Part II

Carbon nanotubes and nanocomposites

6

Synthesis, characterization and application of carbon nanotubes: the case of aerospace engineering

M. REGI, University of Rome 'La Sapienza', Italy

6.1 Introduction

Nanotechnology is the design, production (synthesis) and application of nanomaterials and nanostructures in advanced macro- and micro-systems, through an understanding of the fundamental relationships between physical properties and materials. This innovative science deals with materials and structures at the nanometer scale, typically from subnanometer to several micrometer (hundred nanometers). Similar to quantum mechanics, in this case, the properties and characterization of a material or structure can significantly differ from the macro-scale conditions. Some nanomaterial properties, for example, tuning semiconductor band gaps by varying the material dimensions, are already known. Ultra-strong and ultra-light multifunctional materials (e.g. carbon nanotubes) can be produced through enhanced nanotechnology. Furthermore, super-conductivity and superior magnetic properties provided by nanomaterials can be valuable in improving the properties of electromagnetic devices (biomedical sensors, thermal management, health monitoring, etc.). An important advantage is component miniaturization made possible by nanotechnology, which has a strong impact on systems performance. To date, it is possible to develop very powerful computers able to simulate some functions of the human brain, smart molecular biosensors (nuclear, bacteriological and chemical (NBC) applications and environment monitoring), micro- and nano-electromechanical systems (MENS/NEMS) or nanorobots that can repair internal damage and remove toxins from human bodies.

Nanotechnology has a very broad range of potential applications in many scientific fields. Therefore, its development requires multidisciplinary teams (engineers, chemists, materials scientists, biologists and others) working together on:

- nanomaterial and nanostructure fabrication;
- nanomaterial and nanostructure characterization, evaluating their properties and possible applications;

- understanding the relationship between physical properties and nanoscale structure;
- designing the nano-device and its integration into a macro-system;
- evaluating the human impact of the nanotechnology.

For each step it is necessary to develop specific and innovative procedures and tools able to satisfy a range of requirements.

The synthesis of nanomaterials and nanostructures is an essential aspect of nanotechnology. A real application is possible only when the nanostructured materials are available with the specific properties desired (size, chemical composition, morphology, physical behaviour). The fabrication of nanomaterials started a long time ago, but it is only in the past ten years that nanotechnology has been a specific scientific sector. Owing to its rapid expansion, it is very difficult to cover all sectors of this innovative science. However, it is important to observe that in nanotechnology many scientific sectors, such as engineering and biology, typically very 'distant' from each other, can work together in the development of nanosystems and devices.

The final target of nanotechnology is the control of materials and apparatus on nanoscale dimensions. A 'nano' material or device can improve the properties and characteristics of many systems. In several sectors, current technologies (e.g. the use of silica in a computer's microchip) have reached their physical limit. Nonetheless, using the *bottom-up* or the *top-down* approach, further improvement is possible.

Time and cost are two other important aspects in nanotechnology. As an innovative scientific sector, nanotechnology requires meaningful schedules and costs to be established. Nanosystems and devices must be economically competitive with respect to other traditional and established methodologies. This is a critical issue, since industry requires greater economic competitiveness for nanotechnology products, with tighter schedules and costs compared with those requested by R&D scientific programs. Consequently, there is a need for a double approach (industrial and scientific) to realize competitive nanotechnology systems and devices, which requires the following:

- synthesis of nanomaterials;
- purification (post-synthesis, useful to obtain a high degree of purification of the nanomaterial);
- characterization (using electronic microscopy, and other techniques of observation);
- functionalization (necessary to 'prepare' the nanomaterial for the next step);
- integration of the nanomaterial, or device, in a macro-advanced system.

In the above phases, control of parameters and reproducibility of results are essential. Therefore, it is clear that nanotechnology activities are very complex and characterized by different specialized scientific sectors, requiring:

- significant time and economic investments;
- 'multidisciplinarity';
- interaction between technicians and researchers of different scientific sectors;
- use of complex and advanced instruments and apparatus.

The possible applications of the nanotechnologies to aerospace engineering are:

- composites (metallic and/or polymeric) with nanoparticles (e.g. carbon nanotubes) embedded in the matrix, for structural applications;
- flat panels for aerospace electronics devices;
- special nanostructured coatings for high-temperature conditions (re-entry space mission phase);
- nanosensors (thermal, electromagnetic, biological, etc.);
- MEMS/NEMS;
- solid nanostructured propellants;
- frequency selective surfaces (FSS) with electromagnetic compatibility;
- thermal management;
- nanodevices (nano-cantilever, -diode, -memories for personal computer, -transistor, etc.);
- astronaut health monitoring;
- biological and biomedical applications;
- development of nanosystems in zero gravity conditions.

These aspects will be illustrated in the following sections.

6.2 The development and structure of carbon nanotubes[1–64]

The first carbon filament possessing a very small diameter (less than 10 nm) was produced in the 1970s by the decomposition of hydrocarbon at high temperature using transition metal catalysts. The 1985 discovery of the third allotropy form of ordered carbon (after the graphite and diamond forms, respectively hybridized sp^2 and sp^3), commonly known as fullerene, spurred the subsequent discovery of a number of related forms of carbon. Among these the most famous are nanotubes (Fig. 6.1), observed for the first time in 1991 by Iijima of the NEC Laboratory in Tsukuba, Japan, using HRTEM (High-Resolution Transmission Electron Microscopy). During the same period, Russian researchers also reported the observation of carbon nanotubes and other forms of carbon nanostructures.

The discovery of these nano-elements and nanostructures offered the opportunity to understand how carbon atoms bond with other carbon atoms, and how carbon reacts with other elements under specific conditions of temperature and pressure. With the benefit of theoretical models and

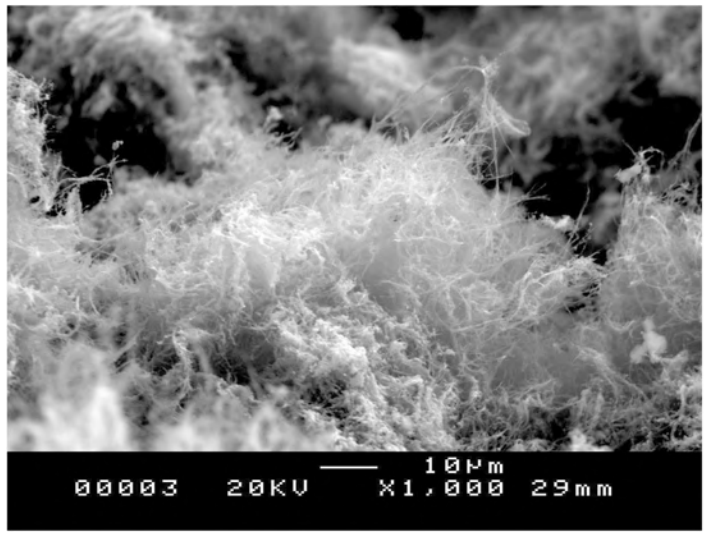

6.1 SEM micrograph of carbon nanotube bundles deposited on the cathode electrode surface.[56]

experimental data, it is now possible to use fullerenes to significantly improve the properties and characteristics of many advanced technologies and systems.

The studies of Kroto, Smalley and coworkers (at Rice University) showed that carbon nanotubes constitute a particular case of the fullerene family. The most famous and most stable of the fullerene molecules is C60, with a computer-simulated image very similar in appearance to a soccer ball. This molecule consists of 20 hexagonal and 12 pentagonal faces, with the carbon atoms at each corner of the individual polygons. C60 stability has been attributed to the 'pentagon rule' and the satisfaction of all valences when the pentagon faces lead to the closure of individual C60 molecules.

The connection between carbon nanotubes and other fullerenes has been defined by the observation that the nanotubes were closed by fullerene-like caps or hemispheres. It is interesting to observe that the smallest reported carbon nanotube diameter is the same as the diameter of C60. This is important in evaluating the minimum dimension of carbon nanostructures. It is necessary to identify all types of nanoparticles and nanostructures of the fullerene family (multiwall and/or single-wall nanotubes, carbon-encapsulated metal nanoparticles, fullerene black and soot, carbon onion, nanowhiskers, etc.). For each nanostructure it is possible to define a set of physical and chemical properties and subsequent applications. It is also interesting to explore the interrelationships between the various nanostructured carbon forms, as well as their relation to the traditional forms of ordered carbon atoms such as diamond and graphite. Carbon is a unique material and can be a good metallic

conductor in the form of graphite, a wide band gap semiconductor in the form of diamond, and a polymer when reacted with hydrogen. As discussed above, carbon provides a significant example of a material showing the entire range of intrinsic nanometer-scaled structures ranging from fullerene, one-dimensional nanoparticles, carbon nanotubes, one-dimensional nanowires, graphite, two-dimensional layered anisotropic materials, fullerene solids, and three-dimensional bulk materials with the fullerene molecules as the fundamental building block of the crystalline phase.

Iijima's discovery of multiwalled carbon nanotubes enabled many scientists to explore the field of nanotechnology, and in particular the world of carbon nanostructures, stimulated initially by the significant one-dimensional quantum effects predicted for their electronic properties, and subsequently by the possibility that the remarkable structure and properties of carbon nanotubes might provide significant improvements in many scientific and technological sectors. Two years after the HRTEM observation of the multiwalled carbon nanotubes, Iijima and his group, in collaboration with the IBM Almaden Laboratory, discovered single-wall carbon nanotubes. This was a very important discovery, because the single-wall configuration represents the fundamental form of carbon nanotubes. It has proved possible to study the fundamental structure by both numerical simulations and experimental tests. The goal is to correlate carbon nanotube properties (mechanical, thermal, electromagnetic, chemical and physical behaviour) to the geometrical characteristics (diameter, length, chirality, hexagon orientation in respect to the nanotubes axis, defects, etc.). It has proved possible to successfully synthesize bundles of carbon nanotubes with very good alignment and a high purity. Control of the parameters used (pressure, temperature, power supply, inert environment condition) is crucial in obtaining a consistent product.

Theoretical and experimental work has focused on the correlation between carbon nanotube morphology and properties. It gives the opportunity to investigate the potential applications in macro-, micro- and nanoscience and technologies. Nanotubes can be utilized, individually or as an assembly, to build functional device prototypes in many scientific sectors, with improved properties and characteristics. The full potential of carbon nanotubes will be reached when growth and synthesis mechanisms are well defined and controlled. Its real application requires the availability of large quantities of material of high quality at low cost. In hydrogen storage, for example, it is necessary to obtain high-quality carbon nanotubes in kilogram quantities using a simple, efficient and cheaper synthesis method. In electronics applications the quantities needed are significantly smaller. The challenge is to produce carbon nanotubes efficiently, obtaining defect-free nanostructures with high length, in large scale with complete dimensional control (length, diameter, chiralities, etc.) provided by a well-defined synthesis process.

6.2.1 The structure of carbon nanotubes[65–91]

The structure of carbon nanotubes is conveniently explained in terms of a seamless array of one or more coaxial cylindrical sheets of graphite with an aspect ratio typically greater than 100 and with outer diameter measuring tens of nanometers, and closed at the end with two semi-domes. The creation of carbon nanotubes can be traced back to the discovery of the fullerene structure C60 (buckyball) in 1985 by Richard Smalley and Harold Kroto. When the buckyball is elongated to form a long and narrow tube with a diameter of approximately 1 nm (10^{-9} m), it provides the basic form of a carbon nanotube (Fig. 6.2). The basic element is graphite, constituted by a series of planes one above the other, held together by van der Waals forces. Each plane has a bidimensional covalent structure. Through a series of processes to fold up these planes of graphite, it is possible to create a tubular seamless structure that does not exist in nature. This structure takes the name of carbon nanotube. Essentially, two families of carbon nanotubes exist (Fig. 6.3):

- SWNT or single-wall nanotubes, that are made up of only one straight tubular unit;
- MWNT or multiwall nanotubes, that are made up of a series of coaxial tubes about 0.34 nm apart (same distance among the various planes of the graphite).

Carbon nanotubes can thus be visualized as a sheet of graphite that has been rolled into a tube. Unlike the diamond (sp^2 hybridization), where the 3D diamond cubic crystal structure is formed with each carbon atom having four

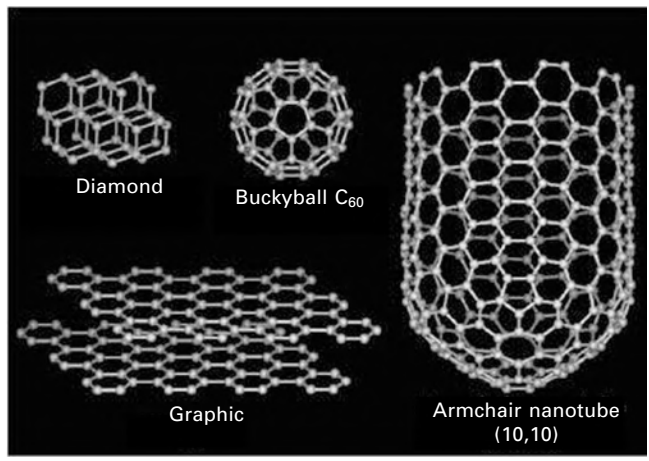

6.2 The carbon family: graphite, diamond, fullerenes and carbon nanotubes.[92]

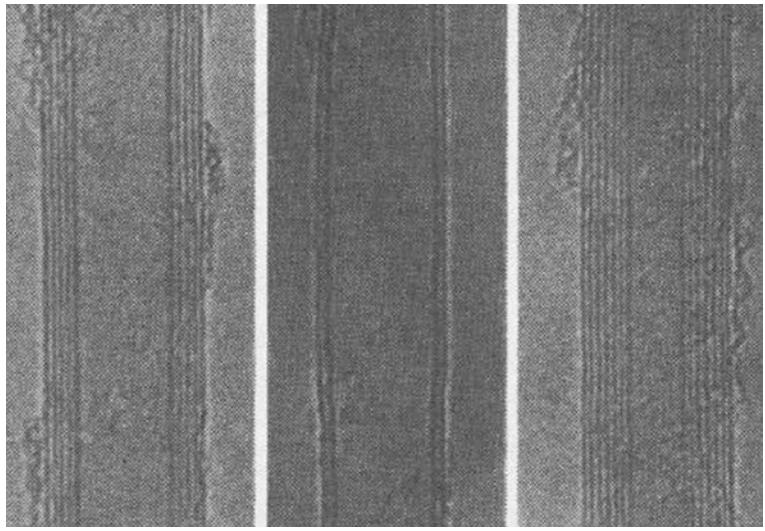

6.3 TEM micrographs of the two principal carbon nanotube typologies: SWNT – single-wall nanotubes (in the center), and MWNT –multiwall nanotubes (on the left and right).[92]

nearest neighbours arranged in a tetrahedron, graphite (sp^3 hybridization) is formed as a 2D sheet of carbon atoms arranged in a hexagonal array. In this case, each carbon atom has three nearest neighbours. 'Rolling' the sheet of graphite into cylinders forms carbon nanotubes. The properties of carbon nanotubes depend on atomic arrangement (how the sheet of graphite is 'rolled'), the diameter and length of the tubes, and the morphology or nanostructure. Using different synthesis methods and specific process parameters, it is possible to obtain different carbon nanotube morphologies and properties, with the potential for multipurpose applications in many scientific fields.

It is possible to define the geometric parameters of carbon nanotubes. The diameter is expressed in terms of the chiral vector (*Ch*) which connects two crystallographically equivalent sites on a 2D graphite sheet (Fig. 6.4):

$$\overrightarrow{Ch} = \overrightarrow{na_1} + \overrightarrow{ma_2} \qquad [6.1]$$

where

$$a_1 = \frac{a\sqrt{3}}{2}x + \frac{a}{2}y \qquad [6.2]$$

and

$$a_2 = \frac{a\sqrt{3}}{2}x - \frac{a}{2}y \qquad [6.3]$$

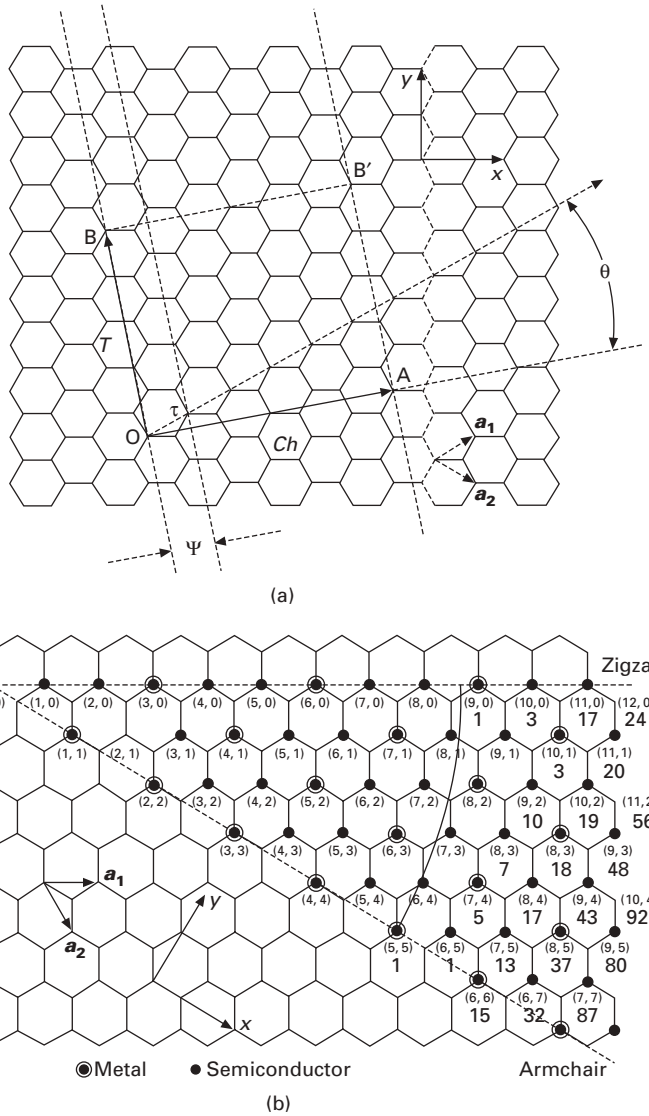

6.4 Geometry construction rule for different carbon nanotube typologies (θ = chiral angle, ψ = length of vector $\boldsymbol{a}_1$, τ indicates direction (dotted line) given by the vector $\boldsymbol{a}_1$).[65]

with $a = 2.46 \Rightarrow$ Å in an (x, y) coordinate system.

The chiral angle (θ) is defined as (Fig. 6.4):

$$\cos(\theta) = \frac{2n + m}{2\sqrt{n^2 + m^2 + nm}} \qquad [6.4]$$

where n and m are two integer numbers. The chiral vector is perpendicular to the tube axis, while the chiral angle is the angle between Ch and the so-called zigzag direction ($\theta = 0°$). The carbon nanotube diameter (d) is calculated by the following formula:

$$d = \frac{|Ch|}{\pi} = \frac{a_{cc}\sqrt{3(n^2 + m^2 + nm)}}{\pi} \quad [6.5]$$

with:

$$1.41\,\text{Å} \leq a_{cc} \leq 1.44\,\text{Å} \quad [6.6]$$

where the inferior extreme corresponds to the graphite, while the superior extreme corresponds to the buckyball C60.

Since Ch, d and θ are expressed as a function of the integers n and m, there is enough to represent any carbon nanotube typology using the following notation:

$$(n, m) \quad [6.7]$$

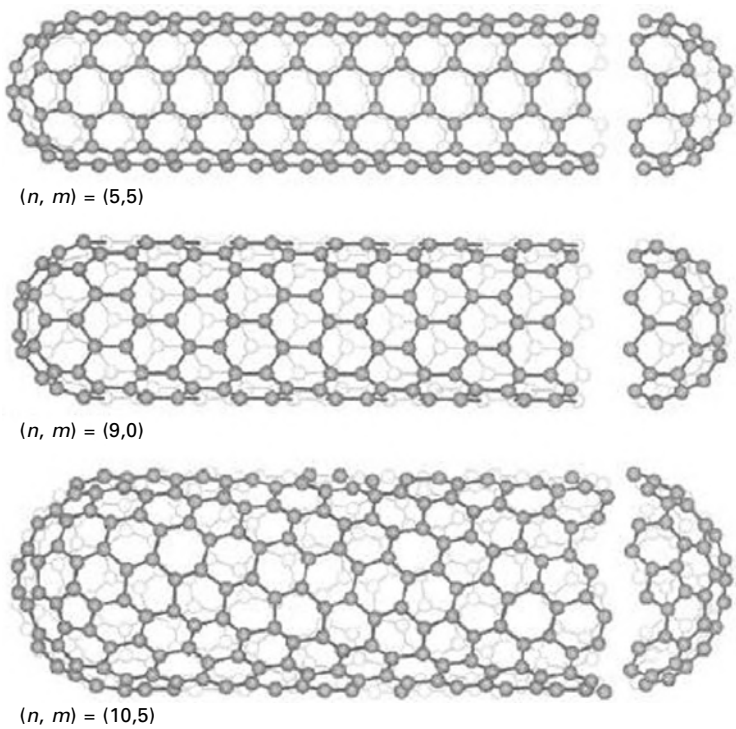

6.5 Carbon nanotube typologies: armchair, zigzag and chiral.[92]

Then, changing the chiral angle (θ), three carbon nanotube families can be distinguished (Fig. 6.5):

1. $\theta = 0° \rightarrow$ *zigzag* carbon nanotubes with (n, 0) or (0, m).
2. $\theta = 30° \rightarrow$ *armchair* carbon nanotubes with $n = m$.
3. $0° < \theta < 30° \rightarrow$ *chiral* carbon nanotubes with $n \neq m$.

If $n \neq m \neq 0$, there is *chiral symmetry*, while if $n = 0$ or $n = m$ there is *achirality*. Each carbon nanotube typology can be characterized in various ways:

- morphological;
- mechanical;
- thermal;
- electromagnetic;
- chemical and physical stability and/or reactivity, etc.

Figure 6.4 indicates the carbon nanotubes that are semiconducting and those that are metallic. It shows the number of distinct fullerene caps that can be used to close the end of (n, m) the nanotubes. The electrical behavior of carbon nanotubes can be determined, using the following simple rule:

$$\begin{cases} n - m = 3q = \text{metallic} \\ n - m \neq 3q = \text{semiconducting} \\ q = \text{integer} \end{cases} \quad [6.8]$$

Table 6.1 summarizes the principal carbon nanotube parameters and Table 6.2 shows their principal properties (mechanics, electrics, thermal, etc.).

Since 1991, great progress has been made in understanding the morphology and properties of carbon nanotubes. There has been a constant fruitful interplay between theoretical models and experimental activity which has enhanced researchers' knowledge in this field. Although there are still many fundamental studies to be done, it is possible to define applications of carbon nanotubes in many sectors. These are mostly related to three unique features of the nanotubes: small dimensions, electronic and mechanical properties. They can be used for example as nanomolds and templates for making small structures of other materials; they can be modified for catalytic purposes and used for gas storage. Conductive carbon nanotubes are excellent for field emissions owing to the high curvature at the tips, while in bulk form they might make good wires. In this case the technological problem is to be able to manipulate the carbon nanotubes individually in a practical way to find use in nanoelectronics devices. In general, bulk applications are most promising at present. Among these, nanotube reinforced materials (polymeric, ceramic, metallic) are excellent candidates. Their exceptionally high strength combined with their light weight makes them ideal for this structural purpose. Nanotubes are the ultimate carbon fibers in terms of strength to weight ratio so it would

Table 6.1 Characteristic parameters of carbon nanotubes

Symbol	Description	Formula	Value
a_{C-C}	Carbon–carbon atom distance	–	$1.42 \Rightarrow$ Å
a	Length of unit vector	$\sqrt{3}a_{C-C}$	$2.46 \Rightarrow$ Å
a_1, a_2	Unit vectors	$\left(\frac{\sqrt{3}}{2}, \frac{1}{2}\right)a, \left(\frac{\sqrt{3}}{2}, -\frac{1}{2}\right)a$	in (x, y) coordinate system
Ch	Chiral vector	$Ch = na_1 + ma_2 \equiv (n, m)$	(n, m): integer
L	Circumference of nanotube	$L = \lvert Ch \rvert = a\sqrt{n^2 + m^2 + nm}$	$0° \le \lvert m \rvert \le 30°$
d	Nanotube diameters	$d = \frac{L}{\pi} = \frac{\sqrt{n^2 + m^2 + nm}}{\pi} a$	
θ	Chiral angle	$\sin \vartheta = \frac{\sqrt{3}m}{2\sqrt{n^2 + m^2 + nm}}$	$0° \le \lvert \vartheta \rvert \le 30°$
		$\cos \vartheta = \frac{2n + m}{2\sqrt{n^2 + m^2 + nm}}$	
		$\tan \vartheta = \frac{\sqrt{3}m}{2n + m}$	

Table 6.2 Principal properties of carbon nanotubes

Parameter	Value
Diameter	O (nanometers)
Length	Several micrometers
Density	1.33–1.40 g/cm^3
Tensile strength	45 GPa
Young's modulus	~1–4 TPa
Electrical properties	Metal or semiconductor
Current density	1×10^9 A/cm^2 (estimated)
Field emission	Activation of phosphorus compounds at ~1–3 V with 1 μm spacing electrodes
Thermal conductivity	6000 W/mK
Thermal stability	Stable up to 2800 °C in vacuum and 750 °C in atmosphere

be surprising if they could not find a niche in this engineering sector. Other possible applications are: health monitoring, biomedical sensors, propulsion and thermal managements.

The critical aspect is their production costs. Until this is brought down to a level competitive with existing fibers, large-scale use of carbon nanotubes will not take place. But, with the right theoretical models and with experimental confirmation of their unique qualities and properties, there will be a greater incentive to develop industrial scale production. In the meantime, the increased know-how brought about by the study of nanotubes is having a strong impact on traditional carbon research and development and on many other fields.

6.3 Synthesis of carbon nanotubes

The first step in the development of advanced nanotechnology systems is the synthesis of the nanomaterial. Regarding carbon nanotubes, three principal methods are available:

- arc discharge (on inert environment, water immersed, plasma arc);
- laser ablation (CO_2, Nd-Yag);
- chemical vapor deposition (CVD; thermal, hot filament, plasma enhanced).

The target is to produce a large quantity of carbon nanotubes (or nanomaterials in general) with a high degree of purity and alignment levels, uniform property distributions and low costs. Producing carbon nanotubes with the above qualities is necessary for current potential applications to become marketable. This requires solving some scientific and technological problems that can be more or less complex depending on each specific synthesis method. One example is the chirality control of carbon nanotubes, with production capability adapted to each specific application (composite material, electronics devices, heat management, etc.). One requirement would be to understand perfectly the mechanism of nanotube nucleation and growth, which remains a key area of research. This problem is partially explained by the complex physical aspects of the synthesis process such as the control of parameters and the reproducibility of results. Thanks to the large number of experimental parameters involved in the synthesis process, and considering the large range of conditions influencing each process, it is legitimate to suppose that many physical and chemical mechanisms affect the synthesis process.

Using the above methods, typical synthesis products are:

- nanoparticles, carbon nanocapsules, nanofibers and whiskers;
- graphite structures;
- carbon nanotubes.

These products use graphite as the base material. In fact, using different precursors (e.g. aluminium, ceramics), with the same technological methods,

it is possible to produce other kinds of nanomaterials (e.g. aluminium nanotubes, ceramic nanoparticles). The principal parameters employed during the synthesis process are:

- temperature;
- pressure;
- gas (inert or not);
- time of synthesis;
- voltage and amperage (and the consequent power provided to the synthesis apparatus);
- base materials (graphite);
- catalysts (yttrium, cobalt, nickel, molybdenum, etc.), used for optimizing the synthesis capability thanks to the improvement of chemical and physical phenomena occurring during the process.

Each parameter is fundamental in order to obtain the specific carbon nanotube typology. In particular, temperature and electrical parameters (voltage, amperage) represent the energy provided to the graphite necessary for the growth of carbon nanotubes. One of the advantages of these different synthesis techniques is the possibility of varying a large number of parameters (described above), allowing the characterization of the optimal conditions for the control of carbon nanotube formation. The major drawback of these techniques is that the carbon nanotubes are never pure, i.e. they are associated with other carbon phases and catalysts, therefore requiring a post-synthesis purification step.

The full application potential of carbon nanotubes will not be realized until the growth mechanisms can be optimized and well controlled. Real-world applications of this innovative material (sometimes called the material of the 21st century) require either large quantities of bulk materials or device integration in scaled-up form. For applications such as structural composites and hydrogen storage, it is necessary to obtain high-quality nanotubes at the kilogram or tonne level (industrialization of the process) using growth methods that are simple, efficient and inexpensive. For devices such as nanotube-based electronics, scale-up will unavoidably rely on self-assembly or controlled growth strategies on surfaces combined with microfabrication techniques. Significant work has been carried out in recent years to tackle these issues. Nevertheless, many challenges remain in the nanotube growth area. First, an efficient growth approach to structurally perfect nanotubes on a large scale is still lacking. Second, growing defect-free nanotubes continuously to macroscopic lengths has been difficult. Third, control is needed over nanotube growth on the surface in order to obtain large-scale ordered nanowire and nanofiber structures. Finally, there is the seemingly formidable task of controlling nanotube chirality by any existing growth method.

Before describing the synthesis methods, it is useful to outline their characteristics.

- *Arc discharge in inert environment*:
  - The simplest and oldest technique.
  - Gives high quantities of carbon nanotubes.
  - Requires a specific control of the environment using inert gases (helium and/or argon).
  - It is necessary to provide an electrode cooling system.
  - The purity and alignment level cannot be optimized without specific parameter control (use of the plasma arc discharge makes it possible to solve these problems).
  - It is very fast.
- *Arc discharge water immersed method*:
  - The use of inert gases is not needed.
  - Thanks to the deionized water, cooling systems are not necessary.
  - The partial evaporation of deionized water may provide arc instability during the synthesis.
- *CVD*:
  - Provides an intrinsic good alignment level of the carbon nanotubes produced.
  - Only small quantities of carbon nanotubes can be produced.
  - High level of purity.
  - Many crystallographic defects in carbon nanotubes produced may be found.
  - It is slow.
- *Laser ablation*:
  - High quantity of carbon nanotubes produced.
  - Better control and repeatability of the process parameters compared to the arc methods.
  - Cost reduction.
  - Complex facilities (lasers, ovens) required.

For realistic use of the carbon nanotubes in advanced applications using the above methods, it is necessary to achieve:

- improved synthesized quantity;
- better parameter control and consistency of product;
- significant cost reduction;
- an industrial scale process, i.e. it is necessary to transform the prototype synthesis facilities into industrial apparatus.

6.3.1 Arc discharge[1–14]

In 1991 Iijima discovered carbon nanotubes in the cathode deposit of an electrode used in the arc discharge. This method is the oldest technique used in nanomaterial synthesis processes. To understand the phenomenon of

nanotube growth in the arc discharge method it is relevant to consider the optimization of other techniques employed (laser ablation, CVD) and, that in general, arc technology is widely employed in several industrial applications. It is also necessary to evaluate the macroscopic phenomena, as per electrode spot, material flow and atomics behavior during the arc process. Typical experimental apparatus used to perform synthesis by the arc method is shown in Fig. 6.6.

The arc was generated between two electrodes with the following parameters:

- Voltage: 20–30 V.
- Current: 60–120 A (there are two possible arc discharge configurations: DC (direct current) and AC (alternating current).
- Pure or doped graphite electrodes.
- Distance between the electrode surface exposed to the arc: 1–3 mm.
- Inert gas: helium and/or argon (the pressure in the synthesis chamber is controlled, and after the process a vacuum is obtained to avoid oxidation of electrodes).
- Discharge time: 10–60 s.

The electrode configuration is an important aspect of this method. Typically, a homo-electrode configuration is employed in which the cathode electrode is made of graphite (pure or doped, diameter: 10–15 mm), and the anode electrode is also made of graphite (pure or doped, diameter: 3–5 mm). Another configuration is the so-called hetero-electrode in which over the graphitic

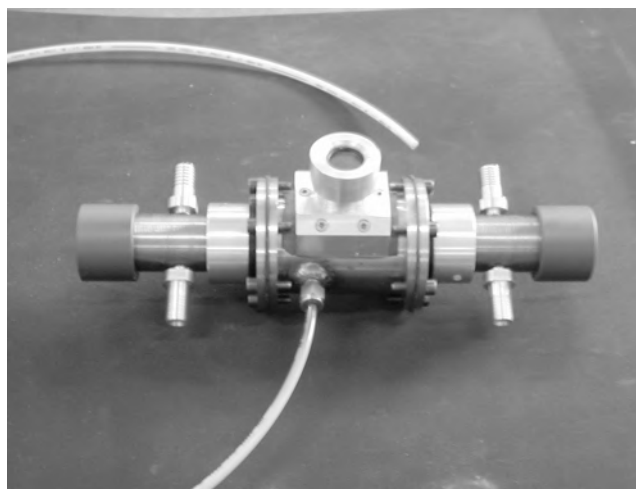

6.6 Arc discharge apparatus in inert environment conditions, consisting of a synthesis chamber, electrode alignment and cooling system, observation window, inert gas ignition and exhausting points, electrode gag control system.[53]

cathode, a metallic anode is used (e.g. molybdenum). The catalysts used to dope the electrodes are: yttrium, cobalt, nickel. They improve the quantity and quality of carbon nanotubes synthesized.

During the process, arc stability is needed (using the methodology of the arc plasma discharge it is possible to obtain a self-sustained arc with an improvement in the synthesis of carbon nanotubes). This can be obtained by accurate control of the electrode gaps (usually an electronic controller is used), and also by using a specific shape of the electrode surfaces exposed to the arc (typically flat or cupped for the cathode, and conical for the anode).

After the process the cathode electrode surface shows several consecutive craters created by the random movement of the generated arc. The areas surrounding the craters appeared shiny gray or silver on visual observation. As shown in Fig. 6.7, on the cathode electrode surface it is possible to distinguish four typical regions, **A**, **B**, **C** and **D**.

- In **A**, the crater spot generated by the arc is visible, and in this region no carbon nanotubes are present, only micro-spheres deposited during the process.
- In **B**, many carbon nanotubes are observed (Fig. 6.8) with a good purity level (some residual catalysts are present), and the alignment depends on

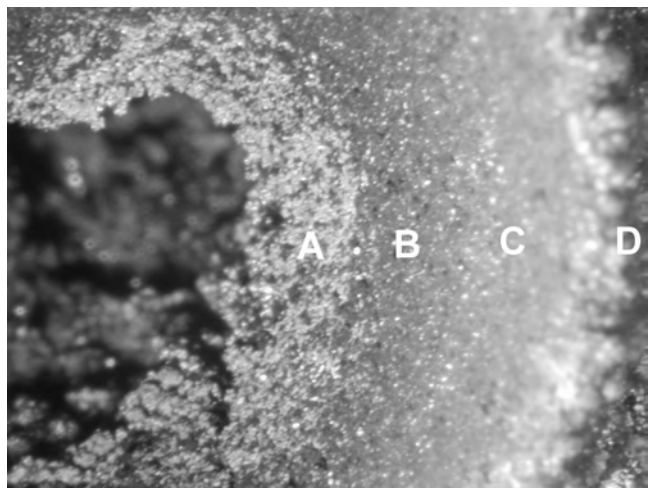

6.7 Cathode electrode surface morphology after the exposure to the arc discharge. Four characteristic regions (**A**, **B**, **C** and **D**) are present: **A** no carbon nanotubes, **B** high quantities of carbon nanotubes (purity and alignment level depends on the parameters employed and by process control), **C** small carbon nanotube quantities and more impurities deposited on the surface, **D** without nanostructured materials (this region is not affected by arc phenomena).[51]

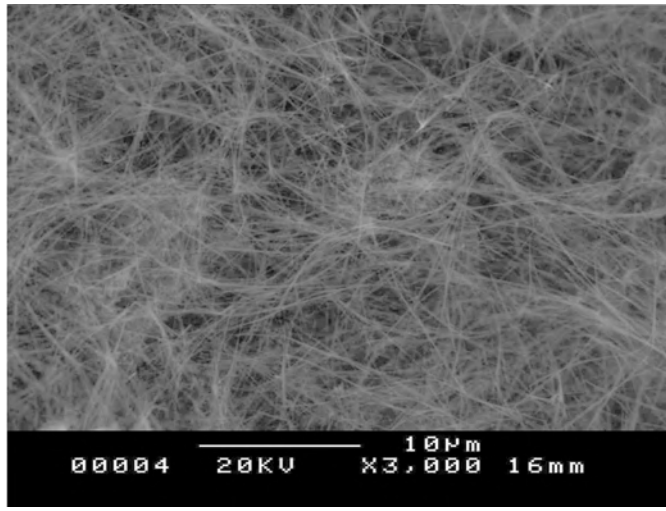

6.8 SEM micrograph with carbon nanotubes produced by the arc discharge method, in the region **B** of Figure 6.7.[55]

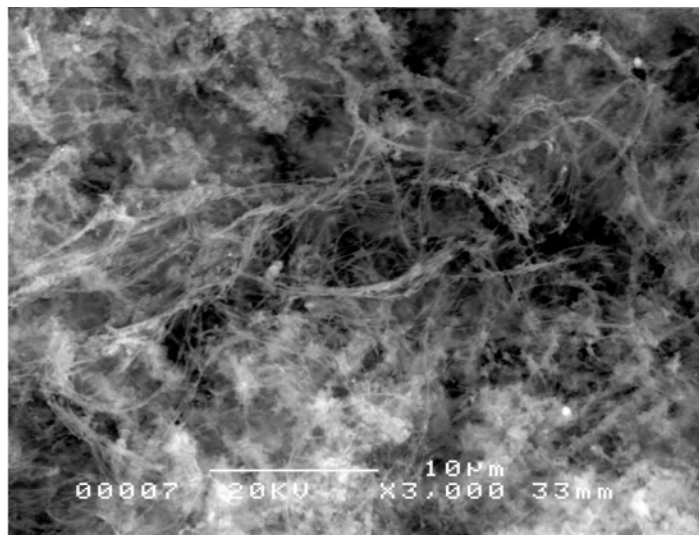

6.9 SEM micrograph with carbon nanotubes produced by the arc discharge method, in the region **C** of Figure 6.7 with residual catalysts and amorphous micro- and nano-carbon particles.[55]

the parameter control used (an intrinsic alignment of the nanotubes is typically provided by the CVD method).

- **C** (Fig. 6.9) is characterized by the presence of carbon nanotubes with major quantities of impurities (catalysts, amorphous carbon, other carbon

micro- and nano-structures) compared with **B**. Usually after the arc process a purification step for the produced nanomaterials is required.

- In **D**, no change caused by the arcing process was observed in the original graphite surface.

The aim of the arc method is to improve the quantity of carbon nanotubes produced (industrialization), maximize region **B** and reduce catalysts and amorphous residuals.

Varying the parameters changes the synthesis results. For example, as shown in Fig. 6.10, changing the electrode gap and increasing the inert gas flow make it possible to modify the geometry and the dimensions of the above four regions. In particular, it is possible to observe an extension of the crater. Naturally, if other parameters are modified (voltage, amperage, discharge time, etc.), further different results are obtainable.

The configuration most often used, the homo-electrode system, consists of both graphitic anode and cathode (C-anode and C-cathode). The cathode deposit is cylindrically composed of two macroscopic parts (in which the above four regions are contained): the outer glossy gray hard shell, and inner dark black soft core. In the homo-electrode system the anode spot is larger than the cathode spot and the mass erosion of the anode is much greater than that of the cathode. This explains the large quantity of carbon nanotubes present in the C-cathode in respect to the C-anode in the DC arc discharge. In the AC arc discharge method, theoretically, it is possible to find the same

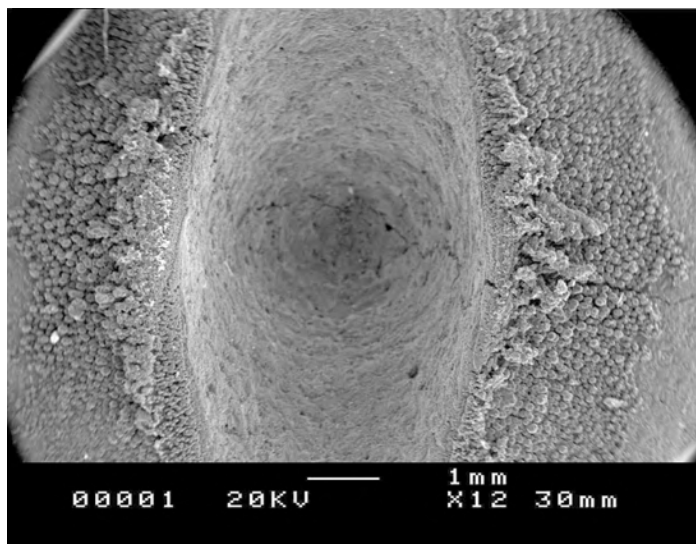

6.10 Using different synthesis parameters (gas flux, pressure, temperature, etc.) makes it possible to change the morphology of the cathode electrode surface.[56]

carbon nanotube quantities in both electrodes, but in this case it is more difficult to control the arc stability, due to the electrical polarity inversion.

In the homo-electrode systems (DC arc discharge), during the arc, carbon atoms, evaporated, due to the high temperature developed from the anode, are deposited on the cathode surface (**B** and **C**). These are then reheated and re-evaporated by the arc, with consequent carbon nanotube growth. In fact, in the central part of the cathode surface involved in the process, nanotubes are synthesized by the random movement of the arc, while on the external region (**D**), materials transferred from the anode are deposited without the reheating and re-evaporation phase. This explains the absence of carbon nanotubes in **D**.

This explanation of the phenomena occurring during arc discharge is just macroscopic; in fact, several theories describe carbon nanotube growth during arc discharge with atomic models. It is necessary to distinguish between models (mainly semi-empirical) useful for an engineering implementation of carbon nanotube synthesis, and theoretical models indispensable for acquiring the know-how on physical and chemical phenomena characterizing carbon nanotube formation. From a technological point of view, the synthesis results depend strongly on a large number of parameters. Complex parametric analysis and scientific investigations are required for a microscopic understanding of carbon nanotube growth mechanism.

Optimizing the arc process produces very interesting results. Figure 6.11a shows the cathode electrode surface in which the four regions (**A**, **B**, **C**, **D**) are well controlled, i.e. with a clean transition from one region to another, with the maximum extension of **B**, thanks to the reduction of the other three regions (**A**, **C** and **D**). Figure 6.11b shows an SEM micrograph of the carbon nanotubes present in **B**, with a very high purity level. The alignment is not excellent, but this is an intrinsic characteristic of the arc discharge method.

Another method is the so-called arc discharge water immersed (using deionized water) method. As shown in Fig. 6.12, vacuum and inert gas systems are not required. In this case the carbon nanotubes on the electrode surfaces, are present in the water suspension. This 'water method' presents some problems:

- the control of the arc stability is very complex;
- the quantity of carbon nanotubes produced is less than that obtained by 'inert environment arc discharge';
- the industrialization of the method seems more complex.

Owing to the many possible configurations applicable and several modifiable parameters, the arc method, which can be considered the traditional carbon nanotube synthesis method, has a greater possibility of being improved.

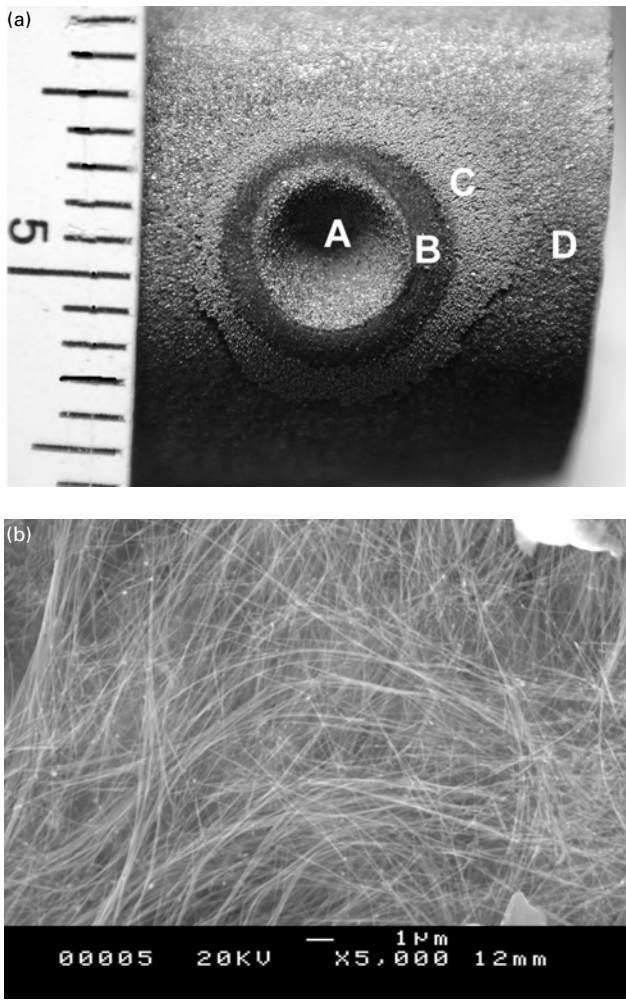

6.11 Optimization of the arc discharge process parameters makes it possible to improve the carbon nanotubes produced by specifically controlling the four characteristic regions and the purity level (as shown by the SEM micrograph in panel b) of the nanomaterials.[56]

6.3.2 Laser ablation[15–24]

This technique is an upgrade of the arc discharge method. Two typical laser methodologies are employed:

- *Nd-Yag*: laser ablation of a carbon rod (graphite pure or doped) at a temperature of 1200 °C in an argon inert flow. A two pulse sequence at 10 Hz from an Nd-Yag laser (wavelength: green at 532 nm; energy: ~50 mJ

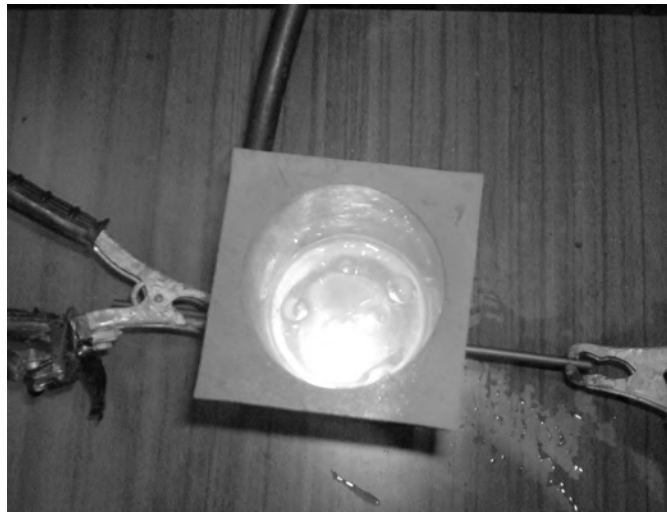

6.12 Water immersed arc discharge prototype apparatus, used to perform a base experimental test of innovative synthesis methods.[55]

per pulse, 6–7 ns) followed by 50 ns delayed second laser pulse at a wavelength of 1064 nm (IR, energy: ~50 mJ per pulse, 4–6 ns) was directed to the above carbon target, with the growth of carbon nanotubes.

- CO_2: laser ablation of a carbon rod (graphite pure or doped) at room temperature (no oven is needed) in an argon inert flow. A single continuous CO_2 laser (wavelength: 1064 nm; power: 400–900 W) was directed to the above carbon target with the growth of carbon nanotubes.

The typical laser experimental set-up used to produce carbon nanotubes is shown in Fig. 6.13. It consists of a quartz tube inside a furnace (not needed in the case of the CO_2 ablation). The tube is sealed and connected to a vacuum system and an inert gas reservoir. The laser beam enters the quartz tube through a special window mounted in a vacuum flange. The carbon target is placed in the center of the quartz tube and is aligned to the laser beam. The distance between the laser and the carbon target is changeable due to a small quartz tube coaxial to the water-cooled metallic collector mounted at the other end of the external tube. During the synthesis process the temperature profile is measured by thermocouples collocated into the tube.

Briefly, the laser ablation process can be summarized as follows:

- The laser beam (double pulsed or continuous) shoots at the carbon target.
- An atomic carbon plume is produced and carried, by the inert gas flow, to the water-cooled metallic (typically aluminum or copper) collector.

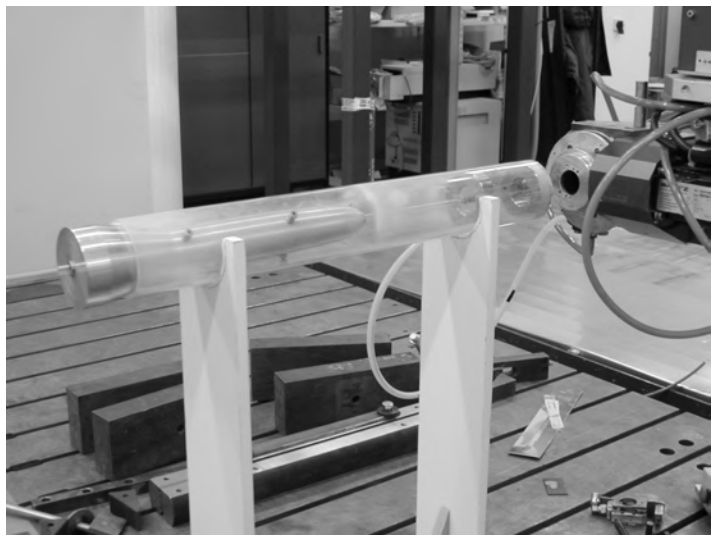

6.13 Laser ablation CO_2 apparatus for carbon nanotube synthesis.[55]

- The nanostructures (carbon nanotubes, fullerenes and other carbon elements) are deposited to the collector surface.

The laser ablation method has been proven to be the most efficient technique for high-purity carbon nanotube production. Many papers focus on studying the effects of processing parameters, i.e. the synthesis optimization (as a function of the catalyst's concentration, furnace temperature, gas flow, pressure, energy provided, etc.). For instance, the experimental tests demonstrate that the bimetallic catalyst mixture (e.g. Ni/Co) is more efficient than the use of a single metal. Moreover, the furnace temperature and gas conditions (flow and pressure) directly influence the production yield of the carbon nanotubes and, in particular, their diameter distribution. The increase in the laser intensity favors the growth of large nanotube diameters. Also the temperature has an important role in the synthesis. In particular, for values less than 800–900 °C the yield of the produced nanostructures decreases, improving the amorphous carbon element deposited on the collector. It is important to observe that the temperature value is proportional to the energy provided to the carbon target.

In general, it is found that the tendency to favor the growth of high carbon nanotube yield is a function of the temperature and the laser intensity. Thus, each optimized laser intensity corresponds with an 'optimal heating' of the carbon target that gives better synthesis results. This is also consistent with the fact that the double pulse configuration, with respect to the continuous laser spot, provides a maximization of the energy absorption by the target surface, leading to a higher carbon nanotube yield.

As for the arc discharge, the phenomena occurring during the laser ablation process are very complex. By *in situ* imaging and spectroscopic diagnostic investigation, it is possible to analyse the carbon nanotube growth mechanism, corresponding to a single laser pulse. Initially the laser pulse produces atomic molecular vapor (plume) containing ~5×10^{16} carbon atoms and ~10^{14} catalyst atoms (this value has been estimated by weighing the target before and after ablation). The evaporated materials remain in the vapor phase until approximately 100 μs after the ablation. Then, laser plasma, which is initially very hot, cools rapidly, increasing the population of the atomic and molecular species. The analysis shows that carbon atoms condense and form clusters after 200 μs from the initial ablation, while the metallic catalyst atoms (typically Ni/Co) condense much later. The atomic catalyst population is maximum at t = 0.8 ms and then condenses by t = 2 ms. At this time all atoms and molecules have converted into clusters and nanoparticles, as evidenced by the vortex ring structures of the plume; with a temperature of ~1400 °C, just above the Ni/C and Co/C eutectic temperatures. By t = 4 ms, the plume has reached the furnace temperature, with the initial formation of carbon nanotubes. Continuing the process, the length of the nanostructures increases. In fact, if for example the process is stopped at ~t = 25 ms, only short carbon nanotubes are obtained, indicating that the majority of the growth takes place after the ablation provided by the laser pulse.

In any case, the laser ablation samples, observed with SEM and HRTEM, exhibit numerous bundles containing a high quantity of carbon nanotubes of excellent purity (carbon nanoparticles and residual catalysts are minimized in respect to the non-optimized arc discharge results). Both the carbon nanotubes and the bundle diameters depend strongly on the process parameters (temperature, pressure, gas flow) and in particular on the laser configuration (single or pulsed, intensity, etc.). For each method (Nd-Yd, CO_2), owing to the experimental activities, it is possible to determine the set of parameters that optimize carbon nanotube synthesis (growth rate, quantity, purity, chirality, single wall or multiwall, metallic or semiconductor).

6.3.3 Chemical vapor deposition[25–39]

CVD is the third method employed in the synthesis of carbon nanotubes. The growth process involves heating a catalyst material to high temperature in a tube furnace and flowing a hydrocarbon gas through the tube reactor for a specific period of time. The key parameters in carbon nanotube CVD growth are:

- hydrocarbons (gas flow and rate);
- catalysts;
- temperature (thermal cycles, described below).

The typical active catalyst species used are transition metal nanoparticles formed on the support (substrate) such as silica (Si) or other materials. Using different CVD typologies (e.g. thermal CVD (TCVD) or plasma enhanced CVD (PHCVD)) the substrate and the catalyst employed can be changed: Si substrate for TCVD, plastic materials for PHCVD.

General nanotube growth in the CVD method is characterized by the dissociation of the hydrocarbon molecules, forming a region rich in carbon atoms reacting with the metallic particles of the substrate, with subsequent carbon nanotube formation (base and tip growth criteria). The CVD method is characterized by four fundamental aspects:

1. The possibility of performing a *free-standing* or *well-aligned* carbon nanotube growth (in the first case the nanostructures on the substrate surface are randomly distributed, while in the second case very good alignment is obtained. This aspect is relevant for the electronics application as nanodevices or MEMS/NEMS).
2. The carbon nanotubes produced have high defect densities (the nature of these defects remains to be thoroughly understood, but is most probably due to the relatively low growth temperature, which does not provide sufficient thermal energy to anneal the nanotubes into perfect crystalline structures. Growing perfect carbon nanotubes with the CVD process remains a challenge because the presence of the above defects strongly influences the carbon nanotube behavior in many applications such as composite nanostructure materials, electronics, thermal management).
3. It is possible to choose a specific pattern of carbon nanotube growth, creating specific distribution of the nanostructures on the substrate thanks to chemical inhibition and/or activation. (This provides the possibility of realizing nanoelectronics circuits or specific paths useful to the controlled thermal dissipation of advanced apparatus and devices).
4. The time scale is not fast (each synthesis requires at least one hour and the quantities of carbon nanotubes produced are much less than by the laser ablation and arc discharge processes, which are, in addition, faster than CVD. In this case the industrialization of the method involves different aspects regarding, principally, the alignment and density defects).

Many CVD configurations have been developed:

- TCVD: thermal CVD;
- HFCVD: hot filament CVD;
- PHCVD: plasma enhanced CVD;
- CCVD: catalytic CVD.

In particular, through using PHCVD it is possible to deposit nanostructures in a low-temperature synthesis condition. This is particularly important in the case of a substrate with a low melting point (plastic materials, for example).

Other methods (TCVD, HFCVD) are normally used with high melting point materials (e.g. Si(100) doped substrate).

The substrate is usually made up of an Si(100) film thermally oxidized and coated with a thin layer (100–200 nm) of metal catalyst.

A typical TCVD facility is shown in Fig. 6.14. The apparatus consists of a quartz tube inside a furnace, with the gas (inert and hydrocarbons) and the vacuum systems. Figure 6.15 illustrates the typical thermal cycles employed in TCVD carbon nanotube synthesis. In particular:

- phase 1: heating the system using an inert gas (argon);
- phase 2: chemical etching (by hydrogen) of the metallic catalyst deposited

6.14 Thermal CVD apparatus.[64]

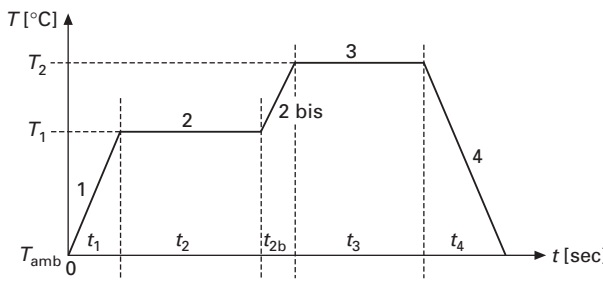

6.15 Typical thermal CVD cycle used in carbon nanotube synthesis: 1, heating phase (inert condition); 2, chemical substrate etching for producing on the surface catalytic nanoparticles useful for the growth of carbon nanotubes; 2 bis, heating phase (inert condition); 3, carbon nanotube growth; 4, final cooling phase (inert condition).[64]

on the Si substrate (T_1 = 500–700 °C, t_2 = 10–20 min). The aim is to create, on the substrate surface, a deposit of high-density metallic nanoparticles (derived from the metal coating) that act as nucleation seeds for carbon nanotube growth (base and tip growth model);
- phase 3: second heating of the system using inert gas (argon);
- phase 4: carbon nanotube growth (T_2 = 800–1200 °C, t_3 = 10–60 min) using hydrocarbon gases (hydrogen, methane, etc.)
- phase 5: cooling the system (t_4 = 30–60 min) with inert gas (argon), to avoid oxidation of the nanostructures synthesized in the previous phase.

Figure 6.16 shows the typical Si(100) doped substrate employed. With CVD it is possible to produce nanostructures and also to realize special nanocoatings, i.e. to deposit materials (nanostructures or simple nanoparticles) on different surfaces (carbon–carbon composites, metallic plates, fibres, multilayer composites, etc). Figure 6.17 shows the nacelle (inserted in the quartz tube) with a carbon–carbon, metallic plate, carbon fiber sample used to perform a TCVD nanocoating test. The results are reported in Figs 6.18–6.21 respectively:

- SEM micrograph of the *free-standing* carbon nanotubes produced (Fig. 6.18).
- Nanoparticles deposited on the metallic plates (this is a possible alternative

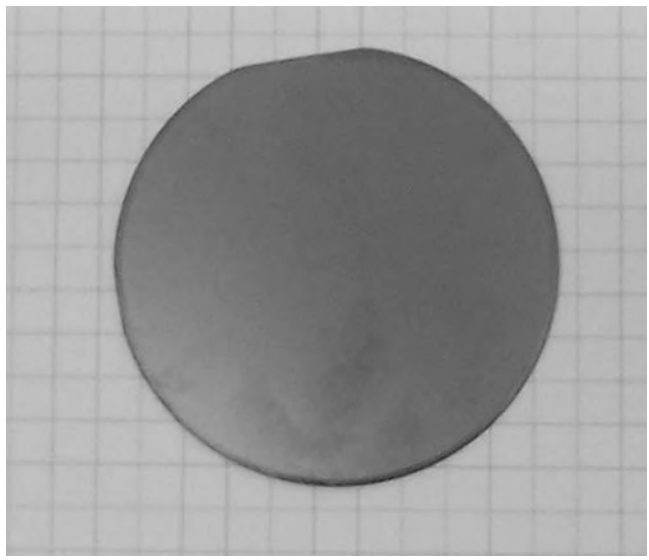

6.16 Silicon, with relative Miller index of 100, doped substrate coated with (ex. nickel) catalyst.[64]

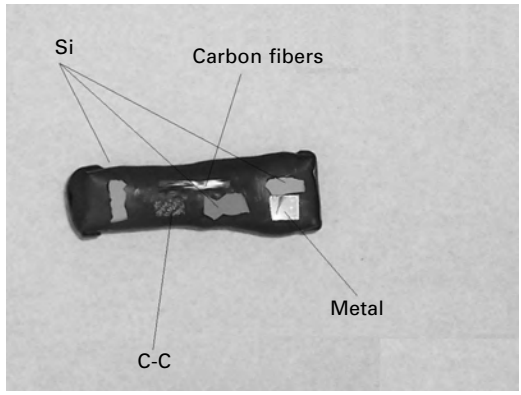

6.17 Different materials used in TCVD.[63]

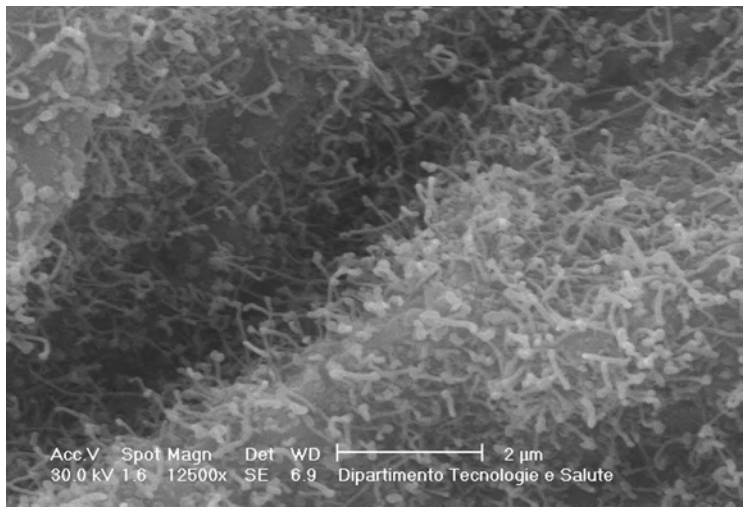

6.18 Bundles of free-standing carbon nanotubes produced by TCVD on the Si(100) doped substrate.[63]

method to plasma spray and traditional technologies used for the coating) (Fig. 6.19).

- Nanoparticles on the carbon fibers (this can represent a fundamental step for chemical bonding between the fibers and the polymeric, or other typology, matrix and for the subsequent mechanical behavior of composite materials) (Fig 6.20).
- Carbon–carbon coating (depositing ceramic materials is possible in order to manufacture a nanostructured thermal barrier useful for aerospace vehicles during the atmosphere re-entry phase of a mission) (Fig. 6.21).

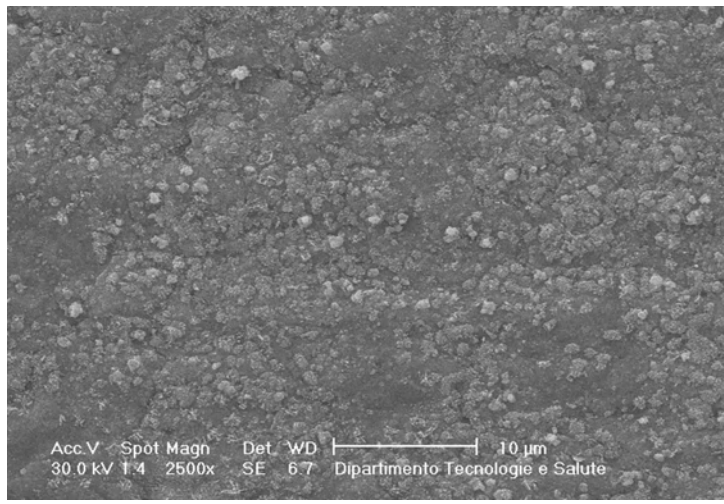

6.19 Carbon coating deposited on the metal plate surface using the TCVD method.[63]

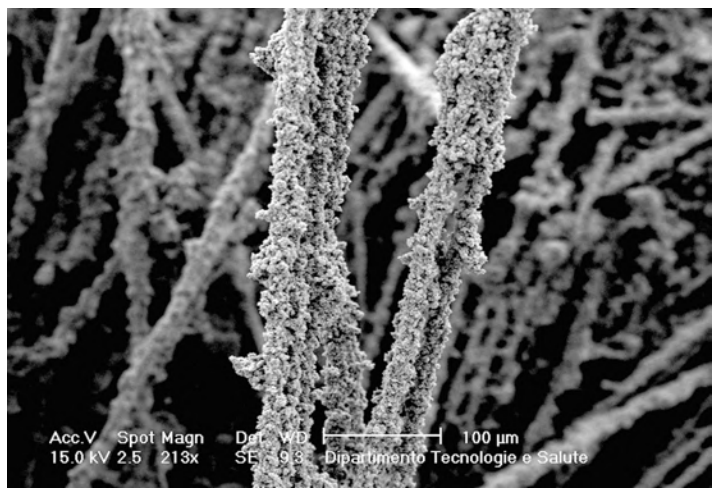

6.20 Carbon coating deposited on the carbon fibers using the TCVD method.[63]

CVD provides the possibility of developing innovative and advanced technological methods useful to improve traditional techniques employed in many scientific sectors.

6.4 Characterization techniques[1, 50–64, 68–73]

In each step in the development of an advanced nanotechnology system/ apparatus the characterization of the nanomaterials and nanostructures

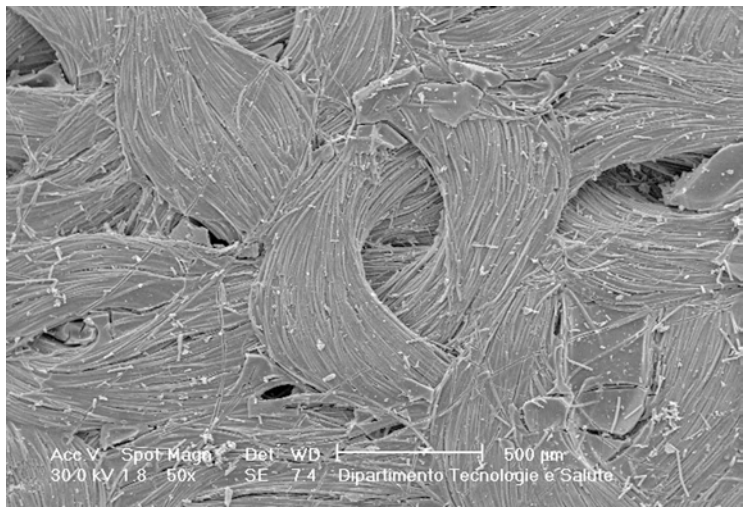

6.21 Carbon coating deposited on the carbon–carbon composite using the TCVD method. Using ceramic materials, with the same technology, it is possible to produce a coating with high mechanical, thermal and chemical characteristics useful for hybrid composite materials employed in space vehicles (for the re-entry phase mission in which the thermal and oxidation conditions are extreme).[63]

employed (synthesized, purified, etc.) is a critical phase. In fact, it is necessary to perform a specific evaluation of the fundamental properties and characteristics of the 'nano-elements' integrated in the above advanced system. To observe and to analyse structures of micro- and nanometric dimensions is not simple but it is necessary to develop a specific standard protocol for every single step, i.e.:

- sample preparation methods;
- analysis criteria;
- evaluation and interpretation of results;
- analysis reliability and repeatability;
- storage procedure for samples.

Several analytical characterization tools have been used successfully in past to determine the principal properties of nanostructures and nanomaterials, but a lack of standard methodologies makes it difficult to compare these measurements. The development of a protocol in which standardized analysis methods and procedures are defined is needed. Typical characterization analyses used in the nanotechnology science are:

- optical microscopy;
- optical laser microscopy;
- SEM (scanning electron microscopy);

- TEM (transmission electron microscopy);
- EDX (energy dispersion X-ray);
- AFM (atomic force microscopy);
- STM (scanning tunneling microscopy);
- Raman spectroscopy.

It is clear that the numerous nanomaterials/structures, available due to the different nanotechnologies developed and modified by different processes (synthesis, purification, integration, etc.), demand close examination when they are used for each application. It is fundamental to have a well-characterized material in order to access the variability of the numerous steps required in the design and development of the previously mentioned applications. For example, the nanocomposite material's preparation and evaluation require measurements that can follow the matrix before and after the addition of nanostructures (e.g. carbon nanotubes). There is a strong need for standard methods to characterize the nanomaterials in order to improve the capability of comparing different samples employed as raw materials. The requested protocol must be characterized by a standard procedure useful for performing a short 'nano-elements' characterization, with high reliability levels.

This section illustrates the techniques available and the typical uses:

- *Optical microscopy*: used to characterize the micromorphologies of the sample surface (e.g. electrode cathode surface after the arc discharge) or micro-powders.
- *Optical laser microscopy*: used for the same purpose as optical microscopy, but with better resolution and the ability to perform 3D surface morphology digital reconstructions.
- *SEM*: used to determine the nature of the nanomaterials obtained (e.g. to define whether the synthesis products are carbon nanotubes or simple amorphous graphite) and to acquire an idea about the material's quality and morphology.
- *TEM*: provides specific characterization. In high-resolution modality, for example, it is possible to determine if the carbon nanotubes analysed are single or multi wall.
- *EDX*: gives a spectra from which the chemical elements present in the studied nanomaterials can be separated and identified.
- *AFM*: allows 3D nanotopography and morphology profiling of the micro- and nanomaterial/structures. In addition, with the cantilever tip of this instrument, it is possible to determine the principal mechanical (Young's modulus) and electrical (*V–I* characteristic) nanostructure properties.
- *STM*: provides 3D real images with subatomic spatial resolution of electrically conductive samples.
- *Raman spectroscopy*: for the specific applications in carbon nanotube science, provides an express, non-destructive and preparation-free estimation of the carbon content in a sample.

The techniques listed enable the following characterization of nanomaterials:

- *Morphology*: evaluation of nanometric geometry and characteristics of the observed nanostructures. For example, to determine the typology (single or multiwall), the chiral angle, the twisted angle, etc. of carbon nanotubes.
- *Homogeneity*: to determine the statistical distribution of the various nanomaterials/structures present in a sample or, for example, dispersed into a matrix or in any device.
- *Dispersability*: to determine the capability of nanostructures to form a stable suspension at specific concentration values in bundles or single elements; or to evaluate the dispersion level of the same materials, into a matrix or in a micro-/macro-system. In particular, three different levels have been defined: macro-, micro- and nano-dispersion.
- *Reactivity*: for each nanomaterial and nanostructure determining the chemical, physical and thermal reactivity is necessary. These are important parameters in each step (synthesis, purification, integration and operative conditions of the 'nano-elements').
- *Purity*: in each phase of their development (synthesis, purification, integration, etc.) the nanomaterials are constituted by nanostructures and amorphous residuals. It is always necessary to evaluate the exact percentage of the each element's typology contained in a sample (powders, massive elements, apparatus, etc.). Clearly, the target is the greatest reduction of impurities.

Each analysis typically requires a specific sample preparation procedure. In the case of massive samples, if requested, it is only necessary to deposit a carbon (or gold) coating on the observed surface to improve the electron microscopy contrast and resolution. In contrast, for the micro- and nano-powders, the preparation procedure is more complex. In fact, generally, the following steps are needed:

- The mechanical removal of powder from the sample surface (for example from the cathode electrodes after the arc discharge synthesis).
- To sonicate the powders in order to separate the single nanostructures, avoiding formation of agglomerates.
- To deposit powder in a holder (characteristic for each microscopy typology: aluminum holders with carbon tape for the SEM, metallic grid with a specific mesh size in the TEM analysis, etc.).
- To perform, when requested, the above-mentioned carbon or gold coating of the sample surface (this is specific for SEM, TEM and EDX).

Some analysis typologies require vacuum conditions (SEM, TEM, EDX), or the electrical conductivity of the sample. Other techniques are more simple and rapid (no sample preparation, no vacuum) and the analysis quality is not reduced, as in AFM.

For each technique, the calibration phase and the comparison of preliminary results with standard measurements are fundamental. They ensure that subsequent analyses can be performed with a high reliability level. The evaluation of results is very difficult in nanotechnological microscopic analysis. In fact, the reduced size of samples, together with the complexity of the instruments and physical and chemical phenomena occurring in nanoscale dimensions (e.g. relativistic effects), introduces numerous stochastic variables, making measurement and relative analysis very complex, with complicated evaluation and interpretation of results.

6.4.1 Optical microscopy

With optical microscopy it is possible to perform an accurate macro-morphology analysis of various sample typologies. Obviously, it is not possible to observe nanostructures, but, for example, one can see the surface of the cathode electrodes before and after the arc discharge, identifying the characteristic four regions (**A**, **B**, **C** and **D**) previously described. In addition, it is possible to characterize the surface (with and without electrical conductivity) and determine the morphologies of the fracture section of composite samples after mechanical (static and dynamic), thermal and corrosion tests. Figures 6.7 and 6.11a show optical images of the cathode electrode surfaces after arc discharge corresponding to different synthesis parameters. As shown, the four regions (A–D) are immediately observable, leading to preliminary studies of process results. The target is to realize an SEM analysis and associate to each region a specific characterization of the nanostructures contained on it. Using the same synthesis parameters it is possible to determine, for comparison, on numerous electrodes, the nanodeposit characterization using only optical microscopy – a cheap and easy analysis method. Figure 6.22 illustrates the fracture section of polymeric nanostructured composite materials after dynamic testing. Much information can be gained from studying these images.

6.4.2 Optical laser microscopy

Optical laser microscopy represents an innovative analysis typology. In fact, in the co-focal no contact mode (using laser light with wavelength (λ) in the order of nanometers – O (nm)), it is possible to build a micrometric 3D topography of the surface. As shown in Fig. 6.23, the cathode electrode surface (treated by arc discharge) is analyzed, permitting the detection of the four characteristic zones with a very high detailed reconstruction of their morphologies. The image acquisition is extremely rapid, and no vacuum and electrical conductivities are required.

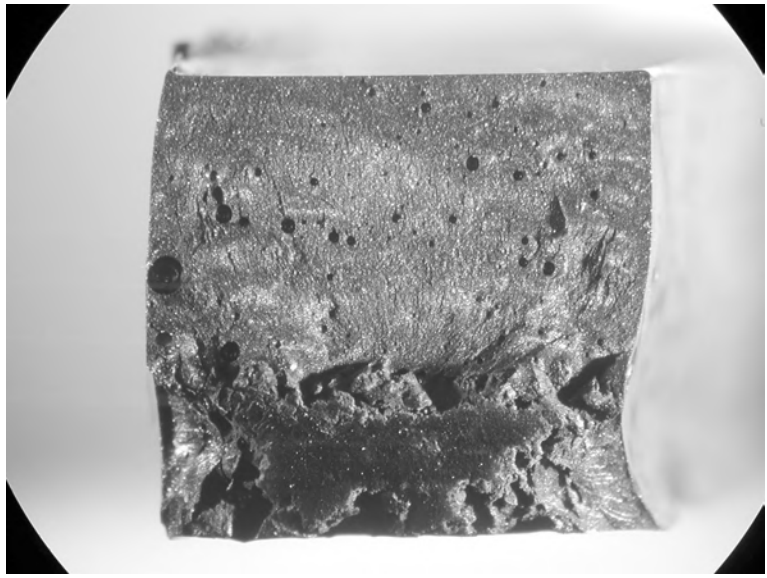

6.22 Fracture section of nanostructured polymeric composite sample used to perform a mechanical test.[53]

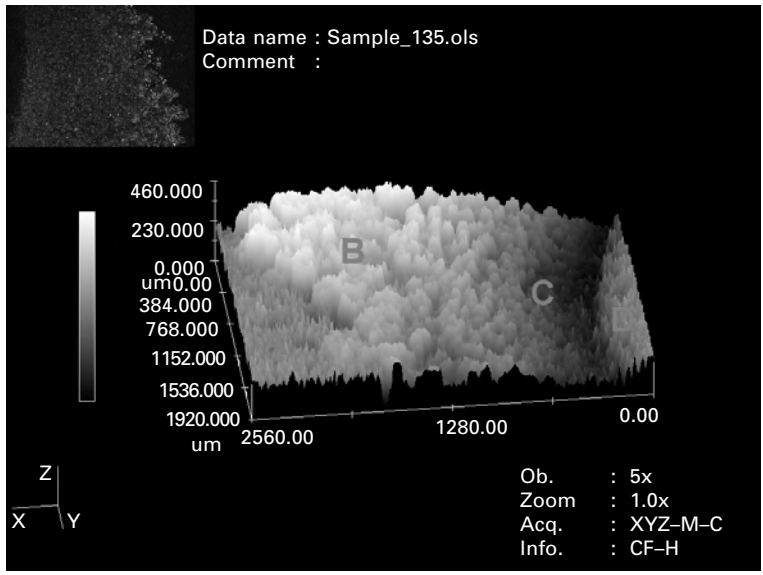

6.23 Optical laser micrographs showing the 3D morphologies of the four characteristic regions present on the cathode surface after the arc discharge process.[60]

6.4.3 Scanning Electron Microscopy (SEM)

SEM micrographs are used to determine the nature of the deposit produced by the synthesis and to acquire a rough idea of the material quality (e.g. purity level). As illustrated, for example, in Figs 6.1 and 6.8, the information acquired by SEM is preliminary; in fact, it is not possible to say whether the observed filaments are bundles of carbon nanotubes or micro-carbon fibers. In addition, in the case of carbon nanotubes data relative to the presence of single walls or multiwalls are not provided. The same applies for other parameters such as chirality, twisted angle, etc.

The micro-mechanics studies of the nanostructured composite are realizable. Figure 6.24(a) shows the micro-fracture line's deviation and interruption due to cavities inside the tested sample. Figure 6.24(b) illustrates the cross-section of a polymeric thin film with carbon nanotubes. By integrating specific software in the SEM it is possible to perform a statistical analysis of nanostructure size. Figure 6.25 shows an SEM picture representation of the carbon particles with different dimensions. From this micrograph the software calculates: area, diameter (max, min and mean) and perimeter of each particle. This is a very important characterization, because in many nanotechnology applications the size of the 'nano-elements' influences strongly the behaviour of apparatus and devices.

6.4.4 Transmission Electron Microscopy (TEM)

Scanning or high-resolution TEM configurations allow the real characteristics of the observed nano-elements to be determined. As mentioned above with SEM, the characterization is incomplete. Only with nanoscale observations is it possible to determine, for example, if a carbon nanotube is single or multiwall. Figure 6.26 gives example of multiwall carbon nanotubes, in which the morphologies and, in particular, their bamboo-like cap end are clearly visible. Typically nanotube extremities contain the catalyst particles useful to the growth process.

6.4.5 Energy Dispersion X-ray (EDX)

Many catalysts are employed to improve the kinetics of nanostructure growth, and quantities and quality (purity level) of synthesized materials, such as cobalt, nickel and yttrium. It is necessary to determine the presence of these elements in order to establish, for each synthesis result, the influence of a specific typology and quantity of catalyst, or a particular mixture. Moreover, an evaluation of the after-purification residual elements (catalysts, amorphous elements) is fundamental for understanding phenomena and subsequent behavior of devices.

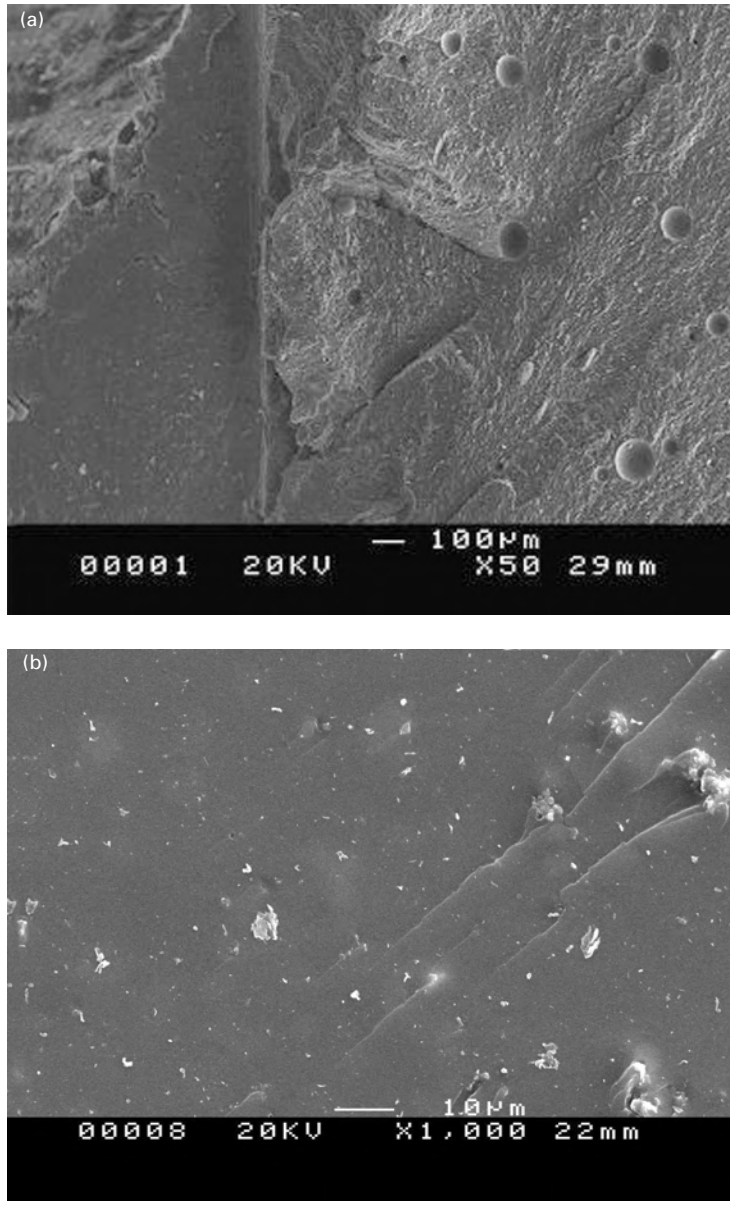

6.24 (a) SEM analysis of the fracture line on the transverse section of a nanostructured composite material after dynamic testing.[50] (b) Cross-section SEM micrograph of polymeric nanostructured thin film.[50]

These data are obtained by EXD, as illustrated by Fig. 6.27, in which it is possible to evaluate the catalysts used and the relative percentage (in this case for nano-powders containing carbon nanotubes and produced by laser

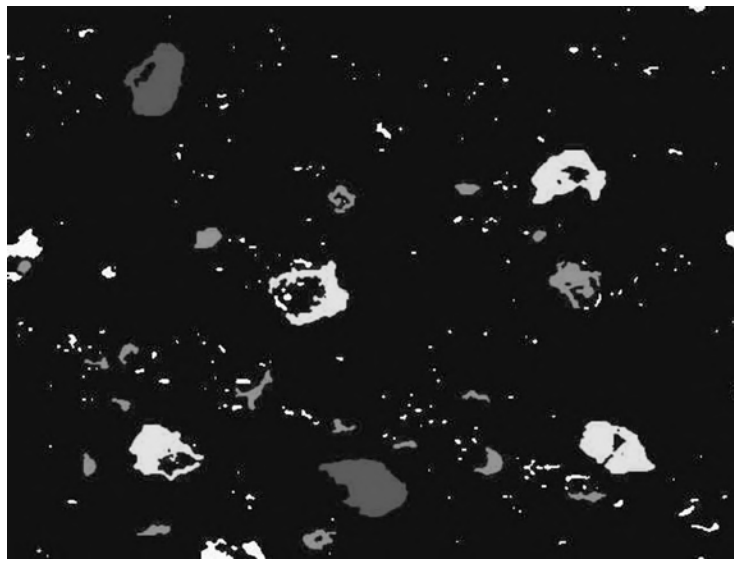

6.25 SEM showing statistical analysis of micro-carbon particles. The software is integrated in the SEM, and through the use of different colors, determines the dimensional ranges of the particles.[64]

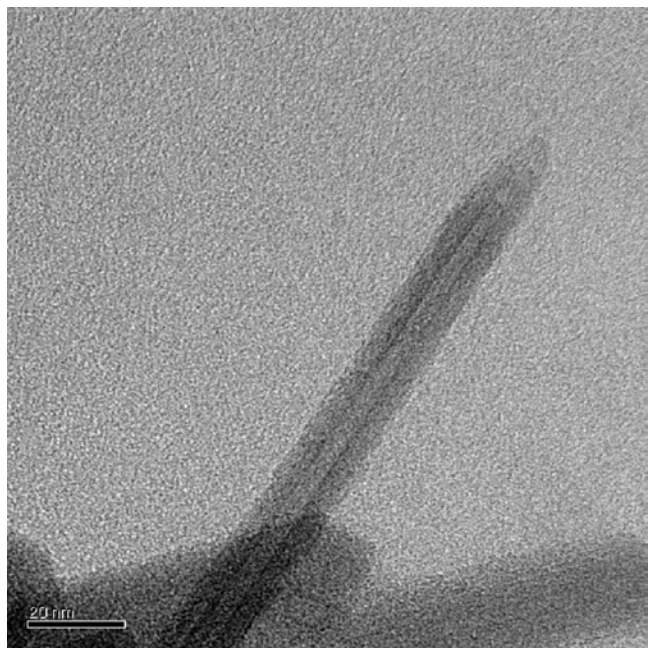

6.26 High-resolution TEM micrograph of a multiwall carbon nanotube synthesized by TCVD.[64]

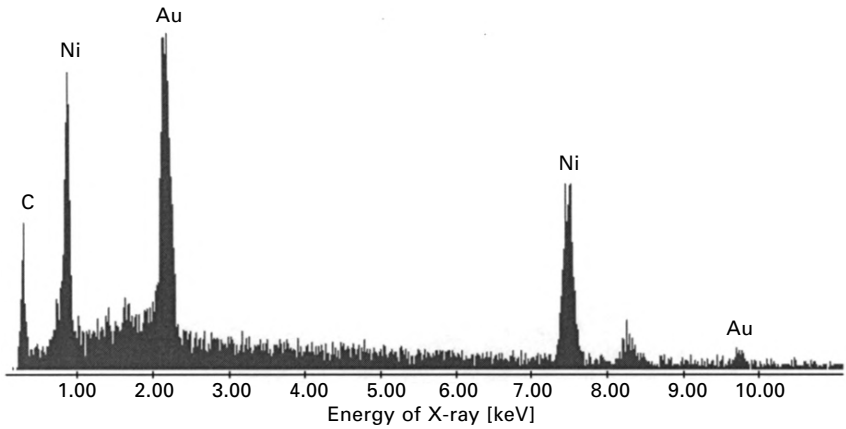

6.27 A typical EDX spectrum used to determine the chemical composition of the nanomaterials produced and purified using different methodologies.[64]

ablation). EDX systems are integrated both in SEM and TEM microscopes, but as described in many protocols reported in the literature, the EDX realized by SEM is more accurate and reliable than that performed by TEM, in which the minor dimension of the analyzed zone can provide unreliable results (with reference to the effective chemical composition of samples, principally due to the interaction between the holders and the measured region).

6.4.6 Atomic Force Microscopy (AFM)

With atomic force microscopy it is possible to realize a 3D nanoscale topography of nanostructures, and define 'nanowrinkledness' profiles. The principal parameters (e.g. Young's modulus) and properties (e.g. *V–I* characteristic) of carbon nanotubes have been determined by the tip of the AFM cantilever. Figure 6.28 illustrates an example of carbon nanotubes deposited on a Si substrate and analysed by AFM. The lines marked as red and green show nanometric sample profiles. The relative statistical characterization is reported in the table.

6.4.7 Raman spectroscopy

Raman spectroscopy is used to corroborate SEM and TEM examinations. All carbon allotropic species (fullerene, graphite, carbon nanotubes and diamonds) are Raman active. All carbon forms contribute to the Raman spectra in the range of 1000–1700 cm^{-1} with two characteristic peaks at 1300 cm^{-1} (D-band) and 1600 cm^{-1} (G-band). The position, width and relative

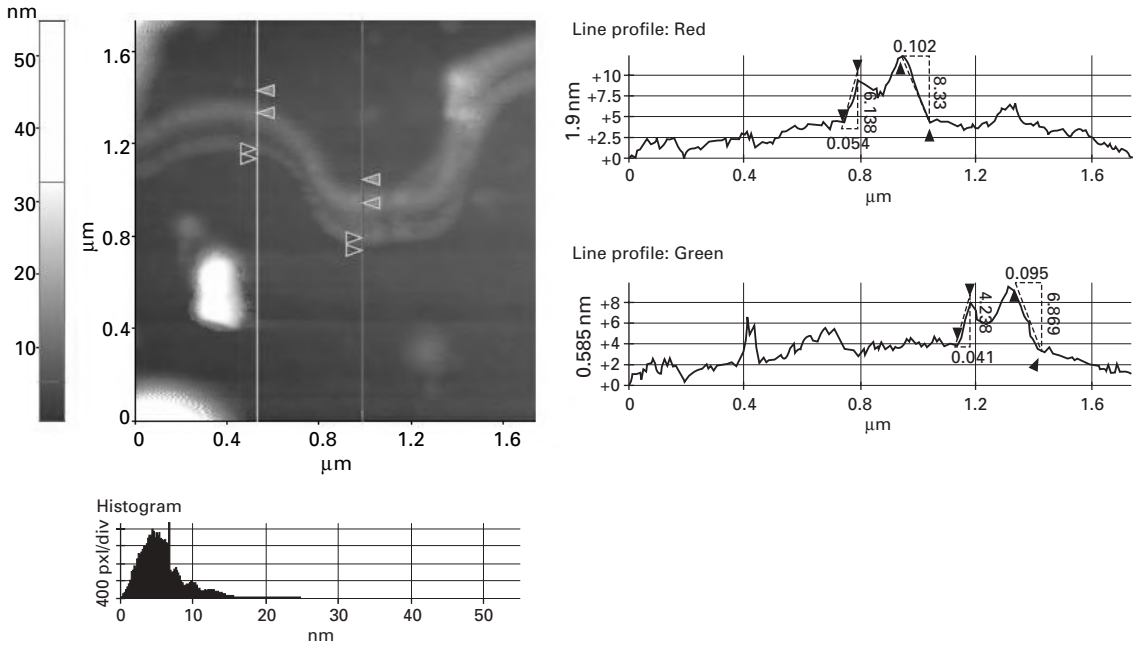

Statistics

Line	Min(nm)	Max(nm)	Mid(nm)	Mean(nm)	Rpv(nm)	Rq(nm)	Ra(nm)	Rz(nm)	Rsk(pm)	Rku(pm)
Red	1.900	14.322	8.111	5.722	12.422	2.623	1.901	4.923	−192.199	657.531
Green	0.585	10.522	5.553	4.058	9.938	1.978	1.490	3.225	−160.973	605.737

6.28 AFM analysis of carbon nanotubes. The graphics and table report the nanotopography analysis useful to characterize nanostructures. In addition, AFM microscopy is used to perform mechanical and electrical characterization of carbon nanotubes.[64]

intensity of peaks vary with carbon allotropes and thus can be used to evaluate the typologies of the 'nano-elements' analyzed. In particular:

- G-Band (~1590 cm^{-1}) is assigned to the tangential radial mode of the graphite. The Breit–Wigner–Fano (BWF) line shape in this band indicates the metallic catalysts in the carbon nanotubes;
- D-Band (~1370 cm^{-1}) is associated with the Raman mode of the amorphous carbon – the G/D ratio provides the purity level of the analyzed carbon nanotubes;
- RBM (radial breathing mode at ~130–300 cm^{-1}) represents, in the low-frequency region of the Raman spectra, the radial breathing mode of carbon nanotubes. The peak position of the RBM ($\omega\,cm^{-1}$) is related to the single-wall carbon nanotube diameter (d) by the following relation:

$$d = \frac{248}{\omega} \qquad [6.9]$$

in the range of 0.8–1.5 nm.

Raman spectroscopy is very useful for a correct carbon nanotube characterization, when SEM and TEM analyses do not provide univocal results. Figure 6.29 shows an example of the carbon nanotube Raman analysis.

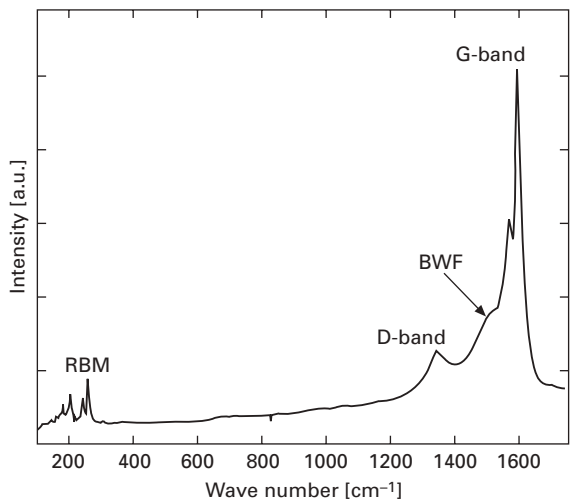

6.29 Raman spectroscopy of nano-powders containing carbon nanotubes. For each band it is possible to associate a specific nanomaterial property.[26]

6.5 Purification techniques[40–49]

After a synthesis process, the produced nanostructures contain some residuals. In particular:

- *graphite* = base materials not transformed in nanostructures (e.g. carbon nanotubes);
- *metallic micro- and nanoparticles* = employed as catalysts to improve the chemical kinetics of the synthesis process and then increasing the quantities of the produced nanostructures;
- *fullerene* = besides carbon nanotubes, the produced deposit can contain other nanostructure typologies (e.g. nanowhiskers, 'buckyballs', buckyonions, etc).

Using different synthesis methods, the quantities of the unwanted residuals can vary. Using laser ablation and CVD facilities the purification level of produced nanomaterials is typically high. Arc discharge, if it is not optimized, may be characterized by a significant presence of residuals, but, as mentioned with specific control of the process parameters this method can provide high quantities of nanomaterials with a significant purification level.

The availability of carbon nanotubes, or in general of nanostructures, of high purification level enables the optimization of the exceptional theoretical properties of these innovative 'nano-elements'. In fact, when developing a nanotechnology system, the effective properties of nanostructures will be inferior to the theoretical predicted values. This depends, principally, on the insufficient purification level of nanostructures, giving a 'nanosystem' that embraces less effective properties than those predicted theoretically. It is important to underline the economic aspect. The high cost of a poorly optimized nanotechnology system (or apparatus) is not justified in respect to a traditional apparatus that provides the requested performance with minor costs. Realistic large-scale use of nanotechnologies will depend, strongly, on a real economic cost reduction with respect to the actual competitive economic level characteristic of nano prototypes and demonstrators.

With devoted purification methodologies it is possible to obtain nanostructures with high purification levels (>80% with respect to the post-synthesis materials employed). The principal purification techniques are:

- sonication;
- chemical etching;
- selective oxidation;
- electrophoresis.

Each method is characteristic of a different synthesis process.

6.5.1 Sonication

Sonication is employed in the sample preparation procedures for microscopy characterization (SEM, TEX, EDX, etc.). It is useful to separate nanostructures from residuals using the following procedures:

- mechanical removal of the nano-powders from the synthesis deposit (e.g. in the case of the arc discharge from the cathode electrode surface);
- dispersion of the removed materials in ethylic alcohol;
- sonication of the liquid solution;
- drying of the above solution and SEM analysis of the just-treated nanomaterials.

By this method it is possible to:

- separate nano-elements from the residual;
- open the edges of carbon nanotubes, removing the caps (this is a typical functionalization, useful for preparing nanotubes for their integration in composite materials or in electronic devices. In fact, the external caps are substituted by other chemical functional groups devoted to the chemical and physical interactions between the nanostructures and the system in which they are dispersed);
- cut the nanostructures, etc.

The principal parameters of this method are time and ultrasound frequency. During the SEM and TEM sample preparations, the materials are sonicated for 3–5 min. In the case of purification (removing of the residual and/or of the cap ends), the time increases. This is a critical aspect. In fact, as shown by Fig. 6.30, after an ultrasound treatment of over 60 min, the carbon nanotube morphologies are very degraded (Fig. 6.30b), with respect to the pre-treatment conditions (Fig. 6.30a). Decreasing the time (Fig. 6.31) reduces post-processing carbon nanotube morphology degradation.

6.5.2 Chemical etching

With chemical etching, using a specific acid solution, it is possible to reduce residuals as a result of the different chemical reactivity of the nanostructures, amorphous particles and catalysts. An example is oxidation with potassium permanganate ($KMnO_4$) in an acidic solution (sulfuric acid H_2SO_4). The chemical reaction useful to remove the undesired residual containing carbon nanotubes proceeds as follows:

$$3C + 4KMnO_4 + 4H^+ \rightarrow 4MnO_2 + 3CO_2 + 4K^+ + 2H_2O$$

After reaction, the mixture is washed in water and dried at ~150 °C for 12 h. Figure 6.32a shows carbon nanotube morphologies before (a) and after (b) chemical treatment.

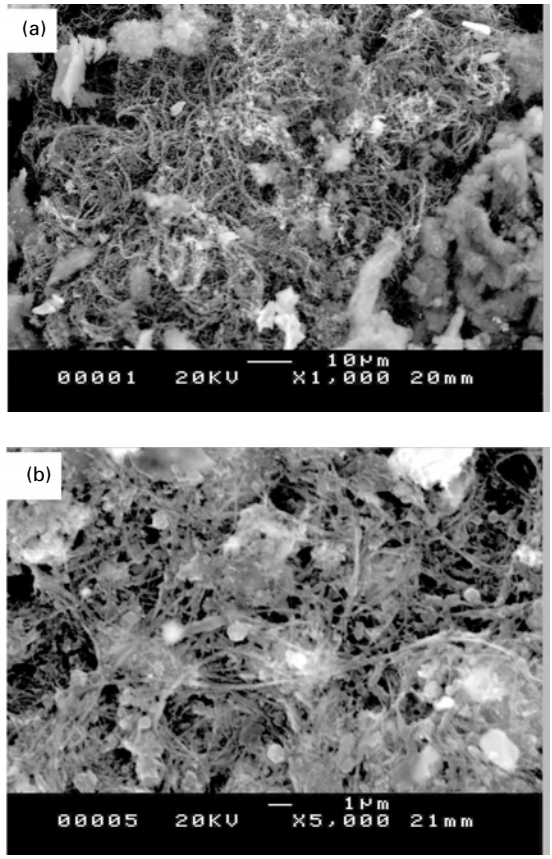

6.30 (a) SEM micrograph of carbon nanotube deposition before the ultrasound purification treatment.[54] (b) SEM micrograph of the same deposit after the treatment. It is not possible to observe good results due to an evident degradation of the carbon nanotube morphology.[54]

Naturally, it is possible to use a different chemical reaction process depending on the specific nanomaterials employed. The chemical reaction with potassium permanganate, for example, is employed for carbon nanotubes produced by laser ablation rather than for those obtained by arc discharge, owing to the different chemical reactivity caused by the different morphologies.

6.5.3 Selective oxidation

Selective oxidation represents the third methodology exploitable to purify nanomaterials and in particular carbon nanotubes. It consists of a selective chemical reaction among carbon nanotubes and residual elements (graphite,

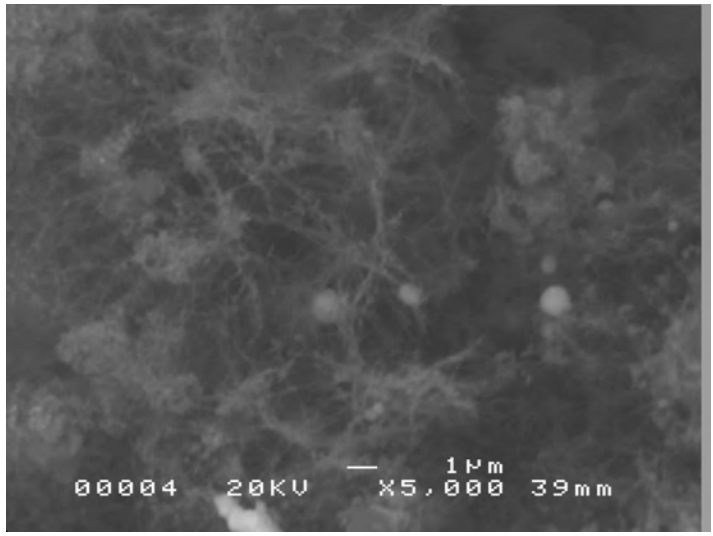

6.31 Reducing the ultrasound treatment time makes it possible to obtain an improvement in the carbon nanotube morphology, as shown by SEM.[54]

amorphous structures, catalysts, etc.) in the presence of an oxidating hot environment. In theory, nanostructures (carbon nanotubes or, more generally, fullerenes) possess a chemical activity less than that of other elements (e.g. amorphous carbon). Using DTA (Differential Thermal Analysis) and TGA (Thermogrametric Analysis), under particular operative conditions, it is possible to obtain a deposit containing carbon nanotubes of high purification.

Figure 6.33 shows a typical DTA–TGA profile employed to purify carbon nanotubes. The line marked 'Temp' indicates the temperature profile characterized by two steps:

- heating phase;
- static thermal operative condition (the optimized temperature value is obtained from repeated testing, useful for determining the condition at which the highest purification level is obtained).

Both phases are carried out in an oxidative environment. Usually, the gases employed are nitrogen (N_2) and oxygen (O_2) with percentages defined by the oxidation 'intensity' required (e.g. 90% N_2 and 10% O_2). The aim is to obtain powders containing the largest quantity of carbon nanotubes, thus minimizing residuals.

The 'TG' line in Fig. 6.33 indicates the mass (m) loss percentage ($\Delta m/\Delta t$). This curve indicates that, during the process, the materials are oxidized. It is necessary to evaluate whether these consist only of residuals or also of

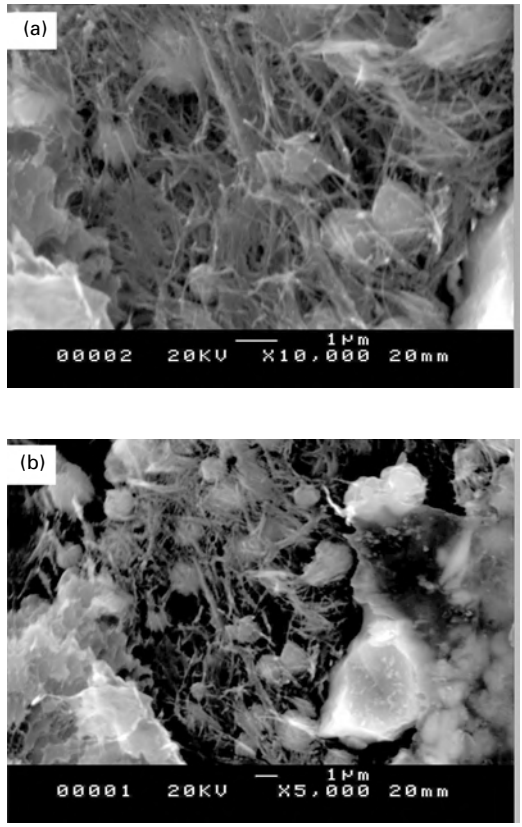

6.32 (a) SEM micrograph of carbon nanotubes before the purification by oxidation with potassium permanganate ($KMnO_4$) in acid solution.[56] (b) Carbon nanotube morphology after the oxidation treatment.[56]

carbon nanotubes. The second hypothesis is more realistic. In fact, by this purification methodology, the real target is to find two simultaneous conditions: the maximum residuals oxidation and minimum carbon nanotube 'destruction'. It is fundamental to observe that all characterizations (SEM, TEM, etc.) and purification methods can modify, in some cases strongly, the morphology and the properties of nanostructures.

The 'DTA' curre in Fig. 6.33 represents the DTA analysis, which indicates the carbon nanotubes mass reduction with respect to an inert mass (e.g. alumina Al_2O_3) used as reference. Figure 6.34 shows a deposit, containing carbon nanotubes, before (a) and after (b) selective oxidation experiments. The reduction of residuals with a deposit prevalently consisting of bundles of carbon nanotubes is shown.

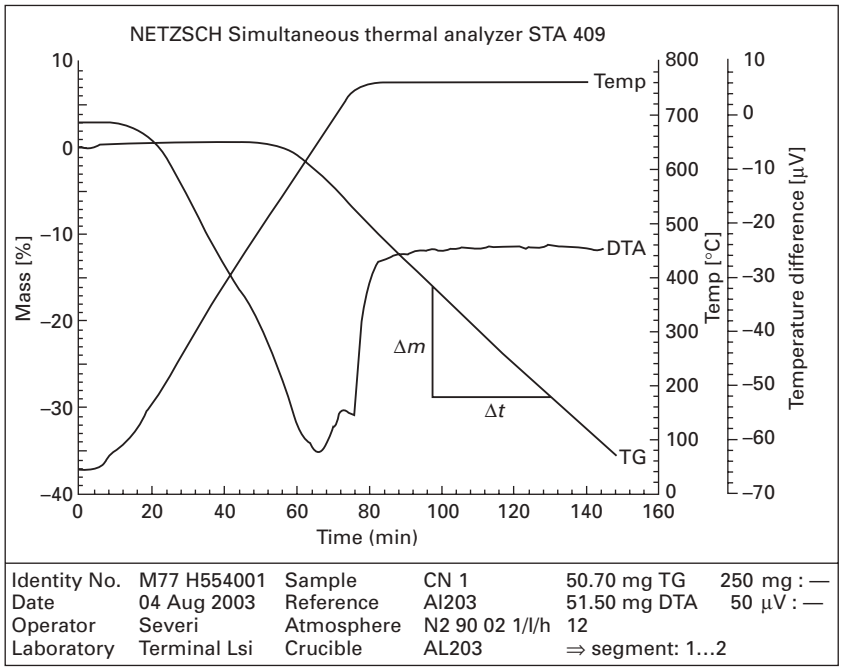

6.33 Typical DTA–TG profile used in the purification of carbon nanotubes using the selective oxidation method.[52]

6.5.4 Electrophoresis

Good carbon nanotube alignment and purification levels are obtainable with electrophoresis. The electrophoresis (DC or AC) technique consists of dispersing nanomaterials (carbon nanotubes and residuals) in isopropyl alcohol dropped onto a coplanar metallic electrode (e.g. Al) with a gap of glass materials. An AC electric field is applied with a specific frequency at room temperature The results consist of well-aligned purified carbon nanotubes. However, carbon particles, contained as impurities, become harder to move (on the electrode surfaces) with increasing frequency, and the degree of nanotube orientation is higher when the frequency is higher and nanotubes are longer. Also in this case parameter optimization is required to obtain carbon nanotubes that are usable in advanced nanotechnology systems.

6.6 The use of carbon nanotubes in aerospace engineering[50–66, 92, 93]

The properties of nanomaterials (mechanical, electrical, thermal, etc.), and in particular those of carbon nanotubes, are considered as key factors for future improvement of technical characteristics of many engineering macro-

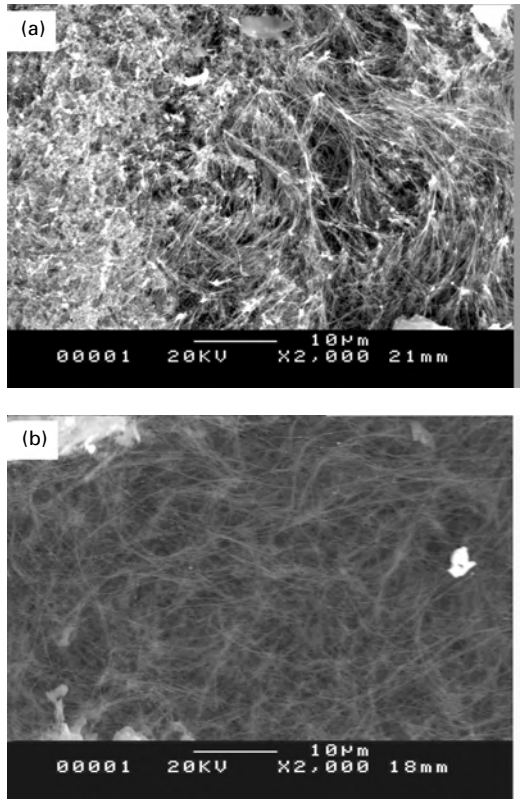

6.34 (a) SEM micrograph of carbon nanotubes before selective oxidation in nitrogen and oxygen.[53] (b) SEM micrographs of the same deposit after the selective oxidation. A significant purification level of the nanomaterials has been obtained.[53]

and nanosystems. The synthesis, purification and characterization of nanomaterials are primary requirements for their realistic use in many engineering sectors. Characterization and functionalization are required steps to prepare nanomaterials for the next phase of the composite manufacturing process or other nanotechnology systems and devices.

Control of the synthesis parameters (voltage, current, laser power, raw materials typology, catalysts used, gas pressure, etc.) is the major hurdlle to obtaining the following requirements:

- producing nanomaterials in high quantity;
- obtaining nanomaterials of high purity and degree of alignment;
- controlling the typology of nanomaterials produced and the relative morphology.

The purified materials (e.g. carbon nanotubes with high or lower degree of

alignment) must be functionalized. This means preparing (for example, with a specific chemical treatment) carbon nanotubes for integration in other systems (a matrix for the composite applications, into a MEMS/NEMS, into a field emission system, sensors, etc). This is a critical phase: in fact, with non-optimized functionalization it is not possible to utilize the properties of carbon nanotubes. To date, the integration of carbon nanotubes in a polymeric matrix with poor chemical functionalization gives poor transmission loads between the matrix and nanomaterials. In addition, the integration of nanomaterials in the matrix (polymeric, metallic and ceramic) is an important step in the realization of innovative nanostructured materials (carbon nanotubes reinforced).

Possible fields of application of these innovative advanced materials are represented by the following aerospace applications:

- nanocomposite materials for structural applications;
- special coatings;
- frequency selective surfaces (FSS);
- thermal barrier for multilayer composite materials (unmanned space vehicles);
- thermal management;
- health monitoring;
- MEMS/NEMS;
- nanosensors and nanodevices.

This new generation of materials has real and interesting applications in aerospace technologies, and the typical research activities are:

- theoretical study of the nanostructured material (e.g. carbon nanotubes reinforced);
- study of nanomaterial synthesis, characterization (optical, SEM, TEM, X-ray and chemical) and its relative functionalization;
- manufacturing process definition;
- sample manufacturing;
- the characterization of materials for specific application (nanocomposite polymeric materials for structural applications, special coatings, FSS, thermal barrier for multilayer composite materials, thermal management).

The properties of these new advanced materials will be calculated with specific tests (considering the probability of the presence of uncertainty within results, a large number of tests will be performed: minimum 10 specimens for each test).

Nanocomposite materials with revolutionary new capabilities constitute an essential element in the design of advanced systems. In particular, carbon nanotube composite materials were identified as those with the highest expectation in terms of performance benefit for many applications and in

particular in the aerospace sector. The general field of nanoscience and technology offers potential as the next great technological revolution. In the field of materials science, we may see a paradigm shift away from the traditional materials role of developing metals, polymers, ceramics and composites to a revolutionary role of developing nanostructured, functionalized, self-assembling materials. Looking to the future, the theoretical potential of these revolutionary new materials will enable technological developments that are barely imaginable today.

Material systems based on carbon nanotubes are a particularly attractive new class of materials. On the basis of computer simulations and limited experimental data, some specific forms of carbon nanotubes appear to possess extraordinary mechanical, thermal and electrical properties. If the properties of carbon nanotubes observed at the molecular level can be translated into useful macro-scale materials, the potential benefits to the aerospace industry include applications to vehicle structures, propulsion systems, thermal management, energy storage, electronic and computing, sensors and devices, and biological and medical applications.

The computer simulation results and limited experimental studies have shown that small diameter, single-wall carbon nanotubes may possess elastic modulus in excess of 1 TPa, and strengths approaching 200 GPa. For example, if small diameter, single-wall tubes can be produced in large quantities, and embedded into a supporting polymeric matrix to form structural materials, the resulting structures could be considerably lighter and stronger than current aluminum alloys and carbon fiber reinforced polymer composites used in conventional aerospace structures.

The mechanical properties of carbon nanotubes give opportunities to develop new advanced materials. It is possible to use different kinds of matrix such as:

- metallic;
- ceramic;
- polymeric.

The composite manufacture requires the following steps:

- selection of materials (matrix, curing agent, nanometric particles);
- studying the sample production methodologies;
- obtaining a uniform distribution of the nanometric particles (with carbon nanotubes of opportune percentage) in the matrix;
- achieving mechanical testing (dynamic and static);
- performing morphological testing;
- studying the mechanical fracture of the composite;
- improving the characteristics of the composite;
- applying the advanced composites in the aerospace systems;

- performing theoretical and numerical analysis of the composite behavior.

With polymeric, metallic and ceramic matrices, it is possible to develop new applications in aerospace engineering:

- lighter structures;
- thermal barriers;
- thermal cooling systems;
- pins;
- special nanostructured coatings, etc.

Sample manufacture is necessary to evaluate the properties of these new materials. In particular:

- studying the theoretical and numerical models;
- synthesizing carbon nanotubes with high quality (enough to produce a sufficient number of samples), high purification and degree of alignment with a perfect control of the typology of nanomaterials synthesized. Price is important in project development;
- performing the characterization and functionalization of carbon nanotubes for their successful integration into a nanosystem/device;
- determining the sample's manufacture procedures and the correlated methodologies of analysis;
- acquiring all the capabilities essential to develop prototypes.

Considering the possible aerospace applications of nanotechnology, the International Space Agencies (e.g. NASA, ESA) have identified the following long-term goals:

- providing safe and affordable orbital transfer and interplanetary transportation capabilities to enable scientific research;
- human and robotic exploration;
- the commercial development of space;
- cost reduction and high reliability.

Numerous scientific and engineering breakthroughs will be required to develop the technology needed to achieve these targets. Critical technologies include advanced vehicle primary and secondary structure, radiation protection, propulsion and power systems, fuel storage, electronics and devices, sensors and science instruments, and medical diagnostics and treatment. Advanced materials with revolutionary new capabilities are an essential element of each of these technologies. Based on a survey of emerging materials with applications to aerospace systems (e.g. vehicle structures and propulsion systems), nanostructured materials have been identified as those with the highest expectation in terms of performance benefit for many applications.

The principal aerospace applications of the nanotechnologies are described below.

6.7 Nanostructured composite materials for aerospace applications[50–64, 92–127]

In aerospace applications, the use of nanostructured materials is finalized to a significant improvement of the mechanical properties, Young's modulus, ultimate strength, Poisson coefficient, etc. and reliability. In other sectors (e.g. electronics) the principal requirements are concentrated on the morphology characteristics of employed nanomaterials. In fact, the required quantities are always limited, and concurrent with their availability. Instead, for composites and structures, considering the large size of aerospace systems, the quantity and the relative costs represent a critical step.

For realistic use of nanostructured composite materials it is fundamental to reduce the costs of developing industrial methodologies (synthesis, purification, integration, etc.) to provide the required quantities while respecting the imposed requirements relative to morphology, typology and purification level. The manufacturing of nanostructured composite samples requires the following specific steps:

- definition of the matrix typology: polymeric (thermoplastic or thermo-setting), metallic, ceramic;
- selection of the specific curing agent, curing process and conditions (temperature, pressure, vacuum, etc.);
- determination of the typology necessary to obtain the properties required;
- definition of the manufacturing and test procedures – for traditional materials numerous standard procedures are available, but in the case of nano-technologies, often, the development of specific non-standard procedures is necessary;
- Analysis of results using: mathematical/theoretical and numerical models, electronic microscopy, fracture mechanics and non-destructive testing.

Comparing theoretical and experimental results allows us to understand the realistic behavior of these innovative materials. In particular, considering the cost of these materials, traditional composite materials are more competitive in terms of economic value and properties. This is a critical aspect with reference to the large dimensions of aerospace components and structures.

During sample manufacturing processes, particular attention is required in the following steps:

- *Matrix de-gassing period*, this is needed to reduce the micro-void embedded in the composite. This represents an important condition not only in the composite sector, but in nanotechnology application areas.
- *Mixing procedure*. During this phase it is essential to obtain uniform distribution of the nanomaterials in the matrix, without void and avoiding random chemical concentrations.

- *Use of the correct curing agent quantities*. In fact, including nanoparticles in the matrix means the ratio of the matrix/curing agent concentrations can vary.
- *Sample characterization and storage*. In this case it is necessary to adapt specific standard procedures of traditional composite materials, to nanostructured composites.

Considering the mechanical aspect, the load transfer properties are the main problem in ensuring high performance of the nanocomposite. This depends strongly on nanostructured functionalization and the interfacial stress between the matrix and embedded nanoparticles. There are three typical load transfer mechanisms:

- micro-mechanical interlock;
- chemical bonding;
- van der Waals interaction forces.

The first mechanism is not influenced by the nanocomposite, since the nanostructured surface typically appears atomically smooth. Some studies demonstrate that the interfacial chemical bonding, between the matrix and nano-elements, could be very high, and the sliding friction between carbon nanotubes and matrix is much greater than that among graphite sheets. With HRTEM analysis of carbon nanotube composite materials, after mechanical testing no fracture has been observed on the carbon nanotube surfaces. Another fundamental result is that if the carbon nanotubes can restore their original undeformed shape when the matrix has been heated, the compressive stress due to the shrinkage (produced by the curing) could be released. It has been observed that using a small percentage of carbon nanotubes embedded in the matrix results in a significant improvement in mechanical properties. This is very interesting carbon nanotube behavior, in respect to problems of bridging, pull out and delaminating (in this case on a nanoscale dimension). In addition, by a random carbon nanotube distribution into a polymeric matrix it is possible to obtain specific electrical properties in order to avoid electrostatic charge, provide sufficient matrix conductivity, etc.

An example of the manufacturing and characterization of a nanostructured composite material is now reported. A complex step is the definition of a procedure aimed at the realization of a homogeneous dispersion of a nanometric powder in epoxy resin. Moreover, adhesion problems related to the interfacial activity of the resin, the powder and the nanotubes must be solved. The materials employed to manufacture the samples were:

- epoxy resin;
- commercial curing agent;
- nanometric graphite powder (granulometria: 20 μm) with a carbon nanotube addition.

The total concentration of the dispersed powder was 10% and 20% in wt. The sample was 10 mm × 10 mm × 120 mm^3 in dimension (Fig. 6.35). The curing process adopted was:

- room temperature for 24 h;
- furnace curing 80 °C for 3 h.

Impact tests were performed, during which the following considerations were relevant:

- the reduction of powder granulometria increased the impact resistance properties;
- good surface finishing improved the mechanical properties.

Figure 6.22 shows the fracture surface appearance of a sample containing 20% of powder. The pre-crack length was 2 mm and the brittle behavior of crack propagation was seen. To understand the fracture-mechanic behavior of the composite, SEM characterization of the fracture surface is necessary. Figure 6.36 shows an SEM image of the sample containing 10% nanocarbon powders. In areas **A** (crack initiation) and **B** (propagation) there is no presence of preferential directions for crack propagation. In contrast, in the sample containing 20% powder, preferential directions of crack propagation are observed (Fig. 6.37 areas **A**, **B**, **C** and **D**). The presence of preferential direction is due to the non-uniformity of powder dispersion in the matrix. A further observation made was that the fracture lines change direction corresponding to cavities (or voids). In Fig. 6.38 two fracture lines (**A** and **B**)

6.35 Nanostructured polymeric composite specimen for mechanical tests.[58]

are diverted by the presence of a void (see points **C** and **D**), and are stopped at point **E**.

The static test shows that using nanometric particles (graphite and carbon nanotubes) the Young's modulus is 12% more than the sample with only resin and curing agent. In theory using only carbon nanotubes (with theoretical Young's modulus: 1 TPa) the mechanical properties of the composite become very interesting. This represents only a preliminary example of nanostructured composite materials. In addition, using the same procedure, it is possible to produce a thin film (Fig. 6.39) that has important applications in electronics, providing devices with specific electromagnetic properties, but also with high mechanical performance. Typically, with traditional technologies, it is very difficult to integrate, in the same material or element, mechanical and electrical properties (or other specific requirements).

Nanostructured composite materials are employed to design and manufacture aerospace structures with high performance, reliability and lightness. An important example is that of the multigrid lattice structures (Fig. 6.40) used for launchers, fuselages and structural elements. Traditional composite technologies can be used to produce such structures, with different shapes and dimensions. The design is carried out using the Vasiliev model, which allows the dimensions of the resistance elements to be determined with respect to the following three conditions:

- minimum mass;

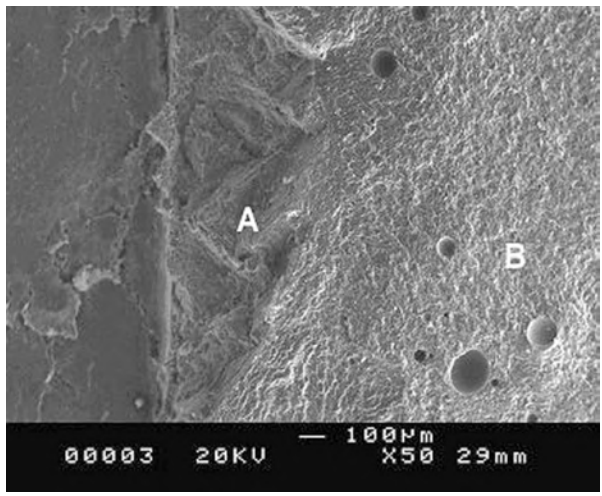

6.36 SEM analysis of the fracture surface of nanostructured composite specimen with 10 wt% carbon nano-powder addition.[55]

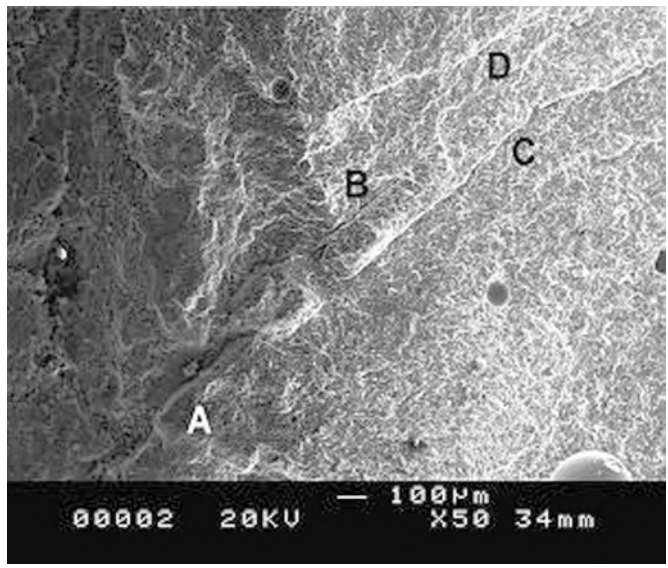

6.37 SEM analysis of fracture surface of nanostructured composite specimen with 20 wt% carbon nano-powder addition, indicating the preferential direction of the fracture line propagation.[55]

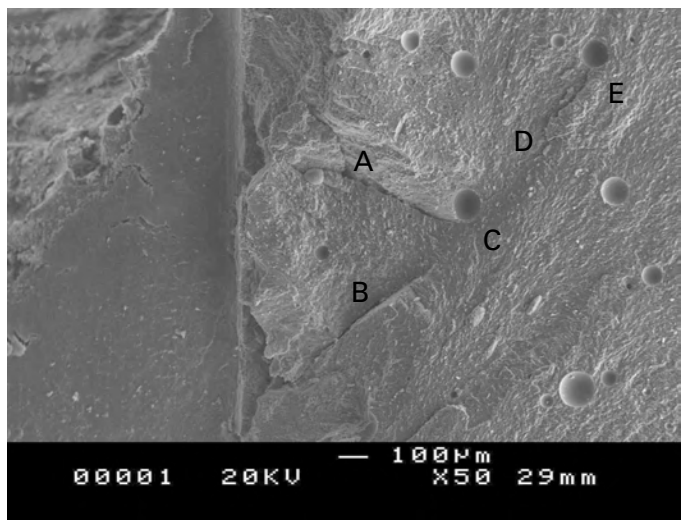

6.38 SEM analysis of fracture surface of nanostructured composite specimen with 20 wt% carbon nano-powders addition, showing the fracture line behavior corresponding to the micro-voids embedded in the matrix.[55]

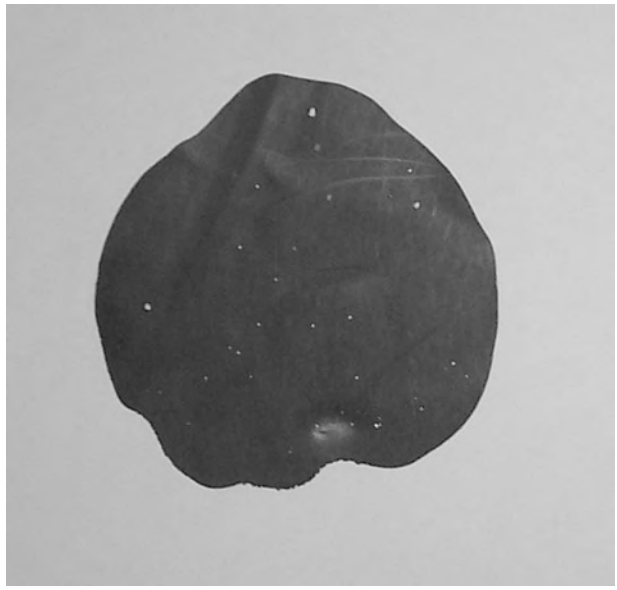

6.39 Nanostructured thin film (polymeric matrix reinforced with carbon nanotubes).[64]

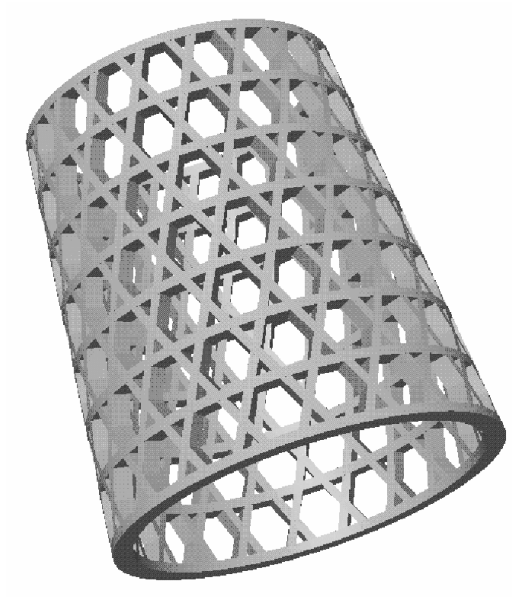

6.40 A 3D CAD (computer-aided design) drawing of a conic anisogrid lattice structure for aerospace application.[59]

- static resistance (the maximum applied load is equal to the ultimate strength of the material employed);
- stability (unitary eigenvalue).

By introducing nanotechnologies, and, in particular, the polymeric composite reinforced with carbon nanotubes, significant improvements in mechanical properties can be obtained. Using the Vasiliev model it is possible to observe that, using a low percentage of carbon nanotubes embedded in a traditional composite, the structures mass reduction, corresponding to the same mechanical behavior, is significant (~20% using only 5 wt% of carbon nanotubes).

The composites are:

- polymeric or metallic matrix reinforced with fibers or particles;
- polymeric or metallic matrix reinforced with nanoparticles or nanostructures;
- hybrid configuration.

Embedding nanoparticles in a matrix changes the manufacturing procedure. In this case, for nanostructured composite materials manufacturing, RTM (Resin Transfer Molding) is the better technology. The following steps for a future industrial and automatic production are used:

- structure design;
- 3D CAD of the positive simulacra of the structure is useful to produce, by rapid prototyping, the positive mold;
- silicone negative mold is produced by using the positive mold. The use of silicone reduces the cost, allows the manufacturing of the complex shape and is reusable. A better dimensional stability is also obtainable.

An example of a flat anisogrid structure is shown in Fig. 6.41.

When using only nanoparticles, RTM technology is the best method. Figure 6.42a illustrates a typical RTM facility used to manufacture a plate of a polymeric composite reinforced with carbon nanoparticles (Fig. 6.42b). The samples have a very smooth surface without macro- and microscopic defects. This structural typology offers, simultaneously, different properties: mechanical, thermal, electrical and magnetic. Using nondestructive testing (NDT) techniques (X-ray and ultrasound systems) it is possible to control the internal morphology. Each specific application aims to obtain an isotropic, continuous and homogeneous material (on macro- and micro-scale): the NDT allows the sample characteristics to be evaluated and then the manufacturing technologies and processes adopted to be validated.

Figure 6.43 shows the NDT tests of the plate reported in Fig. 6.42b. The features of the nanostructured polymeric composite materials have been broadly investigated. Some observations are useful to the metallic and ceramic matrices. Metal matrix nanostructured composites have been little investigated. These materials are generally produced using metallurgical methodologies

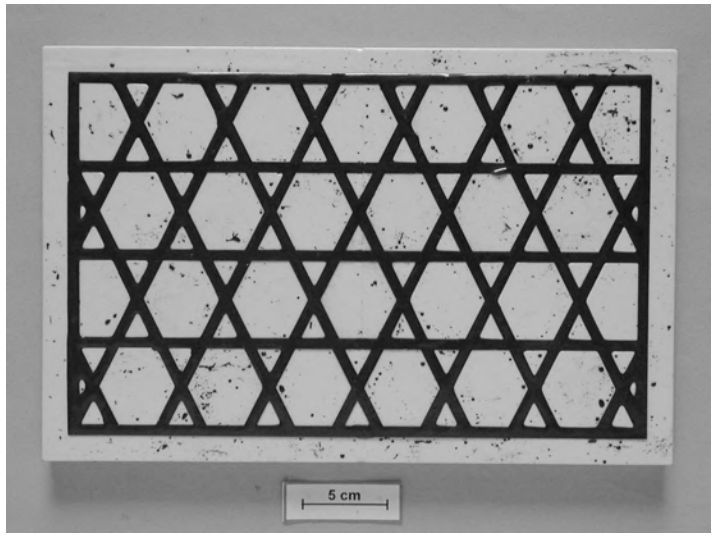

6.41 Flat anisogrid lattice structures produced in a silicone mold with a polymeric composite material reinforced with nanoparticles of graphite and carbon nanotubes.[51]

but the nanoparticles, and in particular carbon nanotubes, are not optimized (quantities, morphologies, etc.). SEM and TEM observations show that the carbon nanotubes embedded in the matrix are not damaged after manufacturing and are well distributed (the alignment degree depends on the manufacturing method adopted). The mechanical test shows that the use of the carbon nanotubes (dispersed for example in a Ti matrix) provide significant improvement of the Young's modulus, hardness, and wear loss and friction coefficient. The nanostructured metallic composites are a significant development of MMC (metal matrix composites).

The ceramic nanoreinforced composites are typically prepared by a mechanical mixing technique using specific precursors and a hot pressing sintering procedure (a sol gel or CVD is also employed). A homogeneous dispersion is observed without no significant damage to the carbon nanotubes embedded in the matrix. The use of carbon nanotubes allows refinement of composite microstructures, a strong reduction of the relative density and an improvement of the toughness and the friction coefficient. In addition, their presence when well-dispersed confers an electrical conductivity to the otherwise insulating ceramic matrix composites. Besides, thermal management using partially stabilized zirconia (PSZ) mixed with carbon nanotubes is important in aerospace applications.

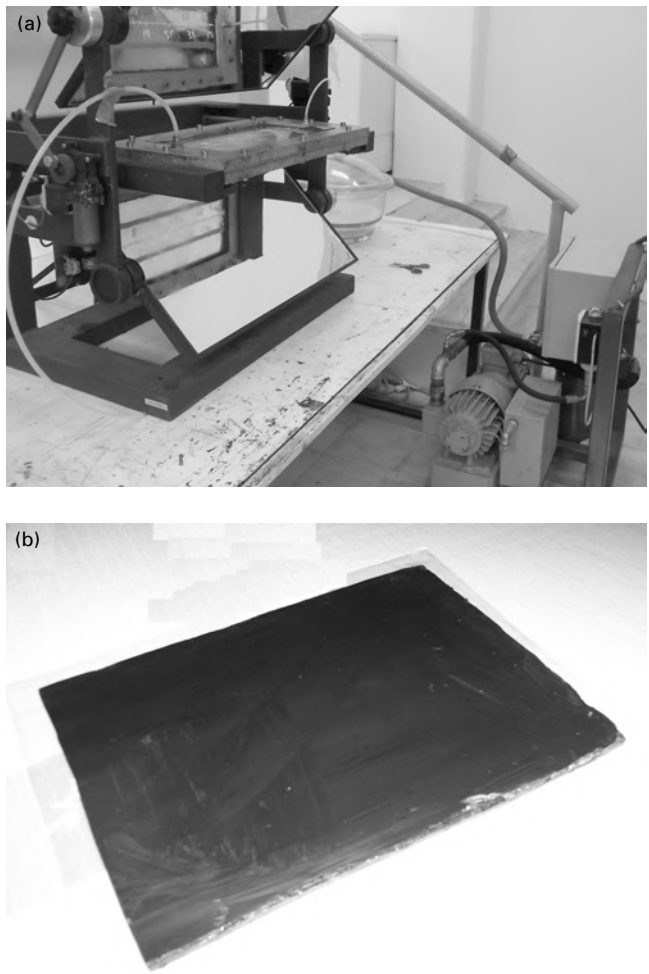

6.42 (a) The RTM facility used to manufacture a plate constituted by nanostructured polymeric composite material.[64] (b) An example of a prototype obtained by RTM.[64]

6.8 Nanostructured solid propellants for rockets[61, 76–79]

Propulsion by means of solid propellant is one of the advanced aerospace and missile fields of research. The remarkable performance, with a technologically more simple system than the liquid propellant jet, put this type of propellant at the heart of many advanced applications. Solid propellant engines find their application in all the 'propelled mission phases' where the reference parameters (Trust Vectoring Control (TVC), time of ignition,

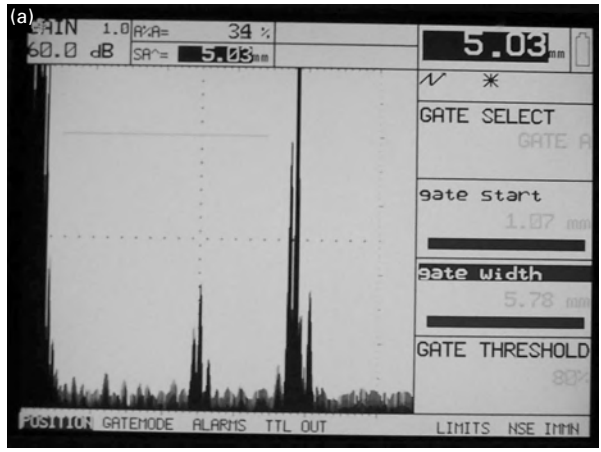

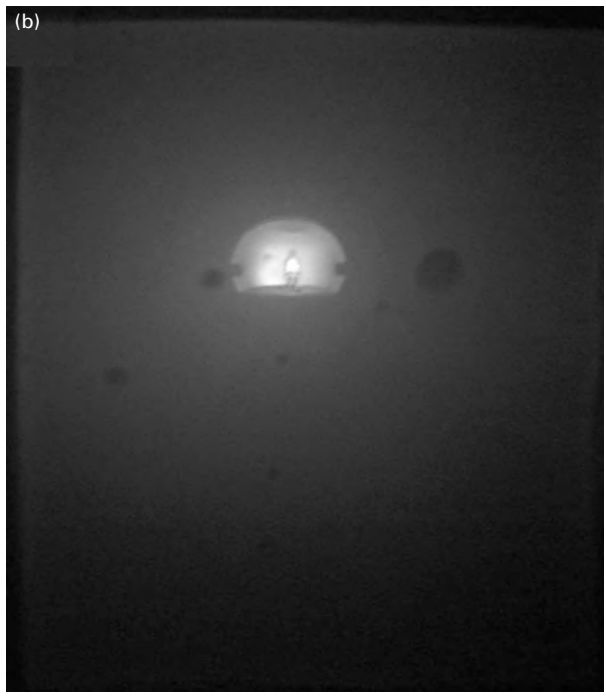

6.43 (a) Ultrasound spectra produced to analyze the morphology of the nanostructured plate produced with the RTM facility (see Fig. 6.42(b)).[64] (b) The analysis of the negative image (obtained from X-ray) of the demonstrator similar to that reported in Fig. 6.42(b). In this case internal defects are observed. This indicates that the RTM process has not been performed correctly.[64]

predefined throw/trajectory and orbital corrections) are defined. Applications such as the orbital corrections of a satellite to avoid ambiguous gravitational perturbations, need liquid propulsion systems that provide a more flexible system. However, such systems are more complex, and have a different intrinsic reliability than a solid propulsion system.

The main reference parameters for the propellant performances are:

- combustion velocity;
- specific impulse;
- stability of the flame front.

The propellant is characterized by an appropriate mixture of a fuel and a comburent (more additives and eventual catalysts).

Apart from the physical effects related to the geometrical/dimensional characterization of the propellant reservoir, all the intrinsic performances of the solid grain depend on the physical /mechanical properties of the fuel–comburent mixture.

The rocket thrust (T) is defined as:

$$T = \dot{m}V_e \qquad [6.10]$$

where: T = thrust
$\dot{m}$ = mass flow
V_e = exhaust gas velocity

and, in particular:

$$\dot{m} = \rho rA \qquad [6.11]$$

where: ρ = propellant density
A = the nozzle exhaust section
r = burning rate

the burning rate (r) is a fundamental parameter and it is defined by the Vielle law:

$$r = \alpha P^n \qquad [6.12]$$

where: α and n = ballistic coefficients
P = combustion chamber pressure.

A solution typically used to increase the performance (r and then T) consists of charging the propellant with metallic micro-particles that are extremely energetic, such as aluminium. During combustion this allows further energy to be supplied that improves the specific impulse.

There are substantial problems associated with this technique such as:

- homogeneous distribution of the powder is necessary in the solid mixture of the grain, in order to avoid localised conglomerates;

- incomplete combustion of the micro-charge, that gives:
  - mechanical degradation of the inner exhaust nozzles,
  - toxicity of the exhausted gas,
  - reduced improvement of the grain performances,
  - thermo-fluid dynamics problems associated with the burned gas, due to the presence of bi-phase flow,
  - in the case of missiles, there is greater intercept opportunity, for the detection of a hot trace due to unburnt solid particulate;
- environmental compatibility of the exhausted gases;
- difficulties in reducing the micro-charge dimensions (to increase the thermal exchange surface) on a nanometric scale;
- energetic limits of the charge itself;
- high costs.

The utilization of different techniques for powder production (Electrical Explosion Wire (EEW), plasma condensation, mechanical shattering) and their coating may lead to significant variations in grain performance. In addition, formulations including not only one, but two, oxides, ammonium perclorate and ammonium nitrate, criteria are under study, with the aim of reducing costs without heavy impact on the performance. Grain characterization, is necessary for any chemical formulation through the following:

- Determination of the combustion velocity as a function of the pressure, the measurement of the ignition delay, the study of the combustion of the propellant under laser radiation (for a stability analysis), the analysis of the combustion residuals. For applications where the engine will be subject to high acceleration, it will be necessary to analyze the eventual effects of the acceleration towards the combustion velocity.
- Dimensional, morphological and chemical characterization of the ingredients, with particular attention to the metallic nano-powders and the combustion residuals, by means of electron microscopy (SEM, TEM, HRTEM), XPS (X-ray photoelectron spectroscopy) and XRD (X-ray diffraction).
- Study of the powder agglomeration at the combustion surface level, by means of high-speed cameras.
- Theoretical–numerical study of the simulation of the combustion processes, needed for a basic understanding of the complex phenomena involved, the development of parametric studies and to address experimental research activities.

With the nanotechnology, using nanoparticles or nanostructures, it is possible to obtain further improvement of the rocket performance. In particular, the combustion of nano-sized elements gives a significant increase of the thermal spatial gradient in the combustion chamber, with a consequent increase of

the burning rate (r) and then of the thrust (T). The possible use of carbon nanotubes has entered the frame of innovative formulation studies, in addition to other materials with nanometric granulometria. Thanks to their covalent unidirectional configuration, the carbon nanotubes may:

- improve the mechanical characteristics of the propellant;
- improve the thermal energy released during the combustion, so improving the specific impulse and the relevant exhaust;
- reduce the environmental pollution problems;
- reduce the mass fraction of the unburnt residuals.

The use of simple graphite with nanometric granulometria, whose plane crystal characterization sp^2 is the same as that of the carbon nanotubes, may give the same performances at macroscopic levels, with a significant cost reduction and a remarkable simplification of the technological processes. To increase rocket performance (burning rate, thrust, combustion stability, etc.) it is possible to decrease the propellant quantities required, with a consequent improvement of the payloads transportable.

The principal objectives of the research programs in nanotechnology propulsion are:

- to implement the manufacturing technologies of the propellants with nanometric metallic particles;
- to test bi-oxidizing solutions (ammonium perclorate and nitrate);
- to study (theoretically and experimentally) carbon-based (graphite, carbon nanotubes) nanometric charges (nanostructured and non-nanostructured);
- to characterize the new solid propellant and evaluate its performances;
- to foresee the eventual use of a metallic charge, associated to a carbon base.

Experimental activity is relevant for the manufacturing of solid propellant that, typically, includes the use of the following base materials:

- commercial aluminum powder charge (micrometric granulometria, typically 30–50 μm);
- nanometric aluminum powder charge (granulometria less than 1 μm);
- micrometric graphite powder charge (<20 μm);
- micrometric graphite powder charge (<20 μm) with the addition of aluminum;
- carbon nanotubes charge;
- carbon nanotubes charge and the addition of aluminum;
- aluminum nitrure nanotubes charge (with and without nanometric aluminum and carbon-based powders).

Figure 6.44 shows a combustion example of the nanostructured solid propellant sample.

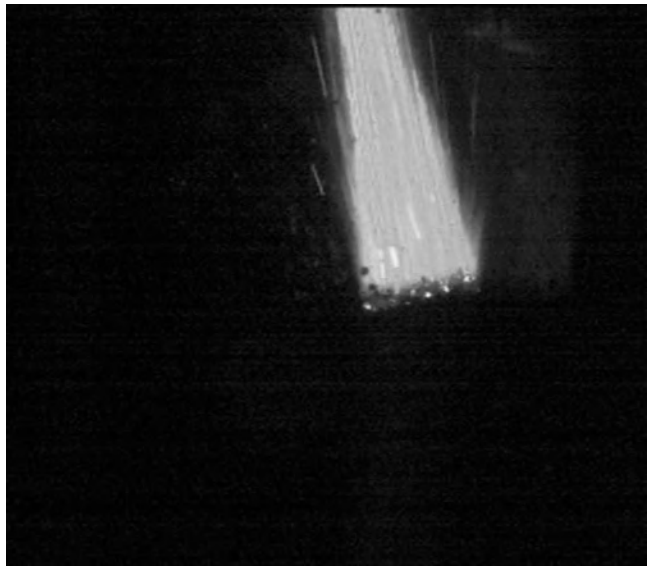

6.44 Experimental combustion test of a nanostructured solid propellant sample for rockets employed in aerospace systems.[61]

The new formulation propellants must be compared with those actually in use. The final goal is to lead to new, innovative formulations to reach the following targets:

- the development of lighter propulsion systems, with improved performances;
- an increased payload mass;
- a cost reduction;
- an environmental pollution reduction;
- improved thermo-mechanical characteristics.

6.9 Frequency selective surfaces for aerospace applications[64, 128–137]

Frequency selective surfaces (FSS) are an important application in many engineering sectors. In particular, it is useful for radomes, filters and radar communications. Traditional FSSs are constituted by two possible configurations: periodically perforated metallic screens, or arrays of metallic patches printed on dielectric substrates. Aeronautic, military and naval applications are the typical technological fields involved in the FSS developments.

The requirements of an FSS are:

- pass-band filter behavior;
- to hide the surface from the external observer.

With a specific design of the traditional FSS, as a result of the Floquet theorem, it is possible to select a unique frequency value for the filter. By solving Maxwell equations, it is possible to determine the theoretical electromagnetic FSS behavior. However, considering the complexity of the phenomena involved, it is only possible to perform a realistic characterization of the FSS with an experimental test.

New kinds of FSS have been introduced that incorporate nanotechnology. In fact, using particular matrices (thermoplastic and thermosetting polymeric resins, silicones, etc.) with homogeneously dispersed, nanoparticles (structured and non-structured) it is possible to produce a material necessary for the electromagnetic, structural and mechanical requirements. In contrast, traditional FSSs provide only electromagnetic properties.

For a nanostructured FSS a particular technological manufacturing process is required to obtain the following micro- and macro-properties: homogeneity, continuity and isotropic characterization (necessary to the imposed requirements). Moreover, these innovative FSSs provide a continuous monolithic structure with a significant improvement in the reliability of the systems in which they are integrated. Traditional FSSs are periodic structures with filtering properties, traditionally manufactured either as periodically perforated metallic screens or as arrays of metallic patches printed on dielectric substrates.

A novel approach is proposed, whereby narrowband filtering properties are created from random composite structures based on the physical resonant properties of the constituents and the geometry of micro- and nano-inclusions. In this manner, a bulk continuous material rather than a lattice formation is used to manipulate and shape the electromagnetic propagation. The novel artificial dielectrics constitute conformal FSSs to be applied by means of a uniform coating process to simple planar or complex curvilinear shapes. The approach is guided by a theoretical design for a random mixture with frequency-selective properties, characterized by a concentric geometry for the inclusions. The frequency dispersion of the proposed composite is driven by the use of a Lorentzian resonant dielectric as one of the constituent media.

The novel complex medium is an amorphous ensemble of micro- and nanospheres composed of a lossy core, coated with a highly resonant dielectric layer and embedded in a dielectric host (a polymeric matrix). This is an innovative application of nanotechnologies in the electronic field.
With these innovative nanostructured FSSs, it is necessary to develop appropriate software useful for evaluating the electromagnetic and mechanical behavior.

The nanostructured FSS consists of a dielectric matrix (polymeric or silicone resin) with micro- and nanoparticles embedded into it. For this composite nanostructured material, it is required to have isotropy, homogeneity and continuity properties. In fact, when the nano-FSS works at high frequency,

all possible material defects can significantly modify the electromagnetic behavior of the element. This is the reason why it is necessary to define a specific sample-manufacturing procedure required to obtain samples with the above characteristics.

Another problem is relevant to the choice of materials. First, a matrix with a specific electromagnetic property is required. It is necessary to study different aspects such as the thermal, mechanical, physical and chemical characterization of the matrix. In fact, the design of an innovative nano-FSS is not limited only to the electromagnetic analysis, but also to its integration in a real operative system with specific requirements, relevant to all the operative aspects and conditions. For example, the resistance to flames and salty water are only two conditions of the possible specific required characterizations to certificate the nano-FSS produced. The surface of the sample must be very smooth to guarantee well-defined control of the electromagnetic behavior. The static and dynamic resistance of the materials are important parameters concerning the mechanical properties. Using a polymeric matrix, it is possible to ensure enough mechanical resistance both for specific electromagnetic instruments (advanced devices) and for naval/aeronautics applications (e.g. nano-FSS panel integrated on a boat and aircraft as an electromagnetic shield). It is possible to think also of a flexible nano-FSS to produce devices with very complex geometries. In this case it is necessary to choose a specific matrix (e.g. silicone materials).

A further aspect is relevant to the nanoparticles employed. The morphological characterization gives the opportunity to evaluate the possible use of a specific kind of micro- and/or nanoparticle that has particular properties (electromagnetic, mechanical, chemical, etc). In this case it is possible to use simple particles (non-nanostructured) or particular elements (carbon nanotubes, for example). The manufacturing procedures for the sample preparation can be very different, with significant changes in the relevant behavior of the nano-FSS. For example, embedding carbon nanotubes on the matrix with different alignments and degrees of purification can provide very different behaviors of the FSS. This gives an idea of the technological problems involved in manufacturing a nano-FSS with characteristics defined by the theoretical and numerical models. The manufacturing procedure is much simpler with the use of simple nanoparticles.

Cost and availability of a suitable quantity of nanostructured materials are two fundamental parameters in the development on these innovative elements. The nano-elements embedded in the matrix can provide other properties. For example, carbon nanotubes are studied for the development of structural composites for aerospace applications, thermal management, electrical systems, etc. In this case it is possible to think of advanced materials with manifold properties (mechanical, thermal, chemical, and mainly electromagnetic). The materials typically employed in nano-FSS manufacture are:

- matrix: polymeric and silicones;
- commercial or specific curing agents;
- particles: micro-powder of non-nanostructured graphite, carbon nanotubes and metal oxides.

It is possible to produce two kinds of nanostructured sample: continuous and multilayer. In each case the uniformity of the sample thickness is fundamental to provide a homogeneous electromagnetic behavior in the studied band (for example the X-band).

The preliminary activities in the nano-FSS design are devoted to defining the sample manufacturing procedures, useful for obtaining materials with specific parameters (dimensions, geometry, porosity, roughness, etc.). With these samples (Fig. 6.35) it is possible to perform a static and dynamic mechanical tests that provide important results on the structural behaviour of this material that will be employed for electromagnetic applications. Using SEM, a fracture-section characterization is also possible (Fig. 6.38). This allows the internal morphology of materials and the micromechanics composite behavior to be investigated.

Also in this case by using specific software integrated in the SEM, a statistical analysis of the particle dimension can be performed. It is necessary to identify a region in which numerous micro- and/or nanoparticles are present, and then to define the range dimensions to study. In this case, the software, using different colors, determines particle groups, each with a specific dimension range. Figure 6.25 shows an SEM micrograph of microparticles with different dimensions and shapes. It is interesting to produce nanostructured thin films that can be used in hybrid multilayer composites dedicated to mechanical and FSS applications (Fig. 6.39).

After the preliminary base material characterizations it is possible to produce nanostructured FSS samples. For example, the materials employed are:

- graphite (0%, 50%, 65% in wt with respect to the resin + curing agent);
- epoxy and polyester resin and silicone;
- curing agent.

For each material a specific curing cycle has been adopted, as specified by the material's datasheet and by the curing test previously performed. It is important to note that the curing process of the matrices can vary in significant ways when the particles are embedded in it. Figure 6.45 shows the various methodologies and phases of the sample manufacturing.

To evaluate the selectivity of the developed nanostructured materials it is necessary to measure (in magnitude and phase) the scattering parameters (S_{ij}). An accurate calibration of the instrument is required, so as to eliminate the effects of the various transitions on the performances of the Device Under Test (DUT).

Considering an analyzer experimental facility (Fig. 6.46) with two ports (1 and 2), the magnitude of the scattering parameter S_{21} (that is, the response at port 2 when port 1 is excited), is defined as:

$$S_{21}(\text{dB}) = 101\text{g}_{10}\frac{P_{\text{out}}}{P_{\text{in}}} \qquad [6.13]$$

where: P_{out} = electromagnetic power measured at port 2
P_{in} = electromagnetic power measured at port 1

In particular, P_{in} indicates the power acting on the nanostructured materials (deposited in the waveguide; see Fig. 6.45), and P_{out} the transmitted power through the nanomaterials themselves.
In a simplified way:

if $P_{\text{out}} = P_{\text{in}} \rightarrow \text{dB} = 0$

if $P_{\text{out}} < P_{\text{in}} \rightarrow \text{dB} < 0$ (in this case the material absorbs the electromagnetic power acting on it).

In the study of FSSs, two other important physical parameters are:

- *electrical permittivity* (ε): providing the electrical behavior of the material $= Re(\varepsilon) + j\ Im(\varepsilon) \Rightarrow \varepsilon_c = \varepsilon - j\ (\sigma/\omega)$, with σ = power loss due to Joule effect, $\omega = 2\pi f$ (f = frequency) with $Re(\varepsilon)$ always > 0 (capacitive effect = electric energy absorption); by Poynting Theorem: $Im(\varepsilon) > 0$ (active material); $Im(\varepsilon) < 0$ (electrical power loss).

6.45 Nanostructured FSS samples (before the final mechanical removal of the residual material on the waveguide surfaces) and the relative manufacturing procedures.[64]

6.46 Agilent portable network analyzer (PNA) E8363B – experimental set-up.[64]

- *magnetic permeability* (μ): providing the magnetic behavior of the material = $Re(\mu) + j\ Im(\mu)$ with Re(μ) always > 0 (inductive effect = magnetic energy absorption); by Poynting theorem: $Im(\mu) > 0$ (active material); $Im(\mu) < 0$ (magnetic power loss).

In the case of FSSs, it is necessary to obtain the following general results: $[Im(\varepsilon), Im(\mu)] < 0$ (the specific values will depend on the materials employed). In the case of a 'metamaterial' it may be: $[Re(\varepsilon), Re(\mu)] < 0$.

Figure 6.47 illustrates an example of the S_{21} measure in the X-band. It is possible to evaluate (in dB):

- mean electromagnetic power loss;
- minimum electromagnetic power loss;
- maximum electromagnetic power loss.

In addition, it is possible to observe that the electromagnetic power absorbed by materials (dielectric + graphite) is increased with respect to the host (only dielectric). This indicates that the micro- and nano-inclusions, embedded on the polymeric matrix, allow the transmitted power to be reduced.

With experimental measures, it is possible to observe that by increasing the quantity of carbon nanoparticles embedded in the polymeric matrix, the electromagnetic power absorption increases and P_{out} decreases (with respect to the same value of P_{in}). In addition, analogous results are obtainable measuring the electrical permittivity (ε) and the magnetic permeability (μ). In fact, if the percentage of the micro- and carbon nanoparticles embedded in the polymeric matrix increases, the following results are obtained:

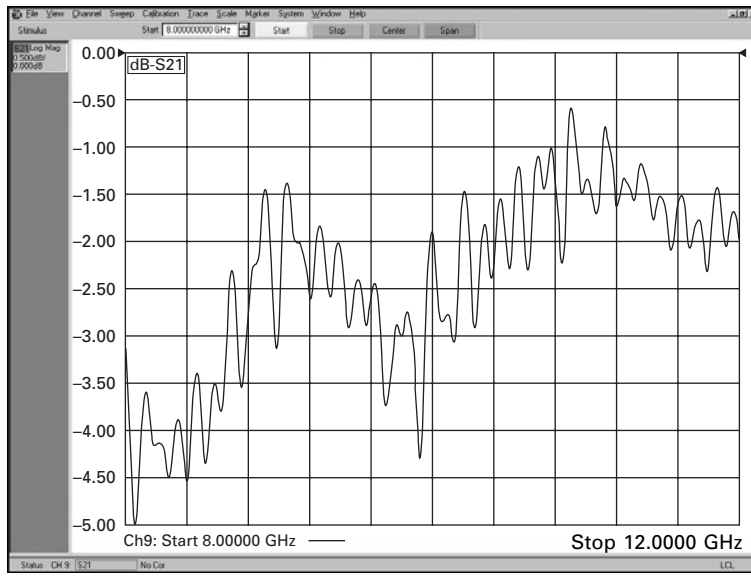

6.47 Frequency response (magnitude in dB) of the sample with nanoparticles of graphite embedded in the matrix.[64]

$$|Im(\varepsilon)| \uparrow \text{ with } Im(\varepsilon) < 0 \text{ and } |Re(\varepsilon)| \uparrow \text{ with } Re(\varepsilon) > 0$$

$$|Im(\mu)| \uparrow \text{ with } Im(\mu) < 0 \text{ and } |Re(\mu)| \uparrow \text{ with } Re(\mu) > 0$$

The use of the silicone materials is indicated due to the possibility of producing flexible FSSs, with the important implication of making FSS elements with a complex shape. Then, the principal characterizations of these innovative materials are:

- to obtain a specific electromagnetic behavior;
- to provide mechanical and thermal properties;
- to select a definite frequency in which $S_{21} \sim 100\%$ and $S_{12} \sim 0\%$ (expressed in terms of the percentage of the external power excitation acting on the FSS surface).

After experimental investigations, it is necessary to analyze, for each sample typology, the selectivity behavior. In particular, for each percentage of the particles embedded in the matrix, it is necessary to determine the specific frequency value at which materials provide the requested selectivity. This is an important goal, with a broad relevance to many scientific sectors and engineering applications.

The principal activities are focused on the technological methods necessary to manufacture the nano-FSS. Particular attention is dedicated to characterization of the base materials (polymeric matrix, curing agent,

nanoparticles) using electron microscopy (SEM, HRTEM and EDX). The degassing phase (used also for the nanostructured composite) is essential to obtain the three following micro- and macro-properties: homogeneity, continuity and isotropic characteristics. Also, the curing phase (temperature, pressure, inert conditions) characterizes the final properties of the produced FSS. Non-destructive testing allows us to verify if the above properties are obtained and then to qualify the technological process employed. The experimental electromagnetic test provides interesting results. In particular, using different quantities of the nanoparticles embedded on the polymeric matrix it is possible to obtain various electromagnetic behaviors. In fact, by increasing the percentage of the particles embedded in the matrix, the sample presents a considerable improvement of the electromagnetic radiation absorbed by the material. For each percentage it is necessary to determine the specific frequency of selectivity.

The future applications of these innovative nanomaterials include the development of multifunctional hybrid nanostructured composite materials able to provide, simultaneously, mechanical, thermal and electromagnetic specific behaviours for aerospace, military, navy and communication applications.

6.10 Other aerospace applications of carbon nanotubes[65, 66, 138]

Nanotechnology can be applied in many other scientific sectors of aerospace engineering.

- *3D NonoTopography*: the good mechanical properties of carbon nanotubes make them an ideal force sensor in scanning probe microscopy with high durability, reliability and capability to reconstruct 3D Images surface with high resolution, resolving the typical limitations of conventional force sensors (typically ceramics)
- *Chemical force microscopy*: nanostructures and in a special way functionalized carbon nanotubes allows selective micrographs to be created based on chemical discrimination (chemical force microscopy). With functionalized nanostructures it is possible to improve the special resolution of the micrographs produced by increasing the chemical reactivity of the samples. The chemical interaction between nanotubes and chemical species present on the observed surface, allows a chemical mapping of the analyzed sample to be performed.
- *Field emission*: carbon nanotubes have been demonstrated to be very efficient field emitters. Using this fundamental property new innovative electronic devices may be developed, including flat panel, computers, X-ray facilities, etc. For example, replacing the traditional glass support of

TV and PC screens with nanostructured polymeric materials would make it possible to produce a flexible screen. In addition, the use of carbon nanotubes gives the possibility of developing devices with high electronic emission stability, mechanical resistance and longer lifetimes.

- *Chemical sensors*: the electrical properties of carbon nanotubes (single wall or multiwall) were recently demonstrated to be very sensitive to chemical composition variations of the surrounding atmosphere at room temperature. This very interesting property would allow an innovative chemical sensor to be designed with high sensibility and capability to detect various chemical substances.
- *Catalyst support*: due to their ability to be tailored to specific needs, carbon nanotubes are candidate supports in heterogeneous catalytic processes. Carbon nanotubes are also employed as catalytic support due to their high surface area, chemical and thermal stability (in a non oxidative environments). Carbon nanofibres, soot and graphite are used in these applications.
- *Adsorption*: significant adsorption and interaction phenomena occur between carbon nanotubes and gases. There are two possible applications for this sector. The first is characterized by the molecular adsorption, which is related to carbon nanotube electrical properties and, then, with the possibility of developing chemical sensors. The second includes gas storage and separation due to the high surface area of carbon nanotubes.
- *Storage*: It is fundamental to develop lightweight and safe hydrogen storage systems in the automotive industry. Due to results obtained with hydrogen storage studies several researchers, using carbon nanotubes, have tried to develop innovative gas storage facilities (oxygen, nitrogen, inert and noble gases, hydrocarbon, etc).
- *Gas separation*: this aspect is a consequence of the above storage application. Due to nanostructure properties, it is possible to control the sorption phenomena with specific conditions (pressure, temperature, nanostructure morphology)
- *Absorbtion*: experimental activities demonstrate that carbon nanotubes are able to absorb toxic gases (e.g. dioxin, fluoride or alcohols). This application is fundamental for military applications (NBC).
- *Biosensors:* attaching molecules to a carbon nanotube surface is a very interesting way to realize nano-biosensors. The use of the internal cavity of carbon nanotubes for drug delivery is another amazing possible application for many sectors (propulsion, health monitoring, medicine, etc.). For example, introducing carbon nanotubes holding specific sensors or chemical elements into the human body, would make it possible to monitor heath. This is a possible application for long-term aerospace missions. Two basic aspects must be investigated: the toxicity and reliability of these systems in respect to traditional medical apparatus.

In each application described above, the functionalization of carbon nanotubes, or of nanostructures in general, represents the fundamental step.

6.11 Conclusions

As described in this chapter nanotechnology offers numerous opportunities for significant improvement in many sectors of the aerospace engineering (structures, composite radar shield, propulsion, etc.). In fact, by introducing nanostructures and nano-elements, it is possible to design devices and apparatus with properties and characteristics that cannot be obtained by traditional technology. Development cost will be the key to realistic use of nanotechnology in aerospace engineering. The possibility of translating base research activities to the industrial scale, with competitive costs, represents the principal challenge of this new branch of science.

Nanotechnologies are characterized by a strong interdisciplinary character, which allows scientific sectors, typically very different from one another, to work jointly to design advanced systems. However, it should be considered that, for each application, a specific set of requirements must be satisfied, employing different specific 'nano-methodologies'. Aerospace engineering is characterized by large dimension systems (launchers, for example) with high performance. For this reason nanotechnology should overcome the limitations of traditional technologies.

Some researchers consider 'nano-elements' to be the materials and structures of the 21st century. The economic, scientific and technological efforts necessary are significant, but with strong collaboration among universities, industries, researchers and scientists the application of nanotechnology science to human life will become a reality.

6.12 Acknowledgments

I would like to thank the following professors and researchers for the important contribution they made to the realization of this chapter:

Prof. Mario Marchetti: Full Professor of Aerospace Structures at the High School of Aerospace Engineering of the University of Rome 'La Sapienza'
Dr Franco Mancia: Researcher at C.S.M. Centro Sviluppo Materiali S.p.A., Rome, Italy
Prof. Gilberto Rinaldi: Professor of Chemistry at the Faculty of Engineering of the University of Rome 'La Sapienza'
Prof. Luciano Galfetti: Full Professor of Aerospace Propulsion at the Politecnico of Milano, Italy
Dr Stefano Bellucci, Dr Giorgio Giannini: Researchers at INFN (Istituto Nazionale di Fisica Nucleare) dei Laboratori Nazionali di Frascati (LNF) – Laboratory of Nanotechnology

Dr Luigi Paoletti, Dr Biagio Bruni: Researchers at ISS Istituto Superiore di Sanità – Health and Technology Department, Rome, Italy
Mr Mario Brecciaroli: Researcher at ENEA of Frascati, Italy
Dr Raffaele Mucciato, Dr Gilberto Gaggiotti: Researchers at 2M Strumenti S.p.A., Italy
Mr Giancarlo Spera: Alitalia Maintenance Division, Fiumicino Airport, Italy

Special thanks go to Dr Vincenzina Fusco, PhD in Food Science and Technology at the University of Naples Federico II, Department of Food Science, Division of Microbiology, for reading this chapter and providing helpful suggestions.

The photos (6.1 and from 6.6 to 6.47) showed in this Chapter are also included in the following Degree Thesis:

1. Marco Regi – "Strutture Multigrid Realizzate Con Compositi Polimerici Rinforzati Connanotubi in Carbonio Per Applicazioni Aerospaziali", Università of Roma "La Sapienza", 2006.
2. Marco Regi – "Studio E Realizzasione Di Materiali Nanostrutturati Per Applicazioni Aerospaziali", Università of Roma "La Sapienza", 2006.

6.13 References

1. Takikama, H., Kusano, O., Sakakibara, T. – 'Graphite cathode spot produces carbon nanotubes in arc discharge', *Appl. Phys.* **32** (1999) 2433–2437
2. Zeng, H., Zhu, L., Hao, G., Sheng R. – 'Synthesis of various forms of carbon nanotubes by ac arc discharge', *Carbon* **36** (1998) 259–261
3. Takikama, H., Ikeda, M., Hirahara, K., Hibi, Y., Tao, Y., Ruiz jr., P. A., Sakakibara, T., Itoh, S., Iijima S. – 'Fabrication of single walled carbon nanotubes and nanohorns by means of a torch arc in open air', *Physica B* **323** (2002) 277–279
4. Bae, J. C., Yoon, Y. J., Lee, S., Baik, H. K. – 'Field emission of carbon nanotubes deposited by electrophoresis', *Physica B* **323** (2002) 168–170
5. Zhen-Hua, L., Miao, W., Xin-Qing, W., Hai-Bin, Z., Huan-Ming, L., Ando Y. – 'Synthesis of large single walled carbon nanotubes by arc discharge', *Chin. Phys. Lett.* **19** (2002) 91–93
6. Tang, D. S., Xie, S. S., Chang, B. H., Sun, L. F., Liu, Z. Q., Zou, X. P., Li, Y. B., Ci, L. J., Liu, W., Zhou, W. Y., Wang, G. – 'Effect of acetylene in buffer gas on the microstructures of carbon nanotubes in arc discharge', *Nanotechnology* **13** (2002) L1–L4
7. Takikama, H., Tao, Y., Miyano, R., Sakakibara, T., Ando, Y., Zhao, X., Hirahara, K., Iijima, S. – 'Carbon nanotubes on electrodes in short-time heteroelectrode arc', *Mater. Sci. Eng. C* **16** (2001) 11–16
8. Dong-Sheng, T., Wei-Ya, Z., Li-Jie, C., Xiao-Qin, Y., Hua-Jun, Y., Zhen-Ping, Z., Ying-Xin, L., Dong-Fang, L., Wei L. – 'Morphologies and microstructures of carbon nanotubes prepared by self-sustained arc discharging', *Chin. Phys.* **11**(5) (2002) 496–501
9. Lange, H., Sioda, M., Huczko, A., Zhu, Y. Q., Kroto, H. W., Walton, D. R. M. –

'Nanocarbon production by arc discharge in water', *Carbon* **41** (2003) 1617–1623

10. Zhang, H., Xue, X., Wang, D., He, Y., Peng S. – 'The effect of different kinds of inert gases and their pressures on the preparation of carbon nanotubes by carbon arc method', *Mater. Chem. Phys*. **58** (1999) 1–5
11. Li, Y., Xie, S., Zhou, W., Tang, D., Liu, Z., Zou, X., Wang, G. – 'Small diameter carbon nanotubes synthesized in an arc discharge', *Carbon* **39** (2001) 1421–1446
12. Lee, S. J., Baik, H. K., Yoo, J., Han, J. H. – 'Large scale synthesis of carbon nanotubes by plasma rotating arc discharge technique', *Diamond Related Mater*. **11** (2002) 914–917
13. Huang, H., Kajiura, H., Murakami, Y., Ata, M. – 'Metal sulphide catalyzed growth of carbon nanofibers and nanotubes', *Carbon* **41** (2003) 579–625
14. Takikama, H., Kusano, O., Sakakibara, T. – 'Graphite cathode spot produces carbon nanotubes in arc discharge', *Appl. Phys.* **32** (1999) 2433–2437
15. Maser, W. K., Munoz, E., Benito, A. M., Martinez, M. T., de la Fuente, G. F., Maniette, Y., Anglaret, E., Sauvajol, J. L. – 'Production of high density single walled nanotube material by a simple laser ablation method', *Chem. Phys. Lett.* **292** (1998) 587–593
16. Yudasaka, M., Yamada, R., Sensui, N., Wilkins, T., Ichihashi, T., Iijima, S. – 'Mechanism of the effect of nico, Ni and Co catalysts on the yeld of single wall carbon nanotubes formed by pulsed Nd:Yag laser ablation', *J. Phys. Chem. B* **103** (1999) 6224–6229
17. Yudasaka, M., Sensui, N., Takizawa, M., Bandow, S., Ichihashi, T., Iijima, S. – 'Formation of single wall carbon nanotubes catalyzed by Ni separation from Y in laser ablation or in arc discharge using a C target containing a NiY catalyst', *Chem. Phys. Lett*. **312** (1999) 155–160
18. Zhang, M., Yudasaka, M., Iijima, S. – 'Single wall carbon nanotubes: a high yield of tubes through laser ablation of a crude-tube target', *Chem. Phys. Lett*. **336** (2001) 196–200
19. Guo, T., Nikolaev, P., Thess, A., Colbert, D. T., Smalley, R. E. – 'Catalytic growth of single walled nanotubes by laser ablation', *Chem. Phys. Lett*. **243** (1995) 49–54
20. Zhang, H., Ding, Y., Wu, C., Chen, Y., Zhu, Y., He, Y., Zhong, S. – 'The effect of laser power on the formation of carbon nanotubes prepared in CO_2 continuous wave laser ablation at room temperature', *Physica B* **325** (2003) 224–229
21. Burakov, V. S., Bokhonov, A. F., Nerdel'ko, M. I., Savastenko, N. A., Tarasenko, N. V. – *Optical Emission Characteristics of Carbon Plasma Produced by Single and Double Pulse Laser Ablation*, Institute of Molecular and Atomic Physics National Academy of Science of Belarus
22. Yudasaka, M., Komatsu, T., Ichihashi, T., Iijima, S. – 'Single wall carbon nanotube formation by laser ablation using double-targets of carbon and metal', *Chem. Phys. Lett*. **278** (1997) 102–106
23. Arepalli, S., Nikolaev, P., Holmes, W., Scott, C. D. – 'Diagnostic of laser-produced plume under carbon nanotube growth conditions', *Appl. Phys. A* **69** (1999) 1–9
24. Scott, C. D., Arepalli, S., Nikolaev, P., Smalley, R. E. – 'Growth mechanisms for single wall carbon nanotubes in a laser ablation process', *Appl. Phys. A* **72** (2001) 573–580
25. Yokomichi, H., Sakai, F., Ichihara, M., Kishimoto, N. – 'Attempt to synthesize carbon nanotubes by hot wire chemical vapor deposition', *Thin Solid Films* **395** (2001) 253–256

26. Okazaki, T., Shinohara, H. – 'Synthesis and characterization of single wall carbon nanotubes by hot filament assisted chemical vapor deposition', *Chem. Phys. Lett.* **376** (2003) 606–611
27. Obraztsov, A., Zolotukhin, A., Ustinov, A., Volkov, A., Svirko, Y. – 'Chemical vapor deposition of carbon films: *in situ* plasma diagnostics', *Carbon* **41** (2003) 836–839
28. Chen, M., Chen, C., Chen, C. F. – 'Preparation of high yield multiwalled carbon nanotubes by microwave plasma chemical vapor deposition at low temperature', *J. Mater. Sci*. **37** (2002) 3561–3567
29. Wang, X., Hu, Z., Chen, X., Chen, Y. – 'Preparation of carbon nanotubes and nanoparticles by microwave plasma enhanced chemical vapor deposition', *Scripta Mater*. **44** (2001) 1567–1570
30. Jung, K., Boo, J., Hong, B. – 'Synthesis of carbon nanotubes grown by hot filament plasma enhanced chemical vapor deposition method', *Diamond Related Mater*. **13** (2004) 299–304
31. Dillon, A., Mahan, A., Alleman, J., Heben, M., Parilla, P., Jones, K. – 'Hot wire chemical vapor deposition of carbon nanotubes', *Thin Solid Films* **430** (2003) 292–295
32. Park, D., Kim, Y., Lee, J. – 'Synthesis of carbon nanotubes on metallic substrates by a sequential combination of PECVD and thermal CVD', *Carbon* **41** (2003) 1025–1029
33. Kong, J., Cassell, A., Dai, H. – 'Chemical vapor deposition of methane for single walled carbon nanotubes', *Chem. Phys. Lett.* **292** (1998) 567–574
34. Pradhan, D., Sharon, M. – 'Carbon nanotubes, nanofilaments and nanobeads by thermal chemical vapor deposition process', *Mater. Sci. Eng. B* **96** (2002) 24–28
35. Mauron, P., Emmenegger, C., Zuttel, A., Nutzenadel, C., Sudan, P., Schlapbach, L. – 'Synthesis of oriented nanotube films by chemical vapor deposition', *Carbon* **40** (2002) 1339–1344
36. Han, J., Choi, S., Lee, T., Yoo, J., Park, C., Jung, T., Yu, S., Yi, W., Han, I., Kim, J. – 'Growth characteristics of carbon nanotubes using platinum catalyst by plasma enhanced chemical vapor deposition', *Diamond Related Mater.* **12** (2003) 878–883
37. Allouche, H., Monthioux, M., Jacobsen, R. – 'Chemical vapor deposition of pyrolytic carbon on carbon nanotubes. Part 1: synthesis and morphology', *Carbon* **41** (2003) 2897–2912
38. Lee, C., Park, J. – 'Growth and structure of carbon nanotubes produced by thermal chemical vapor deposition', *Carbon* **39** (2001) 1891–1896
39. Grujicic, M., Cao, G., Gersten, B. – 'Optimization of chemical vapor deposition process for carbon nanotubes fabrication', *Appl. Surface Sci*. **191** (2002) 223–239
40. Bonard, J., Stora, T., Salvetat, J., Maier, F., Stockli, T., Duschl, C., Forrò, L., Heer, W., Chatelain, A. – 'Purification and size selection of carbon nanotubes', *Adv. Mater.* **9(10)** (1997) 827
41. Colomer, J., Piedigrosso, P., Willems, I., Journet, C., Bernier, P., van Tendeloo, G., Fonseca, A., Nagy, J. – 'Purification of catalytically produced multi wall nanotubes', *J. Chem. Soc., Faraday Trans.*, **94** (1998) 3753–3758
42. Bandow, S., Rao, A., Williams, K., Thess, A., Smalley, R., Eklund, P. – 'Purification of single wall carbon nanotubes by microfiltration', *J. Phys. Chem B* **101** (1997) 8839–8842
43. Yamamoto, K., Akiya, S., Nakayama, Y. – 'Orientation and purification of carbon nanotubes using AC electrophoresis', *Appl. Phys.* **31** (1999) L34–L36

44. Shelimov, K., Esenaliev, R., Rinzler, A., Huffman, C., Smalley, R. – 'Purification of single wall carbon nanotubes by ultrasonically assisted filtration', *Chem. Phys. Lett*. **282** (1998) 429–434
45. Hafner, J., Bronikowski, M., Azamian, B., Nikolaev, P., Rinzler, A., Colbert, D., Smith, K., Smalley, R. – 'Catalytic growth of single wall carbon nanotubes from metal particles', *Chem. Phys. Lett*. **296** (1998) 195–202
46. Dai, H., Rinzler, A., Nikolaev, P., Thess, A., Colbert, D., Smalley R. – 'Single wall nanotubes produced by metal catalyzed disproportionation of carbon monoxide", *Chem. Phys. Lett*. **260** (1996) 471–475
47. Flahaut, E., Govindaraj, A., Peigney, A., Laurent, C., Rousset, A., Rao, C. – 'Synthesis of single walled carbon nanotubes using binary (Fe, Co, Ni) alloy nanoparticles prepared in situ by the reduction of oxide solid solution', *Chem. Phys. Lett*. **300** (1999) 236–242
48. Yamamoto, K., Akiya, S., Nakayama, Y. – 'Orientation and purification of carbon nanotubes using AC electrophoresis', *Appl. Phys.* **31** (1999) L34–L36
49. Morishita, K., Takarada, T. – 'Scanning electron microscope observation of the purification behaviour of carbon nanotubes', *J. Mater. Sci*. **34** (1999) 1169–1174
50. Regi, M., Mancia, F., Marchetti, M., Amantini, L. – 'Study of carbon nanotubes process for their application in the aerospace engineering', *IX Workshop on Microwave Engineering, Metamaterials and Special Materials for Electromagnetic Applications and TLC*, Aula Magna University of 'ROMA TRE', 5 April 2004, Proceeding of Ronchi Foundation **1–2** (2005) 267
51. Regi, M., Mancia, F., Marchetti, M. – 'Design and characterization of anisogrid lattice structures with carbon nanotubes', *Proceedings International Workshop on MEMS and Nanotechnology Integration (MNI): Application*, 10–11 May 2004, Montreux (Svizzera)
52. Regi, M., Marchetti, M., Mancia, F., Allegri, G. – 'Synthesis of carbon nanotubes and their application in "anisogrid lattice structures" ', *Proceedings SEM X International Congress & Exposition on Experimental and Applied Mechanics, 5th International Symposium on MEMS and Nanotechnology*, 7–10 June 2004, Costa Mesa, California, USA
53. Regi, M., Mancia, F. – 'Synthesis and characterization of carbon-nanotubes and their application in the aerospace engineering', *Proceedings Polymer Fibres 2004*, 14–16 July 2004, UMIST Conference Centre, Manchester, UK
54. Regi, M., Mancia, F., Marchetti, M. – 'Synthesis of carbon nanotubes and their application in "anisogrid lattice structures" ', *Proceedings International Conference on Experimental Mechanics ICEM12*, 29 August–2 September 2004, Bari, Italy
55. Regi, M., Mancia, F., Marchetti, M., Totaro, G., De Nicola, F., Vasiliev, V. V., Rasin, A. F. – 'Nanostructured composite materials and anisogrid lattice structures for aerospace applications, Part A: synthesis of carbon nanotubes and their application in "anisogrid lattice structures", Part B: optimized design of isogrid and anisogrid lattice structures', *Proceedings 55th IAC International Astronautical Congress IAF*, 4–8 October 2004, Vancouver, Canada
56. Mancia, F., Regi, M., Marchetti, M. – 'Optimization of the synthesis of carbon nanotubes using the arc discharge method', *Proceedings of* "*School and Workshop on Nanotubes and Nanostructures*" NN2004, LNF – INFN, Frascati, 14–20 October 2004
57. Bellucci, S., Balasubramanian, C., Mancia, F., Marchetti, M., Regi, M., Tombolini, F. – 'Electrical and mechanical properties of composite materials based on carbon nanotubes for aerospace applications', *Proceedings (Poster + Paper) Canues 2004,*

Conference on Micro-Nano-Technologies for Aerospace Applications: From Concepts to Systems, 1–5 November 2004, Monterey, CA
58. Bellucci, S., Balasubramanian, C., Mancia, F., Marchetti, M., Regi, M., Tombolini, F. – 'Composite materials based on carbon nanotubes for aerospace applications', *Proceedings ICEM04 International Conference on Experimental Mechanics*, 29 November–1 December 2004, Singapore
59. Marchetti, M., Regi, M., Mancia, F. – 'Damage response of anisogrid lattice aerospace structures', *Proceedings dell'ICOSAAR2005 9th International Conference on Structural Safety and Reliability*, Rome, Italy, 19–23 June 2005
60. Regi, M., Marchetti, M., Mancia, F. – 'Ricostruzione laser 3D della morfologia superficiale di elettrodi di grafite contenenti nanotubi in carbonio', *Tutto Misure* **4** (2005)
61. Galfetti, L., De Luca, L. T., Meda, L., Marra, G., Marchetti, M., Regi, M., Bellucci, S. – 'Nanoparticles for solid rocket propellants', *Nanoscience and Nanotechnology NN2005*, INFN–LNF, Villa Mondragone Monteporzio Catone, Frascati, Rome, 14–16 November 2005
62. Regi, M., Mucciato, R., Bellucci, S., Marchetti, M., Gaggiotti, G., Borin, P., Giannini, G. – 'Study and characterization of carbon nanotubes with the atomic force microscopy (AFM)', *Nanoscience and Nanotechnology NN2005*, INFN–LNF, Villa Mondragone Monteporzio Catone, Frascati, Rome, 14–16 November 2005
63. Bellucci, S., Balasubramanian, C., Giannini, G., Borin, P., Regi, M., Micciulla, F. – 'Field emission studies from multiwalled carbon nanotubes', *Nanoscience and Nanotechnology NN2005*, INFN–LNF, Villa Mondragone Monteporzio Catone, Frascati, Rome, 14–16 November 2005
64. Marchetti, M., Frezza, F., Regi, M., Mazza, F., Carnà, E. – 'Development and characterization of nanostructured frequency selective surfaces (FSS)', *Proceeding 46th IACAS – Israel Annual Conference on Aerospace Structures*, 1–2 March 2006
65. Dresslhaus, M. S., Dresslhaus, G., – *Carbon Nanotubes*: *Synthesis, Structure, Properties and Application*, Springer Verlag Berlin Heidelberg New York, 2001
66. Guozhong, C. – *Nanostructures and Nanomaterials*, Imperial College Press, 2004
67. Nan, C., Shi, Z., Lin, Y. – 'A simple model for thermal conductivity of carbon nanotube based composites', *Chem. Phys. Lett.* **375** (2003) 666–669
68. Arepalli, S., Nikolaev, P., Gorelik, O., Hadjiev, V., Holmes, W., Files, B., Yowell, L. – 'Protocol for the characterization of single walled carbon nanotube material quality', *Carbon* **42** (2004) 1783–1791
69. Morishita, K., Takarada, T. – 'Scanning electron microscope observation of the purification behaviour of carbon nanotubes', *J. Mater. Sci.* **34** (1999) 1169–1174
70. Feng, S. Q., Yu, D. P., Hu, G., Zhang, X. F., Zhang, Z. – 'The HRTEM observation of cross-sectional structure of carbon nanotubes', *J. Phys. Chem. Solids* **58**(11) (1997) 1887–1892
71. Hirsch, P., Howie, A., Nocholson, R., Pashley, D. W., Whelan, M. J. – *Electron Microscopy of Thin Crystals*, Krieger Publishing Company, 1997
72. Thomas, G., Goringe, M. J. – *Transmission Electron Microscopy of Materials*, John Wiley & Son, 1979
73. Valentini, L., Biagiotti, J., Kenny, J., Santucci, S. – 'Morphological characterization of single walled carbon nanotubes-pp composites', *Composites Sci. Technol*. **63** (2003) 1149–1153
74. Nan, C., Shi, Z., Lin, Y. – 'A simple model for thermal conductivity of carbon nanotube based composites', *Chem. Phys. Lett.* **375** (2003) 666–669.

75. Chambers, A., Park, C., Baker, R., Rodriguez, N. – 'Hydrogen storage in graphite nanofibres', *J. Phys. Chem. B* **102**(22) (1998) 4253–4256
76. Dokhan, A., Price, E. W., Sigman, R. K., Seitman, J. M. – 'The effect of the Al particle size on the burning rate and residual oxide in aluminized propellants', *Proceedings of 37th AIAA/ASME/SAE/ASEE Joint Propulsion Conference and Exhibition* '*Fundamentals of Solid Propellant Combustion*', AIAA–2001–3581, American Institute of Aeronautics and Astronautics (2001) 1–11
77. Désilets, S., Brousseau, P., Coté, S. – 'Ignition of energetic materials containing carbon nanotubes', *34th International Annual Conference of ICT*, 24–27 June 2003
78. Ramaswamy, A., Kaste, P., Trevino, S. – *Studies in Nanopropulsion for Environmentally Benign Propellants*, University of MD, College Park, MD, Army Research Laboratory
79. Dokhan, A., Price, E., Sigman, R., Seitzman, J. – 'The effects of al particle size on the burning rate and residual oxide in aluminized propellants', *AIAA 2001-3581 37th AIAA/ASME/SAE/ASEE Joint Propulsion Conference*, 2001
80. Peigney, A., Laurent, C., Flahaut, E., Rousset, A. – 'Carbon nanotubes in novel ceramic matrix nanocomposites', *Ceramics Int.* **26** (2000) 677–683
81. Roche, S. – 'Carbon nanotubes: exceptional mechanical and electronic properties', *Ann. Chim. Sci. Mat.* **25**, (2000) 529–532
82. Hammel, E., Tang, X., Trampert, M., Schmitt, T., Mauthner, K., Eder, A., Potschke, P. – 'Carbon nanofibers for composite applications', *Carbon* **42** (2004) 1153–1158
83. Sax, N. I., Feiner, B. – '*Dangerous Properties of Industrial Materials*', Nostrand Reinold, 1984
84 Garg, A., Sinnott, S. – 'Effect of chemical functionalization on the mechanical properties of carbon nanotubes', *Chem. Phys. Lett.* **295** (1998) 273–278
85. Little, R. – 'Mechanistic aspects of carbon nanotubes nucleation and growth', *J. Cluster Sci*. **14** (2) (2003)
86. Shyu, Y., Hong, F. – 'Low-temperature growth and field emission of aligned carbon nanotubes by chemical vapor deposition', *Mater. Chem. Phys*. **72** (2001) 223–227
87. Lee, N., Park, C., Lee, S., Kang, J., Kim, C., Yun, M., Park, N., Han, I., Kim, J., Jung, J., Kim, J. – 'New emitter techniques for field emitter displays', *Sixth Applied Diamonds Conference/Second Frontier Carbon Technology*, Auburn University, July 2001, NASA/CP-2001-210948
88. Dean, K., Chalamala, B., Coll, B., Talin, A., Trujillo, J., Wei, Y., Jaskie, J. – 'Fundamental properties of nanotube field emitters for large area electron sources', *Sixth Applied Diamonds Conference/Second Frontier Carbon Technology*, Auburn University, July 2001, NASA/CP-2001-210948
89. Jeong, S., Hwang, H., Lee, K. – 'Multiwall carbon nanotubes growth in nano-template and their application to a field emission device', *Sixth Applied Diamonds Conference/Second Frontier Carbon Technology*, Auburn University, July 2001, NASA/CP-2001-210948
90. Wong, W., Au, F., Bello, L., Lee, C., Lee, S. – 'Field emission from carbon nanotubes grown on plasma treated nickel/silicon substrate', *Sixth Applied Diamonds Conference/Second Frontier Carbon Technology*, Auburn University, July 2001, NASA/CP-2001-210948
91. Fu, W., Xiao, B., Albin, S. – 'Field emission properties of ultra fine multi wall carbon nanotubes grown by microwave plasma CVD', *Sixth Applied Diamonds Conference/Second Frontier Carbon Technology*, Auburn University, July 2001, NASA/CP-2001-210948

92. Lau, K., Hui, D. – 'The revolutionary creation of new advanced materials-carbon nanotubes composites', *Composite: Part B* **33** (2002) 263–277
93. Thostenson, E. T., Ren, Z., Chou, T. – 'Advances in the science and technology of carbon nanotubes and their composites', *Composites Sci. Technol.* **61** (2001) 1899–1912
94. Andrews, R., Rantell, T., Haddon, R., Dickey, E., Bergosh, R., Hu, H., Landis, C., Meier, M. – 'Composite materials from modified carbon nanotubes', *Sixth Applied Diamonds Conference/Second Frontier Carbon Technology*, Auburn University, July 2001, NASA/CP-2001-210948
95. Ruoff, R. – 'Mechanics of carbon nanotubes', *Sixth Applied Diamonds Conference/ Second Frontier Carbon Technology*, Auburn University, July 2001, NASA/CP-2001-210948
96. Kimura, A., Mizutani, A., Toriyama, T., Oguri, K., Tonegawa, A., Nishi, Y. – 'Fracture stress enhancement by EB treatment of carbon fibres', *Sixth Applied Diamonds Conference/Second Frontier Carbon Technology*, Auburn University, July 2001, NASA/CP-2001-210948
97. Cagin, T., Che, J., Deng, W., Xu, X., Goddard, W. – 'Computational studies on formation and properties of carbon nanotubes', *Sixth Applied Diamonds Conference/ Second Frontier Carbon Technology*, Auburn University, July 2001, NASA/CP-2001-210948
98. Kalamamkarov, A. – *Composite and Reinforced Elements of Construction*, John Wiley & Sons Ltd, 1992
99. Fortscue, P., Stark, J., Swinerd G. – *Spacecraft Systems Engineering*, John Wiley & Sons Ltd, third edition 2003
100. Gou, J., Miniaie, B., Wang, B., Liang, Z., Zhang, C. – *Computational and Experimental Study of Interfacial Bonding of Single Walled Nanotubes Reinforced Composites*, Department of Mechanical Engineering, University of South Alabama, USA
101. Cooper, C., Cohen, S., Barber, A., Wagner, H. – 'Detachment of nanotubes from a polymeric matrix', *Appl. Phys. Lett.* **81**(20) (2002) 3873–3875
102. Lourie, O., Cox, D., Wagner, H. – 'Buckling and collapse of embedded carbon nanotubes', *Phys. Rev. Lett.* **81**(8) (1998) 1638–1641
103. Wei, C., Cho, K. – 'Chemical bonding of polymer on carbon nanotube', *MRS 2001 Spring Meeting Proceeding Paper*
104. Barber, A., Cohen, S., Wagner, H. – 'Measurement of carbon nanotubes polymer interfacial strength', *Appl. Phys. Lett.* **82**(23) (2003) 4140–4142
105. Ruoff, R., Qian, D., Liu, W. – 'Mechanical properties of carbon nanotubes: theoretical prediction and experimental measurements', *C. R. Physique* **4** (2003) 993–1008
106. Salvetat, J., Bonard, J., Thomson, N., Kulik, A., Forrò, L., Beniot, W., Zuppiroli, L. – 'Mechanical properties of carbon nanotubes', *Appl. Phys. A* **69** (1999) 255–260
107. Cooper, C., Ravich, D., Lips, D., Mayer, J., Wagner, H. – 'Distribution and alignment of carbon nanotubes and nanofibrils in a polymer matrix', *Composites Sci. Technol.* **62** (2002) 1105–1112
108. Alloui, A., Bai, S., Cheng, H., Bai, J. – 'Mechanical and electrical properties of a MWNT/epoxy composite', *Composites Sci. Technol.* **62** (2002) 1993–1998
109. Ruoff, R., Lorents, D. – 'Mechanical and thermal properties of carbon nanotubes', *Carbon* **33** (7) (1995) 925–930

110. Frankland, S., Harik, V., Odegard, G., Brenner, D., Gates, T. – 'The stress–strain behaviour of polymer nanotube composites from molecular dynamics simulation', *Composites Sci. Technol.* **63** (2003) 1655–1661
111. Valentini, L., Biagiotti, J., Kenny, J., Santucci, S. – 'Morphological characterization of single walled carbon nanotubes-PP composites', *Composites Sci. Technol*. **63** (2003) 1149–1153
112. Lau, K., Hui, D. – 'The revolutionary creation of new advanced materials–carbon nanotube composites', *Composites: Part B* **33** (2002) 263–277
113. Wagner, H., Lourie, O., Zhou, X. – 'Macrofragmentation and microfragmentation phenomena in composite materials', *Composites: Part A* **30** (1999) 59–66
114. Xiao, Q., Zhou, X. – 'The study of multi walled carbon nanotube deposited with conducting polymer for super capacitor', *Electrochimica Acta* **48** (2003) 575–580
115. Peigney, A., Laurent, C., Flahaut, E., Rousset, A. – 'Carbon nanotubes in novel ceramic matrix nanocomposites', *Ceramics Int*. **26** (2000) 677–683.
116. Koratkar, N., Wei, B., Ajayan, P. – 'Multifunctional structural reinforcement featuring carbon nanotube film', *Composites Sci. Technol.* **63** (2003) 1525–1531
117. Binnott, S., Shenderova, O., White, C., Brenner, D. – 'Mechanical properties of nanotubule fibres and composites determined from theoretical calculations and simulations', PII: S0008-6223(97)00144-9
118. Stephan, C., Nguyen, T., Chapelle, M., Lefrant, S., Journet, C., Bernier, P. – 'Characterization of single walled carbon nanotubes-PMMA composites,' *Synthetic Metals* **108** (2000) 139–149
119. Garg, A., Sinnott, S. – 'Effect of chemical functionalization on the mechanical properties of carbon nanotubes', *Chem. Phys. Lett*. **295** (1998) 273–278
120. Andler, J., Shaffer, M., Prasse, T., Bauhofer, W., Schulte, K., Windle, A. – 'Development of dispersion process for carbon nanotubes in a epoxy matrix and the resulting electrical properties', *Polymer* **40** (1999) 5967–5971
121. Currao, S., Davey, A., Coleman, J., Dalton, A., McCarthy, B., Maier, S., Drury, A., Gray, D., Brennan, M., Ryder, K., de la Chapelle, M., Journet, C., Bernier, P., Byrne, H., Carroll, D., Ajayan, P., Lefrant, S., Blau W. – 'Evolution and evaluation of polymer/nanotube composite', *Synthetic Metals* **103** (1999) 2559–2562
122. Odegard, G., Gates, T., Nicholson, L., Wise, K. – 'Equivalent continuum modelling of nano structured materials', *Composites Sci. Technol*. **62** (2002) 1869–1880
123. Hammel, E., Tang, X., Trampert, M., Schmitt, T., Mauthner, K., Eder, A., Potschke, P. – 'Carbon nanofibers for composite applications', *Carbon* **42** (2004) 1153–1158
124. Vasiliev, V., Barynin, V., Rasin, A. – 'Anisogrid lattice structures – survey of development and application', *Composite Structures* **54** (2001) 361–370
125. Slinchenko, D., Verijenko, V. – 'Structural analysis of composite lattice shells of revolution on the basis of smearing stiffness', *Composite Structures* **54** (2001) 341–348
126. Vasiliev, V. V., Jones, R. M. – *Mechanics of Composite Structures*, Taylor & Francis, 1993
127. Vasiliev, V. V., Morozov, E. V. – *Mechanics and Analysis of Composite Materials*, Elsevier Science Ltd, 2001
128. Kyriazidou, C., Diaz, R., Alexopoulos, N. – 'Novel material with narrow band transparency window in the bulk', *IEEE Trans. Antenna Propagation* **48**(1) (2000) 107–116.
129. Campos, F., D'Assuncao, A., Neto, G. – 'Scattering characteristics of FSS on two anisotropic layers for incident co-polarized plane waves', *Microwave Optical Technol. Lett.* **33**(1) (2002) 57–61

130. Lu, C., Chern, R., Chang, C. – *Analysis of Frequency Selective Surfaces by Spectral Galerkin Method*, Institute of Applied Mechanics, National Taiwan University
131. Cui, S., Weile, D. – *Efficient Analysis of Scattering for Periodic Structures Composed of Arbitrary Inhomogeneous and Anisotropic Materials using FE-BI Method Accelerated by FFT*, Dept. of Electrical & Computer Engineering, University of Delaware, Newark, DE
132. Chakravarty, S., Mittra, R. – 'Application of micro genetic algorithm to the design of spatial filters with frequency selective surfaces embedded in dielectric media', *IEEE Trans. Electromagnetic Compatibility* **44**(2) (2002) 338–346.
133. Chakravarty, S., Mittra, R. – 'Design of a frequency selective surface (FSS) with very low cross-polarization discrimination via parallel micro genetic algorithm', *IEEE Trans. Antennas Propagation* **51**(7) (2003) 1664–1668
134. Lynch, J., Colburn, J. – 'Modelling polarization mode coupling in frequency selective surfaces', *IEEE Trans. Microwave Theory Techniques* **52**(4) (2004) 1328–1338
135. Kristensson, G. – *On the Generation of Surface Waves in Frequency Selective Structures*, Department of Electroscience Electromagnetic Theory, Lund Institute of Technologies, Sweden, 2003
136. Li, Z., Papalambros, P., Volakis, J. – 'Frequency selective surface design by integrating optimisation algorithms with fast full wave numerical methods', *IEE Proc. Microwave Antennas Propagation* **149**(3) (2002) 175–180
137. Munk, B. – *Frequency Selective Surfaces*, John Wiley & Sons Inc., 2000
138. Bhushan, B. – *Handbook of Nanotechnology*, Springer, 2004

7

Carbon nanotube and nanofibre reinforced polymer fibres

M. S. P. SHAFFER, Imperial College London, UK and
J. K. W. SANDLER, University of Bayreuth, Germany

7.1 Introduction

Carbon nanotubes (CNTs) can be seen as a bridge between traditional carbon fibres and the fullerene family;[1] this intermediate position between the molecular and continuum domains is the classic signature of a nanomaterial. Research on these structures blossomed only recently, following the electric-arc synthesis of multiwalled nanotubes by Iijima, in 1991;[2] since then, in excess of 10 000 papers have appeared discussing the science of CNTs, including a large fraction on polymer composites. This interest was initially stimulated by the recognition of the relationship with the closed, curved, carbon shells of the fullerene family that had been discovered a few years previously, in 1985.[3] However, although Iijima is often credited with the discovery of CNTs, there are earlier reports in the literature, notably by Endo in 1976, of the synthesis of tubular carbon structures using hydrocarbon decomposition,[4] as well as earlier in the catalysis literature of the 1950s, and possibly even the late 19th century.[5] In fact, nanotubes are now known to occur naturally, having been observed in 10 000-year-old ice cores[6] and metallic swords.[7] The investigation of nanotubes today is driven by their elegant and diverse structures, and their emerging remarkable intrinsic properties.

CNTs have typical diameters in the range of ~1–50 nm and lengths of many micrometres (even centimetres in special cases).[8] They can consist of one or more concentric graphitic cylinders. In contrast, commercial (polyacrylonitrile (PAN) and pitch) carbon fibres are typically in the 7–20 μm diameter range, while vapour-grown carbon fibres (VGCFs) have a broad range of possible diameters (see Fig. 7.1). Compared with carbon fibres, the best nanotubes can have almost atomistically perfect structures; indeed, there is a general question as to whether the smallest CNTs should be regarded as very small fibres or heavy molecules, especially as the diameters of the smallest nanotubes are similar to those of common polymer molecules.

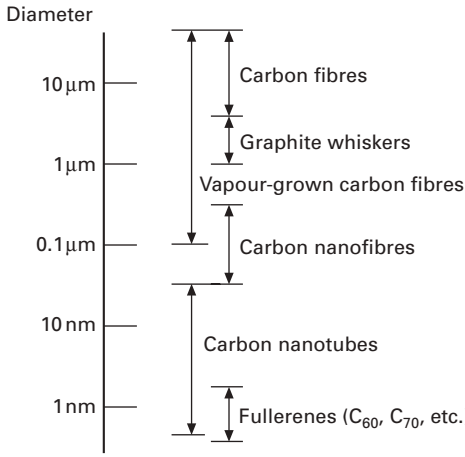

7.1 Comparison of diameters of various fibrous carbon-based materials.

Consequently, it is not yet clear to what extent conventional fibre composite understanding can be extended to CNT composites.

Structurally, CNTs are very diverse depending on their origins. Fundamentally, a single wall carbon nanotube (SWCNT) consists of a single layer of graphite rolled into a seamless cylinder; the orientation of the graphite lattice to the cylinder axis defines the *chirality* or *helicity* of the nanotube.[9] Nanotube shells have large surface areas and prefer to gain van der Waals stabilisation[10] either by forming parallel bundles of SWCNTs[11–14] or by nesting concentrically to form a multiwalled carbon nanotube (MWCNT). The outer diameter of such MWCNTs can vary between 2 and a somewhat arbitrary upper limit of about 50 nm; the inner diameter is often (though not necessarily) quite large, about half that of the whole tube. As-grown, each nanotube is closed by a hemispherical, fullerenic cap associated with pentagonal rather than hexagonal rings in the graphitic structure. In addition, a wide range of defects can exist including vacancies, extraneous non-hexagonal rings, edge dislocations, local sp^3 hybridisation, and non-carbon functional group defects which can give rise to longer range morphological changes in the structure, such as kinks/bends, and changes in diameter. The formation of kinks during synthesis is particularly significant as it encourages the development of an entangled network of nanotubes that is difficult to disperse.[15] Straight nanotubes, on the other hand, are less likely to be entangled, can be aligned more easily, and are likely to have better performance in composites.[16] Figure 7.2 shows a comparison of aligned and entangled MWCNTs. In addition to variations in the structure of the nanotubes, other contaminating materials can be present, including, for example, amorphous carbon, graphitic nanoparticles and catalyst metals, which can be difficult to remove.

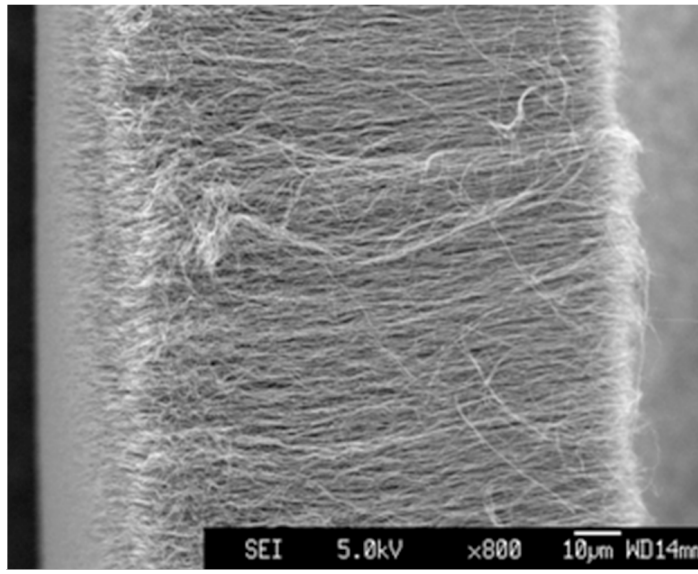

(a)

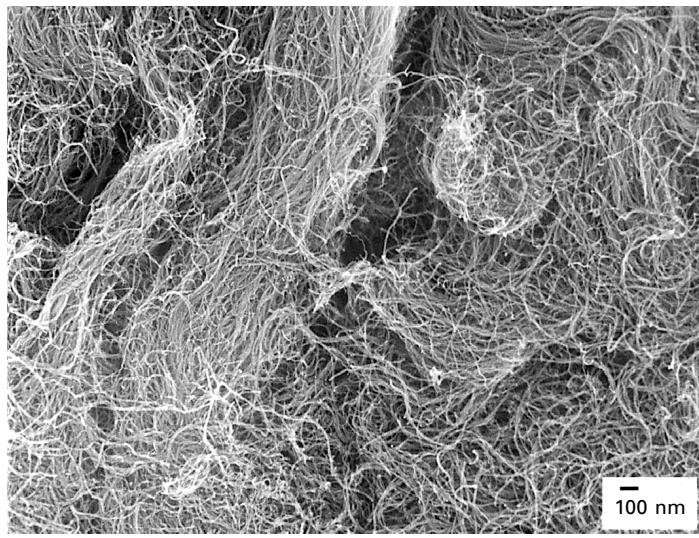

(b)

7.2 Scanning electron micrographs of (a) aligned and (b) commercial entangled MWCNTs produced by chemical vapour deposition (CVD) methods.

Carbon nanofibres (CNFs) are mainly differentiated from nanotubes by the orientation of the graphene planes: whereas the graphitic layers are parallel to the axis in nanotubes, nanofibres can show a wide range of orientations of the graphitic layers with respect to the fibre axis. They can be visualised as

stacked graphitic discs or (truncated) cones, and are intrinsically less perfect as they have graphitic edge terminations on their surface. Nevertheless, these nanostructures can be in the form of hollow tubes with an outer diameter as small as ~5 nm, although 50–100 nm is more typical. The stacked cone geometry is often called a 'herringbone fibre' due to the appearance of the longitudinal cross-section. Slightly larger (100–200 nm) fibres are also often called CNFs, even if the graphitic orientation is approximately parallel to the axis. An example of the complicated structure of a commercial CNF material is shown in Fig. 7.3.

7.2 Synthesis and properties of carbon nanotubes

Both MWCNTs and SWCNTs can be produced by a variety of different processes which can broadly be divided into two categories: high-temperature evaporation using arc-discharge[11, 12, 17–19] or laser ablation,[13, 20] and various chemical vapour deposition (CVD) or catalytic growth processes.[14, 21–23] In the high-temperature methods, MWCNTs can be produced from the evaporation of pure carbon, but the synthesis of SWCNTs requires the presence of a metallic catalyst. The CVD approach requires a catalyst for both types of CNTs but also allows the production of CNFs. The products of the high-temperature routes tend to be highly crystalline, with low defect concentrations, but are relatively impure, containing other, unwanted carbonaceous impurities. These methods usually work on the gram scale and are, therefore, relatively expensive. For the use of nanotubes in composites, large quantities of nanotubes are required at low cost, ideally without the requirement for complicated

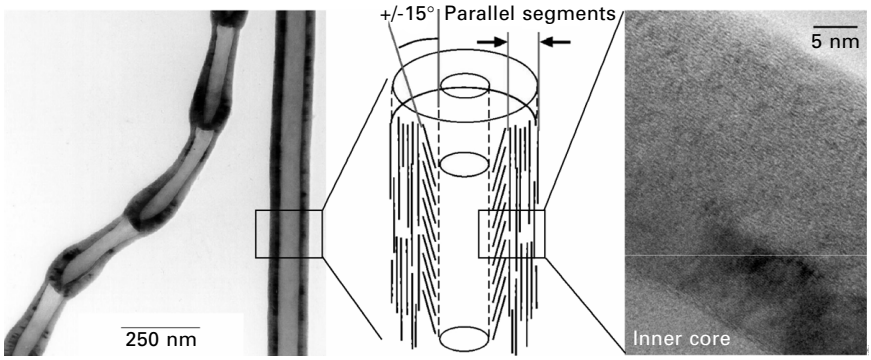

7.3 Representative transmission electron micrographs of commercial carbon nanofibres, highlighting structural variations both in overall morphology and in the orientation of the graphitic planes. The leftmost image shows a 'bamboo' and a 'cylindrical' CNF, while the rightmost image shows a high magnification image of one wall of the cylindrical fibre which reveals the graphitic arrangement sketched in the central panel.

purification. At present, only CVD-grown nanotubes satisfy these requirements and, as such, tend to be the materials of choice for composite work, both in academia and in industry;[24] a number of companies have scaled up such processes to 100 tonnes per year or more. The main contaminants in CVD materials are residual catalyst particles which are mostly incorporated into the nanotubes. On the other hand, these gas-phase processes operate at lower temperatures and lead to structurally more imperfect nanotubes, as shown by the deviation from the ideal cylindrical structure in Fig. 7.4.

7.2.1 Mechanical properties

The interest in carbon nanotubes, particularly their application in composites, has been driven by their remarkable intrinsic properties; however, these properties depend critically on the structural characteristics mentioned above, with crystalline quality and orientation being especially important. The fundamental mechanical properties of nanotubes are quite difficult to determine, but a number of attempts have been made, based on transmission electron microscopy (TEM) studies of thermal vibrations,[25, 26] bending measurements using atomic force microscopy (AFM),[27, 28] direct nano-tensile tests,[29–31] fragmentation/deformation under load in a composite,[32–34] and experiments on macroscopic aligned bundles,[35, 36] as well as various computational approaches.[37–41] The errors in such measurements are often large because of sample variability and the challenging experimental environment; in addition, the calculations generally assume a classical mechanical behaviour, and usually use the van der Waals thickness of the graphitic sheet(s) to calculate the appropriate normalising cross-sectional area (in fact, the presence of the hollow core reduces the real effective modulus, which, in any case, is hard

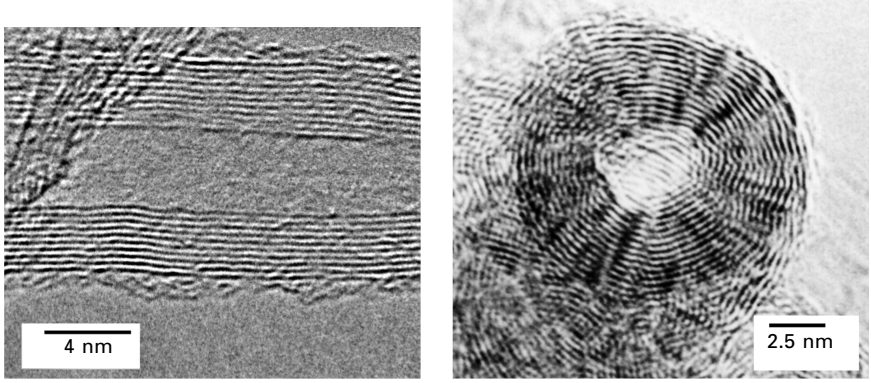

7.4 Transmission electron micrographs of commercial MWCNTs grown by CVD methods, with the beam perpendicular (left) and parallel (right) to the axis.

to define in bending).[42] Despite these difficulties, there is a reasonably clear picture emerging that highly crystalline SWCNTs or individual shells of MWCNTs, grown at high temperatures, have axial stiffnesses similar to the in-plane properties of graphite (1.1 TPa), and strengths of around 50 GPa, implying high strains to failure (~10%). Under bending deformation, nanotubes are highly resilient, undergoing reversible kinking.[43–46] These values match or exceed all other materials (specific properties are even more impressive given the low density) and have stimulated significant efforts to exploit the performance at the macroscopic scale,[47] as discussed in a later section. One problem is that CVD-grown material, which is otherwise highly suitable for composites applications, has a high defect concentration. These defects dramatically degrade the intrinsic properties of the nanotubes. Although point defects can be significant,[48] deviations from a perfectly parallel alignment of the graphitic layers to the axis is particularly detrimental owing to the high anisotropy of graphite. Reductions in strength and stiffness of up to one to two orders of magnitude have been measured,[49–51] with typical values around 2 GPa, and 50–100 GPa, respectively.

The high anisotropy of graphite has a further consequence; namely, that individual MWCNTs and SWCNT bundles can suffer internal failures due to the low shear strength parallel to the graphene layers. The result is that only the outer layer(s) of an MWCNT or SWCNT bundle actually carries the tensile load when embedded in a polymer matrix. Whether end effects, high aspect ratios or modest defect concentrations can alleviate this problem remains to be seen. Shear failures have been observed in nano-tensile tests[29–31] and scanning tunneling microscope (STM) observations[52] of neat nanotubes and in some composite experiments.[33, 53] For these reasons, some have suggested that individually dispersed SWCNTs should be the ideal reinforcement; however, other problems with flexibility, processing and large interfacial areas may be worse.

7.2.2 Transport properties

Theoretical studies of the electronic properties of SWCNTs indicate that nanotube shells are one-dimensional conductors with characteristic Van Hove singularities in their density of states. Depending critically on helicity, they can be either metallic or semiconducting,[54–56] with a small or moderate band gap (for semiconducting tubes) inversely proportional to the tube radius.[57, 58] On average, approximately one-third of SWCNTs are metallic and two-thirds semiconductors.[54] Since MWCNTs have larger diameters, confinement effects disappear, and the transport properties approach those of turbostratic graphite.[59] Interlayer interactions which might be important in small diameter MWCNTs are thought to be weak.[60, 61] However, structural defects as well as bends or twists again have a strong effect on the transport properties.[62]

Experimental electronic transport measurements on individual CNTs using bottom[63–65] or top[66] contacts, or scanning tunnelling spectroscopy (STS),[67,68] have broadly confirmed these theoretical predictions. The predicted Van Hove singularities have been observed in STS experiments and a wide range of visible/near IR, fluorescence and Raman spectroscopy studies.[69,70] Typical room temperature conductivity is in the range 10^5–10^6 S/m and 10 S/m for metallic and semiconducting nanotubes, respectively. The conductivity of SWCNT bundles, which is influenced by the significant semiconductor content,[71] has been found to be between 1×10^4 and 3×10^6 S/m[72,73,74] at room temperature, depending on sample type. Metallic nanotubes thus approach the in-plane conductivity of graphite (2.5×10^6 S/m).[75] Conductivities of individual MWCNTs have been reported to range[66] between 20 and 2×10^7 S/m, depending on the helicities of the outermost shells[76] or the presence of defects.[77] The electronic properties of larger diameter MWCNTs approach those of graphite. Smaller MWCNTs exhibit ballistic conductivity over micrometre lengths, with scattering occurring only at the contacts.[78]

Lastly, the axial thermal conductivity of individual, perfect CNTs is expected to be very high,[79] greater than that of diamond. Experimental values for individual MWCNTs have reached 3300 W/m K,[80] and aligned SWCNT arrays have been shown to be highly anisotropic.[81]

7.2.3 Physical properties

Carbon nanotubes burn in air at temperatures in the range of 450–750 °C depending on the crystallinity, size, purity and surface chemistry of the sample. In inert atmospheres, MWCNTs are essentially stable up to 3000 °C or more, although graphitisation may occur;[82] SWCNTs begin to reform into MWCNTs from around 1500 °C. The density of CNTs relates to that of graphite (2200 kg/m^3), but is effectively reduced, as long as the central hole remains empty, by an amount that depends on the ratio of the internal and external diameters. Typical values for MWCNTs and CNFs are in the range of 1600–2000 kg/m^3. The density of SWCNTs varies systematically with diameter in the approximate range 1300–1600 kg/m^3 and has been used to separate them by centrifugation.[83] The surface areas generally follow the classical geometric expectation, although it can be increased by surface activation of MWCNTs.[84] Typical values for MWCNTs are hundreds of m^2/g, with closed SWCNTs reaching 1340 m^2/g in theory, although the experimental value is generally reduced by bundling.[85] The value for SWCNTs is particularly high as every atom lies on the surface; if the inner surface is accessible to the probe, the total area is even higher, with every atom present on two surfaces.

7.3 Developing nanotube/nanofibre–polymer composites

There are at least three general experimental methods to produce bulk polymer nanocomposites: mixing in the liquid state, solution-mediated processes and *in-situ* polymerisation techniques. The direct melt-blending approach is much more commercially attractive than the latter two methods, as both solvent processing and *in-situ* polymerisation are less versatile and more environmentally contentious. Although various mixing methodologies are commonly used, final sample fabrication usually is by injection-moulding or hot pressing.

The literature on processing and evaluating macroscopic nanotube/nanofibre–polymer composites is still in its infancy but developing rapidly. This situation is not surprising, given that initial attempts to produce such nanocomposites were hindered by the small quantities of nanotubes available. The focus on CVD synthesis techniques has opened the door to the manufacture of large-scale polymer nanocomposites.

7.3.1 Nanotube dispersion

A high-quality nanotube dispersion in any polymer matrix is a crucial prerequisite for good mechanical composite performance, and is often difficult to achieve. Each nanotube should be loaded separately and equally; if the filler is agglomerated, some nanotubes will be shielded from the mechanical load. In addition, the agglomerates will act as defects, leading to stress concentration and premature failure. Good dispersion becomes harder to achieve as the particle size shrinks into the nanoscale; as surface areas increase, particles become more mobile, the distances between them decrease and shear forces become harder to apply. Nanoparticles have a strong tendency to agglomerate, and the high aspect ratio of nanotubes only makes matters worse as they sweep out large hydrodynamic volumes and can easily become entangled (see the rheology discussion in Section 7.5). High loading fractions favour agglomeration not only because the particles come into contact more often, but also because there can be a shortage of polymer matrix to 'wet out' the surface of the filler. The problem of debundling SWCNTs is particularly acute, as the van der Waals forces between the deformable nanotubes are strong, and the amount of polymer required to wet the surface is large. A trivial estimate suggests that in a 1 vol% composite containing individual SWCNTs, all the polymer chains are touching a nanotube surface (assuming a 5 nm radius of gyration); it is then easy to understand why it might be hard to add additional SWCNTs. Indeed, it is quite a common result for nanocomposites in general that properties increase at low loading fractions but cannot be increased further due to agglomeration above a few volume

percent. The situation is more ambiguous when addressing transport properties, especially electrical conductivity, as a network of touching nanotubes is desired. However, even in this case, best results may be obtained by generating a good dispersion initially, and then allowing the network to form.[16]

A particular practical problem is that dispersion is very hard to quantify. In fact, no good objective measures are available. Characterisation typically consists of a qualitative assessment of a freeze–fracture surface studied under an SEM. This approach is quite successful for discovering dense aggregates (typical of CNTs synthesised in the electric arc) or looser agglomerates in low volume fraction systems. However, it is less useful at high loading fractions where the filler is necessarily densely packed; here it is hard to distinguish between closely packed but isolated CNTs and an agglomerated network, since any contacts may not lie in the fracture plane. Optical microscopy or even optical clarity is another useful guide, again chiefly for low loading fractions. Since nanotubes are usually at least micrometres long, agglomerates are generally visible. Optical clarity is, therefore, a necessary though not sufficient condition for well-isolated CNTs, although at higher loadings, samples simply become very dark. Rheological measurements can also provide an indication of dispersion, particularly as data can be collected during the dispersion process; as discussed further in Section 7.5.

The primary method of dispersion is usually physical. Substantial shear forces appear to be necessary during the initial composite processing steps, in order to disperse either CNTs or CNFs in the (pre)polymer melt or polymer solution, especially when using the filler in the as-produced state or at high-volume fractions. For high-viscosity systems, particularly thermoplastic melts, twin-screw extrusion has been frequently applied and found to be effective for up to 60 wt% CNFs[86] and about 30 wt% MWCNTs.[87] The high intrinsic viscosity of thermoplastic matrices in general has the dual advantage of increasing the shear applied to the aggregates (even breaking the individual CNTs/CNFs) and minimising the opportunity for reaggregation. In the case of nanotubes especially, the degree of dispersion depends strongly on the entanglement state of the as-received material, since even extensive twin-screw extrusion does not lead to a complete break-up of the entanglements in commercially available catalytically grown MWCNTs,[88–90] although some materials seem to be more easily processed,[87–91] particularly those based on aligned CNTs.[92] CNFs tend to break more easily during processing, leading to the removal of entanglements;[93] SWCNT bundles are not generally broken up by thermoplastic processing. Other high-shear processes can be applied, for example, the use of ball milling of the raw filler material prior to processing;[94] however, this approach degrades the aspect ratio of individual particles significantly more than shear-intensive melt processing.[95]

Solvent processing is popular as an alternative to melt processing, or as a preliminary step. Dispersion in low-viscosity solutions is typically achieved

using ultrasound; the high intensity used separates CNT aggregates and even SWCNT bundles, but can also cause damage.[96] Reagglomeration may be prevented by the presence of the polymer in solution which can adsorb onto the exposed CNT surfaces or even become grafted due to chain scission.[97] Amphiphilic polymers dissolved in water,[98] such as poly(hydroxyaminoether) (PHAE),[99, 100] poly(vinyl alcohol) (PVA),[101, 102] and PVA/poly(vinyl pyrrolidone) (PVP)[103] have proved particularly effective, although organic systems have also been explored, based on polystyrene (PS),[104–106] ultra-high molecular weight polyethylene (UHMWPE)[107] and polypropylene (PP).[108] In addition, surfactants,[103, 109] polymer-functionalised nanotubes[110, 111] and other chemical treatments of the constituents[112–114] are often employed. Some of the most successful nanotube–polymer composites have been created by *in-situ* polymerisation, such that the nanotubes become grafted to or ensnared in the growing polymer.[115–119] In all low-viscosity systems, the individual nanotubes should form an inherently electrostatically or sterically stabilised dispersion, with a long lifetime relative to the subsequent processing. Once the solvent is removed, thermoplastic processing can be applied without necessarily losing the good dispersion.[87, 91, 95, 114, 120, 121] The chemical methods of providing stabilisation, particularly those that encourage a strong, or even covalent interaction with the polymer, tend to have a positive impact on subsequent composite properties through improved load transfer.

7.3.2 Mechanical properties of nanotube/nanofibre–polymer composites

Although many nanotube/nanofibre composite systems have been prepared, the mechanical enhancements have been significant but somewhat limited compared with theoretical predictions. The main challenges lie in obtaining a good dispersion, optimising the interface between polymer and filler, and obtaining high-quality structures in sufficient quantities (as discussed above, CVD-grown nanotubes are used commonly in composites but have relatively poor properties). As in any fibre reinforced composite system, the interfacial shear strength is an important parameter, although difficult to assess. A growing body of computational work[122–124] as well as some initial experimental work[33, 125–127] has addressed this issue. Both approaches have shown significant spread in the data, yet the overlap seems to suggest values in the range of 50–100 MPa for non-covalently bonded composites[47] although much higher values are anticipated for covalently bonded nanotubes.[122]

The published mechanical data show that the tensile modulus of nanotube/nanofibre–thermoplastic composites is generally improved, although a detailed comparison of the data is difficult due to the different types of fillers, surface treatments, matrices, processing techniques and test methods that have been used. In general, the stiffening effect of nanotubes and nanofibres appears to

be more prominent in semicrystalline rather than amorphous thermoplastics, possibly due to nucleation effects commonly observed in such nanocomposites.[108, 128–130]

Even when a homogeneous dispersion of the nanoscale filler is claimed for all concentrations, the stiffness enhancement is usually most prominent for low filler weight fractions, with the critical concentration depending on the specific materials and processing conditions used. This observation might relate to decreasing nanofiller alignment or increasing void content with increasing weight fraction,[95, 106, 131] although alignment variations of the polymer matrix often have not properly been taken into account. In semicrystalline matrices the (often unanalysed) variations in crystallinity can also be a source of non-linearity. Furthermore, in most cases, there are likely to be changes in dispersion, as the larger surface areas associated with high loading fractions become increasingly difficult to accommodate within the polymer; similar effects have been seen in nanoclay-filled polymers.[132] However, even in the presence of nanotube clusters, enhancements in composite stiffness can be observed.[133]

A concise overview of reported mechanical nanocomposite properties is presented by Coleman *et al.*[47] Composites based on chemically-treated nanotubes show the best results on average. This conclusion is not surprising, given that nanotube functionalisation should significantly improve both the dispersion as well as the stress transfer. In comparison to solution-based composites, the average reinforcement effect seen in melt-processed systems is somewhat disappointing, most likely reflecting alignment issues in bulk samples. Yet, the best individual results reported[134, 135] have shown stiffness improvements approaching the maximum predicted by conventional composite theories, while strength improvements are generally low. Lastly, it is interesting to note that MWCNTs appear to outperform SWCNTs in many cases, most likely reflecting the difficulties in obtaining straight, debundled SWCNTs. Compared to stiffening, enhancements in composite yield stress, strength and toughness generally appear more difficult to achieve, especially for filler loading fractions exceeding about 10 wt%. These properties depend more on the homogeneity of specimens achieved during processing, as well as on interfacial issues relating to the specific filler types and matrices. For example, the impact properties of nanofibre– polycarbonate (PC) composites are significantly decreased, even at low nanofibre contents, most likely as a result of aromatic hydrocarbons on the nanofibre surface enhancing chemical stress cracking of the polycarbonate.[136] The most prominent strength enhancements of bulk nanocomposites have been achieved for well-dispersed and aligned nanofibres in poly(ether ether ketone) (PEEK),[137] up to filler loading fractions of 10 vol%, and in PP,[95] at nanofibre loading fractions as low as 5 vol%. CNTs and CNFs are also interesting additives for tribological applications;[138, 139] they can significantly reduce the wear rate of polymers,

apparently without much dependence on the degree of dispersion achieved during compounding. Benefits are obtained even when compounded with established tribological aids, but are potentially accessible in components (such as fibres) in which conventional additives cannot be incorporated.

7.3.3 Physical properties of nanotube/nanofibre–polymer composites

As well as mechanical reinforcement, there is considerable interest in the exploitation of other physical properties of nanotubes, particularly the high thermal and electrical conductivities. Electrically conductive polymer composites, for example, are used in antistatic packaging applications, as well as in highly specialised components in the electronics, automotive and aerospace sectors. The incorporation of conductive filler particles into an insulating polymer host can lead to sufficient bulk conductivities to exceed the antistatic limit of 10^{-6} S/m. Common conductive fillers are metallic or graphitic particles in any shape (spherical, platelet-like or fibrous) and size. However, the incorporation of CNTs allows for a low percolation threshold, a high-quality surface finish, a robust network and good mechanical properties – a combination not obtained with any other filler. The use of CNTs/CNFs as a conductive filler is their biggest current application, and is widespread across the automotive and electronic sectors.

The electrical properties of nanofibre–thermoplastic composites exhibit a characteristic percolation behaviour,[140–142] with a rapid increase in conductivity as the loading fraction passes through the critical threshold. In the case of untreated CNFs, the threshold is around 5–10 vol% and depends on aspect ratio, surface chemistry, dispersion and alignment. Similarly, the electrical percolation threshold of thin MWCNT–thermoplastic films also depends on the type of nanotube and the processing route. Threshold values range from around 5 wt% for oxidised catalytic MWCNTs in PVA[101] to around 0.06 wt% and 0.5 wt% for arc-discharge MWCNTs in PVA[143] and PMMA[144], respectively. In bulk, thermosetting systems,[145–150] CNT-based composites tend to have higher conductivities and lower percolation thresholds than either carbon black or CNF-based ones. Indeed, a CNT-based epoxy system currently shows the lowest percolation threshold observed in any system, at around 0.0025 wt%.[146] It is tempting to attribute this and other low thresholds simply to the high aspect ratio of the conductive filler. However, these low values can be explained only in the light of a complicated dispersion and reaggregation behaviour during processing; in essence, well-dispersed nanotubes are destabilised and trapped just as a network forms.[151] This network formation behaviour can be manipulated not only by temperature and shear rate, but also by the application of external electrical fields.[152] Interestingly, low loading fractions of nanotubes in thin

films may allow a useful level of conductivity while retaining optical transparency.[118]

Effects to increase thermal conductivity have been less successful. Increases have been modest and linear; percolation does not play a major role due to the less dramatic difference in conductivity between filler and matrix.[95, 131, 141] Results are similar to those observed for short carbon fibres in similar systems.[141, 153]

7.4 Adding nanotubes and nanofibres to polymer fibres

The fundamental motivation for adding nanotubes to polymer fibres is similar to those outlined above for other composite systems: namely, that there is an opportunity to improve the mechanical and functional properties of the matrix by drawing on the unique properties of the nanotubes. However, there are some additional attractions. At the current stage of development, bulk nanotube composites appear to offer only comparable properties to systems reinforced with conventional chopped fibres. However, unlike the nanotubes, such conventional fillers cannot be accommodated within fine polymer fibres. Thus, CNTs/CNFs offer a new route to nano-reinforced polymer fibres, and can provide unique improvements in performance. These improvements can be significant even at the current level of development of nanotube composites, using existing commercial CVD materials, because no other established filler can compete in the confined environment of the polymer fibre.

In addition to acting as a reinforcing agent, such nanoscale fillers can also act as critical processing aids by modifying the polymer rheology; in particular, the elongational flow properties that are relevant at the high extension rates typically encountered during fibre-spinning operations.[154] Last but not least, initial work on such fibre systems requires only small quantities of nanotubes, allowing a wide range of scarce, experimental nanotube materials or modifications to be tested in composite form.[92] Polymer fibre systems thus also provide a useful test-bed for developing our understanding of nanotube composites in general and moving towards the full exploitation of their fundamental properties.

This type of basic development is additionally helped by the fact that the nanotubes tend to become aligned to the fibre axis during processing, naturally providing the optimal orientation. Perhaps most significant of all, this uniaxial orientation is almost certainly the most plausible arrangement for fully exploiting the anisotropic, intrinsic properties of the nanotubes. The aligned arrangement not only provides the optimal loading geometry, but also maximises the volume content of nanotubes, since rods pack more efficiently when aligned;[155] the ultimate (possibly unobtainable) goal of many researchers is a perfectly aligned infinite crystal of nanotubes.[156]

There are, therefore, two strands to nanotube–polymer fibre composites. On the one hand, there is interest in improving the properties of existing polymer fibre systems either by improving critical properties of high-performance fibres (see, for example, the discussion of PEEK below), or by upgrading the performance of commodity polymers to an 'engineering' standard (e.g. PP). On the other hand, there are ongoing attempts to generate fibres with an absolutely higher level of mechanical performance than any existing system, based either on improving the current top performers (such as poly(*p*-phenylenebenzobisoxazole), PBO) or by developing new, high CNT content fibres. Finally, there are interesting attempts to exploit the potential of nanotubes to produce functional fibres that can, for example, act as electronic devices.

Processing is, of course, crucially important in determining nanotube dispersion and orientation, as well as the more traditional but equally important factors associated with polymer morphology. Polymer nanocomposite fibres may be spun from solution or from the melt, often following an initial dispersion step, as discussed in Section 7.3.1 above. Much of the initial work has been exploratory in nature, and there remains considerable scope for applying the wider understanding of fibre spinning to these systems.

7.4.1 Solution spinning

Solution spinning is a widespread and attractive route for the production of polymer fibres, and has been applied to a variety of CNT systems. A particularly interesting possibility is the use of a lyotropic nematic nanotube solution as a route to a highly aligned fibre. Much of this work is directed at high loadings of nanotubes and examples include the use of surfactant-stabilised dispersions of CNTs injected into a PVA[157, 158] or poly(ether imide) (PEI)[159] bath, to form a fibre that can be handled and drawn, and the use of pure SWCNT dispersions in 'superacid'.[160, 161]

A number of other, lower-volume fraction systems have also been spun from nanotube/polymer solutions, although the 'spinning' process is often a relatively rudimentary small-scale demonstration. Solvent routes are particularly attractive for SWCNTs as pure melt-mixing does not lead to adequate exfoliation of the bundles; matrix/solvent (maximum CNT content) examples include polyaniline/dichloroacetic acid (0.3%),[162] chitosan/water (4.8%),[163] polyacrylonitrile/*N*, *N*-dimethylformamide (DMF) (1%)[164] and PVOH/DMSO/H_2O (polyvinyl alcohol/dimethylsulphoxide/water) (3%),[165] although the highest content system[163] was poorly dispersed. An interesting variant is based on the use of caprolactam as both solvent and monomer for an *in-situ* ring opening polymerisation of nylon-6 to produce nanocomposite fibres (1.5%).[166] More straightforwardly, the *in situ* polymerisation can be carried out in the presence of the solvent before spinning, as in the case of SWCNTs added to the rigid rod polymer PBO.[116] Lastly, both MWCNTs and CNFs

have also been processed into polyetherketone (PEK) fibres following an *in situ* polymer grafting reaction (10%).[167]

It is also possible to produce nano-reinforced polymer fibres by electrospinning nanotube polymer solutions;[168] however, this topic will not be discussed further as it is covered at length elsewhere in this book (see Chapters 1–5)

7.4.2 Melt spinning

The majority of nanotube/nanofibre-filled thermoplastic fibres are made by variants of melt spinning, or approximations based on sample collection from rheometers and the like, representing an optimisation of previous alignment approaches based on die designs[95] and simple melt strand or film stretching.[91] While conventional melt processing of the nanocomposite dope is desirable for economical reasons, initial solution-blending is often performed in the case of SWCNT-filled polymers,[120, 121] yet the effectiveness of this approach remains debatable.

Although the amount of nanocomposite material is often limited, the principal applicability of traditional fibre processing technology for the manufacture of nanotube/nanofibre-filled systems has been demonstrated. As such, most studies have focused on low to medium draw ratios and a whole range of fibre diameters ranging from a few to hundreds of micrometres. In addition, experimental efforts aimed at maximising alignment of both filler and matrix are still at early stages; initial cold- and hot-drawing approaches following spinning have not yet been optimised. It can be anticipated that production techniques will improve as a more fundamental understanding of nanocomposite rheology and thermal properties emerges and more nanocomposite material is prepared.

7.5 Analysing the rheological properties of nanotube/nanofibre–polymer composites

The addition of a nanofiller to a polymer melt can significantly affect the rheological properties; in certain cases, both processing and final composite properties can be enhanced with the same filler. To date, rheological studies of nanotube/nanofibre-filled systems have focused mainly on the shear behaviour;[88, 136, 140, 169–171] however, shear tests alone cannot characterise the melt elongation properties that are important for foaming, film-blowing or fibre-spinning processes. There are as yet limited data available on the elongational viscosity of nanocomposite melts at low extension rates related to foaming processes[172, 173] and very little[174] at the high extension rates typically encountered during fibre-spinning operations. In addition, interactions between filler and melt occurring during processing can also

have pronounced impacts on the resulting matrix morphology[129, 154] (see Section 7.6.1).

7.5.1 Shear properties

For particle-filled thermoplastic melt systems, oscillatory shear experiments are common and avoid issues with time-dependent alignment effects. As expected, the shear viscosity of such nanocomposites generally increases with loading fraction, to an extent that depends on the nature of the filler and matrix. Percolation effects have been observed, generally at low shear, although even low nanotube concentrations can lead to significant viscosity increases;[170] at high shear rates, thinning associated with the polymer dominates, particularly if the filler can fragment. For example, CNF loadings up to 10 wt% had no significant influence on the shear viscosity of PP[140] and PEEK[154] composites in the shear rate regime typically encountered during thermoplastic processing. In case of a PC matrix, the shear viscosity was even reduced with increasing nanofibre content up to 10 wt%,[136] most likely as a result of pronounced shear alignment of the filler, a well-known behaviour for short fibre-filled polymers.[175]

With increasing strain amplitude, nanotubes and nanofibres gradually align parallel to the flow direction, thus reducing the tube–tube or fibre–fibre interactions, as it has been observed in nanoclay systems.[176] The formation or presence of filler network structures and/or aggregates at elevated contents is reflected by a pronounced increase in shear viscosity, especially at low shear rates (Fig. 7.5 shows the behaviour of nanofibre reinforced PEEK as an example.[154] Such behaviour is typical for highly filled nanoparticulate systems, independent of filler type and geometry[140, 170, 171] and is associated with a transition to an elastic pseudo solid-like response. This rheological percolation threshold depends on the nanotube/nanofibre type and treatment as well as on the polymer matrix and generally indicates the onset of interactions between individual filler particles or clusters. Often (for example the PEEK system shown in Fig. 7.5), strong shear thinning is observed;[154] the effect can be attributed to the alignment of the nanofibres which, given their large size and rigidity, will experience a larger torque and have longer relaxation times than the polymer molecules. It is also interesting to note that melt-compounded nanocomposites tend to have similar rheological and electrical thresholds,[154] although nanocomposites prepared by the coagulation method[177, 178] have shown relatively lower rheological thresholds; an effect that is attributed to the fact that denser nanotube networks are required to achieve electrical conductivity than to restrict polymer motion.

The comparatively high rheological percolation threshold (between 10 and 15 wt%) observed for this particular PEEK/CNF system (Fig. 7.5) is in agreement with studies on similar systems[140, 169] but is much higher than that

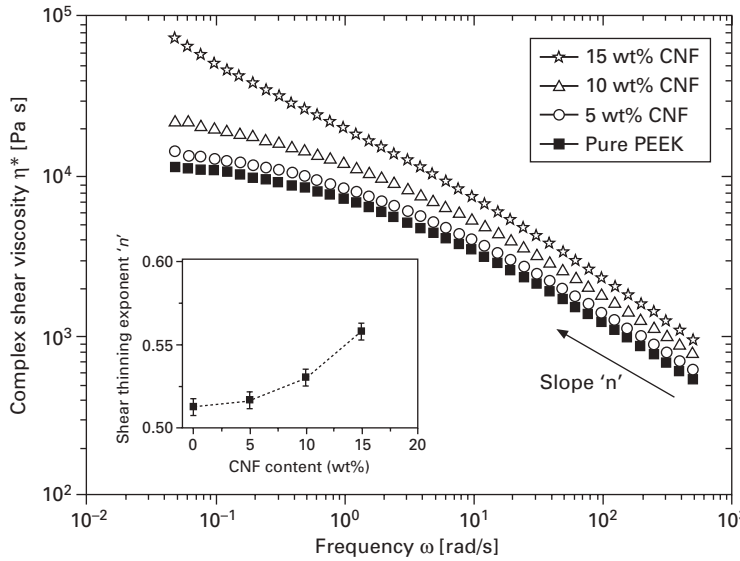

7.5 Complex shear viscosity of carbon nanofibre reinforced PEEK composites as a function of frequency, at a temperature of 360 °C, in the linear viscoelastic regime. The insert shows the resulting shear thinning exponent as a function of nanofibre content.

observed in many MWCNT-filled thermoplastics.[170, 171, 179] The most likely explanation is that the CNF aspect ratio is much more significantly degraded during processing owing to their larger absolute dimensions and lower strength. Comparison with the classic Guth equation[180] suggests an aspect ratio of 15, much lower than that of the as-grown CNFs. Yet, degradation of aspect ratio during processing has also been reported by Kuriger *et al.*[95] and Kharchenko *et al.*,[179] investigating both CNF- and MWCNT-filled PP, respectively, as well as by Ma *et al.*[181] evaluating melt-spun CNF/polyethylene terephthalate (PET) fibres.

7.5.2 Elongational properties

Although-the shear rheology data do not indicate any particular degradation of melt processability when adding such carbon nanofillers, they do not explain variations in flow behaviour or microstructure arising from elongation of the melt as it occurs during foaming,[182] fibre-spinning,[183] and film blowing.[184] Uniaxial extension at high strain rates relevant for fibre-spinning can be explored using the Rheotens test:[185] the force required to elongate a melt strand is measured as a function of a linearly accelerated draw-down velocity, under quasi-isothermal conditions.[186] The force required to rupture

the strand is commonly defined as the 'melt strength' and the maximum draw-down velocity or draw-down ratio is defined as the 'elongation to failure' or 'drawability'.

The experimental data shown in Fig. 7.6 clearly highlight a substantial increase in PEEK melt strength and drawability with increasing nanofibre content, effects that can be attributed to a 'reinforcement' of the melt.[154] A direct conversion of such Rheotens data into an elongational viscosity is complex[187, 188] but it is possible to compare the drawing behaviour of different polymer nanocomposites at defined experimental conditions.[189] For the PEEK–CNF system, the calculated elongational viscosity (Fig. 7.7) indicates an increase in initial elongational viscosity and an earlier onset of elongational thinning with increasing CNF content. Thus, the processing window relevant for operations such as foaming and fibre-spinning can be usefully adjusted. Both the increasing melt strength as well as the higher drawability of the PEEK nanocomposites explain the relatively good melt-spinnability of this system.[190] In general, such effects may also allow significantly finer filaments to be spun, in the future, without early rupture of the melt strand. For example, fine nanofibre-reinforced polyester PET fibres with diameters as low as 25 µm have been produced under stable conditions.[181]

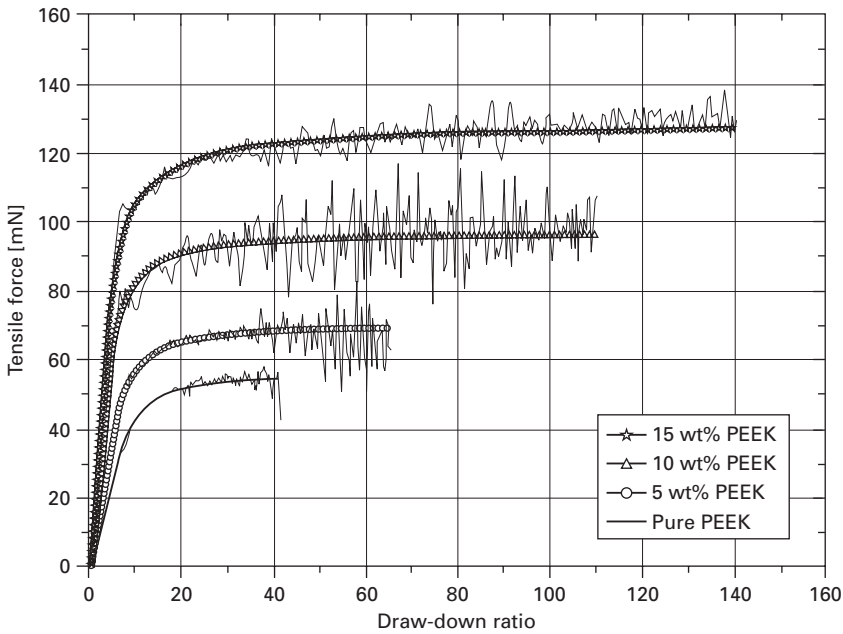

7.6 Experimental average Rheotens curves for PEEK–CNF nanocomposites at 360 °C. The lines represent a Levenberg–Marquardt fit of the data according to Wagner *et al.*[187]

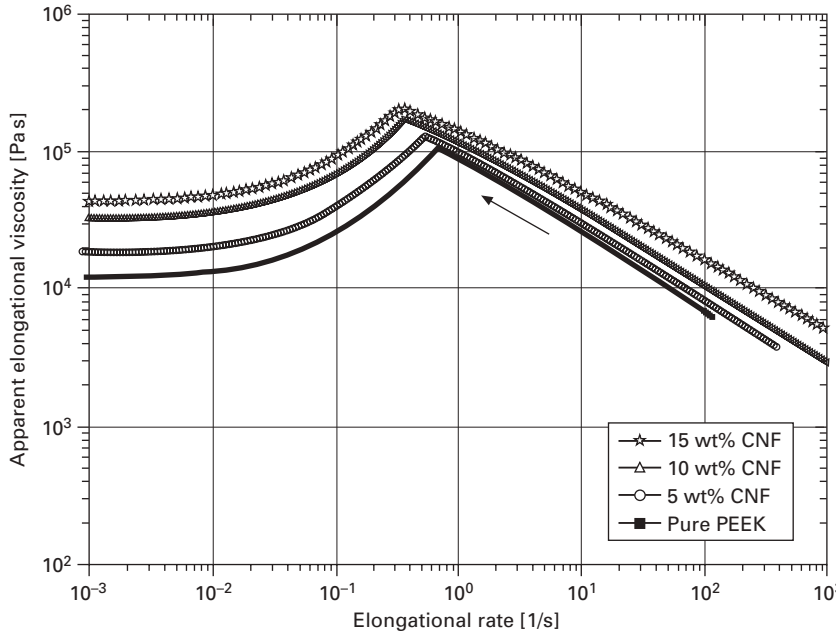

7.7 Apparent elongational viscosity as a function of elongation rate for carbon nanofibre reinforced PEEK at 360 °C, calculated using the Wagner model.[187]

7.6 Analysing the microstructure of nanotube/nanofibre–polymer composites

As outlined in Section 7.4, most experimental approaches towards nanocomposite fibre spinning are still at early stages, operating on small-scale material quantities. These initial attempts have, nevertheless, demonstrated a significant potential of producing good-quality nanocomposite fibres. Obviously, as in the case of bulk nanocomposites, both the general melt or solution spinnability as well as the fibre surface finish are strongly related to the quality of nanofiller dispersion achieved during processing prior to spinning. Both the use of highly entangled raw nanotube materials, as well as insufficient shear mixing or excessive post-shear reagglomeration, lead to clusters which can prohibit melt-spinning completely[191] or induce rather low-quality fibre surfaces.[92] Rather than reinforcing the melt and even enhancing its drawability[154] as highlighted in Section 7.5.2, nanofibre or nanotube agglomerates induce significant stress concentrations leading to a severe reduction of melt elongation. Intermediate levels of dispersion or the presence of very small agglomerates induce voids, rough surface finishes and/or diameter variations,[92] as illustrated in Fig. 7.8.

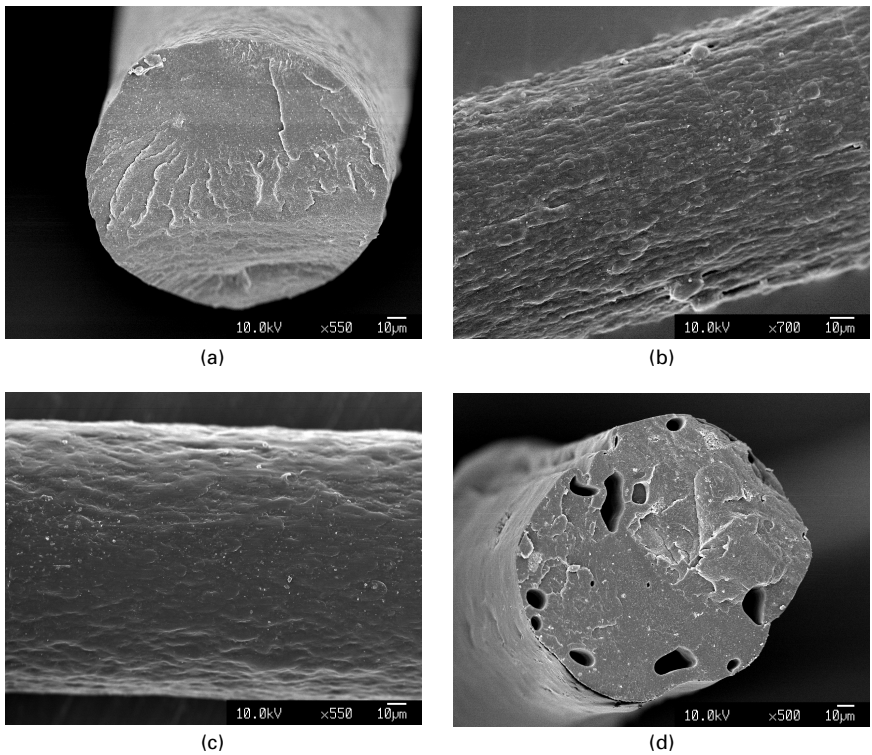

7.8 Comparative SEM micrographs of melt-spun polyamide-12 nanocomposite fibres containing (a) 10 wt% CNFs, (b) 10 wt% entangled catalytic MWCNTs, (c) 5 wt% aligned CVD MWCNTs, and (d) 5 wt% arc-grown MWCNTs. Reproduced from Ref. 92.

The variations in fibre quality can be directly related to the nanotube/nanofibre dispersion which, in turn, reflects the condition of the as-produced materials. Arc-grown material often is fused together by contaminating graphite; catalytically-grown MWCNTs separate well given sufficient shear forces but often retain some entanglements, while straighter and unentangled CVD-grown MWCNTs and most nanofibre types disperse most successfully.

Efforts aimed at spinning SWCNT-reinforced composite fibres face related difficulties. At high loading fractions, exceeding a few weight percent, variations in the rheological behaviour prevent uniform and stable melt-spinning conditions.[192] Furthermore, debundling of the SWCNTs remains a challenge; even solvent-blending prior to melt-compounding and spinning did not lead to individually dispersed nanotubes in polycarbonate fibres.[121] Nevertheless, some successful nanotube-filled fibres have been spun at lower loading fractions.[120, 193]

7.6.1 Matrix microstructure

As mentioned before, the addition of carbon nanotubes and nanofibres to a polymer matrix can have significant implications on the resulting matrix microstructure. In the case of semicrystalline thermoplastics especially, crystallisation kinetics are often strongly affected by high surface area fillers, altering the degree of crystallinity, the crystalline orientation, and even the preferred crystal structure. The impact of CNTs and CNFs in highly oriented systems such as nanocomposite fibres has not yet been fully established, although related behaviour is known for conventional additives such as colouring pigments.[194] Such effects are critical to the understanding of nanocomposite performance in general, but are too often ignored when evaluating the observed improvements in fibre properties with regard to the intrinsic properties of the filler. In the case of polyvinyl alcohal (PVOH), it has been suggested that ordering of PVOH around CNTs is the dominant determinant of the mechanical performance, rather than direct reinforcement.[195]

As for conventional polymer fibres, spectroscopy, diffraction[196] and thermal analysis are commonly used to evaluate the final matrix microstructure of the nanocomposite fibre. As in the bulk case, significant variations in these microstructural features have been observed in semicrystalline fibre systems, depending on the filler type, treatment and content, as well as on the specific processing conditions. An example for melt-spun PEEK–CNF fibres is shown in Fig. 7.9; the differential scanning calorimetry (DSC) data indicate a significant increase in matrix crystallinity with the addition of nanofibres, although apparently independently of filler content. The two-chain orthorhombic crystal I form of PEEK usually seen for melt-spun and annealed monofilaments[197] is maintained for the nanocomposites,[190] yet the increased glass transition temperature of the neat polymer fibre (Fig. 7.9) strongly implies a significant variation in molecular alignment prior to quenching, in agreement with the elongational rheology behaviour of this particular system discussed in Section 7.5.2. In polyamide[92] and polypropylene[193] nanocomposite fibres, nucleation effects of the additives were observed, although no changes in the favoured crystal structure were reported.

Laser Raman spectroscopy as well as wide-angle X-ray diffraction are commonly used for the characterisation of SWCNT and MWCNT/CNF alignment, respectively; although quantitative interpretation of the data can be challenging. For example, in the case of carbon nanofibres,[92, 181, 190] an apparent lower degree of alignment is often determined from 2D wide-angle X-ray scattering (WAXS) patterns due to misalignment of the graphitic planes relative to the nanofibre axis (Section 7.1). In polypropylene fibres for example,[198, 199] evaluation is further complicated by the superposition of graphitic and polymer peaks. Raman spectroscopy yields a much stronger signal when polarised parallel to the nanotube axis, and, once calibrated, can

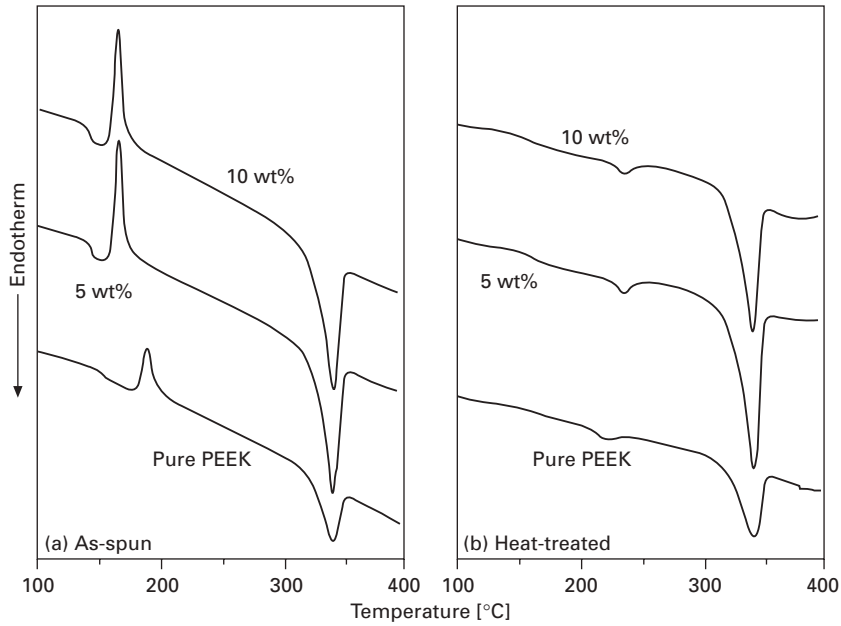

7.9 Representative DSC traces of melt-spun PEEK–CNF fibres, (a) after melt-spinning and (b) following subsequent annealing at 220 °C, obtained on composite fibre bundles heated at 10 °C/min. Curves have been shifted for clarity.

indicate degree of alignment; an example of the resulting data for SWCNTs[121] is shown in Fig. 7.10.

As expected, overall, the data suggest a greater degree of both nanotube/nanofibre and polymer alignment in fibre systems than in bulk nanocomposites. Some discrepancies remain, reflecting the significant variations in materials, experimental conditions and data analysis techniques. Filler alignment in general appears to critically depend on the quality of the initial dispersion, independently of processing technology; the lack of additional alignment of multiwalled structures during cold-drawing[92] suggests that the nanofillers are fully aligned by the relatively low draw ratios applied during melt-spinning; the remaining misorientation is likely to reflect both the misorientation of the graphitic layers, and the intrinsic 'waviness' of the CNTs/CNFs. That the nanofillers align easily is not suprising given their large size, long relaxation times and rigidity compared to the matrix polymer, and is consistent with the rheology data discussed above. The intrinsic 'waviness' that is characteristic of CVD-grown material and that cannot apparently be removed, at least for multiwalled structures, is likely to have a major, limiting effect on the maximum performance that can be achieved.[200] In principle, more flexible SWCNT bundles may suffer from this effect to a lesser extent, but data so far seem to suggest a similar behaviour both in solution and in the melt.

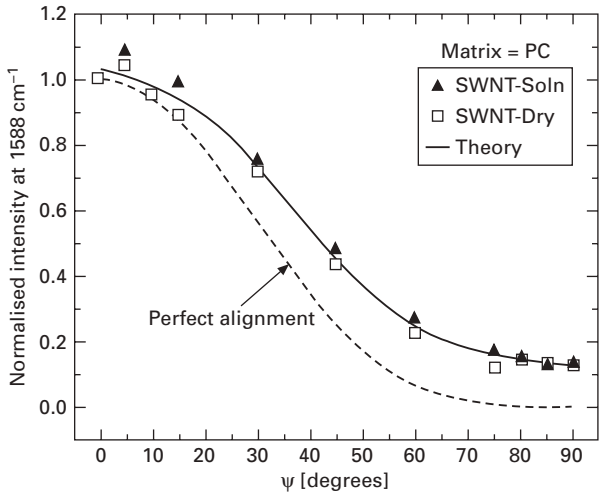

7.10 Raman intensity of the tangential mode at 1588 cm^{-1} of SWCNTs in melt-spun PC fibres, containing 5 wt% of SWCNTs, as a function of the fibre angle. Reproduced from Ref[121] The dashed line represents the relationship between relative intensity and fibre angle for perfect or unidirectional alignment of SWCNTs along the fibre axis. The label 'SWNT-Soln' refers to an initially solution-blended SWCNT/PC system that was subsequently extruded and melt-spun in an identical manner to the 'SWCNT-Dry' sample.

7.7 Mechanical, electrical and other properties of nanocomposite fibres

As outlined above, well-dispersed nanotubes and nanofibres tend to align with the molecular flow and can experience a significant load transfer in the molten state during fibre spinning.[154] Such reinforced melt systems show a good spinnability, leading to high-quality fibres even at elevated draw ratios. Similarly, the drawability and strain to failure of both as-prepared and treated solid-state nanocomposite fibres also critically depend on the quality of the filler dispersion, alignment and interfacial bonding. As an example, the stress–strain behaviour of both as-prepared and annealed melt-spun PEEK–CNF composite fibres is shown in Fig. 7.11.[190] In most fibre systems, stiffness and strength increase, but strain to failure decreases with increasing filler entanglement and content. However, for some high loading fraction, solution-spun fibres and significant improvements in fibre toughness have been reported.[157, 158]

Overall, there is considerable variability in the published mechanical data due to the largely different systems and experimental approaches. Nevertheless, a tentative comparison of data for melt-spun fibres to the typical data for bulk systems processed in the melt (see Section 7.5.2)[47, 201] indicates a more

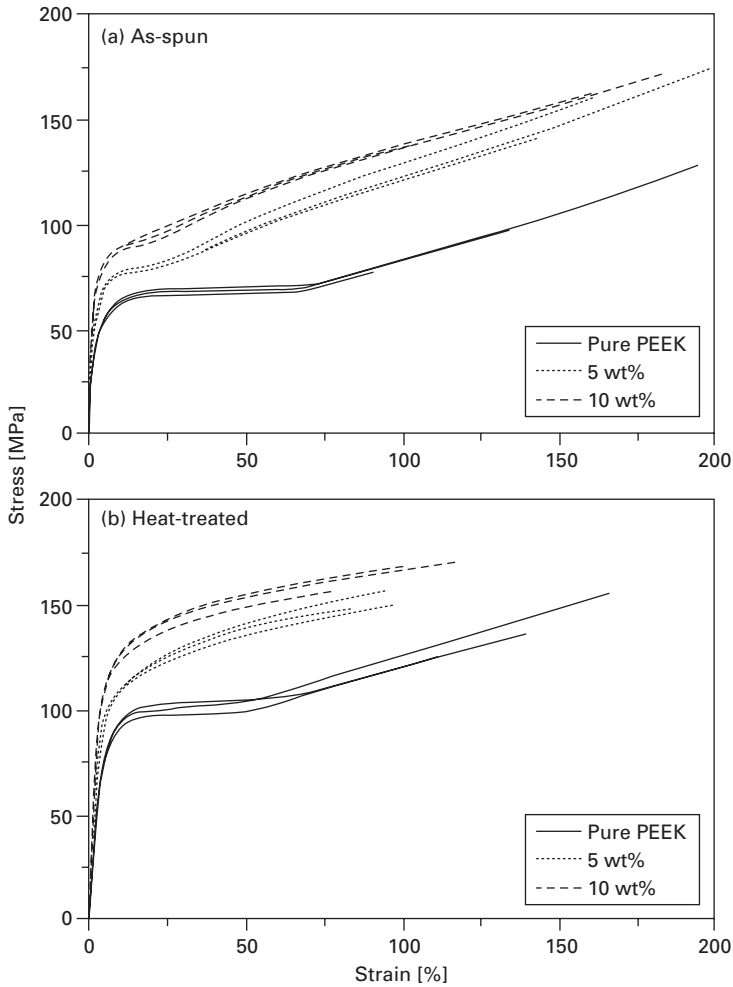

7.11 Representative engineering stress–strain diagrams of (a) as-spun and (b) heat-treated PEEK–CNF nanocomposite fibres as a function of nanofibre content. (Tensile tests were based on a constant force ramp.[190])

pronounced reinforcement in fibrous nanocomposites. This observation can be attributed to the improved alignment of the filler to the loading direction; a conventional short fibre interpretation based on the Krenchel model suggests that orientation efficiency of nanofibres may behave similarly[137] although issues of fibre waviness are also important.[200]

As in the case of bulk nanotube composites, absolute values of the mechanical properties are mostly disappointing relative to the expectations generated by the mechanical properties of perfect nanotubes; the reasons are

likely to be similar: the relative imperfection of the CVD nanotubes used, difficulties with dispersion, and the need to optimise interfacial stress transfer without chemically damaging the nanotubes. A detailed analysis of the literature is complicated, as variations in the polymer microstructure, particularly of semicrystalline matrices, have not always been considered. Yet there is evidence that, all else being equal, the crystalline quality of the filler is important[92] with dispersed MWCNTs outperforming CNFs; Fig. 7.12, for example, summarises the fibre modulus and yield stress for melt-spun polyamide-12

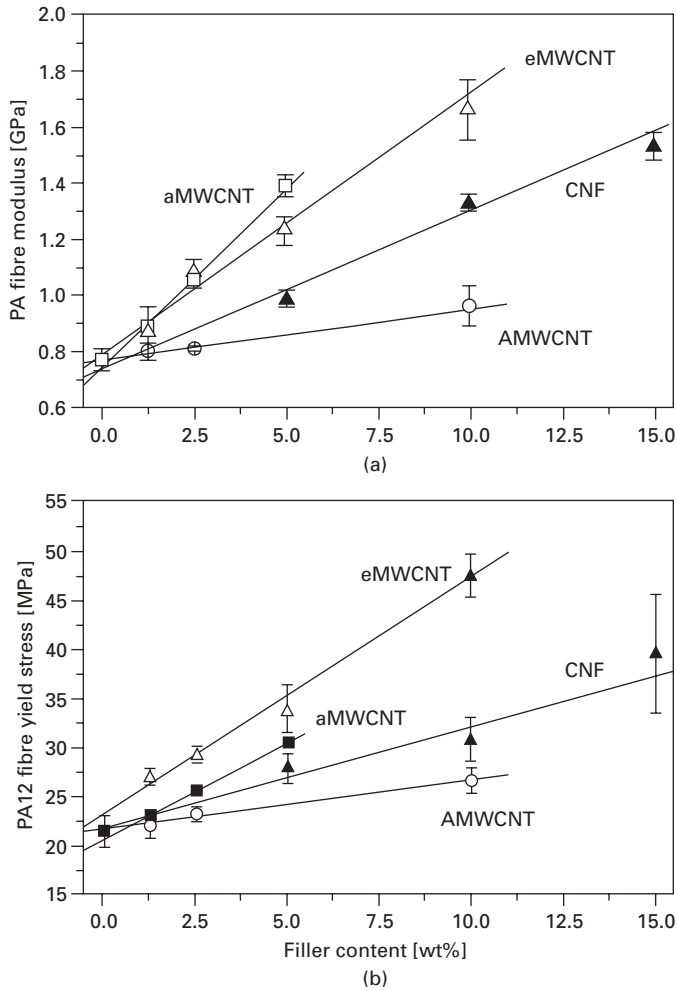

7.12 Plots summarising the relationship between (a) tensile modulus and (b) yield stress of melt-spun polyamide-12 nanocomposites and nanoscale filler weight fraction for CNFs, arc-grown (aMWCNT) entangled (eMWCNT) and aligned (aMWCNT) multiwall structures. (Tensile tests were based on a constant force ramp.[92])

nanocomposite fibres containing different multiwalled fillers. It is not yet clear what size of nanotube will prove to be ideal; small diameter MWCNTs may be the best choice, as higher loading fractions of individual tubes can be realised as compared to most SWCNT systems, while retaining a relatively high degree of perfection and surface area.

The deformation micro-/nano-mechanics of such fibrous nanocomposites are only slowly emerging; the picture is complicated by the quite pronounced variations in matrix microstructure following nanocomposite spinning. Some attempts have been made both to determine interfacial phenomena and to define the laws that govern their properties, for instance, the nanoscale scaling of flaw violations.[202] However, the main focus remains on experimental methodologies to study the evolution of the microstructure during deformation. Laser Raman spectroscopy, for example, not only delivers static information regarding the local dispersion and alignment of nanotubes within a fibre, but also allows mapping of the local deformation in a composite by following the molecular deformation of the reinforcement.[203] These molecular deformations are evidenced by a shift in Raman band position as a function of stress or strain applied to the composite during *in-situ* deformation experiments and sensitively highlight nanotube/matrix interactions and the degree of load transfer.[204, 205] Alternatively, synchrotron X-ray sources can be used to study more explicitly the relationship of polymer and filler deformation and orientation, using a combination of small- and wide-angle studies.[206, 207] For example, functionalised SWCNTs have been shown to suppress the reconstruction of lamellae stacks in poly(ethylene-propylene) fibres.[114] Although individual polymer systems will need to be studied in detail, such techniques will shed light on the filler/matrix interactions in nanotube/nanofibre composite fibres and may lead to new micromechanical concepts for polymer fibre deformation in general.

7.7.1 Electrical properties

A range of interesting properties beyond straightforward mechanical reinforcement are expected.[208] One interesting possibility is that nanotube-filled fibres may provide convenient, robust, electrically conductive textiles for a range of 'intelligent' applications, although the simplest advantage may be in electrostatic dissipation. Static build-up in textiles is not only be uncomfortable but can be dangerous in many industrial environments. Existing alternative approaches include post-spinning coating with nanoparticles[209] or intrinsically conductive polymers,[210] but often lack cohesion and long-term stability. As in the case of bulk nanocomposites, carbon nanotubes/nanofibres are well suited to the formation of electrically conductive percolating networks (see Section 7.3.3 above). In principle, a good dispersion of high aspect ratio nanotubes can percolate at modest loadings, although the alignment

of straight nanotubes is expected to increase the percolation threshold.[155] In reality, the intrinsic curvature and waviness of dispersed nanotubes, although detrimental for mechanical reinforcement, is beneficial for percolation. Nevertheless, the alignment induced by spinning has been shown to reduce or remove the conductivity observed in the bulk nanocomposites for both PC[211] PP[213].

An early study in 1999 highlighted a significant decrease in volume resistivity of an isotropic pitch fibre containing 5 wt% of SWCNTs.[192] Yet, SWCNT loading fractions of up to 10 wt% did not induce a measurable improvement in conductivity of rigid-rod PBO polymer fibres prepared by solution-spinning, again taken as evidence for a high degree of filler alignment.[116] For comparison, solution-spun polyamide-11 fibres containing intrinsically conductive polyaniline showed a percolation threshold at around 5 wt% due to phase separation and fibrillation.[212] In this case, the fibre conductivity even increased with increasing draw ratio, whereas nanofibre-filled PP fibres showed the reverse trend,[213] as highlighted by the normalised current–voltage characteristics of such PP–CNF nanocomposite fibres shown in Fig. 7.13. Yet, a promising compromise between electrical and mechanical properties was attained at relatively low filler contents, verifying the potential of using such carbon nanostructures to accomplish electrically conductive thermoplastic fibres.

7.7.2 Other properties

An important feature of nanocomposite fibres is the reduced axial shrinkage[116, 214] during both spinning and post-treatments, although these

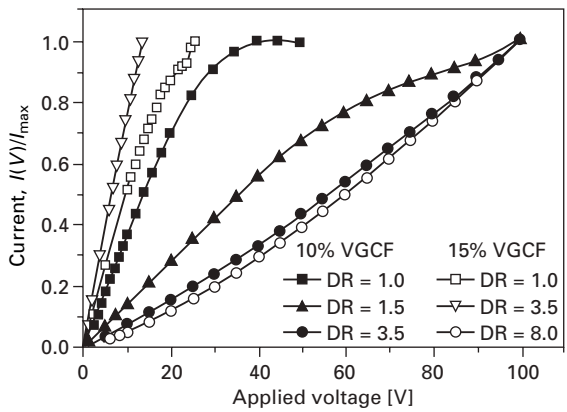

7.13 Normalised current–voltage characteristics of melt-spun PP fibres containing 10 and 15 vol% of carbon nanofibres drawn to different draw ratios (DR). Reproduced from Ref. 213.

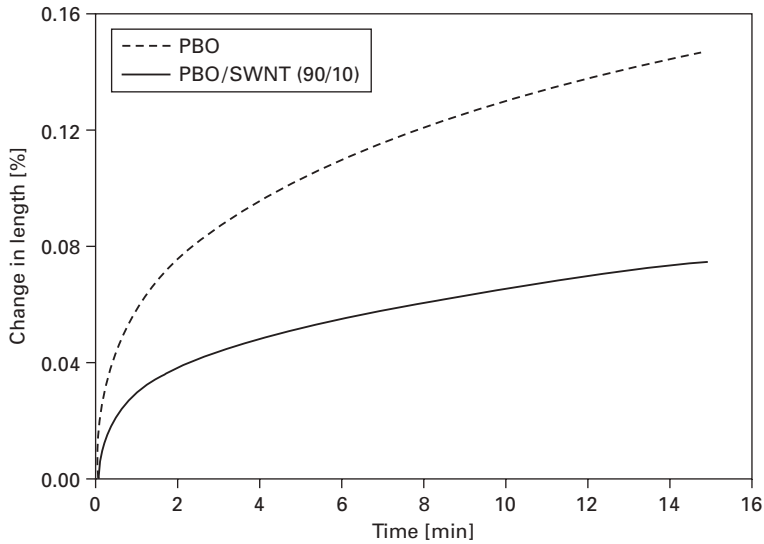

7.14 Creep behaviour of neat PBO and PBO nanocomposite fibres containing 10 wt% of SWCNTs at 400 °C and a stress of 250 MPa. Reproduced from Ref. 116.

effects may be particularly pronounced due to the preliminary nature of the spinning studies. The ability of the nanofillers to constrain the polymer matrix will strongly depend on the dispersion and polymer microstructure,[215] as well as on the effective surface area and chemical interactions. One positive example is the significantly improved axial creep behaviour of solution-spun high-performance PBO fibres containing 10 wt% of SWCNTs at elevated temperatures, shown in Fig. 7.14.[116]

Enhancements in other properties such as flame retardance,[216] wear resistance,[138] and thermal conductivity[95, 131, 141] have been observed in bulk nanocomposite systems and are likely to be relevant to polymer fibres, although they are, as yet, much less thoroughly investigated. Indeed, the wear improvement observed in PEEK[138] is already in a system that can be spun into fibres.[190]

7.8 Future trends

The introduction of nanotubes and nanofibres into polymer fibres is an appealing prospect, and a natural embodiment of this nanocomposite system. As discussed in the motivation section (Section 7.4) above, there is scope to provide immediate mechanical enhancements, using existing nanotube and nanofibre materials, that cannot be obtained using other fillers. Nanocomposite fibres may represent a useful and early mechanical application of carbon

nanomaterials. In addition, the presence of the nanofiller, if well dispersed, may aid the spinning process by increasing the melt strength and/or drawability of the polymer. While developing these potentially useful systems, a number of challenges associated with nanotube composites in general can be addressed.

The long-term goal must be to access the properties of individual perfect nanotubes on a macroscopic scale. As in the case of bulk applications, the performance of such fibrous nanocomposites critically depends on the quality of nanostructure dispersion achieved prior to spinning and drawing. The manufacture of nanocomposite fibres with uniform diameter and good surface finish relies on well-dispersed filler particles, even at low draw ratios. Methods to improve both dispersion and to optimise the interface between polymer and filler are emerging, based particularly on chemical functionalisation of the surfaces. Probably the most central remaining difficulty is to identify the nature of the ideal nanotube for use in composites and then to synthesise sufficiently large quantities at low enough cost for practical usage. Although a variety of synthesis methods now exist to produce carbon nanotubes and nanofibres, the products differ greatly in terms of diameter, aspect ratio, crystallinity, crystalline orientation, purity, entanglement, surface chemistry and straightness. These structural variations dramatically affect intrinsic properties, processing and behaviour in composite systems. However, it is not yet clear which type of nanotube material is most suitable for composite applications, nor is there much theoretical basis for rational design. Ultimately, the selection will depend on the matrix material, processing technology and the property enhancement required. Further comparative studies are needed, together with theoretical understanding of the nanomechanical mechanisms at work and their interaction with the polymer microstructure. Many questions remain outstanding but there are rich rewards to be gained, if the true potential of carbon nanotubes can be harnessed.

7.9 References

1. Ebbesen, T., '*Carbon Nanotubes, Preparation and Properties*', CRC Press, Boca Raton (1997)
2. Krätschmer, W., Lamb, L.D., Fostiropoulos, K., Huffmann, D.R. 'Solid C_{60}: A new form of carbon', *Nature* **347**(6291) (1990), 354–358
3. Kroto, H.W., Heath, J.R., O'Brian, S.C., Curl, R.F., Smalley, R.E. 'C_{60}: Buckminsterfullerene', *Nature* **318**(6042) (1985), 162–163
4. Oberlin, A., Endo, M., Koyama, T. 'Filamentous growth of carbon through benzene decomposition', *J. Cryst. Growth* **32**(3) (1976), 335–349
5. Monthioux, M., Kuznetsov, V.L. 'Who should be given the credit for the discovery of carbon nanotubes?', *Carbon* **44**(9) (2006), 1621–1623
6. Esquivel, E.V., Murr, L.E. 'A TEM analysis of nanoparticulates in a Polar ice core', *Mater. Charact.* **52**(1) (2004), 15–25
7. Reibold, M., Paufler, P., Levin, A.A., Kochmann, W., Pätzke, N., Meyer, D.C. 'Carbon nanotubes in an ancient Damascus sabre', *Nature* **444**(7117) (2006), 286

8. Zheng, L.X., O'Connell, M.J., Doorn, S.K., Liao, X.Z., Zhao, Y.H., Akhadov, E.A., Hoffbauer, M.A., Roop, B.J., Jia, Q.X., Dye, R.C., Peterson, D.E., Huang, S.M., Liu, J., Zhu, Y.T. 'Ultralong single-wall carbon nanotubes', *Nature Mater*. **3**(10) (2004), 673–676
9. Meyyappan, M., '*Carbon Nanotubes: Science and Applications*', CRC Press, Boca Raton (2005)
10. Tersoff, J., Ruoff, R.S. 'Structural properties of a carbon-nanotube crystal', *Phys. Rev. Lett*. **73**(5) (1994), 676–679
11. Bethune, D.S., Kiang, C.H., de Vries, M.S., Gorman, G., Savoy, R., Vazquez, J., Beyers, R. 'Cobalt-catalysed growth of carbon nanotubes with single-atomic-layer walls', *Nature* **363**(6430) (1993), 605–607
12. Journet, C., Master, W.K., Bernier, P., Loiseau, A., Lamy de la Chapelle, M., Lefrant, S., Deniard, P., Lee, R., Fischer, J.E. 'Large-scale production of single-walled carbon nanotubes by the electric-arc technique', *Nature* **388**(6644) (1997), 756–758
13. Thess, A., Lee, R., Nikolaev, P., Dai, H., Petit, P., Robert, J., Xu, C., Lee, Y.H., Kim, S.G., Rinzler, A.G., Colbert, D.T., Scuseria, G.E., Tomanek, D., Fischer, J.E., Smalley, R.E. 'Crystalline ropes of metallic carbon nanotubes', *Science* **273**(5274) (1996), 483–487
14. Cheng, H.M., Li, F., Su, G., Pan, H.Y., He, L.L., Sun, X., Dresselhaus, M.S. 'Large-scale and low-cost synthesis of single-walled carbon nanotubes by the catalytic pyrolysis of hydrocarbons', *Appl. Phys. Lett*. **72**(25) (1998), 3282–3284
15. Endo, M., Takeuchi, K., Igarashi, S., Kobori, K., Shiraishi, M., Kroto, H.W. 'The production and structure of pyrolytic carbon nanotubes (PCNTs)', *J. Phys. Chem. Solids* **54**(12) (1993), 1841–1848
16. Sandler, J.K.W., Kirk, J.E., Kinloch, I.A., Shaffer, M.S.P., Windle, A.H. 'Ultra-low electrical percolation threshold in carbon-nanotube–epoxy composites', *Polymer* **44**(19) (2003), 5893–5899
17. Ebbesen, T.W., Ajayan, P.M. 'Large-scale synthesis of carbon nanotubes', *Nature* **358**(6383) (1992), 220–222
18. Colbert, D.T., Zhang, J., McClure, S.M., Nikolaev, P., Chen, Z., Hafner, J.H., Owens, D.W., Kotula, P.G., Carter, C.B., Weaver, J.H., Rinzler, A.G., Smalley, R.E. 'Growth and sintering of fullerene nanotubes', *Science* **266**(5188) (1994), 1218–1222
19. Cadek, M., Murphy, R., McCarthy, B., Drury, A., Lahr, B., Barklie, R.C., in het Panhuis, M., Coleman, J.N., Blau, W.J. 'Optimisation of the arc-discharge production of multi-walled carbon nanotubes', *Carbon* **40**(6) (2002), 923–928
20. Rinzler, A.G., Liu, J., Dai, H., Nikolaev, P., Huffman, C.B., Rodriguez-Macias, F.J., Boul, P.J., Lu, A.H., Heymann, D., Colbert, D.T., Lee, R.S., Fischer, J.E., Rao, A.M., Eklund, P.C., Smalley, R.E. 'Large-scale purification of single-wall carbon nanotubes: process, product, and characterization', *Appl. Phys. A* **67**(1) (1998), 29–37
21. Endo, M., Takeuchi, K., Igarashi, S., Kobori, K., Shiraishi, M., Kroto, H.W. 'The production and structure of pyrolytic carbon nanotubes (PCNTs)', *J. Phys. Chem. Solids* **54**(12) (1993), 1841–1848
22. Rao, C.N.R., Govindaraj, A., Sen, R., Satishkumar, B.C. 'Synthesis of multi-walled and single-walled nanotubes, aligned-nanotube bundles and nanorods by employing organometallic precursors', *Mater. Res. Innovat*. **2**(3) (1998), 128–141.
23. Andrews, R., Jacques, D., Rao, A.M., Derbyshire, F., Qian, D., Fan, X., Dickey,

E.C., Chen, J. 'Continuous production of aligned carbon nanotubes: A step closer to commercial realization', *Chem. Phys. Lett*. **303**(5–6) (1999), 467–474
24. Tibbetts, G.G., Gorkiewicz, D.W., Alig, R.L. 'A new reactor for growing carbon-fibers from liquid-phase and vapor-phase hydrocarbons', *Carbon* **31**(5) (1993), 809–814.
25. Treacy, M.M.J., Ebbesen, T.W., Gibson, J.M. 'Exceptionally high Young's modulus observed for individual carbon nanotubes', *Nature* **381**(6584) (1996), 678–680
26. Krishnan, A., Dujardin, E., Ebbesen, T.W., Yianilos, P.N., Treacy, M.M.J. 'Young's modulus of single-walled nanotubes', *Phys. Rev. B* **58**(20) (1998), 14013–14019
27. Falvo, M.R., Clary, G.J., Taylor, R.M., Chi, V., Brooks Jr., F.P., Washburn, S., Superfine, R. 'Bending and buckling of carbon nanotubes under large strain', *Nature* **389**(6651) (1997), 582–584
28. Wong, E.W., Shehan, P.E., Lieber, C.M. 'Nanobeam mechanics: elasticity, strength and toughness of nanorods and nanotubes', *Science* **277**(5334) (1997), 1971–1975
29. Yu, M.-F., Lourie, O., Dyer, M.J., Moloni, K., Kelly, T.F., Ruoff, R.S. 'Strength and breaking mechanism of multiwalled carbon nanotubes under tensile load', *Science* **287**(5453) (2000), 637–640
30. Yu, M.-F., Files, B.S., Arepalli, A., Ruoff, R.S. 'Tensile loading of ropes of single wall carbon nanotubes and their mechanical properties', *Phys. Rev. Lett*. **84**(24) (2000), 5552–5555
31. Nardelli, M.B., Yakobson, B.I., Bernholc, J. 'Brittle and ductile behavior in carbon nanotubes', *Phys. Rev. Lett*. **81**(21) (1998), 4656–4659
32. Lourie, O., Cox, D.M., Wagner, H.D. 'Buckling and collapse of embedded carbon nanotubes', *Phys. Rev. Lett*. **81**(8) (1998), 1638–1641
33. Wagner, H.D., Lourie, O., Feldmann, Y., Tenne, R. 'Stress-induced fragmentation of multiwall carbon nanotubes in a polymer matrix', *Appl. Phys. Lett*. **72**(2) (1998), 188–190
34. Li, F., Chai, H.M., Bai, S., Su, G., Dresselhaus, M.S. 'Tensile strength of single-walled carbon nanotubes directly measured from their macroscopic ropes', *Appl. Phys. Lett*. **77**(20) (2000), 3161–3163
35. Walters, D.A., Ericson, L.M., Casavant, M.J., Liu, J., Colbert, D.T., Smith, K.A., Smalley, R.E. 'Elastic strain of freely suspended single-wall carbon nanotube ropes', *Appl. Phys. Lett*. **74**(25) (1999), 3803–3805
36. Pan, Z.W., Xie, S.S., Lu, L., Chang, B.H., Sun, L.F., Zhou, W.Y., Wang, G., Zhang, D.L. 'Tensile tests of ropes of very long aligned multiwall carbon nanotubes', *Appl. Phys. Lett*. **74**(21) (1999), 3152–3154
37. Liu, J.Z., Zheng, Q., Jiang, Q. 'Effect of a rippling mode on resonances of carbon nanotubes', *Phys. Rev. Lett*. **86**(21) (2001), 4843–4846
38. Yakobson, B.I., Brabec, C.J., Bernholc, J. 'Nanomechanics of carbon tubes: Instabilities beyond linear response', *Phys. Rev. Lett*. **76**(14) (1996), 2511–2514
39. Yakobson, B.I., Smalley, R.E. 'Fullerene nanotubes: $C_{1,000,000}$ and beyond', *Am. Sci.* **85**(6) (1997), 324–337
40. Bernholc, J., Brabec, C.J., Nardelli, M.B., Maiti, A., Roland, C., Yakobson, B.I. 'Theory of growth and mechanical properties of nanotubes', *Appl. Phys. A* **67**(1) (1998), 39–46
41. Belytschko, T., Xiao, S.P., Schatz, G.C., Ruoff, R.S. 'Atomistic simulation of nanotube fracture', *Phys. Rev. B* **65**(235430) (2002)
42. Govindjee, S., Sackman, J.L. 'On the use of continuum mechanics to estimate the properties of nanotubes', *Solid State Commun*. **110**(4) (1999), 227–230

43. Pantano, A., Parks, D.M., Boyce, M.C. 'Mechanics of deformation of single- and multi-wall carbon nanotubes', *J. Mech. Phys. Solids* **52**(4) (2003), 789–821
44. Despres, J.F., Daguerre, E., Lafdi, K. 'Flexibility of graphene layers in carbon nanotubes', *Carbon* **33**(1) (1995), 87–92
45. Ruoff, R.S., Lorents, D.C. 'Mechanical and thermal properties of carbon nanotubes', *Carbon* **33**(7) (1995), 925–930
46. Iijima, S., Brabec, C., Maiti, A., Bernholc, J. 'Structural flexibility of carbon nanotubes', *J. Chem. Phys*. **104**(5) (1996), 2089–2092
47. Coleman, J.N., Khan, U., Blau, W.J., Gun'ko, Y.K. 'Small but strong: a review of the mechanical properties of carbon nanotube–polymer composites', *Carbon* **44**(9) (2006), 1624–1652
48. Chandra, N., Namilae, S. 'Tensile and compressive behavior of carbon nanotubes: effect of functionalization and topological defects', *Mech. Adv. Mater. Struct*. **13**(2) (2006), 115–127
49. Salvetat, J.-P., Kulik, A.J., Bonard, J.-M., Briggs, G.A.D., Stökli, T., Metenier, K., Bonnamy, S., Beguin, F., Burnham, N.A., Forro, L. 'Elastic modulus of ordered and disordered multiwalled carbon nanotubes', *Adv. Mater*. **11**(2) (1999), 161–165
50. Enomoto, K., Kitakata, S., Yasuhara, T., Ohtake, N., Kuzumaki, T., Mitsuda, Y. 'Measurement of Young's modulus of carbon nanotubes by nanoprobe manipulation in a transmission electron microscope', *Appl. Phys. Lett*. **88**(15) (2006), 153115
51. Pan, Z.W., Xie, S.S., Lu, L., Chang, B.H., Sun, L.F., Zhou, W.Y., Wang, G., Zhang, D.L. 'Tensile tests of ropes of very long aligned multiwall carbon nanotubes', *Appl. Phys. Lett*. **74**(21) (1999), 3152–3154
52. Ge, M.H., Sattler, K. 'Bundles of carbon nanotubes generated by vapor-phase growth', *Appl. Phys. Lett*. **64**(6) (1994), 710–711
53. Schadler, L.S., Giannaris, S.C., Ajayan, P.M. 'Load transfer in carbon nanotubes epoxy composites', *Appl. Phys. Lett*. **73**(26) (1998), 3842–3844
54. Saito, R., Fujita, M., Dresselhaus, G., Dresselhaus, M.S. 'Electronic structure of chiral graphene tubules', *Appl. Phys. Lett*. **60**(18) (1992), 2204–2206
55. Hamada, N., Sawada, S.-I., Oshiyama, A. 'New one-dimensional conductors: graphitic microtubules', *Phys. Rev. Lett*. **68**(10) (1992), 1579–1581
56. Mintmire, J.W., Dunlop, B.I., White, C.T. 'Are fullerene tubules metallic?', *Phys. Rev. Lett*. **68**(5) (1992), 631–634
57. White, C.T., Robertson, D.H., Mintmire, J.W. 'Helical and rotational symmetries of nanoscale graphitic tubules', *Phys. Rev. B* **47**(9) (1993), 5485–5488
58. Mintmire, J.W., White, C.T. 'Electronic and structural properties of carbon nanotubes', *Carbon* **33**(7) (1995), 893–902
59. Benedict, L.X., Crespi, V.H., Louie, S.G., Cohen, M.L. 'Static conductivity and superconductivity of carbon nanotubes: relations between tubes and sheets', *Phys. Rev. B* **52**(20) (1995), 14935–14940
60. Tanaka, K., Aoki, H., Ago, H., Yamabe, T., Okahara, K. 'Interlayer interaction of two graphene sheets as a model of double-layer carbon nanotubes', *Carbon* **35**(1) (1997), 121–125
61. Lambin, P., Meunier, V., Rubio, A. 'Electronic structure of polychiral carbon nanotubes', *Phys. Rev. B* **62**(8) (2000), 5129–5135
62. Kane, C.L., Mele, E.J. 'Size, shape, and low energy electronic structure of carbon nanotubes', *Phys. Rev. Lett*. **78**(10) (1997), 1932–1935
63. Langer, L., Stockman, L., Heremans, J.P., Bayot, V., Olk, C.H., van Haesendonck, C., Bruynseraede, Y., Issi, J.P. 'Electrical resistance of a carbon nanotube bundle', *J. Mater. Res*. **9**(4) (1994), 927–932

64. Heremans, J.P., Olk, C.H., Morelli, D.T. 'Magnetic susceptibility of carbon structures', *Phys. Rev. B* **49**(21) (1994), 15122–15125
65. Tans, S.J., Devoret, M.H., Dai, H., Thess, A., Smalley, R.E., Geerligs, L.J., Dekker, C. 'Individual single-wall carbon nanotubes as quantum wires', *Nature* **386**(6624) (1997), 474–477
66. Ebbesen, T.W., Lezec, H.J., Hiura, H., Bennett, J.W., Ghaemie, H.F., Thio, T. 'Electrical conductivity of individual carbon nanotubes', *Nature* **382**(6586) (1996), 54–56.
67. Odom, T.W., Huang, J.-L., Kim, P., Lieber, C.M. 'Atomic structure and electronic properties of single-walled carbon nanotubes', *Nature* **391**(6662) (1998), 62–64
68. Wildöer, J.W.G., Venema, L.C., Rinzler, A.G., Smalley, R.E., Dekker, C. 'Electronic structure of atomically resolved carbon nanotubes', *Nature* **391**(6662) (1998), 59–62
69. Bachilo, S.M., Strano, M.S., Kittrell, C., Hauge, R.H., Smalley, R.E., Weisman, R.B. 'Structure-assigned optical spectra of single-walled carbon nanotubes', *Science* **298**(5602) (2002), 2361–2366
70. Telg, H., Maultzsch, J., Reich, S., Hennrich, F., Thomsen, C. 'Chirality distribution and transition energies of carbon nanotubes', *Phys. Rev. Lett*. **93**(17) (2004), 177401
71. Bockrath, M., Cobden, D.H., McEuen, P.L., Chopra, N.G., Zettl, A., Thess, A., Smalley, R.E. 'Single-electron transport in ropes of carbon nanotubes', *Science* **275**(5308) (1997), 1922–1925
72. Kim, G.T., Choi, E.S., Kim, D.C., Suh, D.S., Park, Y.W., Liu, K., Duesberg, G., Roth, S. 'Magnetoresistance of an entangled single-wall carbon-nanotube network', *Phys. Rev. B* **58**(24) (1998), 16064–16069
73. Fischer, J.E., Dai, H., Thess, A., Lee, R., Hanjani, N.M., Dehaas, D.L., Smalley, R.E. 'Metallic resistivity in crystalline ropes of single-wall carbon nanotubes', *Phys. Rev. B* **55**(8) (1997), 4921–4924
74. Bozhko, A.D., Sklovsky, D.E., Nalimova, V.A., Rinzler, A.G., Smalley, R.E., Fischer, J.E. 'Resistance vs. pressure of single-wall carbon nanotubes', *Appl. Phys. A* **67**(1) (1998), 75–77
75. Charlier, J.R., Issi, J.-P. 'Electrical conductivity of novel forms of carbon', *J. Phys. Chem. Solids* **57**(6–8) (1996), 957–965
76. Lee, J.-O., Park, C., Kim, J.-J., Kim, J., Park, J.W., Yoo, K.-H. 'Formation of low-resistance ohmic contact between carbon nanotubes and metal electrodes by a rapid thermal annealing method', *J. Phys. D: Appl. Phys*. **33**(16) (2000), 1953–1956
77. Dai, H., Wong, E.W., Lieber, C.M. 'Probing electrical transport in nanomaterials: conductivity of individual carbon nanotubes', *Science* **272**(5261) (1996), 523–526
78. Poncharal, P., Berger, C., Yi, Y., Wang, Z.L., de Heer, W.A. 'Room temperature ballistic conduction in carbon nanotubes', *J. Phys. Chem. B* **106**(47) (2002), 12104–12118
79. Hone, J., Whitny, M., Zettl, A. 'Thermal conductivity of single-walled carbon nanotubes", *Synth. Metals* **103**(1–3) (1999), 2498–2499
80. Kim, P., Shi, L., Majumdar, A., McEuen, P.L. 'Thermal transport measurements of individual multiwalled nanotubes', *Phys. Rev. Lett*. **87**(21) (2001), 215502
81. Hone, J., Llaguno, M.C., Nemes, N.M., Johnson, A.T., Fischer, J.E., Walters, D.A., Casavant, M.J., Schmidt, J., Smalley, R.E. 'Electrical and thermal transport properties of magnetically aligned single walled carbon nanotube films', *Appl. Phys. Lett*. **77**(5) (2000), 666–668

82. Andrews, R., Jacques, D., Qian, D., Dickey, E.C. 'Purification and structural annealing of multi-walled carbon nanotubes at graphitization temperatures', *Carbon* **39**(11) (2001), 1681–1687
83. Arnold, M.S., Green, A.A., Hulvat, J.F., Stupp, S.I., Hersam, M.C. 'Sorting carbon nanotubes by electronic structure using density differentiation', *Nature Nanotechnol*. **1** (2006), 60–65
84. Niu, C.M., Sichel, E.K., Hoch, R., Moy, D., Tennet, H. 'High power electrochemical capacitors based on carbon nanotube electrodes', *Appl. Phys. Lett*. **70**(11) (1997), 1480–1482
85. Peigney, A., Laurent, C., Flahaut, E., Bacsa, R.R., Rousset, A. 'Specific surface area of carbon nanotubes and bundles of carbon nanotubes', *Carbon* **39**(4) (2001), 507–514
86. Lozano, K., Barrera, E.V. 'Nanofiber-reinforced thermoplastic composites I: Thermoanalytical and mechanical analyses', *J. Appl. Polym. Sci*. **79**(1) (2001), 125–133
87. Jin, Z., Pramoda, K.P., Xu, G., Goh, S.H. 'Dynamic mechanical behavior of melt-processed multi-walled carbon nanotube/poly(methyl methacrylate) composites', *Chem. Phys. Lett*. **337**(1–3) (2001), 43–47
88. Pötschke, P., Fornes, T.D., Paul, D.R. 'Rheological behavior of multiwalled carbon nanotube/polycarbonate composites', *Polymer* **43**(11) (2002) 3247–3255
89. Pötschke, P., Dudkin, S.M., Alig, I. 'Dielectric spectroscopy on melt processed polycarbonate-multiwalled carbon nanotube composites', *Polymer* **44**(17) (2003), 5023–5030
90. Meincke, O., Kaempfer, D., Weickmann, H., Friedrich, C., Vathauer, M., Warth, H. 'Mechanical properties and electrical conductivity of carbon-nanotube filled polyamide-6 and its blends with acrylonitrile/butadiene/styrene' *Polymer* **45**(3) (2004), 739–748
91. Thostenson, E.T., Chou, T.-W. 'Aligned multi-walled carbon nanotube-reinforced composites: processing and mechanical characterization', *J. Phys. D: Appl. Phys*. **35**(16) (2002), 77–80
92. Sandler, J.K.W., Pegel, S., Cadek, M., Gojny, F., van Es, M., Lohmar, J., Blau, W.J., Schulte, K., Windle, A.H., Shaffer, M.S.P. 'A comparative study of melt-spun polyamide-12 fibres reinforced with carbon nanotubes and nanofibres', *Polymer* **45**(6) (2004), 2001–2015
93. Sato, E., Takahas, T., Koyama, K. 'Comparison of the length of vapor-grown carbon fiber before and after mixing process', *Kobunshi Ronbunshu* **61**(2) (2004), 144–148
94. Tibbetts, G.G., McHugh, J.J. 'Mechanical properties of vapor-grown carbon fiber composites with thermoplastic matrices', *J. Mater. Res*. **14**(7) (1999), 2871–2880
95. Kuriger, R.J., Alam, M.K., Anderson, D.P., Jacobsen, R.L. 'Processing and characterization of aligned vapor grown carbon fiber reinforced polypropylene', *Comp. Part A* **33**(1) (2002), 53–62
96. Lu, K.L., Lago, R.M., Chen, Y.K., Green, M.L.H., Harris, P.F., Tsang, S.C. 'Mechanical damage of carbon nanotubes by ultrasound', *Carbon* **34**(6) (1996), 814–816
97. Koshio, A., Yudasaka, M., Zhang, M., Iijima, S. 'A simple way to chemically react single-wall carbon nanotubes with organic materials using ultrasonication', *Nano Lett*. **1**(7) (2001), 361–363
98. O'Connell, M.J., Boul, P., Ericson, L.M., Huffman, C., Wang, Y., Haroz, E., Kuper,

C., Tour, J., Ausman, K.D., Smalley, R.E. 'Reversible water-solubilization of single-walled carbon nanotubes by polymer wrapping', *Chem. Phys. Lett*. **342**(3–4) (2001), 265–271
99. Jin, L., Bower, C., Zhou, O. 'Alignment of carbon nanotubes in a polymer matrix by mechanical stretching', *Appl. Phys. Lett*. **73**(9) (1998), 1197–1199
100. Bower, C., Rosen, R., Han, J., Zhou, O. 'Deformation of carbon nanotubes in nanotube–polymer composites', *Appl. Phys. Lett*. **74**(22) (1999), 3317–3319
101. Shaffer, M.S.P., Windle, A.H. 'Fabrication and characterization of carbon nanotube/poly(vinyl alcohol) composites', *Adv. Mater*. **11**(11) (1999), 937–941
102. Cadek, M., Coleman, J.N., Barron, V., Hedicke, K., Blau, W.J. 'Morphological and mechanical properties of carbon-nanotube-reinforced semicrystalline and amorphous polymer composites', *Appl. Phys. Lett*. **81**(27) (2002), 5123–5125
103. Zhang, X., Liu, T., Sreekumar, T.V., Kumar, S., Moore, V.C., Hauge, R.H., Smalley, R.E. 'Poly(vinyl alcohol)/SWCNT composite film', *Nano Lett*. **3**(9) (2003), 1285–1288
104. Qian, D., Dickey, E.C., Andrews, R., Rantell, T. 'Load transfer and deformation mechanisms in carbon nanotube–polystyrene composites', *Appl. Phys. Lett*. **76**(20) (2000), 2868–2870
105. Watts, P.C., Hsu, W.K., Chen, G.Z., Fray, D.J., Kroto, H.W., Walton, D.R.M. 'A low resistance boron-doped carbon nanotube-polystyrene composite', *J. Mater. Chem*. **11**(10) (2001), 2482–2488
106. Safadi, B., Andrews, R., Grulke, E.A. 'Multiwalled carbon nanotube polymer composites: synthesis and characterization of thin films', *J. Appl. Polym. Sci*. **84**(14) (2002), 2660–2669
107. Ruan, S.L., Gao, P., Yang, X.G., Yu, T.X. 'Toughening high performance ultrahigh molecular weight polyethylene using multiwalled carbon nanotubes', *Polymer* **44**(19) (2003), 5643–5654
108. Assouline, E., Lustiger, A., Barber, A.H., Cooper, C.A., Klein, E., Wachtel, E., Wagner, H.D. 'Nucleation ability of multiwall carbon nanotubes in polypropylene composites', *J. Polym. Sci. B*: *Polym. Phys*. **41**(5) (2003), 520–527
109. Dufresne, A., Paillet, M., Putaux, J.L., Canet, R., Carmona, F., Delhaes, P., Cui, S. 'Processing and characterization of carbon nanotube/poly(styrene-co-butyl acrylate) nanocomposites', *J. Mater. Sci*. **37**(18) (2002), 3915–3923
110. Paiva, M.C., Zhou, B., Fernando, K.A.S., Lin, Y., Kennedy, J.M., Sun, Y.-P. 'Mechanical and morphological characterization of polymer–carbon nanocomposites from functionalized carbon nanotubes', *Carbon* **42**(14) (2004), 2849–2854
111. Lin, Y., Zhou, B., Fernando, K.A.S., Liu, P., Allard, L.A., Sun, Y.-P. 'Polymeric carbon nanocomposites from carbon nanotubes functionalised with matrix polymer', *Macromolecules* **36**(19) (2003), 7199–7204
112. Mitchell, C.A., Bahr, J.L., Arepalli, S., Tour, J.M., Krishnamoorti, R. 'Dispersion of functionalized carbon nanotubes in polystyrene', *Macromolecules* **35**(23) (2002), 8825–8830
113. Shaffer, M.S.P., Fan, X., Windle, A.H. 'Dispersion and packing of carbon nanotubes', *Carbon* **36**(11) (1998), 1603–1612
114. Chen, X.M., Burger, C., Fang, D.F., Sics, I., Wang, X.F., He, W.D., Somani, R.H., Yoon, K., Hsiao, B.S., Chu, B. '*In-situ* X-ray deformation study of fluorinated multiwalled carbon nanotube and fluorinated ethylene-propylene nanocomposite fibers', *Macromolecules* **39**(16) (2006), 5427–5437
115. Jia, Z.J., Wang, Z.Y., Xu, C.L., Liang, J., Wei, B.Q., Wu, D.H., Zhu, S.W. 'Study

on poly(methyl methacrylate)/carbon nanotube composites', *Mater. Sci. Eng. A* **271**(1–2) (1999), 395–400
116. Kumar, S., Dang, T.D., Arnold, F.E., Bhattacharyya, A.R., Min, B.G., Zhang, X., Vaia, R.A., Park, C., Adams, W.W., Hauge, R.H., Smalley, R.E., Ramesh, S., Willis, P.A. 'Synthesis, structure, and properties of PBO/SWNT composites', *Macromolecules* **35**(24) (2002), 9039–9043
117. Barraza, H.J., Pompeo, F., O'Rear, E.A., Resasco, D.E. 'SWNT-filled thermoplastic and elastomeric composites prepared by miniemulsion polymerization', *Nano Lett.* **2**(8) (2002), 797–802
118. Ounaies, Z., Park, C., Wise, K.E., Siochi, E.J., Harrison, J.S. 'Electrical properties of single wall carbon nanotube reinforced polyimide composites', *Comp. Sci. Tech.* **63**(11) (2003), 1637–1646
119. Roslaniec, Z., Broza, G., Schulte, K. 'Nanocomposites based on multiblock polyester elastomers (PEE) and carbon nanotubes (CNT)', *Comp. Interfaces* **10**(1) (2003), 95–102
120. Kearns, J.C., Shambaugh, R.L. 'Polypropylene fibers reinforced with carbon nanotubes', *J. Appl. Polym. Sci.* **86**(8) (2002), 2079–2084
121. Fornes, T.D., Baur, J.W., Sabba, Y., Thomas, E.L. 'Morphology and properties of melt-spun polycarbonate fibers containing single- and multi-wall carbon nanotubes', *Polymer* **47**(5) (2006), 1704–1714
122. Frankland, S.J.V., Caglar, A., Brenner, D.W., Griebel, M. 'Molecular simulation of the influence of chemical cross-links on the shear strength of carbon nanotube-polymer interfaces', *J. Phys. Chem. B* **106**(12) (2002), 3046–3048
123. Liao, K., Li, S. 'Interfacial characteristics of a carbon nanotube–polystyrene composite system', *Appl. Phys. Lett.* **79**(25) (2001), 4225–4227
124. Wong, M., Paramsothy, M., Xu, X.J., Ren, Y., Li, S., Liao, K. 'Physical interactions at carbon nanotube-polymer interfaces', *Polymer* **44**(25) (2003), 7757–7764
125. Cooper, C.A., Cohen, S.R., Barber, A.H., Wagner, H.D. 'Detachment of nanotubes from a polymer matrix', *Appl. Phys. Lett.* **81**(20) (2002), 3873–3875
126. Barber, A.H., Cohen, S.R., Wagner, H.D. 'Measurement of carbon nanotube-polymer interfacial strength', *Appl. Phys. Lett.* **82**(23) (2003), 4140–4142
127. Barber, A.H., Cohen, S.R., Kenig, S., Wagner, H.D. 'Interfacial fracture energy measurements for multi-walled carbon nanotubes pulled from a matrix', *Comp. Sci. Tech.* **64**(15) (2004), 2283–2289
128. Xie, X.L., Aloys, K., Zhou, X.P., Zeng, F.D. 'Ultrahigh molecular mass polyethylene/carbon nanotube composites – crystallization and melting properties', *J. Therm. Anal. Calorim.* **74**(1) (2003), 317–323
129. Sandler, J., Broza, G., Nolte, M., Schulte, K., Lam, Y.-M., Shaffer, M.S.P. 'Crystallization of carbon nanotube and nanofiber polypropylene composites', *J. Macromol. Sci. – Phys. B* **42**(3–4) (2003), 479–488
130. Grady, B.P., Pompeo, F., Shambaugh, R.L., Resasco, D.E. 'Nucleation of polypropylene crystallization by single-walled carbon nanotubes', *J. Phys. Chem. B* **106**(23) (2002), 5852–5858
131. Patton, R.D., Pittman Jr., C.U., Wang, L., Hill, J.R. 'Vapor grown carbon fiber composites with epoxy and poly(phenylene sulfide) matrices', *Comp. Part A* **30**(9) (1999), 1081–1091
132. Ray, S.S., Okamoto, M. 'Polymer/layered silicate nanocomposites: a review from preparation to processing', *Prog. Polym. Sci.* **28**(11) (2003), 1539–1641
133. Tang, W., Santare, M.H., Advani, S.G. 'Melt processing and mechanical property

characterization of multi-walled carbon nanotube/high density polyethylene (MWNT/HDPE) composite films', *Carbon* **41**(14) (2003), 2779–2785
134. Coleman, J.N., Cadek, M., Blake, R., Nicolosi, V., Ryan, K.P., Belton, C., Fonseca, A., Nagy, J.B., Gun'ko, Y.K., Blau, W.J. 'High-performance nanotube-reinforced plastics: understanding the mechanism of strength increase', *Adv. Funct. Mater.* **14**(8) (2004), 791–798
135. Putz, K.W., Mitchell, C.A., Krishnamoorti, R., Green, P.F. 'Elastic modulus of single-walled carbon nanotube/poly(methyl methacrylate) nanocomposites', *J. Polym. Sci. Part B – Polym. Phys.* **42**(12) (2004), 2286–2293
136. Carneiro, O.S., Covas, J.A., Bernado, C.A., Caldeira, G., Van Hattum, F.W.J., Ting, J.-M., Alig, R.L., Lake, M.L. 'Production and assessment of polycarbonate composites reinforced with vapour-grown carbon fibres', *Comp. Sci. Technol.* **58**(3–4) (1998), 401–407
137. Sandler, J., Werner, P., Shaffer, M.S.P., Demchuk, V., Altstädt, V., Windle, A.H. 'Carbon-nanofibre-reinforced poly(ether ether ketone) composites', *Comp. Part A* **33**(8) (2002), 1033–1039
138. Werner, P., Altstädt, V., Jaskulka, R., Jacobs, O., Sandler, J.K.W., Shaffer, M.S.P., Windle, A.H. 'Tribological behaviour of carbon-nanofibre-reinforced poly(ether ether ketone)', *Wear* **257**(9–10) (2004), 1006–1014
139. Zoo, Y.S., An, J.W., Lim, D.P., Lim, D.S. 'Effect of carbon nanotube addition on tribological behavior of UHMWPE', *Tribol. Lett.* **16**(4) (2004), 305–309
140. Lozano, K., Bonilla-Rios, J., Barrera, E.V. 'A study on nanofiber-reinforced thermoplastic composites II: Investigation of the mixing rheology and conduction properties', *J. Appl. Polym. Sci.* **80**(8) (2001), 1162–1172
141. Gordeyev, S.A., Macedo, F.J., Ferreira, J.A., Van Hattum, F.W.J., Bernado, C.A. 'Transport properties of polymer-vapour-grown carbon fibre composites', *Physica B* **279**(1–3) (2000), 33–36
142. Finegan, I.C., Tibbetts, G.G. 'Electrical conductivity of vapor-grown carbon fiber/thermoplastic composites', *J. Mater. Res.* **16**(6) (2001), 1668–1674
143. Kilbride, B.E., Coleman, J.N., Fraysse, J., Fournet, P., Cadek, M., Drury, A., Hutzler, S., Roth, S., Blau, W.J. 'Experimental observation of scaling laws for alternating and direct current conductivity in polymer–carbon nanotube composite thin films', *J. Appl. Phys.* **92**(7) (2002), 4024–4030
144. Stephan, C., Nguyen, T.P., Lahr, B., Blau, W.J., Lefrant, S., Chauvet, O. 'Raman spectroscopy and conductivity measurements on polymer-multiwalled carbon nanotubes composites', *J. Mater. Res.* **17**(2) (2002), 396–400
145. Bai, J.B., Allaoui, A. 'Effect of the length and the aggregate size of MWCNTs on the improvement efficiency of the mechanical and electrical properties of nanocomposites – experimental investigation', *Comp. Part A* **34**(8) (2003), 689–694
146. Sandler, J., Shaffer, M.S.P., Prasse, T., Bauhofer, W., Schulte, K., Windle, A.H. 'Development of a dispersion process for carbon nanotubes in an epoxy matrix and the resulting electrical properties', *Polymer* **40**(21) (1999), 5967–5971
147. Allaoui, A., Bai, S., Cheng, H.M., Bai, J.B. 'Mechanical and electrical properties of a MWNT/epoxy composite', *Comp. Sci. Technol.* **62**(15) (2002), 1993–1998
148. Barrau, S., Demont, P., Peigny, A., Laurent, C., Lacabanne, C. 'DC and AC conductivity of carbon nanotubes–polyepoxy composites', *Macromolecules* **36**(14) (2003), 5187–5194
149. Prasse, T., Cavaille, J.-Y., Bauhofer, W. 'Electric anisotropy of carbon nanofibre/

epoxy resin composites due to electric field induced alignment', *Comp. Sci. Technol.* **63**(13) (2003), 1835–1841

150. Valentini, L., Puglia, D., Frulloni, E., Armentano, I., Kenny, J.M., Santucci, S. 'Dielectric behavior of epoxy matrix/single-walled carbon nanotube composites', *Comp. Sci. Technol.* **64**(1) (2004), 23–33
151. Martin, C.A., Sandler, J.K.W., Shaffer, M.S.P., Schwarz, M.-K., Bauhofer, W., Schulte, K., Windle, A.H. 'Formation of percolating networks in multi-wall carbon-nanotube-epoxy composites', *Comp. Sci. Technol.* **64**(15) (2004), 2309–2316
152. Martin, C.A., Sandler, J.K.W., Windle, A.H., Schwarz, M.-K., Bauhofer, W., Schulte, K., Shaffer, M.S.P. 'Electric field-induced aligned multi-wall carbon nanotube networks in epoxy composites', *Polymer* **46**(3) (2005), 877–886
153. Fu, S.-Y., Mai, Y.-W. 'Thermal conductivity of misaligned short-fiber-reinforced polymer composites', *J. Appl. Polym. Sci.* **88**(6) (2003), 1497–1505
154. Bangarusampath, D.S., Ruckdäschel, H., Sandler, J.K.W., Altstädt, V., Shaffer, M.S.P. 'Melt rheology of carbon nanofibre-reinforced poly(ether ether ketone) under shear and elongational flow', *J. Rheol* (2007), submitted to *J. Rheol*
155. Rahatekar, S.S., Koziol, K.K.K., Butler, S.A., Elliott, J.A., Shaffer, M.S.P., Mackley, M.R., Windle, A.H. 'Optical microstructure and viscosity enhancement for an epoxy resin matrix containing multiwall carbon nanotubes', *J. Rheol.* **50**(5) (2006), 599–610
156. Pugno, N.M. 'On the strength of the carbon nanotube-based space elevator cable: from nanomechanics to megamechanics', *J. Phys.: Condens. Matter* **18**(33) (2006), S1971–S1990
157. Vigolo, B., Penicaud, A., Coulon, C., Sauder, C., Pailler, R., Journet, C., Bernier, P., Poulin, P. 'Macroscopic fibers and ribbons or oriented carbon nanotubes', *Science* **290**(5495) (2000), 1331–1334
158. Dalton, A.B., Collins, S., Munoz, E., Razal, J.M., Ebron, V.H., Ferraris, J.P., Coleman, J.N., Kim, B.G., Baughman, R.H. 'Super-tough carbon-nanotube fibres – these extraordinary composite fibres can be woven into electronic textiles", *Nature* **423**(6941) (2003), 703
159. Munoz, E., Suh, D.S., Collins, S., Selvidge, M., Dalton, A.B., Kim, B.G., Razal, J.M., Ussery, G., Rinzler, A.G., Martinez, M.T., Baughman, R.H. 'Highly conducting carbon nanotube/polyethyleneimine composite fibers', *Adv. Mater.* **17**(8) (2005), 1064
160. Ericson, L.M., Fan, H., Peng, H.Q., Davis, V.A., Zhou, W., Sulpizio, J., Wang, Y.H., Booker, R., Vavro, J., Guthy, C., Parra-Vasquez, A.N.G., Kim, M.J., Ramesh, S., Saini, R.K., Kittrell, C., Lavin, G., Schmidt, H., Adams, W.W., Billups, W.E., Pasquali, M., Hwang, W.F., Hauge, R.H., Fischer, J.E., Smalley, R.E. 'Macroscopic, neat, single-walled carbon nanotube fibers', *Science* **305**(5689) (2004), 1447–1450
161. Zhou, W., Vavro, J., Guthy, C., Winey, K.I., Fischer, J.E., Ericson, L.M., Ramesh, S., Saini, R., Davis, V.A., Kittrell, C., Pasquali, M., Hauge, R.H., Smalley, R.E. 'Single wall carbon nanotube fibers extruded from super-acid suspensions: preferred orientation, electrical, and thermal transport', *J. Appl. Phys.* **95**(2) (2004), 649–655
162. Mottaghitalab, V., Spinks, G.M., Wallace, G.G. 'The development and characterisation of polyaniline–single walled carbon nanotube composite fibres using 2-acrylamido-2 methyl-1-propane sulfonic acid (AMPSA) through one step wet spinning process', *Polymer* **47**(14) (2006), 4996–5002

163. Spinks, G.M., Shin, S.R., Wallace, G.G., Whitten, P.G., Kim, S.I., Kim, S.J. 'Mechanical properties of chitosan/CNT microfibers obtained with improved dispersion', *Sens. Actuat. B – Chem.* **115**(2) (2006), 678–684
164. Chae, H.G., Minus, M.L., Kumar, S. 'Oriented and exfoliated single wall carbon nanotubes in polyacylonitrile', *Polymer* **47**(10) (2006), 3494–3504
165. Zhang, X.F., Liu, T., Sreekumar, T.V., Kumar, S., Hu, X., Smith, K. 'Gel spinning of PVA/SWNT composite fiber', *Polymer* **45**(26) (2004), 8801–8807
166. Gao, J.B., Itkis, M.E., Yu, A.P., Bekyarova, E., Zhao, B., Haddon, R.C. 'Continuous spinning of a single-walled carbon nanotube-nylon composite fiber', *J. Am. Chem. Soc.* **127**(11) (2005), 3847–3854
167. Oh, S.-J., Lee, H.-J., Keum, D.-K., Lee, S.-W., Wang, D.H., Park, S.-Y., Tan, L.-S., Baek, J.-B. 'Multi-walled carbon nanotubes and nanofibres grafted with polyetherketones in mild and viscous polymeric acids', *Polymer* **47**(4) (2006), 1132–1140
168. Ko, F., Gogotsi, Y., Ali, A., Naguib, N., Ye, H.H., Yang, G.L., Li, C., Willis, P. 'Electrospinning of continuous carbon nanotube-filled nanofiber yarns', *Adv. Mater.* **15**(14) (2003), 1161
169. Lozano, K., Yang, S.Y., Zeng, Q. 'Rheological analysis of vapor-grown carbon nanofiber-reinforced polyethylene composites', *J. Appl. Polym. Sci.* **93**(1) (2004), 155–162
170. Pötschke, P., Abdel-Goad, M., Alig, I., Dudkin, S., Lellinger, D. 'Rheological and dielectrical characterization of melt mixed polycarbonate-multiwalled carbon nanotube composites', *Polymer* **45**(26) (2004), 8863–8870
171. McNally, T., Pötschke, P., Halley, P., Murphy, M., Martin, D., Bell, S.E.J., Brennan, G.P., Bein, D., Lemoine, P., Quinn, J.P. 'Polyethylene multiwalled carbon nanotube composites', *Polymer* **46**(19) (2005), 8222–8232
172. Ramesh, N.S., Lee, S.T. 'Blowing agent effect on extensional viscosity calculated from fiber spinning method for foam processing', *SPE Foams '99* (1999), 85–96
173. Werner, P., Verdejo, R., Wöllecke, F., Altstädt, V., Sandler, J.K.W., Shaffer, M.S.P. 'Carbon nanofibres allow foaming of semicrystalline poly(ether ether ketone)', *Adv. Mater.* **17**(23) (2005), 2864–2869
174. Joseph, R., Martyn, M.T., Tanner, K.E., Coates, P.D., Bonfield, W. 'Rheological characterisation of hydroxyapatite filled polyethylene composites Part 1–Shear and extensional behaviour', *Plast. Rubber Comp.* **30**(5) (2001), 197–204
175. Ramazani, A., Ait-Kadi, A., Grmela, M. 'Rheological modelling of short fiber thermoplastic composites', *J. Non-Newton. Fluid Mech.* **73**(3) (1997), 241–260
176. Krishnamoorti, R., Ren, J.X., Silva, A.S. 'Shear response of layered silicate nanocomposites', *J. Chem. Phys.* **114**(11) (2001), 4968–4973
177. Hu, G., Zhao, C., Zhang, S., Yang, M., Wang, Z. 'Low percolation thresholds of electrical conductivity and rheology in poly(ethylene terephthalate) through the networks of multi-walled carbon nanotubes', *Polymer* **47**(1) (2006), 480–488
178. Du, F., Scogna, R.C., Zhou, W., Brand, S., Fischer, J.E., Winey, K.I. 'Nanotube networks in polymer nanocomposites: rheology and electrical conductivity', *Macromolecules* **37**(24) (2004), 9048–9055
179. Kharchenko, S.B., Douglas, J.F., Obrzut, J., Grulke, E.A., Migler, K.B. 'Flow-induced properties of nanotube-filled polymer materials', *Nature Mater.* **3**(8) (2004), 564–568
180. Guth, E. 'Theory of filler reinforcement', *J. Appl. Phys.* **16**(1) (1945), 20–25
181. Ma, H., Zeng, J., Realff, M.L., Kumar, S., Schiraldi, D.A. 'Processing, structure,

and properties of fibers from polyester/carbon nanofiber composites', *Comp. Sci. Technol*. **63**(11) (2003), 1617–1628
182. Stange, J., Münstedt, H. 'Rheological properties and foaming behaviour of polypropylenes with different molecular structures', *J. Rheol*. **50**(6) (2006), 907–923
183. Han, C.D., Kim, Y.W. 'Studies on melt spinning. 5. Elongational viscosity and spinnability of two-phase systems', *J. Appl. Polym. Sci*. **18**(9) (1974), 2589–2603
184. Münstedt, H., Steffl, T., Malmberg, A. 'Correlation between rheological behaviour in uniaxial elongation and film blowing properties of various polyethylenes', *Rheol. Acta* **45**(1) (2005), 14–22
185. Meissner, J. 'Dehnungsverhalten von Polyäthylen-Schmelzen', *Rheol. Acta* **10** (1971), 230–242
186. Muke, S., Ivanov, I., Kao, N., Bhattacharya, S.N. 'Extensional rheology of polypropylene melts from the Rheotens test', *J. Non-Newton. Fluid Mech*. **101**(1–3) (2001), 77–93
187. Wagner, M.H., Bernnat, A., Schulze, V. 'The rheology of the rheotens test', *J. Rheol*. **42**(4) (1998), 917–928
188. Laun, H.M., Schuch, H. 'Transient elongational viscosities and drawability of polymer melts', *J. Rheol*. **33**(1) (1989), 119–175
189. Prasad, R., Pasanovic-Zujo, V., Gupta, R.K., Cser, F., Bhattacharya, S.N. 'Morphology of EVA based nanocomposites under shear and extensional flow', *Polym. Eng. Sci*. **44**(7) (2004), 1220–1230
190. Sandler, J., Windle, A.H., Werner, P., Altstädt, V., van Es, M., Shaffer, M.S.P. 'Carbon-nanofibre-reinforced poly(ether ether ketone) fibres', *J. Mater. Sci*. **38**(10) (2003), 2135–2141
191. Sennett, M., Welsh, E., Wright, J.B., Li, W.Z., Wen, J.G., Ren, Z.F. 'Dispersion and alignment of carbon nanotubes in polycarbonate', *Mat. Res. Soc. Symp. Proc*. **706** (2002), Z3.31.1–6
192. Andrews, R., Jacques, D., Rao, A.M., Rantell, T., Derbyshire, F., Chen, Y., Chen, J., Haddon, R.C. 'Nanotube composite carbon fibers', *Appl. Phys. Lett*. **75**(9) (1999), 1329–1331
193. Bhattacharyya, A.R., Sreekumar, T.V., Liu, T., Kumar, S., Ericson, L.M., Hauge, R.H., Smalley, R.E. 'Crystallization and orientation studies in polypropylene/single wall carbon nanotube composite', *Polymer* **44**(8) (2003), 2373–2377
194. Marcincin, A. 'Modification of fiber-forming polymers by additives', *Prog. Polym. Sci*. **27**(5) (2002), 853–913
195. Coleman, J.N., Cadek, M., Ryan, K.P., Fonseca, A., Nagy, J.B., Blau, W.J., Ferreira, M.S. 'Reinforcement of polymers with carbon nanotubes. The role of an ordered polymer interfacial region. Experiment and modelling', *Polymer* **47**(26) (2006), 8556–8561
196. Young, R.J., Eichhorn, S.J. 'Deformation mechanisms in polymer fibres and nanocomposites', *Polymer* **48**(1) (2007), 2–18
197. Liu, T.X., Wang, S.E., Mo, Z.S., Zhang, H.F. 'Crystal structure and drawing-induced polymorphism in poly(aryl ether ether ketone). IV', *J. Appl. Polym. Sci*. **73**(2) (1999), 237–243
198. Kumar, S., Doshi, H., Srinivasarao, M., Park, J.O., Schiraldi, D.A. 'Fibers from polypropylene/nano carbon fiber composites', *Polymer* **43**(5) (2002), 1701–1703
199. Chatterjee, A., Deopura, B.L. 'High modulus and high strength PP nanocomposite filament', *Comp. Part A* **37**(5) (2006), 813–817

200. Fisher, F.T., Bradshaw, R.D., Brinson, L.C. 'Effects of nanotube waviness on the modulus of nanotube-reinforced polymers', *Appl. Phys. Lett*. **80**(24) (2002), 4647–4649
201. Coleman, J.N., Khan, U., Gun'ko, Y.K. 'Mechanical reinforcement of polymers using carbon nanotubes', *Adv. Mater*. **18**(6) (2006), 689–706
202. Gao, H.J., Ji, B.H., Jäger, I.L., Arzt, E., Fratzl, P. 'Materials become insensitive to flaws at nanoscale: lessons from nature', *Proc. Natl Acad. Sci. USA* **100**(10) (2003), 5997–5600
203. Zhao, Q., Wagner, H.D. 'Raman spectroscopy of carbon-nanotube-based composites', *Proc. Trans. Royal Soc. London Ser. A* **362**(1824) (2004), 2407–2424
204. Cooper, C.A., Young, R.J., Halsall, M. 'Investigation into the deformation of carbon nanotubes and their composites through the use of Raman spectroscopy', *Comp. Part A* **32**(3–4) (2001), 401–411
205. Zhao, Q., Wood, J.R., Wagner, H.D. 'Stress fields around defects and fibers in a polymer using carbon nanotubes as a sensor', *Appl. Phys. Lett*. **78**(12) (2001), 1748–1750
206. Chen, X.M., Yoon, K.W., Burger, C., Sics, I., Fang, D.F., Hsiao, B.S., Chu, B. '*In-situ* X-ray scattering studies of a unique toughening mechanism in surface-modified carbon nanofiber/UHMWPE nanocomposite films', *Macromolecules* **38**(9) (2005), 3883–3893
207. Kelarakis, A., Yoon, K., Sics, I., Somani, R.H., Hsiao, B.S., Chu, B. 'Uniaxial deformation of an elastomer nanocomposite containing modified carbon nanofibers by *in situ* synchrotron X-ray diffraction', *Polymer* **46**(14) (2005), 5103–5117
208. Karst, D., Yang, Y.Q. 'Potential advantages and risks of nanotechnology for textiles', *AATCC Rev*. **6**(3) (2006), 44–48
209. Huang, C.-Y., Wu, C.-C. 'The EMI shielding effectiveness of PC/ABS/nickel-coated-carbon-fibre composites', *Europ. Polym. J*. **36**(12) (2000), 2729–2737
210. Hirase, R., Hasegawa, M., Shirai, M. 'Conductive fibers based on poly(ethylene terephthalate)–polyaniline composites manufactured by electrochemical polymerization', *J. Appl. Polym. Sci*. **87**(7) (2003), 1073–1078
211. Pötschke, P., Brünig, H., Janke, A., Fischer, D., Jehnichen, D., 'Orientation of multi-walled carbon nanotubes in composites with polycarbonate by melt spinning', *Polymer* **46**(23) (2005), 10355–10363
212. Zhang, Q.H., Jin, H.F., Wang, X.H., Jing, X.B. 'Morphology of conductive blend fibers of polyaniline and polyamide-11', *Synth. Metals* **123**(3) (2001), 481–485
213. Gordeyev, S.A., Ferreira, J.A., Bernardo, C.A., Ward, I.M. 'A promising conductive material: highly oriented polypropylene filled with short vapour-grown carbon fibres', *Mat. Lett*. **51**(1) (2001), 32–36
214. Zeng, J., Saltysiak, B., Johnson, W.S., Schiraldi, D.A., Kumar, S. 'Processing and properties of poly(methyl methacrylate)/carbon nano fiber composites', *Comp. Part B* **35**(2) (2004), 173–178
215. Chae, H.G., Sreekumar, T.V., Uchida, T., Kumar, S. 'A comparison of reinforcement efficiency of various types of carbon nanotubes in polyacrylonitrile fiber', *Polymer* **46**(21) (2005), 10925–10935
216. Schartel, B., Pötschke, P., Knoll, U., Abdel-Goad, M. 'Fire behaviour of polyamide6/multiwall carbon nanotube nanocomposites', *Europ. Polym. J*. **41**(5) (2005), 1061–1070

8

Structure and properties of carbon nanotube-polymer fibers using melt spinning

R. E. GORGA, North Carolina State University, USA

8.1 Introduction

The fabrication of advanced fibers for protective applications continues to be of utmost interest. This chapter focuses on the mechanical and morphological properties of polymer/carbon nanotubes composites via melt processing. In particular, this chapter will focus on (1) melt processing optimization for improved nanotube dispersion; (2) the effect of fiber draw ratio on morphology and mechanical properties; (3) the effect of nanotube type and geometry on morphology and mechanical properties; and (4) details on future trends for the technology and potential applications as well as a section outlining further resources for the interested reader.

Carbon nanotubes are graphitic sheets rolled into seamless tubes (i.e. arrangements of carbon hexagons into tube-like fullerenes) and have diameters ranging from about a nanometer to tens of nanometers with lengths up to centimeters. Nanotubes have received much attention due to their interesting properties (high modulus and electrical/thermal conductivity) since their discovery by Iijima in 1991.[1, 2] For example, theoretical calculations and preliminary experimentation have shown that carbon nanotubes have excellent mechanical properties, electrical conductivity (5.1×10^{-6} to $5.8\,\Omega$ cm),[3] and thermal conductivity (1750–5800 W/m K).[4] Treacy *et al*.[5] found the Young's modulus of individual nanotubes to be in the range of 1 TPa using intrinsic thermal vibrations.

Although carbon nanotubes show exceptional properties on the nano-scale, the difficulty lies in creating a material that exhibits carbon nanotube properties on the macro-scale. Incorporating the nanotubes as filler into polymer matrices is the most common method currently explored.[6–15] Similar to other composites made from chopped fiber in a polymer matrix, filler dispersion and orientation are essential to achieve optimal property improvements. Researchers have used many different techniques to attempt to disperse nanotubes in polymer matrices including solution chemistry to functionalize the nanotube surface,[16–21] the use of polymers to coat the nanotube

surface,[22] *in situ* polymerization of the nanocomposite,[23, 24] ultrasonic dispersion in solution,[14, 25] melt processing,[10, 26–30] the use of surfactants,[21, 31] electrospinning,[32] gelation/crystallization[33] and electrode chemistry.[34] Furthermore, research has shown improved mechanical properties via nanotube orientation by melt drawing after melt compounding in a poly(methyl methacrylate) (PMMA) matrix with low levels (~1 wt%) of multiwall carbon nanotubes (MWNTs).[27]

Polypropylene (PP) has been a common matrix used for carbon nanotube composites. Both single wall[26, 35–38] and multiwall[11, 39–41] nanotubes have been used to study crystallization behavior in PP and polymer morphology as well as mechanical properties. Results have been mixed, especially for mechanical properties, where one study[26] showed no significant improvement in mechanical properties, and others have shown moderate improvements in tensile strength, but decreased toughness.[38]

8.2 Producing carbon nanotube-polymer fibers

Exxon Mobil Type 3155 Polypropylene with a melt flow rate of 36 g/10 min, density of 0.9 g/cm^3, and molecular weight distribution of 2.8, was utilized as the matrix. MWNTs were supplied by Nano-Lab (Newton, MA). These nanotubes (with purity > 95%) were produced via plasma-enhanced chemical vapor deposition (PE-CVD) using acetylene and ammonia with iron catalyst particles on a mesoporous silica substrate.[42] The diameter is specified as 20–50 nm with lengths ranging between 5 and 20 μm.

The PP pellets were ground into a powder using a SPEX® CertiPrep Freezer Mill (Metuchen, NJ). The pellets were precooled for 5 min followed by three 2 min grinding cycles at 10 Hz. Between each cycle the sample was cooled for a 1 min interval. Nanocomposites were created by dry blending the PP powder with a given ratio of MWNTs (0.25, 0.50, 1 and 3 wt%).

The preblend was then fed into a Haake Mini-Lab twin screw extruder and processed for 10 min at 100 rpm and 200 °C (conditions previously optimized via a controlled experiment). After 10 min, the composite was extruded through a 1.75 mm cylindrical die. Oriented samples were created using a specially designed winding apparatus with melt and solid drawing capabilities. The winding apparatus consists of three PP rollers each driven by variable speed motors. The center to center distance for the first and second rollers is 15 in (380 mm), and for the second and third rollers is 24.75 in (630 mm). Each motor is capable of linear speeds on the outer roller surface of 45–450 in/min (1.1–11 m/min). The rollers can all be controlled independently. For melt drawing, the material is drawn using the first roller and the sample is collected using the third roller. Using this procedure, melt-drawn samples had a nominal draw ratio of 12:1. In coupled melt/solid

drawing, the material is wound around the first roller at one speed, and then wound around the second roller at a faster speed, and is collected by the third roller at the same speed as that for the second roller. Using this procedure, coupled melt/solid-drawn samples had nominal draw ratios of 23:1 and 24:1. After extruding both oriented and unoriented samples (i.e. no drawing via the winding apparatus), the mechanical and morphological properties were characterized using the techniques described in the following sections.

8.3 Thermal characterization

A Perkin Elmer Pyris 1 Thermal Gravimetric Analyzer (TGA) was used to determine the weight percent concentration of nanotubes in the composite samples. Approximately 20 mg of each sample was heated from 25 to 950 °C at a rate of 20 °C/min in a nitrogen environment. As the sample is heated, the mass is measured as function of temperature. The mass retained is calculated by dividing the mass at the temperature of interest by the initial mass. Once the polymer has degraded, the remaining mass is assumed to be the mass of the MWNTs since the MWNTs are thermally stable in nitrogen to temperatures above 1000 °C (from discussion with David Carnahan, President of Nano-Lab).

Owing to the high thermal stability of carbon nanotubes, the PP matrix will degrade several hundred degrees before nanotubes in a nitrogen environment (from discussion with David Carnahan, President of Nano-Lab). Figure 8.1 shows a comparative plot of the 100% PP sample with nanocomposites ranging from 0.25 to 3 wt% MWNTs. Owing to the thermal

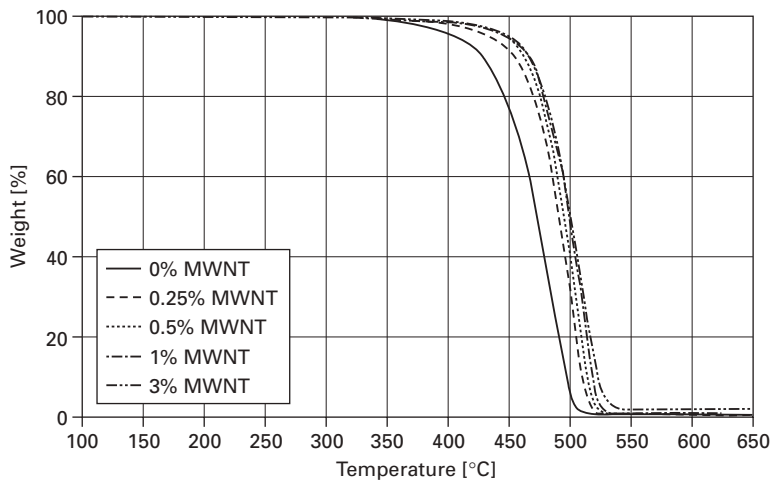

8.1 TGA plot of PP nanocomposites as a function of MWNT loading.

stability of the nanotubes, the 3 wt% composite sample shows thermal stability (i.e. no mass loss) to 192 °C (80 °C higher than that for pure PP).

8.3.1 Differential scanning calorimetry

The crystallinity of the composite samples was studied using a Perkin Elmer Diamond differential scanning calorimeter. Each sample was heated from 25 to 200 °C at a rate of 10 °C/min. The thermograms were used to determine the onset melting temperature, peak melting temperature, peak area and enthalpy of melting (ΔH). To achieve more accurate values for these temperatures, a straight baseline was drawn connecting each flat side of the melting peak. The shapes of the curves at different loading levels were evaluated qualitatively to determine changes in crystal structure. Finally, the overall percent crystallinity was calculated by dividing the enthalpy of melting for the sample (ΔH) by the enthalpy of melting for 100% crystalline PP (ΔH_f^o = 207.1 J/g).[43]

Figure 8.2 shows the melting endotherms from differential scanning calorimetry (DSC) for 0, 1 and 3 wt% drawn samples (to a 12:1 draw ratio), respectively. The crystallinity was calculated using a ΔH_f^o value of 207.1 J/g for 100% crystalline PP[43] and Equation 8.1, shown below (where ΔH is the enthalpy measured from the experiment). The percent crystallinity, onset temperature and melting peak temperature are tabulated in Table 8.1.

$$\% \text{ Crystallinity} = \frac{\Delta H}{\Delta H_f^o} \times 100 \qquad [8.1]$$

Figure 8.2 shows the melting peak has a similar shape at the different loading levels. Table 8.1 shows little quantitative change in the overall percent crystallinity and peak melting temperature. The addition of up to 3 wt% MWNTs in PP did not significantly alter the overall crystallinity as observed by DSC, which is consistent with results from the literature.[26, 39, 40]

8.4 Fiber morphology

The morphology of the PP/nanotube composite samples was observed both qualitatively and quantitatively. The dispersion and orientation of the nanotubes was verified through transmission electron microscopy (TEM) and scanning electron microscopy (SEM). Finally, the polymer crystal structure and orientation was investigated quantitatively through wide-angle X-ray diffraction (WAXD).

8.4.1 Transmission electron microscopy

A Jeol Inc. model 100S transmission electron microscope operating at 100 kV was utilized to view the orientation of the nanotubes. Both drawn and undrawn

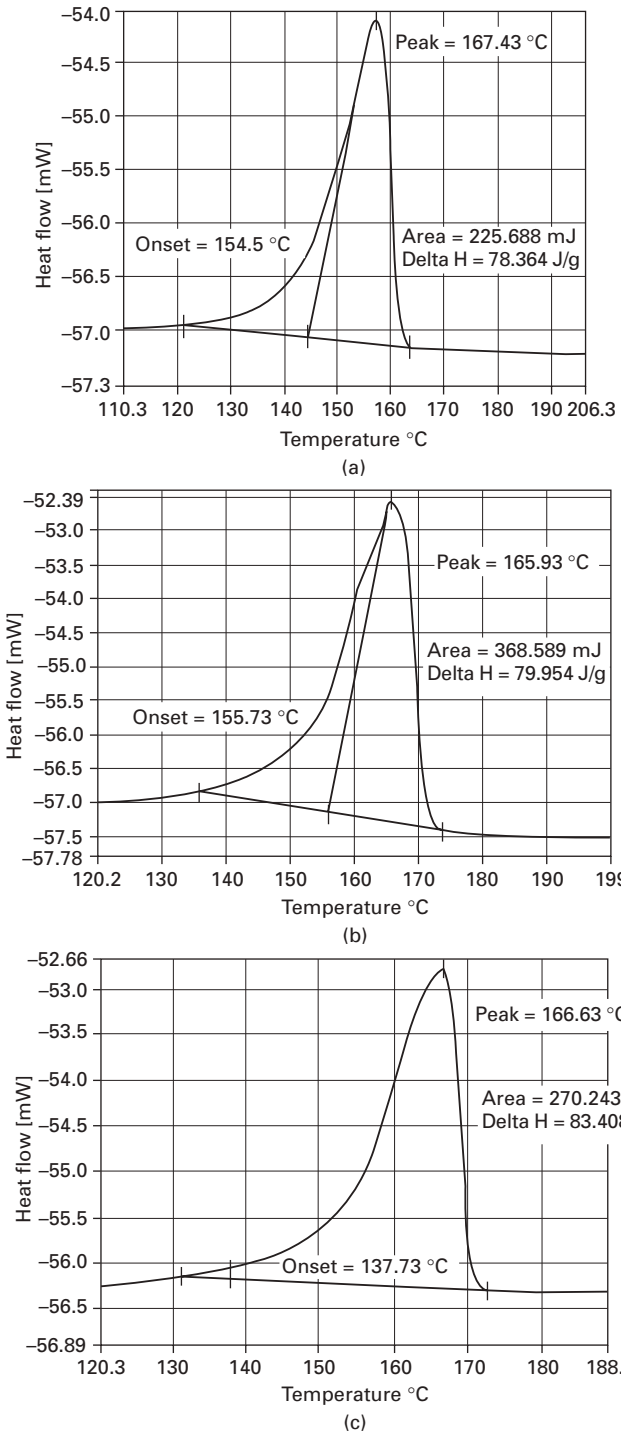

8.2 DSC melting peaks for (a) 0 wt%, (b) 1 wt%, and (c) 3 wt% MWNTs in PP.

Table 8.1 Percentage crystallinity and peak melting temperature

Figure 8.2	MWNT (wt%)	Draw ratio	Crystallinity (%)	Peak melting temperature (°C)
(a)	0	12:1	38	167
(b)	1	12:1	39	166
(c)	3	12:1	40	167

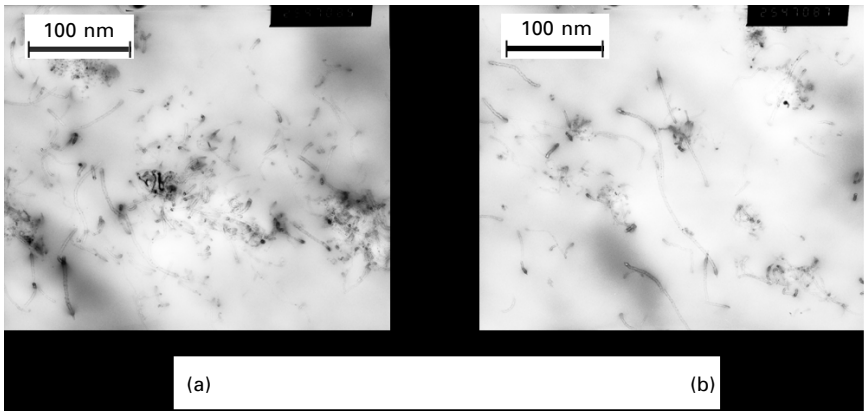

8.3 TEM images of 3 wt % MWNT in PP: (a) unoriented, (b) oriented, 12:1 draw ratio.

samples were observed to determine the extent of orientation for the nanotubes. Ultrathin cross-sections of the fiber sample were microtomed and placed on standard TEM grids. Images were captured at magnifications of 25 000× and 50 000×.

Figure 8.3 shows TEM images of 3 wt% MWNTs in PP both unoriented (no draw) and oriented at 12:1 draw ratio. These images depict the cross-section of the fiber parallel to the drawing direction. Comparing the two images reveals how melt drawing the nanocomposite orients the nanotubes. In the unoriented image (Fig. 8.3a) whole nanotubes lying at various oblique angles are observed; whereas the image of the drawn sample (Fig. 8.3b) shows nanotubes that run parallel to the fiber axis, therefore indicating flow-induced orientation along the fiber axis.

8.4.2 Scanning electron microscopy

A Jeol Inc. Field Emission model J600F scanning electron microscope, operating at 5 kV, was utilized to further examine the orientation of the nanotubes. Both drawn and undrawn samples were imaged to determine the effect of melt drawing on nanotube orientation. The samples were cleaved

with a sharp razor normal to the fiber axis. Next, the samples were coated with an Au/Pd film approximately 100 Å thick to reduce charging. After coating, they were mounted with the microscope looking down the fiber axis, depicting the cross-section of the fiber normal to the drawing direction. Images were captured at magnifications of 20 000×, 30 000× and 40 000×.

Figure 8.4 shows SEM images of 3 wt% MWNTs in PP both unoriented (no draw) and oriented at 12:1 draw ratio. These images depict the cross-section of the fiber normal to the drawing direction. Comparing the two SEM images further reveals how drawing the nanocomposite orients the nanotubes. Since the samples are cleaved, the fracture plane will propagate along the weakest section of the composite, namely the interface between the nanotube and the matrix. In the case where the nanotubes are unoriented, the fracture plane will contain nanotubes lying at various oblique angles. As is shown in Fig. 8.4a, whole nanotubes are observed indicating the random orientation of the nanotubes, whereas, the image of the drawn sample (Fig. 8.4b) shows only the tips of the nanotubes (which run parallel to the fiber axis), therefore indicating flow-induced orientation along the fiber axis.

Qualitative evidence of nanotube alignment is observed in both the transmission and scanning electron microscopy images. Therefore as the material is being extruded and melt-drawn, the extensional flow causes nanotube orientation along the fiber axis. As a result, the maximum load transfer can be achieved, leading to the property improvements discussed in Section 8.5.

8.4.3 Wide-angle X-ray diffraction

A Bruker AXS wide-angle X-ray diffractometer with a Cu Kα average source (λ = 1.5418 Å) was utilized to look at the crystalline structure of the overall composite sample and to calculate the Herman orientation factor. The samples were run in transmission and reflection modes. In the reflection mode, the

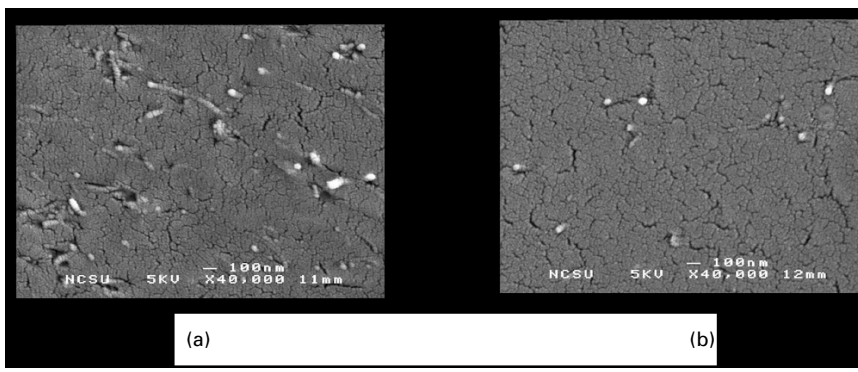

8.4 SEM images of 3 wt% MWNT in PP: (a) unoriented, (b) oriented, 12:1 draw ratio.

fibers were mounted on a 1 cm × 1 cm silicon wafer. When mounting the sample in the unit, the fiber axis was oriented in the vertical direction. In this mode, the beam hits the sample at a predetermined angle, and the X-rays diffract into the detector creating the diffraction pattern. The instrument was set to run the scan with ω set at 15°. The scan was run for 900 seconds. From the diffraction pattern, the intensity is measured as a function of 2Θ, and plots of intensity versus 2Θ are created. In the transmission mode, the fiber axis is oriented in the horizontal direction. The beam passes through the sample, and the X-rays diffract off the sample to the detector, creating cones seen as rings on the diffraction pattern. From these diffraction patterns, the intensity around each ring is measured and plotted against χ, the angle around the ring starting at 6 o'clock moving counter-clockwise. The data were then corrected for background scattering. Using ImageJ software, the transmission images were transformed to plots of intensity versus scattering vector, q.

Figure 8.5 shows the 2D wide-angle X-ray diffraction patterns and corresponding scattering vector versus intensity plots for drawn samples (12:1) at 0 and 3 wt% MWNT loading. The plots both reveal the four peaks corresponding to the four-ring pattern common to PP fiber X-ray diffraction. However, all four peaks for the 3 wt% sample (Fig. 8.5b) are more distinct and intense than the peaks for the 0 wt% sample (Fig. 8.5a). Similar transitions for intensity were observed by Broda[44] in pure PP fiber extruded with increasing take-up speeds. The study concluded the decrease in intensity resulted from the presence of a mesophase coupled with the PP α phase. Based on comparison with Broda's X-ray diffraction plots, the 0 wt% sample contains mesophase coupled with α phase PP crystals. However, the 3 wt% sample contains only α phase PP crystals indicating a more ordered crystal structure as a result of the aligned MWNTs. Although different PP crystal phases can be responsible for changes in the mechanical properties,[43] the strengthening mechanism proposed here is primarily due to load transfer from the polymer matrix to the nanotube.

Using the intensity as a function of angle, χ, around each diffraction ring, Herman's orientation factor can be determined. Herman's orientation factor (P_2) is defined in Equation 8.2:

$$P_2 = \frac{3 < \cos^2 \chi > - 1}{2} \qquad [8.2]$$

In Equation 8.2, $<\cos^2\chi>$ is the average cosine squared value for the diffraction ring and is calculated using the following equation:

$$< \cos^2 \chi > = \frac{\sum_{i=0}^{90} I_i \cos^2 \chi_i \sin \chi_i}{\sum_{i=0}^{90} I_i \sin \chi_i} \qquad [8.3]$$

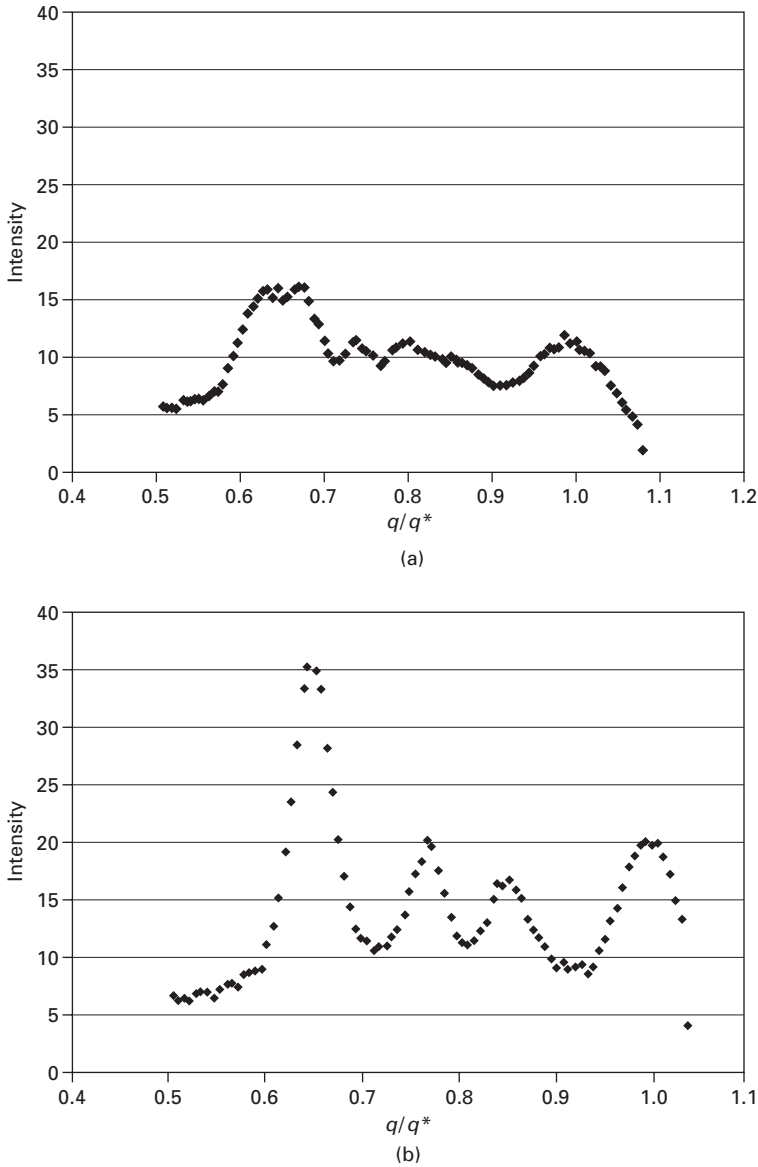

8.5 WAXD patterns for (a) 0 wt% and (b) 3 wt% MWNTs in PP with 12:1 draw ratio.

In Equation 8.3, I_i and χ_i are the intensity and angle at the ith (0.5° step) position along the diffraction ring. The diffraction data were corrected to shift the background intensity to a value of zero. After correcting the background, Herman's orientation factors for each crystallographic ring of a

Table 8.2 Herman's orientation factors

Sample	110	040	130	$13\bar{1}$
0% Unoriented	0.42	–0.22	–0.08	–0.18
0% Oriented	0.76	–0.37	–0.33	–0.24
3% Unoriented	–0.10	–0.08	–0.11	–0.27
3% Oriented	0.43	–0.34	–0.26	–0.22

Table 8.3 ΔP_2 values

Ring	0 wt% MWNT	3 wt% MWNT
110	0.34	0.53
040	–0.15	–0.26
130	–0.25	–0.15
$13\bar{1}$	–0.06	0.05

virgin PP sample and a 3 wt% MWNT loaded sample were calculated using Equations 8.2 and 8.3. The results are tabulated in Table 8.2.

Herman's orientation factor can vary between –0.5 to 1. If the factor is –0.5, the crystal plane is oriented perpendicular to the reference direction of $\chi = 0$, the direction of draw, whereas a factor of 1 denotes orientation parallel to the reference direction. Random orientation is observed when the factor equals 0. Herman's orientation analysis can be used to quantify crystal orientation as a function of nanotube concentration and polymer and nanotube orientation. In the as-extruded (or undrawn) samples, the nanotube addition promotes isotropization of the composite as demonstrated by the P_2 coefficients being slightly negative but close to zero (for nanotube filled samples). Further examination of the change in the P_2 coefficients ($\Delta P_2 = P_{2,\text{oriented}} - P_{2,\text{unoriented}}$) from the unoriented to the oriented state demonstrates the effects of drawing both pure PP and filled PP (with 3 wt% MWNT). The ΔP_2 factors are tabulated in Table 8.3. As shown by Table 8.3, drawing the fiber samples results in improved orientation overall. The 110 crystal planes become more oriented along the fiber axis, whereas the 040 and 130 planes become more oriented perpendicular to the fiber axis. However, the $13\bar{1}$ plane remains randomly oriented. It is germane to note that the orientation along the fiber axis for the 110 plane is more highly oriented for the nanotube loaded sample. Likewise, the orientation perpendicular to the fiber direction for the 040 plane is more highly oriented in the nanotube loaded sample. This indicates that the crystal structure becomes more oriented with nanotube orientation, whereas the opposite is true of the 130 plane.

8.5 Mechanical properties of fibers

Tensile tests were preformed to measure the tensile toughness (MJ/m^3), modulus (MPa) and yield strength (MPa) of the oriented and unoriented samples at each loading level. The tests were performed on an Instron® Model 5544 using the Bluehill® Version 1.00 software package. Ten replicates of each sample were run to obtain average, standard deviation and standard error values. Each experiment was conducted with a gauge length of 25.4 mm, crosshead speed of 25.4 mm/min and data acquisition rate of 50 points/second. To obtain the elastic modulus, a linear regression technique was utilized to define the slope of the stress–strain curve in the initial region before yield. The toughness was calculated using the product of the energy at break at 98% maximum load and the sample volume. The energy at break was defined as the area under the force–elongation curve up to the break point, which was defined as 98% of the maximum load. The volume was defined for a cylinder with initial diameter, d, and initial length, l, as follows:

$$V = \pi*(d^2/4)*l \qquad [8.4]$$

Therefore, the defined calculation for toughness equals the energy at break divided by the volume of the sample. The yield strength was calculated using the slope threshold algorithm from the BlueHill® software package. In the algorithm, the yield is calculated as the point where the slope of the stress/strain curve decreases to a user-selected percentage of the modulus slope. After experimenting with several different percentages, the value chosen was 2%, because the marker placed on the stress–strain curve most closely approximated the appropriate location for yield in a polymer system.

Figure 8.6 shows a representative set of stress–strain curves for the 12:1 melt-drawn samples at each nanotube concentration. The addition of nanotubes significantly alters the stress–strain behavior of the fibers. The ultimate stress, yield stress and modulus increase with the addition of nanotubes. In contrast, the ultimate elongation slightly decreases with the addition of nanotubes. The significant increases in ultimate and yield stress combined with a small decrease in ultimate elongation lead to the observed increases in toughness.

Figure 8.7 shows the results for the tensile toughness (Fig. 8.7a), modulus (Fig. 8.7b) and yield stress (Fig. 8.7c) as a function of nanotube concentration (from 0 to 3 wt%) and orientation (no draw, or unoriented, and oriented with a draw ratio of 12:1, 23:1 and 24:1). The white bars represent undrawn samples, the black bars represent fibers melt-drawn to a 12:1 ratio, the vertical striped bars represent fibers that are melt and then cold drawn to a 23:1 ratio, and the horizontal striped bars represent fibers coupled melt/solid drawn to a 24:1 ratio. The error bars are based on the standard error of ten samples tested at each concentration level. Because of the difficulty of drawing the PP/3 wt% MWNT samples to the 24:1 draw ratio, homogeneous samples could not be collected. In both the tensile toughness and modulus, optimal

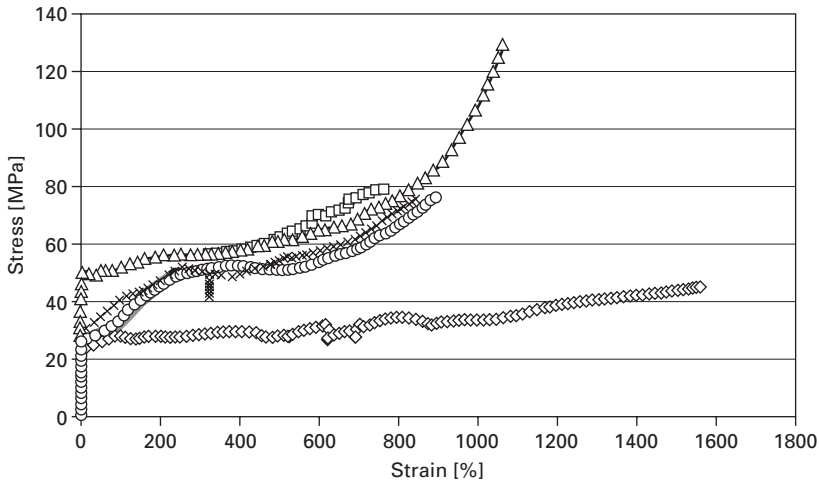

8.6 Stress–strain curves for 12:1 melt-drawn fibers (◇ PP, □: PP/0.25, △: PP/0.5, × PP/1, ○ PP/3).

loading was achieved at 0.25 wt%. For the yield strength, the maximum occurred at about 1 wt%.

As observed in Fig. 8.7a, the toughness of the unoriented (no draw) material is so low at all concentrations that it does not show up on the scale of the figure. Therefore, the orientation of PP alone improves tensile toughness. However, with the addition of nanotubes, the oriented samples show a statistically significant improvement at concentrations of 0.25–0.5 wt% MWNTs. As proposed by Gorga and Cohen[27] the toughness increase in amorphous materials results from the crack bridging ability of the nanotubes. As microcracks form, the nanotubes bridge the gap formed by the crack, slowing down the crack propagation and increasing the overall material toughness. Synonymously, in semicrystalline materials, such as polypropylene, the nanotubes act as tie molecules between crystalline regions rather than crack bridges, thereby also acting as toughners. At concentrations greater than 0.5 wt%, toughness decreases. The decrease results as the nanotubes begin to aggregate, forming stress concentrations similar to those caused by voids in composite systems as discussed by Wilbrink *et al.*[45]

Similarly, Fig. 8.7b shows an increasing modulus with concentrations up to 0.25 wt% followed by a decrease for both undrawn and drawn samples. Figure 8.7b shows orientation of PP alone increases the modulus but not to the level attained with the addition of nanotubes. Adding low levels of nanotubes to PP improves the mechanical properties up to an optimal concentration (0.25 wt%) above which nanotube aggregation leads to property decreases via stress concentrations (as discussed above). Although modulus decreases above 0.25 wt%, the filled samples with orientation exhibit improved modulus

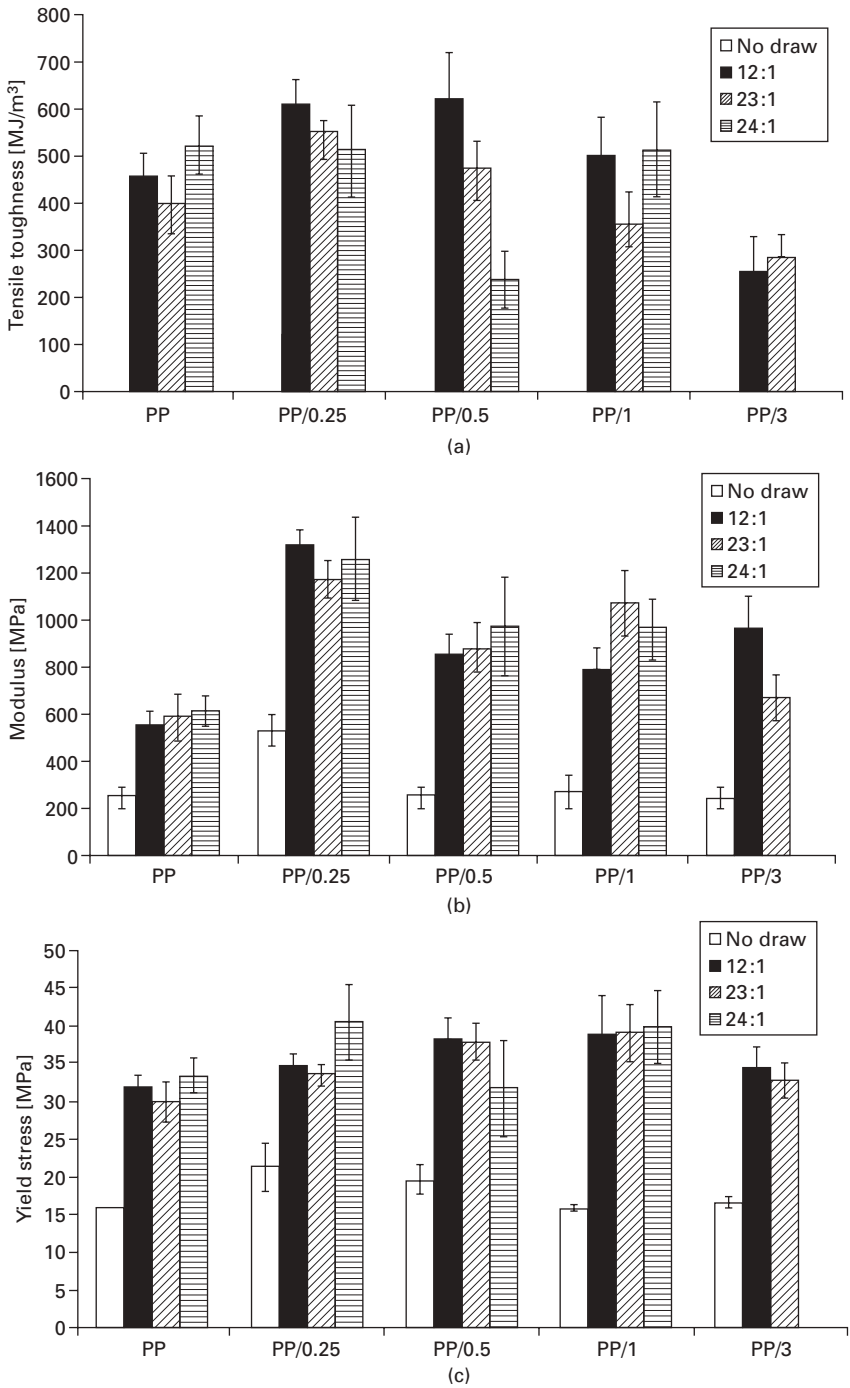

8.7 (a) Tensile toughness (MJ/m^3), (b) modulus (MPa) and (c) yield stress (MPa) as a function of nanotube loading in PP for several draw ratios.

over that of the drawn PP for all nanotube concentrations studied. The modulus increase can either be attributed to load transfer (from matrix to particle) or crystallinity changes in PP due to the addition of MWNTs (although none was detected via DSC). According to the rule of mixtures, the maximum modulus should reach 2.2 GPa for a 0.25 wt% sample, assuming nanotube modulus of 1 TPa and PP modulus of 550 MPa. However, owing to less than optimal load transfer, the maximum modulus achieved at a loading of 0.25 wt% is 1.3 GPa. As shown by electron microscopy (Sections 8.4.1 and 8.4.2), the nanotubes are not perfectly aligned. Poor adhesion to the matrix material and imperfections and defects in the nanotube structure will also result in a reduced composite modulus.

Likewise, Fig. 8.7c shows statistically significant increases in the yield stress with the addition of nanotubes to PP. Furthermore, the increase to a maximum value followed by a decrease is also observed. However, the maximum occurs at a higher concentration range of about 0.5–1 wt% MWNTs. Additionally, the increase is not as significant and pronounced as in the case of the toughness and modulus, indicating that the nanotubes are not as effective at resisting plastic deformation.

Additionally, little to no statistical difference between the melt-drawn (12:1) samples and the coupled melt/solid-drawn (23:1, 24:1) samples is observed (as shown by the error bars). However, the toughness for the 0.5 wt% sample is significantly lower for reasons we cannot explain, but appears to be an anomaly. Therefore, the addition of fibers that are melt and then solid-drawn does not affect the values and trends achieved by melt drawing alone. The ability to melt-draw to higher levels could possibly lead to further property improvements. Table 8.4 gives a summary of the average mechanical properties for each loading level and draw ratio.

8.5.1 Dynamic mechanical analysis

Dynamic mechanical analysis (DMA) was used to investigate the viscoelastic properties of the sample. The Q800 Dynamic Mechanical Analyzer from TA Instruments was used for these experiments. The fiber clamp was used for the oriented samples, and the film clamp was used for the unoriented samples. The samples were run using a DMA multi-frequency–strain procedure with a temperature step and frequency sweep. All samples were cylindrical with length l and diameter d. The temperature was stepped from 30 to 150 °C with 20 °C increments. The frequency sweep was 0.01–100 Hz on a logarithmic scale with 3 points per decade. Time–temperature superposition master curves were created by selecting a reference temperature in the middle of the experimental temperature range, 90 °C, and shifting the other curves in relation to the reference curve. The storage modulus, loss modulus and tan δ master curves were analyzed for trends as a function of nanotube loading.

Table 8.4 Summary of mechanical properties for PP and composite samples as a function of nanotube concentration and fiber draw ratio

Sample name	MWNT (wt%)	Draw ratio	Tensile toughness (MJ/m^3)	Modulus (MPa)	Yield stress (MPa)
PP	0	0	0.8	257	15.8
PP	0	12:1	457	551	31.8
PP	0	23:1	397	585	29.9
PP	0	24:1	523	611	33.3
PP/0.25	0.25	0	1.1	528	21.2
PP/0.25	0.25	12:1	608	1312	34.6
PP/0.25	0.25	23:1	549	1167	33.4
PP/0.25	0.25	24:1	512	1250	40.3
PP/0.5	0.5	0	1.7	254	19.4
PP/0.5	0.5	12:1	620	852	38.0
PP/0.5	0.5	23:1	474	877	37.7
PP/0.5	0.5	24:1	237	967	31.7
PP/1	1	0	0.7	266	15.8
PP/1	1	12:1	500	782	38.8
PP/1	1	23:1	355	1064	38.8
PP/1	1	24:1	511	949	40.0
PP/3	3	0	0.9	238	16.4
PP/3	3	12:1	254	957	34.2
PP/3	3	23:1	286	662	32.6

Additionally, the activation energy of the composite fibers was calculated using the Arrhenius equation and was analyzed for trends as a function of nanotube loading.

The experiments were performed at several temperature intervals and shifted to a reference temperature (90 °C). The storage modulus was measured as a function of frequency for seven temperatures (ranging from 30 to 150 °C) for the 0.25 wt% MWNT sample. At each temperature the frequency ranged from 0.01 to 100 Hz.

Horizontally shifting the curves around a reference temperature, i.e. 90 °C, produced the master curve. The *x*-axis shift factor, a_T, for each temperature was plotted as a function of the temperature. The data can be fit using the Arrhenius equation (Equation 8.5) as a mathematical model (as shown in Fig. 8.8):

$$\ln a_T = \frac{-E_a}{R}\left(\frac{1}{T_0} - \frac{1}{T}\right) \qquad [8.5]$$

In Equation 8.5, E_a is the activation energy of the polymer system, a_T is the time-based shift factor, R is the gas constant, T is the measurement temperature, and T_0 is the reference temperature (in absolute units). As the polymer is strained, it must overcome an energy barrier to allow the chains to move and rotate about the main chain bonds. The energy barrier is known as the activation energy of the polymer system.[46] Figure 8.9 shows a plot of this activation

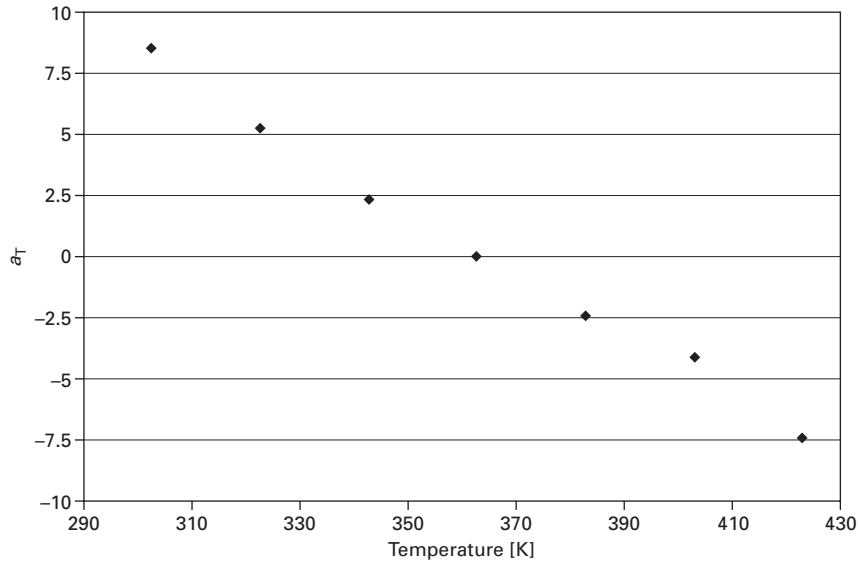

8.8 Shift factor as a function of temperature for 0.25 wt% MWNTs in PP (12:1 draw ratio) with Arrhenius model.

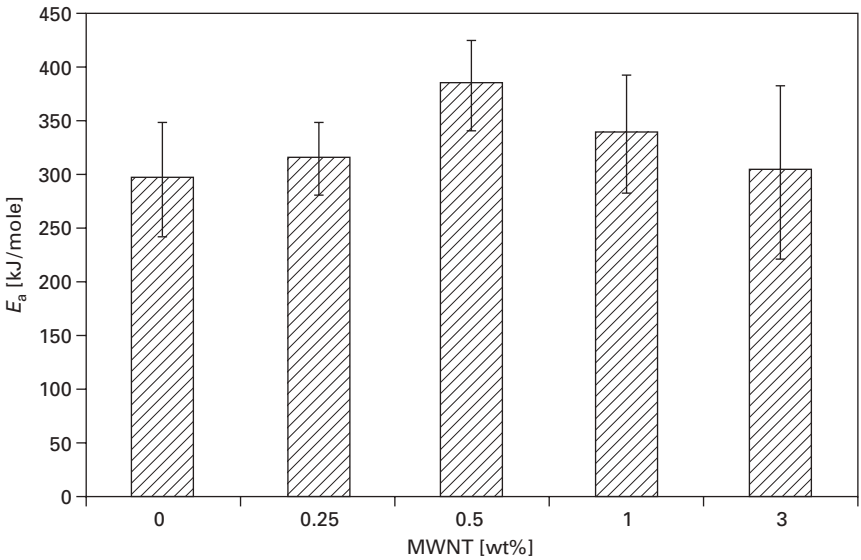

8.9 Activation energy of fibers as a function of nanotube loading with 12:1 draw ratio.

energy as a function of nanotube loading with errors bars representing the standard error of the Arrhenius model fit for the 0.25 wt% sample at the 12:1 draw ratio.

Similar to the tensile data, a maximum, with the addition of nanotubes, is seen in the activation energy. However, the trend is only marginally statistically significant as shown by the error bars. With the addition of high modulus nanotubes, the resistance to strain should increase similar to that for the toughness (resistance to rupture) and modulus (resistance to deformation). However, as the concentration of nanotubes increases to concentrations greater than 0.5 wt%, aggregates of the nanotubes form, therefore decreasing the reinforcing effect.

8.6 Conclusions and future trends

Dispersion and orientation of MWNTs in PP simultaneously created a tougher and stiffer material. The tensile properties increased as a function of loading to a maximum value at a loading level of 0.25 wt% MWNTs. Toughness increases up to 32% over pure PP were due to the nanotubes acting as tie molecules between the crystalline regions. Modulus increases of up to 138% were due to load transfer from polymer matrix to nanotube. The activation energy, calculated from dynamic mechanical experiments, also revealed a maximum as a function of nanotube loading. Therefore, the mechanical properties (modulus, toughness, yield and activation energy) all exhibited a maximum at a low nanotube loadings (<1 wt% MWNTs). The DSC results showed no change in overall crystallinity. Wide-angle X-ray diffraction indicates a crystal structure change from α phase coupled with mesophase to α phase only with nanotube loading in oriented samples; however, the trend in mechanical properties as a function of nanotube loading supports stiffening as a function of load transfer. In drawn samples, the nanotubes were shown by transmission electron microscopy and scanning electron microscopy to be highly aligned. Although nanotube orientation was revealed through these techniques, isotropization (for randomly dispersed nanotubes) and increased orientation for the melt-drawn (or oriented) samples was quantified by Herman's orientation factor analysis of the wide-angle X-ray diffraction patterns. Through this work, the processing parameters and morphological and mechanical properties of a promising nanocomposite material were developed for potential use in advanced fiber and material applications. Future work will focus on the thermal and electrical conductivity of these nanocomposite fibers.

The current results reinforce the need to design the nanotube/polymer interface so that sufficient load transfer occurs. Improved adhesion and stress transfer across the interface would enable the exceedingly high modulus value of the nanotubes to contribute in the expected way to the nanocomposite modulus. At the same time, it is important to tailor the surface adhesion properly to capitalize on the role of nanotubes in the toughening of the nanocomposites. If the interfaces of the bridging nanotubes are exceedingly well bonded, fracture would occur at very high stresses, but without significant

development of strain, thereby producing strong but brittle materials. A properly designed polymer/nanotube interface would adhere at low stresses to provide modulus enhancement while providing frictional slip modes at higher stresses for energy dissipation. Therefore future work should focus on the ability to engineer the interface to promote both load transfer and provide frictional energy dissipation. Additionally, researchers are also making nanotube ropes (without a polymer matrix). With this methodology, one can imagine that the strength of the ropes should approach that of the individual nanotubes. Issues here will include ductility, abrasion resistance and processability.

8.7 Sources of further information and advice

In addition to the references cited throughout this chapter, there are some good review sources for polymer nanotube composites. These include:

- Thostenson, E.T., Ren, Z. and Chou, T.W., Advances in the science and technology of carbon nanotubes and their composites: a review. *Composites Science and Technology*, 2001. **61**(13): p. 1899–1912.
- Harris, P.J.F., Carbon nanotube composites. *International Materials Review*, 2004. **49**(1): p. 31–43.
- Lau, K.T. and Hui, D., The revolutionary creation of new advanced materials – carbon nanotube composites. *Composites Part B – Engineering*, 2002. **33**(4): p. 263–277.

Another source which discusses polymer nanocomposites (not specific to carbon nanotubes) is:

- Krishnamoorti, R. and Vaia, R.A., *Polymer Nanocomposites: Synthesis, Characterization, and Modeling*. ACS Symposium Series, 2002. **804**.

For detailed information on carbon nanotubes, the following will provide the reader with a solid foundation:

- Dresselhaus, M.S. and Dai, H., Advances in carbon nanotubes. *MRS Bulletin*, 2004. **29**(4).
- Dresselhaus, M.S., Dresselhaus, G., Charlier, J.C. and Hernandez, E., Electronic, thermal and mechanical properties of carbon nanotubes. *Philosophical Transactions of the Royal Society of London Series A – Mathematical Physical and Engineering Sciences*, 2004. **363**(1823): p. 2065–2098.

8.8 Acknowledgments

The author would like to thank William Dondero for running the experiments, collecting the data, and performing the analyses. The author gratefully acknowledges Professor Richard Spontak for useful discussions regarding

the analysis of the X-ray diffraction data. In addition, the author thanks Professor Jon Paul Maria for use of the X-ray facility and training. This work was supported by the North Carolina State University Faculty Research and Professional Development Program and the NCSU Nanotechnology Initiative.

8.9 References

1. Iijima, S., Helical microtubules of graphitic carbon. *Nature*, 1991. **354**(6348): p. 56–58.
2. Iijima, S. and T. Ichihashi, Single-shell carbon nanotubes of 1-nm diameter. *Nature*, 1993. **363**(6430): p. 603–605.
3. Ebbesen, T.W., *et al*., Electrical conductivity of individual carbon nanotubes. *Nature*, 1996. **382**(6586): p. 54–56.
4. Hone, J., *et al*., Thermal conductivity of single-walled carbon nanotubes. *Physical Review B*, 1999. **59**(4): p. R2514–R2516.
5. Treacy, M.M.J., T.W. Ebbesen, and J.M. Gibson, Exceptionally high Young's modulus observed for individual carbon nanotubes. *Nature*, 1996. **381**(6584): p. 678–680.
6. Bower, C., *et al*., Deformation of carbon nanotubes in nanotube–polymer composites. *Applied Physics Letters*, 1999. **74**(22): p. 3317–3319.
7. Cooper, C.A., *et al*., Distribution and alignment of carbon nanotubes and nanofibrils in a polymer matrix. *Composites Science and Technology*, 2002. **62**(7–8): p. 1105–1112.
8. Haggenmueller, R., *et al*., Aligned single-wall carbon nanotubes in composites by melt processing methods. *Chemical Physics Letters*, 2000. **330**(3,4): p. 219–225.
9. Jin, L., Bower, C. and Zhou, O. Alignment of carbon nanotubes in a polymer matrix by mechanical stretching. *Applied Physics Letters*, 1998. **73**(9): p. 1197–1199.
10. Jin, Z., *et al*., Dynamic mechanical behavior of melt-processed multi-walled carbon nanotube/poly(methyl methacrylate) composites. *Chemical Physics Letters*, 2001. **337**(1,2,3): p. 43–47.
11. Kearns, J.C. and R.L. Shambaugh, Polypropylene fibers reinforced with carbon nanotubes. *Journal of Applied Polymer Science*, 2002. **86**(8): p. 2079–2084.
12. Lozano, K. and E.V. Barrera, Nanofiber-reinforced thermoplastic composites. I. Thermoanalytical and mechanical analyses. *Journal of Applied Polymer Science*, 2001. **79**(1): p. 125–133.
13. Potschke, P., Fornes, T.D. and Paul, D.R. Rheological behavior of multiwalled carbon nanotube/polycarbonate composites. *Polymer*, 2002. **43**(11): p. 3247–3255.
14. Safadi, B., Andrews, R. and Grulke, E.A. Multiwalled carbon nanotube polymer composites: synthesis and characterization of thin films. *Journal of Applied Polymer Science*, 2002. **84**(14): p. 2660–2669.
15. Schadler, L.S., Giannaris, S.C. and Ajayan, P.M. Load transfer in carbon nanotube epoxy composites. *Applied Physics Letters*, 1998. **73**(26): p. 3842–3844.
16. Chen, J., *et al*., Solution properties of single-walled carbon nanotubes. *Science* 1998. **282**(5386): p. 95–98.
17. Mitchell, C.A., *et al*., Dispersion of functionalized carbon nanotubes in polystyrene. *Macromolecules*, 2002. **35**(23): p. 8825–8830.
18. Bubert, H., *et al*., Characterization of the uppermost layer of plasma-treated carbon nanotubes. *Diamond and Related Materials*, 2003. **12**(3–7): p. 811–815.
19. Eitan, A., *et al*., Surface modification of multiwalled carbon nanotubes: toward the

tailoring of the interface in polymer composites. *Chemistry of Materials*, 2003. **15**(16): p. 3198–3201.
20. Jang, J., Bae, J. and Yoon, S.H. A study on the effect of surface treatment of carbon nanotubes for liquid crystalline epoxide–carbon nanotube composites. *Journal of Materials Chemistry*, 2003. **13**(4): p. 676–681.
21. Shaffer, M.S.P., Fan, X. and Windle, A.H. Dispersion and packing of carbon nanotubes. *Carbon*, 1998. **36**(11): p. 1603–1612.
22. Star, A., *et al*., Preparation and properties of polymer-wrapped single-walled carbon nanotubes. *Angewandte Chemie*, *International Edition*, 2001. **40**(9): p. 1721–1725.
23. Jia, Z., *et al*., Study on poly(methyl methacrylate)/carbon nanotube composites. *Materials Science and Engineering A*, 1999. **A271**: p. 395–400.
24. Deng, J., *et al*., Carbon nanotube–polyaniline hybrid materials. *European Polymer Journal*, 2002. **38**(12): p. 2497–2501.
25. Qian, D., *et al*., Load transfer and deformation mechanisms in carbon nanotube–polystyrene composites. *Applied Physics Letters*, 2000. **76**(20): p. 2868–2870.
26. Bhattacharyya, A.R., *et al*., Crystallization and orientation studies in polypropylene/single wall carbon nanotube composite. *Polymer*, 2003. **44**(8): p. 2373–2377.
27. Gorga, R.E. and R.E. Cohen, Toughness enhancements in poly(methyl methacrylate) by addition of oriented multiwall carbon nanotubes. *Journal of Polymer Science Part B – Polymer Physics*, 2004. **42**(14): p. 2690–2702.
28. Potschke, P., Bhattacharyya, A.R. and Janke, A. Melt mixing of polycarbonate with multiwalled carbon nanotubes: microscopic studies on the state of dispersion. *European Polymer Journal*, 2004. **40**(1): p. 137–148.
29. Siochi, E.J., *et al*., Melt processing of SWCNT – polyimide nanocomposite fibers. *Composites Part B – Engineering*, 2004. **35**(5): p. 439–446.
30. Tang, W.Z., Santare, M.H. and Advani, S.G. Melt processing and mechanical property characterization of multi-walled carbon nanotube/high density polyethylene (MWNT/HDPE) composite films. *Carbon*, 2003. **41**(14): p. 2779–2785.
31. Gong, X., *et al*., Surfactant-assisted processing of carbon nanotube/polymer composites. *Chemistry of Materials*, 2000. **12**(4): p. 1049–1052.
32. Dror, Y., *et al*., Carbon nanotubes embedded in oriented polymer nanofibers by electrospinning. *Langmuir*, 2003. **19**(17): p. 7012–7020.
33. Bin, Y.Z., *et al*., Development of highly oriented polyethylene filled with aligned carbon nanotubes by gelation/crystallization from solutions. *Macromolecules*, 2003. **36**(16): p. 6213–6219.
34. Chen, G.Z., *et al*., Carbon nanotube and polypyrrole composites: coating and doping. *Advanced Materials (Weinheim, Germany)*, 2000. **12**(7): p. 522–526.
35. Grady, B.P., *et al*., Nucleation of polypropylene crystallization by single-walled carbon nanotubes. *Journal of Physical Chemistry B*, 2002. **106**(23): p. 5852–5858.
36. Valentini, L., *et al*., Effects of single-walled carbon nanotubes on the crystallization behavior of polypropylene. *Journal of Applied Polymer Science*, 2003. **87**(4): p. 708–713.
37. Valentini, L., *et al*., Morphological characterization of single-walled carbon nanotubes-PP composites. *Composites Science And Technology*, 2003. **63**(8): p. 1149–1153.
38. Moore, E.M., *et al*., Enhancing the strength of polypropylene fibers with carbon nanotubes. *Journal of Applied Polymer Science*, 2004. **93**(6): p. 2926–2933.
39. Assouline, E., *et al*., Nucleation ability of multiwall carbon nanotubes in polypropylene

composites. *Journal of Polymer Science Part B – Polymer Physics*, 2003. **41**(5): p. 520–527.
40. Sandler, J., *et al*., Crystallization of carbon nanotube and nanofiber polypropylene composites. *Journal of Macromolecular Science – Physics*, 2003. **B42**(3–4): p. 479–488.
41. Xia, H.S., *et al*., Preparation of polypropylene/carbon nanotube composite powder with a solid-state mechanochemical pulverization process. *Journal of Applied Polymer Science*, 2004. **93**(1): p. 378–386.
42. Ren, Z.F., *et al*., Synthesis of large arrays of well-aligned carbon nanotubes on glass. *Science*, 1998. **282**(5391): p. 1105–1107.
43. Karger-Kocsis, J., ed. *Polypropylene: An A-Z Reference*. 1999, Kluwer Academic Publishers: Boston.
44. Broda, J., Polymorphism in polypropylene fibers. *Journal of Applied Polymer Science*, 2003. **89**(12): p. 3364–3370.
45. Wilbrink, M.W.L., *et al*., Toughenability of nylon-6 with $CaCO_3$ filler particles: new findings and general principles. *Polymer*, 2001. **42**(26): p. 10155–10180.
46. McCrum, N.G., Buckley, C.P. and Bucknall, C.B. *Principles of Polymer Engineering*. Second ed. 1997, Oxford University Press: New York.

9

Multifunctional polymer nanocomposites for industrial applications

S. J. BULL, University of Newcastle, UK

9.1 Introduction

The development of composite materials with nanostructured reinforcements is well documented; such composites may have metallic (Michalski *et al*., 2003), ceramic (Ohji, 1999) or polymeric (Merinska *et al*., 2004) matrices and be developed in bulk or thin film form (Pavoor *et al*., 2004). Reinforcements are often chosen to improve the structural performance of the composite without compromising other properties though in some cases it is possible to enhance both structural and functional properties considerably. This has led to emerging applications in a number of industries, particularly the automotive and sports goods industries.

For textile applications polymer matrix composites are the most relevant. In polymer nanocomposites the reinforcements are typically selected to increase the strength of the material and many workers have demonstrated the benefits of adding exfoliated clays, nanoparticles and even carbon nanotubes. The major problems arise in ensuring reliability of processing and achieving a uniform dispersion and distribution of the reinforcement. However, the benefits in structural strength are not always much greater than can be achieved with traditional reinforcements, and to get the greatest benefits from such nanocomposites, additional functionality must be considered. Since a given improvement in mechanical properties can be achieved by a smaller volume fraction of nanoscale reinforcement, there is volume available for the addition of particles which can deliver other properties rather than structural strength and stiffness. Thus there is considerable potential for multifunctional nanocomposite materials, both as bulk composite materials and fibres.

In this chapter the development of nanocomposites for mechanical, tribological and fire-protection applications will be introduced and the potential for multifunctional nanocomposite fibres will be discussed.

9.2 The development of functional polymer nanocomposites

Making good samples of polymer nanocomposites is a challenge and a range of processing techniques are being actively developed at present including melt mixing (Chan *et al.*, 2002), *in situ* polymerisation (Yang *et al.*, 1998, Reynaud *et al.*, 2001) and other approaches. A full discussion of the technologies available is beyond this chapter but the interested reader is referred to the review of Jordan *et al.* (2005). A single processing approach is unlikely to deliver viable composites in every system and the different processing techniques often do not give the same results (Park *et al.*, 2001). One of the main issues in preparing good polymer matrix nanocomposites is the good dispersion of the nanoparticles in the polymer matrix which is a strong function of the preparation technique. This is a particular problem as the volume fraction of the particles increases.

An important group of nanocomposites is those based on clay reinforcement where the processing critically depends on the final morphology required for the reinforcement within the composite, i.e. particulate, exfoliated or intercalated (Komarneni, 1992). In the intercalated form the matrix polymer molecules are introduced between ordered layers of clay resulting in an increase in the interlayer spacing. However, in the exfoliated form the clay layers are separated and distributed randomly within the matrix. It is possible that some portion of a particular composite will form the intercalation morphology whereas another part will form the exfoliated structure – this is determined by balancing the interaction between the polymer matrix and silicate platelets against interactions between the silicate platelets themselves and may depend on attractive and steric interactions (Koo *et al.*, 2003). Exfoliation of layered materials is often hampered by the fact that the materials exhibit a strong tendency to agglomerate due to their large surface areas. However, in general, exfoliated materials show better properties than intercalated materials with the same nanoplatelet concentration and this has driven the development of exfoliated composite systems.

Intercalated nanocomposites are usually formed by mixing in the melt or *in situ* polymerisation whereas exfoliation may require more complex processing depending on the properties of the clay (Usuki *et al.*, 1993). However, such layered silicate-based polymer nanocomposites have attracted considerable recent interest after the commercialisation of polypropylene- and nylon-6-based materials (Krishnamoorti and Yurekli, 2001, Kiersnowski and Piglowski, 2004). The major barrier to commercialisation has been developing techniques to ensure a reliable and reproducible product which has now been addressed for clay-based composites some thirty or so years after they were first developed.

The use of carbon nanotubes (CNT) in polymer composites has attracted

considerable attention (Wagner *et al*., 1997, Shaffer and Kinloch, 2004). The high aspect ratio of the carbon nanotubes and their exceptional mechanical properties could provide the ultimate reinforcement for structural composite materials and improved electrical and thermal conductivity are also possible due to the low percolation limit of CNT. However, the planar graphitic surface of these nanotubes provides relatively few sites for easy chemical modification and bonding to a matrix material and hence processing viable composites can be difficult. Furthermore, the properties of the nanocomposites made with carbon nanotubes vary considerably; in part this is due to the fact that mixtures of single and multiwall nanotubes are produced by most manufacturing techniques and this will vary from process to process and even from batch to batch. Another source of variation is the different defect densities which are observed for nanotubes from different sources. Considerable improvements in reliability and reproducibility will be required if CNT are to be used in composites in the same way that clay systems are used today.

To date much of the development of polymer nanocomposites has been for structural applications with current commercial applications such as the step assist for the Chevrolet Astro van introduced by General Motors in 2002. However, there are other composite functions, such as tribological resistance, low friction or fire retardancy which are important in other applications and with nanoscale reinforcements it is possible to mix several different types of reinforcement to generate improvements in a range of properties. The following sections discuss how such properties are improved in nanocomposites.

9.3 Improving the mechanical properties of polymer nanocomposites

Many workers have reported that the elastic modulus of nanocomposites increases as the size of the reinforcement is reduced, provided that there was a good interaction between the filler and the polymer matrix (Vollenberg and Heikens, 1989, Chan *et al*., 2002). For some nanocomposites with very small reinforcement particles, Young's modulus is greater than might be expected from the volume law of mixtures of the constituents and this is attributed to the modification to the structure of the matrix surrounding the nanoparticles due to their high surface area (Akita and Hattori, 1999). For polymer systems where a high degree of crystallinity is possible, the increase in modulus with a reduction in particle size is found to be even greater unless there is poor interaction between filler and matrix. The modulus increases with the volume fraction of the reinforcement as expected until aggregation of the particles occurs when the modulus can be reduced in some systems (Akita and Hattori, 1999).

The yield strength of a polymer nanocomposite is critically dependent on the interaction between the reinforcement and the matrix. Where this interaction is strong the yield stress tends to increase with increasing volume fraction of reinforcement and decreasing particle size. This changes when there is poor interaction where an increase in volume fraction leads to a yield stress decrease from the value for the unreinforced matrix, regardless of the filler concentration or size. The ultimate tensile strength follows a similar pattern to the yield stress. Thus, to achieve nanocomposites with good mechanical properties it is critical that the matrix–reinforcement interfacial chemistry is controlled to give strong adhesion.

As the stiffness of the nanocomposite increases, so, in general, does its strength and this is accompanied by a reduction in its strain to failure. The strain to failure for a nanocomposite material is often higher than when the reinforcement is micrometre-sized (Petrovic *et al*., 2000). However, there are exceptions to this and, as with strength, it critically depends on the bonding between the reinforcement and the matrix – if this is poor then both the strength and strain to failure are reduced (Chan *et al*., 2002).

For clay-reinforced nanocomposites, increases in modulus compared with the unfilled polymer matrix have been observed in many systems with the effect increasing with filler content as expected but the properties are highly sensitive to microstructure (Luo and Daniel, 2003). In general, to maximise stiffness (and thermal properties) it is necessary to achieve full exfoliation and dispersion which is not readily achieved (Vu *et al*., 2001, Zhang *et al*., 2004).

Filler particles are added to composite materials to improve their viscoelastic properties. The heat distortion temperature for nanocomposites tends to be higher than that of the unfilled matrix or microreinforced materials because of an increase in viscosity during composite manufacture and a reduction in viscous deformation afterwards. For nanocomposites the storage modulus increases with an increase in the reinforcement content for both clay reinforced (Shelley *et al*., 2001) and silica nanoparticle reinforced nylon (Reynaud *et al*., 2001). Similar results have been observed for silica–polyurethane composites (Petrovic *et al*., 2000). Morphological details such as exfoliation, intercalation or matrix cross-linking also have a significant effect on the viscoelastic response. In epoxy–clay nanocomposites an increase in the amount of exfoliation is associated with an increase in viscosity and a relatively large increase in storage modulus (Park and Jana, 2003). In general, the resistance to viscoelastic deformation tends to be higher in polymer nanocomposites than in pure polymer systems. Where there are strong matrix–reinforcement interactions the storage modulus increases with increasing volume fraction of filler and increases as the reinforcement size decreases.

The increase in tensile strength or Young's modulus for nanocomposites compared with microcomposites can partly be explained by the details of the interaction between the filler and the matrix. Good adhesion between matrix

and particle results in less debonding when a stress is applied and consequently the strength is improved. The polymer in the proximity of a particle to which there is good adhesion tends to have higher density which also results in an increase in stiffness (Vollenberg and Heikens, 1989). The polymer adjacent to this high-density region will have a lower density as the chains are moved towards the particle to make the high-density region. For large particles this lower density region will be relatively large and the contribution of the high modulus filler will be diminished compared with the case when the filler particle is small. For nanocomposites, the number of particles for a given volume fraction is much larger and the particles will be much closer to each other. If the reinforcement particles are very densely packed then the high-density boundary layer will make up a larger proportion of the matrix and the modulus will increase. Thus, the major improvements to the mechanical properties of nanocomposites arise from the small particle spacing, rather than directly from the size or volume fraction of the reinforcement particles used.

The use of CNT in polymer composites has also received considerable attention (Kuriger *et al*., 2002, Shaffer and Kinloch, 2004). The combination of the high aspect ratio and extreme mechanical properties (strength and stiffness) of CNT provides the ultimate reinforcement for composite materials. Even with only 1% by weight of CNT added to a polymer matrix increases in strength and stiffness in excess of 40% have been measured (Lozano and Barrera, 2001). However, the properties of most CNT are very variable, since single and multiwall nanotubes with differing numbers of defects may be used for composite manufacture. For this reason the properties of nanotube composites can be very variable and considerable work is necessary to develop a reliable supply of material to generate CNT reinforced composites with controlled properties.

9.4 Improving the fire-retardant properties of polymer nanocomposites

Polymer–clay nanocomposites have been shown to greatly improve the barrier properties and fire retardancy of polymers as might be expected from their highly distributed inorganic material content (Gilman *et al*., 1997). This has been reviewed by several authors for both polymer–clay and polymer–nanoparticle composites (Porter *et al*., 2000, Koo and Pilato, 2005, Yang *et al*., 2005). Intercalated and exfoliated complexes show increased thermal stability compared with the unreinforced polymer. The fire properties of materials are evaluated in many different ways including by cone calorimetry (ASTM E1354), radiative gasification and limiting oxygen index measurement (ASTM D2863, ISO4589). Cone calorimetry is the most widely used laboratory method to assess nanocomposites – this technique generates information on

the heat which is released during combustion of the material and the reduction in peak heat release rate (PHRR) is often used to characterise potential fire-retardant materials (Schartel *et al*., 2005). For instance, in polystyrene–clay nanocomposites, Zhu and Wilkie (2000) reported that the peak heat release rate may be decreased by up to 58% depending on the composite structure and filler content.

Improvements in fire performance have been reported for polymer–clay nanocomposites with a range of polymer matricies including polyethylene (Bergaya *et al*., 2005), polypropylene (Tidjani, 2005), polyamide (Lei *et al*., 2004), epoxy (Camino *et al*., 2005), polystyrene (Chigwada *et al*., 2006a), acrylonitrile butadiene styrene (ABS, Chigwada *et al*., 2006a) and ethylene–vinyl acetate copolymer (EVA, Szep *et al*., 2006). In most cases the fire performance of a polymer–clay nanocomposite is dictated by its composition, rather than by the details of the microstructure, in contrast to the mechanical properties of the composite. The benefits increase as the clay content increases and further improvements can be achieved by the use of compatibilisers (Modesti *et al*., 2006). Good dispersion of the clay is essential for the most reliable materials (Duquesne *et al*., 2003). Modification of the clay with different salts can improve performance, e.g. by the addition of quinolinium and pyridinium surfactants to polystyrene (Chigwada *et al*., 2006b). It has also been shown that the use of synthetic clays to improve fire performance is more effective than the use of natural clays in the composite (Morgan *et al*., 2005).

In many cases the clay catalyses the formation of a clay reinforced carbonaceous char which is responsible for the lower flammability of the nanocomposites (Hull *et al*., 2003, Preston *et al*., 2004, Zanetti *et al*., 2004). The fire retardancy of polymer/clay nanocomposites is thus controlled by a change in the degradation pathway of a polymer by incorporation of the clay (Jang *et al*., 2005). Since the clay layers act as a barrier to mass transport and lead to superheated conditions in the matrix, extensive random scission of the products formed by radical recombination is an additional degradation pathway of polymers in the presence of clay. The polymers that show good fire retardancy upon nanocomposite formation exhibit significant intermolecular reactions, such as inter-chain aminolysis/acidolysis, radical recombination and hydrogen abstraction. This increases as the clay loading increases (Jang and Wilkie, 2005). In the case of the polymers that degrade through a radical pathway, the relative stability of the radical is the most important factor for the prediction of the effect that nanocomposite formation has on the reduction in the peak heat release rate. The more stable is the radical produced by the polymer, the better is the fire retardancy, as measured by the reduction in the peak heat release rate, of the polymer/clay nanocomposite.

Improvements in fire performance have also been reported for nanocomposites reinforced with nanoparticles. For instance, PMMA–silica

nanocomposites show improved thermal stability compared with the unreinforced polymer (Yang and Nelson, 2004) and polyimide–silica nanocomposites show improved fire retardancy (Liu *et al*., 2000). Oxide nanoparticles generate a decrease in PHRR with a range of fillers and the effect increases with filler content. Synergistic effects have also been reported with the combination of TiO_2 and organoclays (Laachachi *et al*., 2005).

The best fire performance is usually achieved by a combination of traditional fire-retardant additives with the nano-reinforcement, whether clay-based or nanoparticles (Zhang and Horrocks, 2003). For instance the combination of magnesium hydroxide and montmorillonites with an EVA matrix results in improved performance (Szep *et al*., 2006). Similarly an improvement in fire-retardancy of clay–polystyrene nanocomposites has been achieved by the addition of an oligomeric material consisting of vinyl benzyl chloride, styrene and dibromostyrene (Chigwada *et al*., 2005). Different clay materials also have differing effects on fire retardancy (Jash and Wilkie, 2005) and combinations of different clays can also generate improved properties (Marosfosi *et al*., 2006). The combination of clay–nanocomposites with added phosphorus-based fire retardants has also been tested and a 92% decrease in PHRR was recorded in the best case (Zhu and Wilkie, 2000). Synergistic effects have been reported in a number of systems, and this, combined with the ability to reduce the fire-retardant content and replace the halogen and phosphorus-containing systems with more environmentally friendly materials, is a major advantage for the nanocomposites currently being developed.

9.5 Improving the tribological properties of polymer nanocomposites

There are a number of ways in which the addition of a particle to a polymer can improve its friction and wear properties and all of these have been exploited in the production of nanocomposites. One approach is to reduce the adhesion of the composite to its sliding counterface by adding friction-modifying reinforcements which may also reduce the heat generated in a sliding contact. These friction modifiers may be in the form of low-friction particles which form low-friction transfer layers at the interface between the composite and its sliding counterface when the surface layers are disrupted by sliding. The fillers may also modify the properties of the transfer layer which forms, reacting chemically with the matrix and counterface materials to produce a low shear material. Another approach is to increase the hardness, stiffness and strength of the material using reinforcement particles as discussed previously. Yet another approach is to use fillers to control the heat transfer through the material in order to dissipate the heat generated by friction. Not all fillers increase the wear resistance of the composite; in the case where the filler decomposes during sliding and the reaction products strongly adhere to

the counterface (Briscoe, 1993) or where the adhesion between the filler and matrix is poor the wear rate will increase (Dasari *et al*., 2005).

To modify friction and adhesion, solid lubricants such as graphite or polytetrafluoroethylene (PTFE) are used. These are either layered structures (e.g. graphite or MoS_2) with low shear strength planes within their structure or smooth molecular species (PTFE) which can become aligned in the sliding direction in a similar manner to combed hair. In both cases these form a modified transfer film on the surface during wear, e.g. a PTFE film (Hager and Davies, 1993). One of the problems with the layered lubricants is the fact that chemical bonding at the edge of the low shear planes can lead to increases in the shear stress required to maintain sliding and a consequent increase in friction. A recent development which addresses this problem is the production of fullerene-like MoS_2 nanoparticles where the low-friction basal planes are wrapped into an approximately spherical shell with a much reduced number of chemical bonding sites, usually at kinks in the planes (Rapoport *et al*., 2005a). This type of material shows low friction and improved life and load bearing capacity compared with conventional flake particles both in composites and as an addition to grease (Rapoport *et al*., 2005b). Another approach is to soak lubricants into a nanoporous composite (Ahn *et al*., 2003).

The reinforcement material composition affects the composition and properties of the transfer layer that forms during sliding which controls friction and wear behaviour in most nanocomposite systems. A uniform, tenacious transfer film is produced in clay–nylon-6 nanocomposites, which leads to a reduction in friction and a lower wear rate (Srinath and Gnanamoorthy, 2005). Similar results are observed for silica nanoparticle reinforcement (Garcia *et al*., 2004).

The use of reinforcement particles that improve the mechanical properties of the composite in order to improve its wear performance is well documented for a range of polymer matrix materials. As the particle size is reduced the improvement in tribological properties tends to increase as smaller regions of matrix material are exposed to the sliding counterface during wear. For instance the wear performance of silica reinforced epoxy composites increases as the particle size is reduced from 500 to 120 nm (Xing and Li, 2004). However, opposite trends were observed for glass reinforced nylon in abrasive wear tests (Friedrich, 1986b). In fact the behaviour is often a complex function of particle size with an increase in wear rate at intermediate size and a reduction at the smallest sizes (Fig. 9.1). For composites with nanoscale particle reinforcement (i.e. less than 100 nm diameter) there is generally an improvement in wear performance as the particle size is reduced (Wang *et al*., 1996, Bahadur and Sunkara, 2005). Optimum wear performance is usually obtained with a fixed volume fraction of filler (Cai *et al*., 2003). For a particular particle size the wear resistance increases with volume fraction up

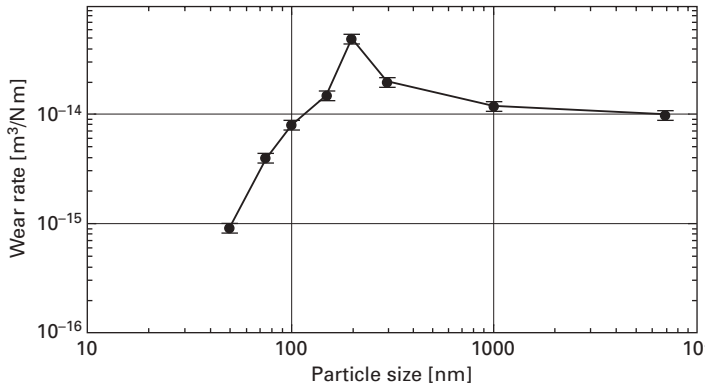

9.1 Effect of reinforcement diameter on wear performance for silica–polyurethane nanocomposites (12 vol%).

to a maximum, usually when the filler particles start to interact with each other. The maximum in performance thus represents a limit imposed by the dispersion of the particles in the matrix. In cases where particle interactions occur, the wear can be very severe and apparently abrasive in nature whereas at lower reinforcement volume fractions the wear mechanism is different (e.g. adhesive and fatigue wear). A strong adhesion between reinforcement and matrix is necessary to prevent pull-out and high wear in nanocomposites designed for tribological applications. This has driven the development of coupling agents and other chemical modifications to improve performance (Zhang *et al*., 2002a,b).

An added advantage of nanocomposites manufactured with small diameter reinforcements is the reduction in surface roughness of the sliding surface. This generally leads to a reduction in the contact stresses at asperity contacts and a resultant reduction in damage to the composite system. The roughness of the counterface is also critical because this dictates the nature of the initial contact with the nanocomposite surface and controls the mechanics of formation of the transfer film (Friedrich, 1986b) – when the roughness of the counterface is less than the particle size, the presence of the nanoparticles tends to increase the wear rate because detached particles get trapped between the sliding surfaces and cannot be taken out of the contact by moving into the roughness valleys. In this case three body abrasion occurs before a protective transfer film forms and the wear rate increases.

Improvements in friction and wear have also been reported with carbon nanotube reinforced polymer composites (Igarashi *et al*., 2005). This is due to both increases in strength of the material and the modification of the transfer layer by fragments of nanotube which can reduce friction. There is an optimum nanotube composition (Cai *et al*., 2004) typically about 10% by weight, for the best wear performance (Werner *et al*., 2004).

9.6 Case-study: development of a nanocomposite sliding seal ring

The problems with developing successful functional applications of nanocomposites can be illustrated with the following example. In this case-study nanocomposite materials were developed for an application in which a composite ring was sliding against a flat steel component in the absence of lubrication. The mean contact pressure at the seal face was 1 MPa. The wear rate and coefficient of friction of the sliding composite part were to be minimised and the sliding speed maximised. A traditional approach to achieve a highly wear-resistant polymer composite is to combine fillers with different functions (e.g. Friedrich, 1986a); this approach has been adopted here. A range of conventional composite and nanocomposite materials has been investigated to determine which is most suitable. Benchmarking newly developed nanocomposites against currently available composite systems is essential to justify their use in any application and in most cases there is a considerable cost implication when selecting a nanocomposite material.

9.6.1 Materials investigated

A range of structural composite materials were produced with different reinforcements for performance assessment. The systems were based on a conventional woven roving/thermosetting resin design but with added nanoscale reinforcement which was mixed with the resin prior to lamination. The systems investigated were:

1. glass reinforced phenolic;
2. glass reinforced polyester;
3. glass reinforced vinyl ester (conventional and scrimp (higher glass content));
4. carbon fibre reinforced epoxy;
5. glass reinforced vinyl ester with added PTFE (100 nm);
6. glass reinforced vinyl ester with added MoS_2 (100 nm);
7. glass reinforced vinyl ester with added MoS_2 (100 nm) + 10% flake graphite (>10 μm);
8. glass reinforced vinyl ester with added flake graphite (>10 μm);
9. glass reinforced vinyl ester with added 3.5–5 μm silica particles;
10. glass reinforced vinyl ester with added 50–70 nm diameter silica particles;
11. glass reinforced vinyl ester with added silica particles; 50% at 50–70 nm and 50% at 3.5–5 μm.

Sample 1 was chosen because the thermal degradation products of phenolic materials are known to be less sticky that the other matrix materials (Vishwanath *et al*., 1993). Sample 2 was chosen because it is cheap and easy to process

but it was expected to have poor wear performance. Silica particles were treated with a titanate coupling agent to aid wetting by the resins; particles were easy to mix with the resin but tended to form clumps in the composite after processing. Sample 4 was chosen because carbon fibre additions to materials such as nylon have been shown to reduce friction in seals by modifying the chemistry of the transfer layer formed. All the additives in samples 6 to 8 are low friction materials that are known to reduce friction in some circumstances as an additive to polymers, composites (Yu *et al.*, 1996), lubricating oils and greases. The main difference with previous studies was the size of the reinforcing particles.

The samples were made by laminating against glass using a release agent; this produced a very smooth surface which is suitable for wear testing. The additives were mixed with the vinyl ester resin prior to hand lamination according to the proportions in Table 9.1. Four samples were made at a time. Some 400 g of the vinyl ester resin was used with the various fillers to lay up the first four layers of the composite and then another four layers were laid up using just the resin. This produces samples with a smooth side (next to the glass) which can be tested and a rough side at the rear. The total sample thickness is sufficiently large that no substrate or backing effects were observed during testing. For the phenolic and polyester matrix materials both the smooth and rough sides were available for testing and both were assessed to determine if roughness has a big effect on the friction and wear results.

The results were compared with a standard steel sample which was tested either in the as-received condition or coated with a layer of lubricating grease. In addition to the modification of structural composites a number of polymer nanocomposites were made by mixing nanoscale reinforcements with a polyurethane resin. In this case the resin was again cast against a glass

Table 9.1 Fillers added to 400 g vinyl ester resin to make the structural composites used in this study

Sample	Glass mat	Filler (1)	Weight (1) [g]	Filler (2)	Weight (2) [g]
Micro silica (3.5–5 μm)	Woven roving 0/90	Silica	300		
Nano silica (50–70 nm)	Woven roving 0/90	Silica	200		
Mixed silica	Woven roving 0/90	Micro-silica	100	Nano-silica	100
PTFE (100 nm)	Woven roving 0/90	PTFE	50		
Graphite	Woven roving 0/90	Graphite	30		
MoS_2 (100 nm)	Woven roving 0/90	MoS_2	100		
Mixed	Woven roving 0/90	MoS_2	90	Graphite	10

block and the smooth side was tested. Silica nanoparticles of a range of different sizes were added to the resin at 5% and multiwall carbon nanotubes were added at 0.5% by weight.

9.6.2 Wear tests

Tribological tests were performed on a modified pin on disc tester fitted with a rotation speed tachometer and friction and wear transducers which were all calibrated prior to use. In this tester a flat-ended pin is loaded against a disc by a dead weight on the end of the loading arm. In each test 60 mm diameter composites discs of approximately 10 mm thickness were used sliding against a 10 mm diameter, 17 mm long steel pin. The disc is rotated by a motor whose speed is controlled by the tachometer. The rotation of the disc forces the loading arm against a load transducer to measure the frictional force and a displacement transducer is placed against the loading arm to measure the total arm displacement during the test. Great care was taken to ensure that the end of the pin was flat and parallel to the disc surface in the test to minimise errors due to misalignment. This was achieved by running in the pin on an unimportant region of disc prior to moving to the test diameter for friction and wear evaluation. All tests were carried out unlubricated. Each test was performed three times and the results averaged; test results were quite consistent with errors of less than 10% except in the case of the nanoscale silica particles where considerable scatter was observed and the extremes of the behaviour observed are shown in the following figures.

Two different types of test were carried out:

- Variation of friction coefficient with sliding speed. In this case tests were carried out on the same track. The sample was rotated at a low speed and left for a few minutes for the friction coefficient to stabilise. A friction measurement was then taken averaged over 60 s of sliding and then the speed was increased and the process repeated. The speed was increased in this manner until seizure occurred and the rotation stopped. This defines the limit in sliding velocity for the composite/pin pair at the normal load chosen.
- Fixed speed test at 6 m/s for a total of 10 km sliding distance to determine wear behaviour.

In all tests a load of 75 N was applied to the pin giving a contact pressure of ~1 MPa. Stylus profilometry was used to assess the depth of the wear scar produced at four places on each track and the results averaged to determine the wear. Friction coefficients were determined by dividing the measured frictional force by the applied normal load.

9.6.3 Friction coefficient measurements

For all materials the friction coefficient was approximately constant as a function of sliding speed until close to seizure when friction increases rapidly. Typical plots are shown in Fig. 9.2 and 9.3. Two important parameters can thus be extracted from the test data:

- the average friction coefficient at all sliding speeds;
- the speed at which seizure occurs under the contact conditions in the test.

The average friction coefficient data for all the samples are collected in Fig. 9.4. It can clearly be seen that most of the composite samples have lower friction coefficients than ungreased steel but all have higher friction than greased steel. As expected the phenolic reinforced with glass shows low friction in dry sliding as does the polyester reinforced with glass and epoxy reinforced with carbon. Only the nanoscale PTFE and MoS_2 additives have been successful at reducing the friction of the glass reinforced vinyl ester (VE). This is consistent with the observation that the scrimp glass reinforced vinyl ester, which has a higher glass content than the other material tested, also shows a higher friction coefficient. It appears that increasing the amount of filler in the material is thus counterproductive if a low friction coefficient

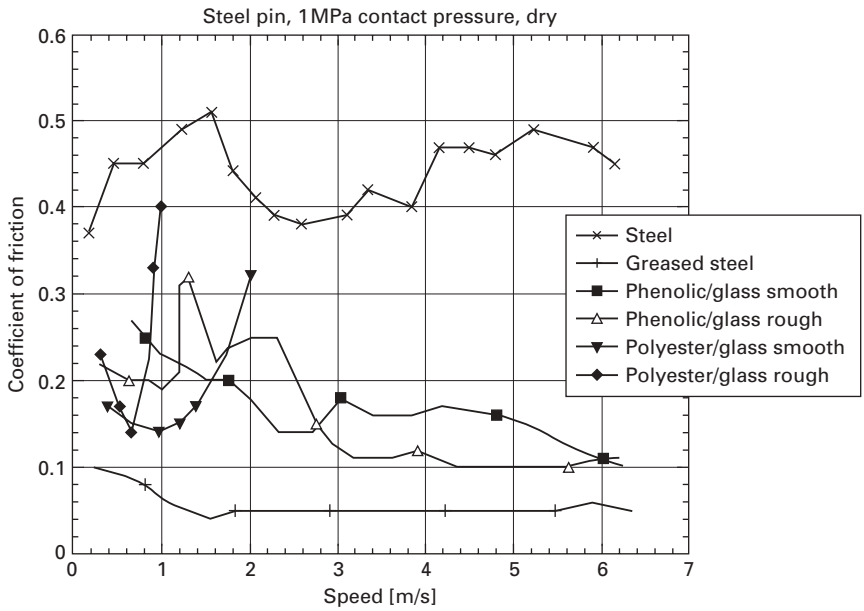

9.2 Variation of coefficient of friction with speed for a range of materials tested against steel at 1 MPa contact pressure in dry sliding.

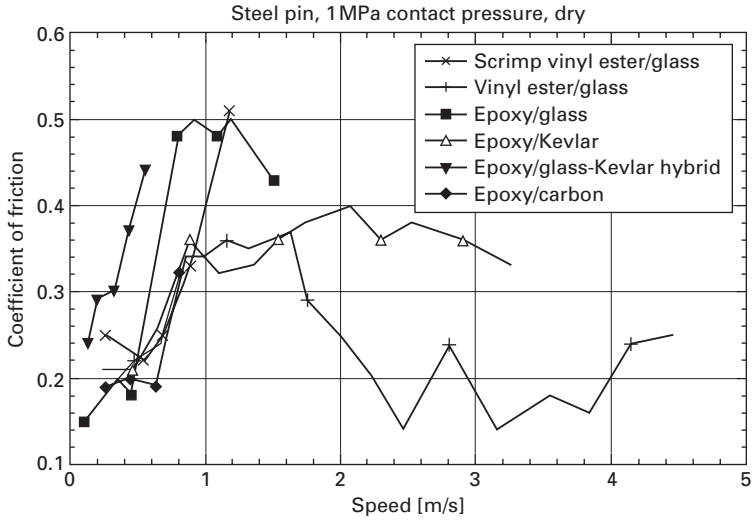

9.3 Variation of friction coefficient against steel with sliding speed for a range of vinyl ester and epoxy matrix composites tested at 1MPa contact pressure in dry sliding.

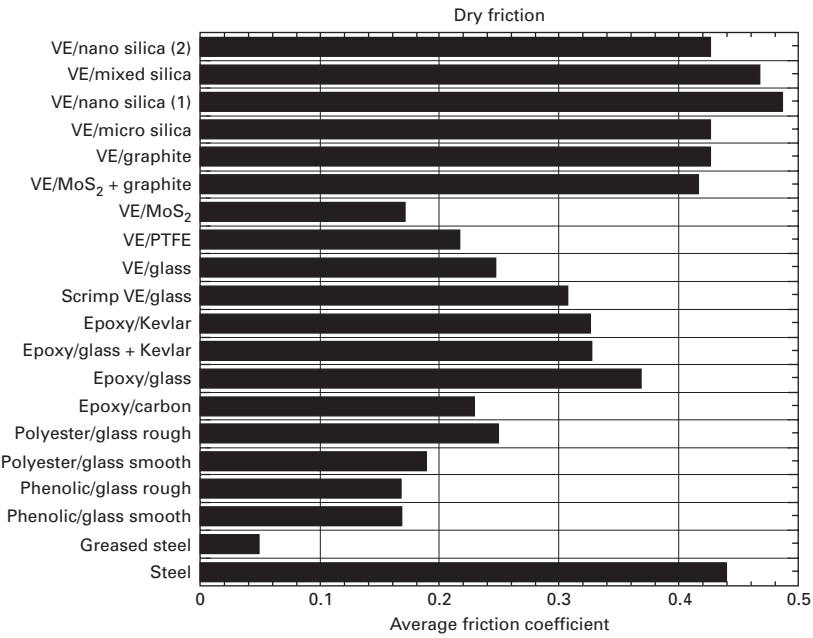

9.4 Average friction coefficient against steel (1MPa contact pressure) as a function of material tested in this programme.

is required unless the filler itself can deliver low friction. It was initially thought that this increase in wear was due to interactions between the reinforcement materials at high loadings. However, temperature measurements showed that increasing the filler content has reduced the thermal conductivity of the composite and thus increased the thermal degradation and stickiness of the contact zone. The highly filled composites show a higher wear rate (see later) and more surface damage is evident. Damage dissipates energy and therefore increases friction. Increasing surface roughness slightly also increases friction for the glass reinforced polyester tested here due to the excessive damage created. This is much less significant for the phenolic matrix material which shows no change in friction with roughness.

The glass reinforced vinyl ester reinforced with nanoscale reinforcement was very different to process and clumps of glass were visible in the composite. Repeat tests on this material show very variable friction and wear performance depending on the location of the glass clumps. This highlights the importance of developing processing methods that generate a uniform dispersion of any reinforcement. The maximum speed before seizure for all the composite materials is very low (Fig. 9.5) but can be increased by the addition of nanoscale MoS_2 reinforcements.

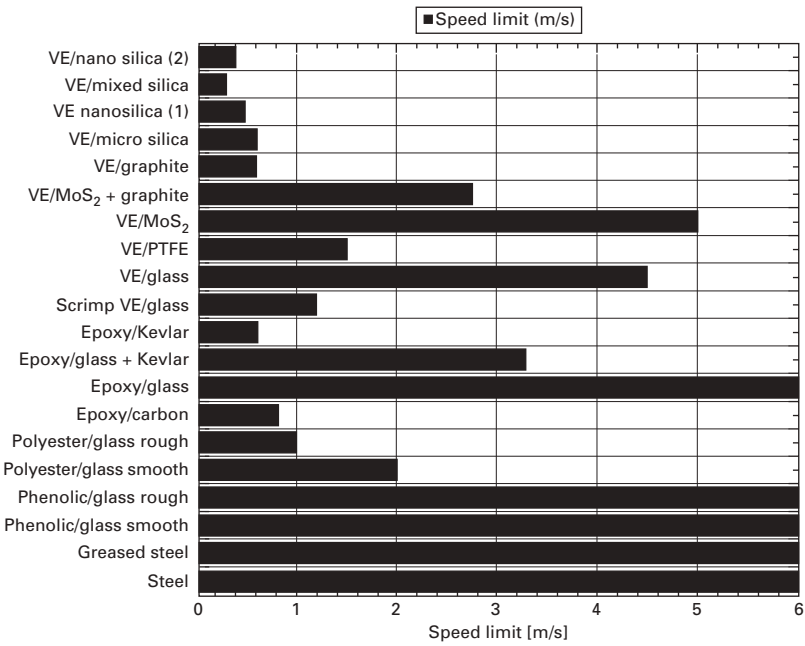

9.5 Maximum speed before seizure for samples tested in this study (1 MPa contact pressure).

9.6.4 Wear

During the wear test experiments it was found that not all samples could be run under the same conditions as originally planned since the maximum speed limit of most of the composites was very low. Wear measurements were thus made on each disc at the highest sliding speed achievable for a total sliding distance of at least 1 km and normalised to 10 km (assuming wear depth is linearly proportional to sliding distance) to compare with the best samples.

Some of the samples show very good wear behaviour (Fig. 9.6). In particular the glass reinforced phenolic shows very low wear rates. The carbon fibre reinforced epoxy has a much higher wear rate than any of the other epoxy matrix composites – the fibres are easily damaged during testing and any advantage that carbon might impart in reducing friction is lost as the roughened damage surface wears. Most of the nano-additions to vinyl ester reduce its wear rate and the silica reinforcement can give major improvements in the best samples. However, as the glass content increases wear is increased due to poor interaction between the particles and the matrix leading to easy pull-out; in the case of the scrimp vinyl ester glass pull-out is very apparent in the wear scar. Of all the additives the nanoscale silica has the greatest effect but the nanoscale MoS_2 offers some advantages. The glass reinforced polyester has a very high wear rate as expected.

The improved wear resistance of nanosilica reinforced vinyl ester prompted a more detailed investigation of the effects of particle size on the wear

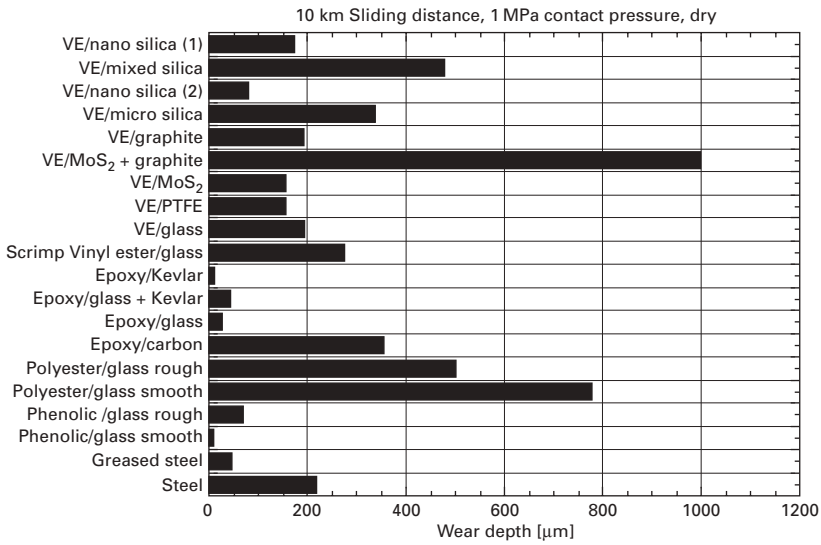

9.6 Maximum wear scar depth of all materials tested in this study after 10 km dry sliding against steel (1 MPa contact pressure).

resistance of a polymer nanocomposite. In this case a polyurethane resin was used, rather than a structural composite, to avoid the complicating effects of macroscale reinforcement. Figure 9.1 shows that the wear rate is critically dependent on particle size, initially increasing as the reinforcement diameter is reduced but dramatically falling as the reinforcement size becomes nanoscaled.

The results presented so far indicate that no single nanoscale reinforcement generates ideal results, either alone or when used in conjunction with more conventional reinforcement materials. To control wear, a hard reinforcement such as silica is preferred whereas to reduce friction a low shear stress reinforcement such as MoS_2 is more effective. Thus a combination of nanoscale reinforcements in vinyl ester resin has been investigated in further tests and the benefits of the mixed compositions on friction (Fig. 9.7) and speed at seizure (Fig. 9.8) have been demonstrated without compromising wear performance.

Visual examination of the worn surfaces of the tested composites shows some evidence of char formation. Thus the high-speed sliding wear performance of these polymer nanocomposite materials is controlled by heat generation and dissipation. The approach of adding particles which generates a reduction in friction has been successful at improving tribological performance by limiting heat generation but an alternative approach would be to add material to the composite which can improve its thermal conductivity so that any heat generated can be more easily dissipated. Potential nanoscale reinforcements which could achieve this include metals and carbon nanotubes since the conductivity along the tube is very high. The best results are achieved with single wall nanotubes but it is currently difficult to obtain this material in

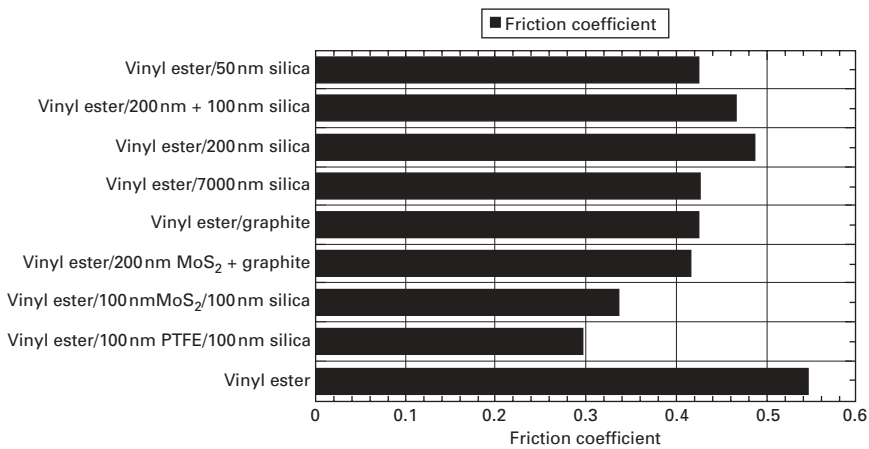

9.7 Friction coefficient of vinyl ester nanocomposites with different reinforcements.

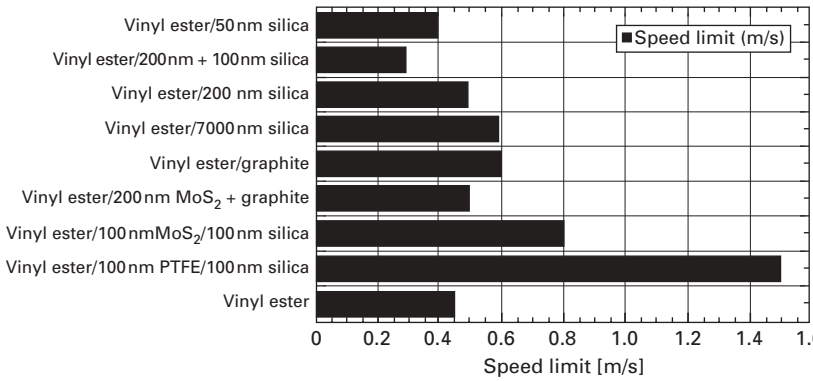

9.8 Speed limit of vinyl ester nanocomposites with different reinforcements.

sufficient quantity for tribological composites. Thus unprocessed multiwall nanotube mats have been incorporated in the polyurethane resin used previously to assess the viability of the approach. At 0.5% loading the tubes have little or no effect on the friction and wear rate of the polyurethane at low sliding speeds as might be expected but the speed limit for seizure for the composite is increased from 1 to 3.5 m/s, indicating that the dissipation of the frictional heat has been improved (Fig. 9.9). More work is necessary to assess this encouraging result further.

The results presented here highlight the need to understand the mechanisms by which a composite fails in a given application if the best material is to be developed. As the functional requirements become more complex this will be more difficult to achieve but the benefits of doing so will be greater as more synergisms can be exploited.

9.7 Enhancing the functionality of polymer nanocomposites

The results presented here demonstrate the benefit of nanoscale reinforcement to improve wear resistance of the composite material but to improve the overall performance of the materials for a sliding seal application no single reinforcement material is suitable. However, a combination of reinforcements can be developed which impart multiple functionality to the composite. For instance, both silica and MoS_2 nanoparticles added to a polyurethane resin matrix can generate improvements in both friction and wear behaviour.

The work here has been carried out with thermosetting resin matrices but there is no reason to suspect that similar results will not be achieved using thermoplastic resins which can be processed into fibres, e.g. by melt electrospinning. Enhanced functionality can be achieved at relatively small

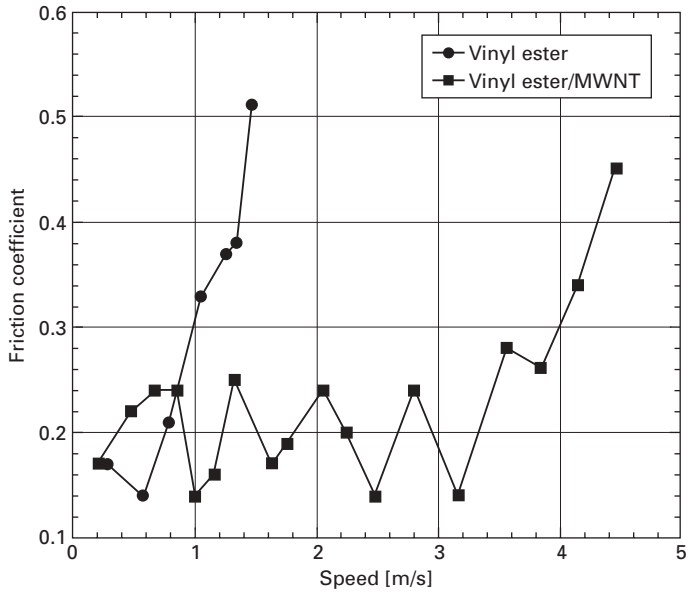

9.9 Variation of coefficient of friction with sliding speed for vinyl ester resin with and without 0.5% multiwall nanotube reinforcement.

particle loadings where the viscosity of the material is not increased too much to process. In many cases the nanocomposite composition range does not need to be tightly controlled as good properties are achieved with a range of reinforcement contents and the processing is quite forgiving in this respect. However, achieving a uniform dispersion of the reinforcement is much more important and this is a major goal of process development. It has been shown that nanotubes at similar loadings to those investigated in this study can be added to thermoplastic matrices and processed by injection moulding (Yalcin and Cakmak, 2004) or spun into fibres (Dalton *et al*., 2003) and fibres containing nano-reinforcements have been produced by electrospinning (Sen *et al*., 2004). The potential for the manufacture of nanocompsite fibres is therefore excellent but more work is necessary to develop and optimise appropriate processing conditions. A reliable source of defect-free nanotubes with reproducible properties will need to be developed if the benefits are to be exploited commercially to any great extent.

It is clear that multifunctional materials may be developed by using several reinforcements in the resin matrix and the choice of these should be based on the required functionality. Many possibilities exist, including:

- high-strength impact management systems;
- fire-retardant systems;
- friction and touch/feel modifiers;

- colourants;
- electrical conductivity modifiers/capacitors/batteries;
- wettability modifiers;
- self-cleaning fibres.

In some cases these functionalities may be achieved by other methods, e.g. by coating or surface texturing after fibre manufacture and the relative merits of the competing technologies will need to be assessed.

One key concern is the cost and availability of the reinforcements used. In this study synthetic nanoparticles and nanotubes have been used but these would not be economic for large-scale composite manufacture at present. Careful control of particle size distribution and the processing of particles is essential and novel processing methods, such as precipitation in the spinning disc reactor (Brechtelsbauer *et al*., 2001), offer great promise in this respect. A range of natural nanoparticles exist which can be obtained from clay deposits which could lead to improvements in strength and fire protection but these need to be investigated in more detail. The characterisation of mineral deposits and the particles that come from them is a key part of this and much progress has been made in recent years.

9.8 Conclusions

Multifunctional nanocomposite materials can be produced by combining a range of nanoscale reinforcement materials with a polymer matrix. Given a knowledge of the performance requirements of a given application it is possible to design a composite with a range of functionalities necessary for successful operation. However, processing of the composite remains a key factor in success and in particular ensuring a uniform dispersion of reinforcement is critical to reliable performance.

There are many potential textile applications of multifunctional composite materials ranging from self-cleaning, water-resistant and fire-retardant fibres, to novel colouration schemes and fabrics with improved toughness and feel. However, much work is necessary to make such applications a reality.

9.9 Acknowledgements

The author would like to thank Katarina Horvathova, Rob McNaught and Thomas Malkow who produced and tested the composite materials.

9.10 References

Ahn, H. S., Julthongpiput, D., Kim, D. I. and Tsukruk, V. V. (2003) Dramatic enhancement of wear stability in oil-enriched polymer gel nanolayers, *Wear,* **255**, 801–807.

Akita, H. and Hattori, T. (1999) Studies on molecular composite. I. Processing of molecular composites using a precursor polymer for poly(*p*-phenylene benzobisthiazole), *Journal of Polymer Science Part B – Polymer Physics*, **37** (3), 189–197.

Bahadur, S. and Sunkara, C. (2005) Effect of transfer film structure, composition and bonding on the tribological behavior of polyphenylene sulfide filled with nano particles of TiO_2, ZnO, CuO and SiC, *Wear*, **258** (9), 1411–1421.

Bergaya, F., Mandalia, T. and Amigouet, P. (2005) A brief survey on CLAYPEN and nanocomposites based on unmodified PE and organo-pillared clays, *Colloid and Polymer Science*, **283** (7), 773–782.

Brechtelsbauer, C., Lewis, N., Oxley, P., Ricard, F. and Ramshaw, C. (2001) Evaluation of a spinning disc reactor for continuous processing, *Organic Process Research and Development*, **5**, 65–68.

Briscoe, B. J. (1993) 'The tribology of composite materials: a preface', in Friedrich, K. (Ed), *Advances in Composite Tribology.* Elsevier, Amsterdam, pp. 3–15.

Cai, H., Yan, F. Y., Xue, Q. J. and Liu, W. M. (2003) Investigation of tribological properties of Al_2O_3-polyimide nanocomposites, *Polymer Testing*, **22** (8), 875–882.

Cai, H., Yan, F. Y. and Xue, Q. J. (2004) Investigation of tribological properties of polyimide/carbon nanotube nanocomposites, *Materials Science and Engineering A – Structural Materials Properties Microstructure and Processing*, **364** (1–2), 94–100.

Camino, G., Tartaglione, G., Frache, A., Manferti, C. and Costa, G. (2005) Thermal and combustion behaviour of layered silicate-epoxy nanocomposites, *Polymer Degradation and Stability*, **90** (2), 354–362.

Chan, C. M., Wu, J., Li, J.-X. and Cheung, Y.-K. (2002) Polypropylene/calcium carbonate nanocompsites, *Polymer*, **43**, 2981–2992.

Chigwada, G., Jash, P., Jiang, D. D. and Wilkie, C. A. (2005) Synergy between nanocomposite formation and low levels of bromine on fire retardancy in polystyrenes, *Polymer Degradation and Stability*, **88** (3), 382–393.

Chigwada, G., Wang, D. Y., Jiang, D. D. and Wilkie, C. A. (2006a) Styrenic nanocomposites prepared using a novel biphenyl-containing modified clay, *Polymer Degradation and Stability*, **91** (4), 755–762.

Chigwada, G., Wang, D. Y. and Wilkie, C. A. (2006b) Polystyrene nanocomposites based on quinolinium and pyridinium surfactants, *Polymer Degradation and Stability*, **91** (4), 848–855.

Dalton, A. B., Collins, S., Munoz, E., Razal, J. M., Ebron, V. H., Ferraris, J. P., Coleman, J. N., Kim, B. G. and Baughman, R. H. (2003) Super-tough carbon nanotube fibres – these extraordinary composite fibres can be woven into electronic textiles, *Nature*, **423**, 703.

Dasari, A., Yu, Z. Z., Mai, Y. W., Hu, G. H. and Varlet, J. L. (2005) Clay exfoliation and organic modification on wear of nylon 6 nanocomposites processed by different routes, *Composites Science and Technology*, **65** (15–16), 2314–2328.

Duquesne, S., Jama, C., Le Bras, M., Delobel, R., Recourt, P. and Gloaguen, J. M. (2003) Elaboration of EVA–nanoclay systems – characterization, thermal behaviour and fire performance, *Composites Science and Technology*, **63** (8), 1141–1148.

Friedrich, K. (1986a) *Friction and Wear of Polymer Composites.* Elsevier, Amsterdam.

Friedrich, K. (1986b) 'Wear of reinforced polymers by different abrasive counterparts', in Friedrich, K. (Ed), *Friction and Wear of Polymer Composites.* Elsevier, Amsterdam, pp. 233–287.

Garcia, M., de Rooij, M., Winnubst, L., van Zyl, W. E. and Verweij, H. (2004) Friction

and wear studies on nylon-6/SiO_2 nanocomposites, *Journal of Applied Polymer Science*, **92** (3), 1855–1862.

Gilman, J. W., Kashiwagi, T. and Lichtenhan, J. D. (1997) Nanocomposites: A revolutionary new flame retardant approach, *Sampe Journal*, **33** (4), 40–46.

Hager, A. M. and Davies, M. (1993) 'Short fibre reinforced, high temperature resistant polymers for a wide field of tribological applications', in Friedrich, K. (Ed), *Advances in Composite Tribology*. Elsevier, Amsterdam, pp. 107–157.

Hull, T. R., Price, D., Liu, Y., Wills, C. L. and Brady, J. (2003) An investigation into the decomposition and burning behaviour of ethylene–vinyl acetate copolymer nanocomposite materials, *Polymer Degradation and Stability*, **82** (2), 365–371.

Igarashi, A., Terasawa, T., Kanie, M., Yamanobe, T. and Komoto, T. (2005) A morphological study of the effect of carbon nanotube filler on tribology of phenol/formaldehyde resin-based composites, *Polymer Journal*, **37** (7), 522–528.

Jang, B. N. and Wilkie, C. A. (2005) The thermal degradation of polystyrene nanocomposite, *Polymer*, **46** (9), 2933–2942.

Jang, B. N., Costache, M. and Wilkie, C. A. (2005) The relationship between thermal degradation behavior of polymer and the fire retardancy of polymer/clay nanocomposites, *Polymer*, **46** (24), 10678–10687.

Jash, P. and Wilkie, C. A. (2005) Effects of surfactants on the thermal and fire properties of poly(methyl methacrylate)/clay nanocomposites, *Polymer Degradation and Stability*, **88** (3), 401–406.

Jordan, J., Jacob, K. I., Tannenbaum, R., Sharaf, M. A. and Jasiuk, I. (2005) Experimental trends in polymer nanocomposites – a review, *Materials Science Engineering A*, **393**, 1–11.

Kiersnowski, A. and Piglowski, J. (2004) Polymer-layered silicate nanocomposites based on poly(e-caprolactone), *European Polymer Journal*, **40**, 1199–1207.

Komarneni, S. (1992) Nanocomposites, *Journal of Materials Chemistry*, **2**, 1219–1230.

Koo, C. M., Kim, S. O. and Chung, I. E. (2003) Study on morphology evolution, orientational behaviour, and anisotropic phase formation of highly-filled polymer-layered silicate nanocomposites, *Macromolecules*, **36**, 2748–2757.

Koo, J. H. and Pilato, L. A. (2005) Polymer nanostructured materials for high temperature applications, *Sampe Journal*, **41** (2), 7–19.

Krishnamoorti, R. and Yurekli, K. (2001) Rheology of polymer layered silicate nanocomposites, *Current Opinion on Colloidal Interface Science*, **6**, 464–470.

Kuriger, R. J., Alam, M. K., Anderson, D. P. and Jacobsen, R. L. (2002) Processing and characterisation of aligned vapour grown carbon fiber reinforced polypropylene, *Composites A*, **33**, 53–62.

Laachachi, A., Leroy, E., Cochez, M., Ferriol, M. and Cuesta, J. M. L. (2005) Use of oxide nanoparticles and organoclays to improve thermal stability and fire retardancy of poly(methyl methacrylate), *Polymer Degradation and Stability*, **89** (2), 344–352.

Lei, S., Yuan, H., Lin, Z. H., Xuan, S. Y., Wang, S. F., Chen, Z. Y. and Fan, W. C. (2004) Preparation and properties of halogen-free flame-retarded polyamide 6/organoclay nanocomposite, *Polymer Degradation and Stability*, **86** (3), 535–540.

Liu, J., Gao, Y., Wang, F. D. and Wu, M. (2000) Preparation and characteristics of nonflammable polyimide materials, *Journal of Applied Polymer Science*, **75** (3), 384–389.

Lozano, E. and Barrera, V. (2001) Nanofiber-reinforced thermoplastic composites I: Thermoanalytical and mechanical analyses, *Journal of Applied Polymer Science*, **79**, 125–133.

Luo, J.-J. and Daniel, I. M. (2003) Characterisation and modelling of mechanical behaviour of polymer–clay nanocomposites, *Composite Science Technology*, **63**, 1607–1616.

Marosfosi, B., Matko, S. and Marosi, P. A. G. (2006) Fire retarded polymer nanocomposites, *Current Applied Physics*, **6** (2), 259–261.

Merinska, D., Kovarova, L., Kalendova, A., Vaculik, J., Weiss, Z., Chimelova, M., Malac, J. and Simonak, J. (2004) *Journal of Polymer Engineering*, **23**, 241.

Michalski, J., Konopka, K. and Trszaska, M. (2003) Description of Al_2O_3 powders coated by Ni-P particles obtained through an electroless chemical reaction and possibilities to obtain an Al_2O_3/Ni-P composite, *Materials Chemistry and Physics*, **81**, 407–410.

Modesti, M., Lorenzetti, A., Bon, D. and Besco, S. (2006) Thermal behaviour of compatibilised polypropylene nanocomposite: effect of processing conditions, *Polymer Degradation and Stability*, **91**, (4) 672–680.

Morgan, A. B., Chu, L. L. and Harris, J. D. (2005) A flammability performance comparison between synthetic and natural clays in polystyrene nanocomposites, *Fire and Materials*, **29** (4), 213–229.

Ohji, T. (1999) Fracture behavior of ceramic based nanocomposites, *Key Engineering Materials*, **2**, 391–396.

Park, C. I., Park, O. O., Lim, J. G. and Kim, H. J. (2001) The fabrication of syndiotactic polystyrene/organophilic clay nanocomposites and their properties, *Polymer*, **42**, 7465–7475.

Park, J. H. and Jana, S. C. (2003) Mechanism of exfoliation of nanoclay particles in epoxy–clay nanocomposites, *Macromolecules*, **36**, 2758–2768.

Pavoor, P. V., Gearing, B. P., Gorga, R. E., Bellare, A. and Cohen, R. E. (2004) Engineering the friction-and-wear behavior of polyelectrolyte multilayer nanoassemblies through block copolymer surface capping, metallic nanoparticles, and multiwall carbon nanotubes, *Journal of Applied Polymer Science*, **92** (1), 439–448.

Petrovic, Z. S., Javni, I., Waddon, A. and Banhegyi, G. (2000) Structure and properties of polyurethane–silica nanocomposites, *Journal of Applied Polymer Science*, **76**, 133–151.

Porter, D., Metcalfe, E. and Thomas, M. J. K. (2000) Nanocomposite fire retardants – a review, *Fire and Materials*, **24** (1), 45–52.

Preston, C. M. L., Amarasinghe, G., Hopewell, J. L., Shanks, R. A. and Mathys, Z. (2004) Evaluation of polar ethylene copolymers as fire retardant nanocomposite matrices, *Polymer Degradation and Stability*, **84** (3), 533–544.

Rapoport, L., Fleischer, N. and Tenne, R. (2005a) Applications of WS_2 (MoS_2) inorganic nanotubes and fullerene-like nanoparticles for solid lubrication and for structural nanocomposites, *Journal of Materials Chemistry*, **15** (18), 1782–1788.

Rapoport, L., Nepomnyashchy, O., Lapsker, I., Verdyan, A., Moshkovich, A., Feldman, Y. and Tenne, R. (2005b) Behavior of fullerene-like WS_2 nanoparticles under severe contact conditions, *Wear*, **259** (1–6), 703–707.

Reynaud, E., Jouen, T., Gautheir, C. and Vigier, G. (2001) Nanofillers in polymeric matrix: a study on silica reinforced PA6, *Polymer*, **42**, 8759–8768.

Schartel, B., Bartholmai, M. and Knoll, U. (2005) Some comments on the use of cone calorimeter data, *Polymer Degradation and Stability*, **88**, (3) 540–547.

Sen, R., Zhao, B., Perea, D., Itkis, M. E., Hu, H., Love, J., Bekgarova, E. and Haddon, R. C. (2004) Preparation of single-walled carbon nanotube reinforced polystyrene and polyurethane nanofibers and membranes by electrospinning, *Nano Letters*, **4**, 459–464.

Shaffer, M. and Kinloch, I. A. (2004) Prospects for nanotube and nanofibre composites, *Composites Science and Technology*, **64** (15), 2281–2282.

Shelley, J. S., Mather, P. T. and de Vries, K. L. (2001) Reinforcement and environmental degradation of nylon-6/clay nanocomposites, *Polymer*, **42**, 5849–5858.

Srinath, G. and Gnanamoorthy, R. (2005) Effect of nanoclay reinforcement on tensile and tribo behaviour of nylon 6, *Journal of Materials Science*, **40** (11), 2897–2901.

Szep, A., Szabo, A., Toth, N., Anna, P. and Marosi, G. (2006) Role of montmorillonite in flame retardancy of ethylene–vinyl acetate copolymer, *Polymer Degradation and Stability*, **91** (3), 593–599.

Tidjani, A. (2005) Polypropylene-graft-malefic anhydride-nanocomposites: II – fire behaviour of nanocomposites produced under nitrogen and in air, *Polymer Degradation and Stability*, **87** (1), 43–49.

Usuki, A., Kojima, Y., Kawasumi, M., Okada, A., Fukushima, Y., Kurauchi, T. and Kamigaito, O. (1993) Synthesis of nylon-6 clay hybrid, *Journal of Materials Research*, **8**, 1179–1184.

Vishwanath, B., Verma, A. P., Rao, C. V. S. K. and Gupta, R. K. (1993) Effect of different matrices on wear characteristics of glass woven roving polymer composites, *Journal of Composites*, **24**, 347–353.

Vollenberg, P. H. T. and Heikens, D. (1989) Particle size dependence of the Young's modulus of filled polymers. 1 Preliminary experiments, *Polymer*, **30**, 1656–1662.

Vu, Y. T., Mark, J. E., Pham, L. H. and Englehardt, M. (2001) Clay nanolayer reinforcement of *cis*-1,4-polyisoprene and epoxidized natural rubber, *Journal of Applied Polymer Science*, **85**, 1392–1403.

Wagner, H. D., Lourie, O., Feldman, Y. and Tenne, R. (1997) Stress-induced fragmentation of multiwall carbon nanofiber in a polymer matrix, *Applied Physics Letters*, **72**, 188.

Wang, Q., Xu, J., Shen, Q. and Liu, W. (1996) An investigation of the friction and wear properties of nanometer Si_3N_4 filled PEEK, *Wear*, **196**, 82–86.

Werner, P., Altstadt, V., Jaskulka, R., Jacobs, O., Sandler, J. K. W., Shaffer, M. S. P. and Windle, A. H. (2004) Tribological behaviour of carbon-nanofibre-reinforced poly(ether ether ketone), *Wear*, **257** (9–10), 1006–1014.

Xing, X. S. and Li, R. K. Y. (2004) Wear behaviour of epoxy matrix composites filled with uniform-sized sub-micron spherical silica particles, *Wear*, **256**, 21–26.

Yalcin, B. and Cakmak, M. (2004) The role of plasticizer on the exfoliation and dispersion and fracture behavior of clay particles in PVC matrix: a comprehensive morphological study, *Polymer*, **45**, 6623–6638.

Yang, F. and Nelson, G. L. (2004) PMMA/silica nanocomposite studies: synthesis and properties, *Journal of Applied Polymer Science*, **91** (6), 3844–3850.

Yang, F., Ou, Y. and Yu, Z. (1998) Polyamide 6 silica nanocomposites prepared by *in situ* polymerization, *Journal of Applied Polymer Science*, **69**, 355–361.

Yang, F., Yngard, R. and Nelson, G. L. (2005) Flammability of polymer–clay and polymer–silica nanocomposites, *Journal of Fire Sciences*, **23** (3), 209–226.

Yu, L. G., Nie, M. D. and Lian, Y. F. (1996) The tribological behaviour and application of rare earth lubricants, *Wear*, **197**, 206–210.

Zanetti, M., Bracco, P. and Costa, L. (2004) Thermal degradation behaviour of PE/clay nanocomposites, *Polymer Degradation and Stability*, **85** (1), 657–665.

Zhang, M. Q., Rong, M. Z., Yu, S. L., Wetzel, B. and Friedrich, K. (2002a) Effect of particle surface treatment on the tribological performance of epoxy-based nanocomposites, *Wear*, **253**, 1088–1095.

Zhang, M. Q., Rong, M. Z., Yu, S. L., Wetzel, B. and Friedrich, K. (2002b) Improvement

of tribological performance of epoxy by the addition of irradiation grafted nano-inorganic particles, *Macromolecular Materials and Engineering*, **287** (2), 111–115.

Zhang, S. and Horrocks, A. R. (2003) A review of flame retardant polypropylene fibres, *Progress in Polymer Science*, **28** (11), 1517–1538.

Zhang, Y.-Q., Lee, L.-H., Jang, H.-J. and Nah, C.-W. (2004) Preparing PP/clay nanocomposites using a swelling agent, *Composite Engineering B*, **35**, 133–138.

Zhu, J. and Wilkie, C. A. (2000) Thermal and fire studies on polystyrene-clay nanocomposites, *Polymer International*, **49** (10), 1158–1163.

10

Nanofilled polypropylene fibres

M. SFILIGOJ SMOLE and
K. STANA KLEINSCHEK,
University of Maribor, Slovenia

10.1 Introduction

Polypropylene (PP) is, besides polyesters, one of the most widely used polymers for producing synthetic fibres, especially for technical applications. PP fibres are mostly used in different technical fields due to their excellent mechanical properties, high chemical stability and processability. However, because of low surface energy, lack of reactive sites and sensitivity to photo- or thermal oxidation the polymer properties are insufficient for some applications. Therefore, several techniques for fibre modification have been reported, e.g. plasma treatment, chemical modification and nanomodification, i.e. production of nanocoated and nanofilled materials.

Polypropylene (PP) fibres have good mechanical properties and can withstand temperatures up to 140 °C (softening point 140–160 °C) before melting at about 170 °C.[1] The low polymer density (0.90 g/cm^3) offers several specific application possibilities.[2] Low costs, good chemical resistance to acid and alkaline environments have greatly influenced the high production quantity of this polymer type.[1, 3] Modifications are needed for some purposes due to PP's high hydrophobicity (moisture regain < 0.1%) and chemical unreactivity and to obtain functional materials with superior physical and mechanical properties for different applications.

There is a wide variety of both synthetic and natural crystalline fillers that are able, under specific conditions, to influence the properties of PP. In PP nanocomposites, particles are dispersed on the nano-scale.[2, 4] The incorporation of one-, two- and three-dimensional nanoparticles, e.g. layered clays,[5] nanotubes,[6, 7] nanofibres,[8, 9] metal-containing nanoparticles,[10] carbon black,[11, 12] etc. is used to prepare nanocomposite fibres. However, the preparation of nanofilled fibres offers several possibilities, such as the creation of nanocomposite fibres by dispersing of nanoparticles into polymer solutions, the polymer melt blending of nanoparticles, *in situ* prepared nanoparticles within a polymeric substrate (e.g. PP/silica nanocomposites prepared *in situ* via sol–gel reaction),[13, 14] the intercalative polymerization of the monomer,

and the introduction of nanoparticles from dispersion into a porous polymer.

Nanomodification creates improved fibre characteristics, e.g. mechanical strength, thermal stability, the enhancement of barrier properties, fire resistance, ion exchange capability, etc., for use in different application fields. In order to follow modification efficiency, various characterization techniques can be used, e.g. X-ray analysis to study composite structure, morphological observations by electron microscopy, mechanical tests, determination of electrokinetic properties, calorimetric measurements. The dispersion of particles within the hybrid system is of fundamental importance, and thus to observe particles a method based on selective etching of the polymer using a plasma or chemical etching can be used.[15–17] The dimensions of spherulites and nanoparticles can be determined by image analysis of the micrographs .[17]

10.2 Polymer layered silicate nanocomposites

Recently, in order to design materials with the desired properties, nanotechnologies have become of great importance since organic–inorganic nano-scale composites frequently exhibit unexpected hybrid properties synergistically derived from the two components.[18, 19] In addition, there are also some property improvements caused by nano-scale material modification that could not be realized by conventional fillers as, for example, a general flame-retardant character and a dramatic improvement in barrier properties. The properties of the particles themselves (size, shape, distribution) can profoundly change the characteristics of a polymer system. Therefore understanding the structure/property relations in polymer/nanoparticle nanocomposites is of major significance.[19, 20]

The idea of mixing polymers with appropriately modified clay minerals and synthetic clays is not new. Polymer layered silicate nanocomposites (PLNC) were reported by Carter and coworkers in patent literature, as early as 1950.[21] However, two major findings have led to its revival. Firstly, researchers from Toyota reported a polyamide 6/montmorillonite (MMT) composite with a remarkable enhancement of thermal and mechanical properties due to very moderate inorganic loading. In addition, it was discovered that it is possible to melt-mix polymers with clays without the use of organic solvents.[19, 22] Since then, the technology for incorporating nanoparticles into a PP matrix has offered several challenges for research, and for industrial applications. Several different nanoparticles for nanofilled composites, e.g. layered silicates,[2, 19, 23–27] silica nanoparticles,[11, 28, 29] carbon black,[11, 12] carbon nanotubes,[6, 7] metal containing nanoparticles,[10] elastomeric nanoparticles[30] and TiO_2,[31] have been reported. The most common PP nanocomposites are composed of organically modified silicates, e.g. MMT and polymeric matrix.

Generally, polymer–clay nanocomposites use smectic-type clays as fillers, such as hectorite, MMT, kaolin or synthetic mica, all minerals with a layered structure.[2, 23, 32, 33] They are of great industrial value because of their high aspect ratio, plate morphology, intercalative capacity, natural abundance and low costs.[23]

The layers are characterized by a thickness of about 1 nm, and the other dimensions vary from 30 nm to several micrometres or more. Several layers are stacked in clay particles, kept together by weak van der Waals forces. The performance of polymer–clay nanocomposites strongly depends on the breaking-up of clay particles in the polymer matrix.[2] However, the most frequently used layered silicate, MMT, is a naturally occurring 2:1 phyllosilicate, which has the same layered and crystalline structure as talc and mica but a different layer charge. A central octahedral sheet of alumina fused between two external silica tetrahedral sheets (the oxygens from the octahedral sheet also belong to the silica tetrahedral) forms the layers of the crystal lattice. Isomorphic substitution within the layers (e.g. Mg^{2+} or Fe^{+2} substitutes Al^{3+}) causes a negative charge, which is defined through the charge exchange capacity (CEC): MMT is typically 90–120 meq/100 g, depending on the mineral's origin.[19, 33] Interlayers or galleries are parallel layers forming stacks with a regular van der Waals gap between them. The negative charge of the pristine MMT is balanced by cations (Na^+, Li^+, Ca^{++}) from the interlayer.[19, 25] There is a considerable difference in polarity between polymer and clay,[2] the pre-treatment of both polymer and clay is, therefore, necessary. Clays are usually modified by cationic surfactants such as organic ammonium salts (e.g. stearyl ammonium[18, 34]) or alkyl phosphonium, that make the clay surface more organophilic.[2] PP's compatibility with organoclays is obtained by grafting polar functional groups such as maleic anhydride, diethyl maleate (DEM),[35] methyl methylacrylate and butylacrylate,[36] and mono-ethanol stearamide and others.

Another approach to enhance the compatibility between PP and modified clay is suggested by Kim *et al.*[37] They prepared PP layered silicate nanocomposites via melt mixing of three components: PP, layered silicates modified with octadecylamine (C18-MMT) and antioxidant.[37]

10.2.1 Preparation of layered silicate polypropylene nanocomposites

Three different techniques can be used to prepare nanocomposites:[25, 38]

1. Dispersing the layered silicate in a solution of the polymer in an organic solvent, followed by either solvent evaporation or polymer precipitation. The limitations of this method are shown by the large amounts of organic solvents, polymer solubility and poor filler dispersion.[25]

2. Melt intercalation of the polymer into previously organo-modified silicates. It is a very effective method when polymers, such as polyamide-6, polysiloxane and even polystyrene are intercalated. For the formation of PP-based nanocomposites, a compatibilizer such as maleic anhydride grafted polypropylene (PP-MA) or acrylic acid grafted PP is involved, which improves the polyolefin–filler interactions.[25]
3. Intercalative polymerization of the monomer. The monomer together with the polymerization initiator or catalyst is intercalated within the silicate layers and polymerization is initiated either thermally or chemically. The macromolecule chains exfoliate in silicate layers and make them disperse in the polymer matrix evenly.[36] This method allows the formation of nanocomposites based on non-polar polymers such as polyolefins.[25]

The dispersion of clay particles in polymers can result in the following:

- Clay sheets may remain stacked in structures called tactoids. Original mineral structure does not contribute to any improvement compared with the usual microcomposites with a low filler loading.[2, 23]
- Intercalated nanocomposite, where some polymer molecules are inserted between individual silicate layers.[23]
- Delaminated or exfoliated nanocomposite in which the layered structure of the clay is disrupted by the silicate layers no longer being close enough to interact with each other, and the nanometric particles are fully dispersed in the matrix.[2, 23, 24] The coherent order of stacked layers strongly depends on the clay content. The grafted polar groups (e.g. maleic anhydride) in the PP-MA chains promote interaction with the clay particles by the diffusion of the PP chain into the space between the silicate galleries (intercalating sites); therefore, the decrement of intercalating sites leads to exfoliation towards the individual silicate layers.[34] In order to favour these morphologies, long chain alkylammonium cations are exchanged for the constitutive cations (Na^+, Li^+) of the layered silicates, making the silicate surface more lipophilic, and appropriate for interacting with the organic polymer.[25]

Above all, the reinforcement effect is observed by exfoliated nanocomposites, since the nanometric dispersion of clay platelets creates a maximal interfacial surface between the filler and the polymer matrix.[25]

10.3 The structure and properties of layered silicate polypropylene nanocomposites

Generally isotactic polypropylene (iPP) is used for nanofilled materials, although nanocomposites prepared from syndiotactic polypropylene (sPP) have also been reported.[39, 40] The degree of crystallinity in PP depends on the

processing conditions, but is usually between 50 and 60%.[1] The common crystalline PP form is α monoclinic, but other forms (β and γ) have been observed. Polymorphism is important for technological reasons, because each phase has different physical and mechanical characteristics. The crystals are chain-folded lamellae and are aggregated into spherulites or row-nucleated structures, depending on the processing conditions.[1]

Some additives in polymers become nucleation centres, leading to an increase of crystal growth in the crystallization process of the polymer. A foreign surface reduces the nucleus size needed for crystal growth through the creation of the interface between polymer crystal and substrate. The important effect of such nucleation is a modification of polymer morphology, which can result in change of crystallographic form. The nucleating efficiency of various organic and inorganic fillers of iPP – talc, chalk, wood flour, nano clay particles, carbon black, chitosan – was studied by Mucha and Królikowski.[41] The best nucleating agents in this research were talc and carbon black. The organic filler as a chitosan powder forms amorphous inclusions in the composites on which iPP molecules cannot be adsorbed. Their presence disturbs a macromolecular diffusion and delays the crystallization process of iPP.[41]

A mixed α and β phase was observed in nanocomposites.[2] The relative amount of β phase never exceeded 30%, denoting a rather uniform crystallization in the bulk and on the samples' surface. The authors presume that the high β content could be attributed to stearic-acid derivatives which were added as processing aid agent and could act as nucleating agent for β phase. Stearic-acid derivatives are known as promoters of β crystallographic phase.[2]

X-ray diffraction (XRD), is commonly used to probe the nanocomposite structure. However, XRD can only detect the periodically stacked clay layers, disordered or exfoliated layers are undetected.[19] In general, in layered silicate-filled polymers a coexistence of exfoliated, intercalated and disordered layers is observed.

The monoclinic crystal structure of neat PP and nanofilled PP shows reflections assigned to planes (100), (040), (130) and others.[23] The peaks recorded between 13° and 26° (14°, 17°, 18.7°, 20°, 21.5°, 25.5°) are associated with the α crystalline structure of the PP corresponding to the basal reflections on the (110), (040), (130) and (111) crystallographic planes.[42]

The formation of an intercalated nanocomposite structure can be defined by analysing the interlayer spacing (d_{001}) of clay, although the diffraction maximum originating from the (002) crystallographic plane can be observed on the scattering curves also.[23] Only when d_{001} in the composite is higher than in the pure clay then the polymer molecules were positioned between clay layers and, hence, an intercalated nanocomposite is produced. If the peak corresponding to d_{001} is not observed in a polymer/clay diffractogram, this implies that an exfoliated nanocomposite structure was most likely obtained.[23]

Pristine MMT shows a characteristic diffraction peak between 6.94°[34] and 7.3°[17] 2θ corresponding to the (001) plane diffraction. It corresponds to an interlayer spacing of 1.2 nm.[17] For modified MMT the interlayer spacing of 1.9 nm obtained from the characteristic peak (001) at 2θ 4.7° was reported.[43] Pure organoclay cloisite 15-A shows a (001) basal signal at 2θ 2.8°, the corresponding d_{001} are 3.15 nm distant from one another.[42] In nanocomposites a shift of this peak towards small angles would be associated with intercalation while its disappearance would be a sign that exfoliation has occurred.[34] However, the disappearance of a basal peak in a wide-angle X-ray scattering (WAXS) diffractogram alone should not be intended as a clear sign of exfoliation, unless it is supported by small-angle X-ray scattering (SAXS) which is sensitive to the crystalline regions organized in lamellar stacks.[42] The SAXS profiles of pure PP samples and nanocomposites registered in the lower angular region show the presence of a maximum, which is associated with the long period resulting from the presence of a macro-lattice formed by centres of adjacent lamellae of the polymer.[43]

Evidence that the nanocomposite structure was not formed is shown by the diffraction peaks due to the presence of MMT in PP polymer which occur in the range of 2θ 2–8°. For PP/unmodified bentonite d_{001} = 1.51 nm (2θ = 5.82°), which is similar to the value observed for the clay (d_{001} = 1.50 nm; 2θ = 5.70°). On the other hand, the system containing PP/modified bentonite forms a diffraction peak at 2θ = 2.18° which is attributed to d_{001} = 4.21 nm, and is much higher than the one for the modified bentonite clay (d_{001} = 2.05 nm, 2θ = 4.32°).[23] This indicates that the organophilic bentonite forms a nanocomposite with PP, as deduced from the increase in the distance between the clay lamellae (d_{001}) caused by the intercalation of polymer molecules.[23]

The characteristics of the coupling agent (molecular weight and grafting content) influence the process of the clay intercalation.[17] The use of a coupling agent with low molecular weight and high grafting content leads to high and uniform intercalation, while exfoliation does not arise. In contrast, high molecular weight and low grafting content leads to more heterogeneous intercalation accompanied with some exfoliation. Disordered and more distanced layer structure is observed.[17] The presence of clay affects the PP morphology, i.e. spherulite size, and brings about crystalline orientation, causes the crystallization at lower temperature, but does not change the PP crystallinity.[17]

10.3.1 Preparation techniques and nanocomposite structure

There are two possibilities for preparing nanocomposites:

1. Master batches containing a high content of clay (e.g. 50% wt of clay) in PP are initially prepared. The master batch is then added to neat PP in

appropriate amounts to obtain nominal contents of 0.5–5 wt% clay in composites. The extrusion temperature usually used is 150–210 °C. The extruded composites are cooled, generally pelletized and then dried[23, 42] and re-extruded using a higher screw speed.

2. Preparation of intercalated PPCNs (PP/clay nanocomposite) using a modified PP and organophilic clay via melt extrusion processing.[18, 34, 44] PP–clay hybrids are prepared by using melt blending technology, i.e. simple melt mixing of three components – i.e. PP, modified PP oligomers and intercalated clays.[18, 45] There are two important factors to achieve the exfoliated and homogeneous dispersion of the layers in the hybrids: the intercalation capability of the oligomers in the layers and the miscibility of the oligomers with PP. Almost completed hybrids were obtained in the case where the PP-MA has both intercalation capability and miscibility.[18]

Mostly nanofilled PP is produced by injection molding; however, composites prepared from iPP and sPP, respectively, and organic layered silicate by the spinning procedure have been reported.[39, 42, 46–48]

The XRD spectra show that both the spun fibres and injection moulded specimens contain a mixture of intercalated and exfoliated organosilicate layered (OSL) structures.[42] On the diffraction curves of nanocomposite fibres no OSL peaks over the full 2θ range from 2° to 30° were observed. In contrast the injection moulded specimens exhibit six distinct OSL peaks in the 2θ region between 2° and 12° and two additional peaks between 26° and 30°. It can be concluded that under melt spinning conditions, the polymer matrix can exfoliate the OSL gallery more effectively than injection moulding. Spinning velocity influences the structure formed, i.e. OSL structures exhibit more improved exfoliation in the fibres spun at higher velocity. The exfoliation of pre-intercalated OSL structures was much more significant under an extensional velocity gradient during melt spinning rather than shear flow in injection molding.[42]

Joshi *et al*. reported that nanoclay reinforced PP nanocomposites could be spun and drawn successfully for 0.5, 1.0 and 1.5 wt% of the modified clay loading. Beyond 1.5 wt% the spinnability is poor.[49] The modified clay content in the range of 0.5-1.0 wt% gives optimum properties.[49]

10.3.2 Properties of layered silicate polypropylene nanocomposites

Nanoparticles are able to provide PP with stiffening, reinforcing and toughening effects at rather low filler concentration. The influence of processing conditions on the nanocomposite structure, i.e. intercalated or exfoliated, and on the enhancement of mechanical properties of PP nanocomposites was studied by different researchers.[44] Most polymer/clay nanocomposites studies report

tensile properties as a function of MMT content.[19] The enhancements are strictly related to the processing conditions, the filler content and the presence of compatibilizer.[44] When comparing properties of neat PP and nanocomposites, there is a sharp increase of the Young's modulus for very small inorganic loadings followed by much slower increase beyond approximately 5 wt%. With increasing MMT content the yield stress does not change markedly compared to the neat polymer value.

Considering the same processing conditions, the elastic modulus is higher in the presence of compatibilizer for different filler contents due to the polymer–inorganic adhesion improvement. This implies that the stress is much more efficiently transferred from the polymer matrix to the inorganic filler, resulting in a higher increase in the Young's modulus.[19, 42] Similar improvements in mechanical properties can also be achieved by other layered fillers; however, much higher filler loadings are required (e.g. by loading 30–60 wt% of talc or mica).[19] Silicate clay can increase the modulus, decomposition temperature, yield strength and fatigue strength, and has no effect on glass transition temperature and melt temperature.[50]

Polymer/silicate nanocomposites are characterized by very strong reduction of gas and liquid permeability and at the same time the solvent uptake decreases accordingly.[19] When single layers are dispersed in a polymer matrix the resulting nanocomposite is optically clear in the visible region, as clays are just 1 nm thick, whereas there is a loss of intensity in the UV region mostly due to scattering by the MMT particles.[19]

Five principal types of generic flame-retardant systems for inclusion in PP fibres have been identified as phosphorus-containing, halogen-containing, silicon-containing, metal hydrate and the more recently developed nanocomposite flame-retardant formulations.[51, 52] The most effective are halogen–antimony and phosphorus–bromine combinations, however their application is limited by ecological criteria.[51] Several kinds of nanocompounds can be used to enhance the flame retardancy of PP, such as modified MMT, TiO_2, Sb_2O_3 and boroxosiloxanes. Of these, the sodium cation exchanged MMT is the most common because of its low price.[19, 51, 53] The general view of the flame-retardant mechanism is that a high-performance carbonaceous silicate char builds up on the surface during combustion: this insulates the underlying material and slows the mass loss rate of decomposition products.[19, 53] All MMT-based composite systems nowadays reported show that MMT must be nanodispersed for it to affect the flammability.[53] Investigations have shown that the largest increase in mechanical properties are obtained in exfoliated nanocomposite forms while the intercalated materials show the best fire performance.[51]

The results for thermal ageing showed that PP compounds based on organically modified bentonite had higher thermal stability than those with natural clay[23] because of the formation of a nanocomposite structure with

reduced oxygen diffusion into the material. However, the thermal degradation of PP with the modified clay is higher than the pure polymer. The phenomenon is attributed to the acidic nature of the clay, the interaction between the clay and PP stabilizers and the decomposition of the organic salt during processing. When the degradation was done in the melt state the thermal stability of the composites may be higher than the pure polymer.[23]

Nanostructured materials, i.e. PP filled with an extra-pure synthetic fluorohectorite modified by means of interlayer exchange of sodium cations for protonated octadecylamine NH_3^+ (ODA) in a weight concentration of maximum 6%, may find new and upgraded application in the electrical and electronic industry, replacing conventional insulation.[54]

10.4 Nanosilica filled polypropylene nanocomposites

The incorporation of inorganic fillers in polymers contributes effectively to the improvement of the mechanical properties and in particular the toughness; however, the procedure is often limited owing to the high filler contents that are needed for desired composite properties. For this reason nanocomposites with unique nano-scale microstructure, obtained by low particle loading represent a particular advantage. However, it is very difficult to disperse nanoparticles in a polymeric matrix homogeneously owing to a strong tendency to agglomerate. An irradiation grafting method for modification of nanoparticles, e.g. nanosilica, presents an appropriate solution.[55] Through irradiation grafting polymerization, nanoparticle agglomerates transform into a nanocomposite microstructure. Grafted monomers of low molecular weight can penetrate into the agglomerated nanoparticles easily and react with the activated sites of the particles inside and outside the agglomerates. Strong interfacial interactions with the polymeric matrix during the subsequent mixing procedure result. Different monomers are appropriate for the process, e.g. styrene, methyl methacrylate, butyl acrylate, ethyl acrylate, methyl acrylic acid, vinyl acetate and others.[56]

Reinforcing and toughening effects were obtained by mixing of modified nanosilica into PP, precisely tensile properties – such as strength, modulus and elongation at break – were increased.[56] Low nanosilica-loaded PP composites were produced by Rong *et al*.[57] by a conventional compounding technique in which the nanoparticles were grafted by polystyrene using irradiation beforehand. The significantly increased hydrophobility of the nanoparticles obtained by the grafted polymers assures better interfacial interaction between the nanoparticles and the polymer. PP-based nanocomposites filled with polystyrene-grafted nano-SiO_2 (SiO_2-g-PS) show an increase of strength with a rise in filler content only to the filler content critical value and afterwards the strength remains constant irrespective of filler content.[57]

Embedded precipitated nanosilica enhances stiffening, reinforcing and toughening of PP nanocomposites at lower concentration as fumed nanosilica. By grafting with polymers such as styrene, methyl methacrylate, butyl acrylate, and ethyl acrylate, the efficiency in the composites' mechanical properties is increased depending on the grafting polymer used.[58]

Nanosilica particles can be prepared *in situ* via a sol–gel reaction. Jain *et al*. reported on PP–silica nanocomposites preparation by the sol–gel procedure[13, 16, 59] from tetraethoxy orthosilicate (TEOS), which was added to PP powder. The effect of *in situ* formed silica nanoparticles on the non-isothermal crystallization kinetics of PP–silica nanocomposites was studied in addition. Silica nanoparticles act as a nucleating agent, thereby a two-stage crystallization process was observed. Within the primary stage, nucleation and spherulitic growth occurred, while the secondary stage includes the perfectioning of crystals; thereby more perfect crystals are formed. The nucleation effect of silica results in a more narrow lamellar thickness distribution.[11] Silica nanoparticles promote β crystallographic phase.[11]

When nanosilica–PP nanocomposites are prepared from isotactic PP and SiO_2 nanoparticles by melt-mixing, a compatibilizer should be added to break off the hydrogen bonds created between the nanoparticles' surface hydroxyl groups. By the addition of PP copolymer with maleic anhydride groups (PP-g-MA), the maleic anhydride groups can react with the surface hydroxyl groups of SiO_2 nanoparticles and, through this, reduce agglomeration.[60] Mechanical properties such as tensile strength at break and Young's modulus are influenced by the content of silica particles and copolymer content.[60] After the critical concentration of nanoparticles (2.5 wt%) has been exceeded, the tensile and impact strength are decreased. This behaviour is attributed to appearance of large silica particle agglomerates.[60]

Furthermore, recently research work has focused on the possibility of using nanofiller as a compatibilizer for immiscible polymer blends. Quin Zhang with co-authors reports an improvement of the compatibility of PP/polystyrene blends with the addition of nano-SiO_2 particles by changing the phase morphology and properties of the two polymers.[61] A drastic reduction of polystyrene phase size and a very homogeneous size distribution were observed by introducing nano-SiO_2 particles at short mixing time, but at longer mixing time an increase of polystyrene size was observed, indicating a kinetics-controlled compatibilization of nano-SiO_2 particles by changing the phase morphology and properties of the two polymers.[61]

Low nanoparticle-loaded polymer composites with improved mechanical performance can be prepared by a conventional melt blending technique in which the nanoparticles are chemically pregrafted by diglycidyl ether of bisphenol-A (DGEBA).[62] Reddy *et al*.[62] prepared a composite by melt blending propylene–ethylene copolymer (EP) with DGEBA-grafted nanosilica. The addition of epoxy resin grafted nanosilica to the polymer matrix produced a

homogeneous dispersion of particles in the form of micro-domains and thereby provides EP with stiffening, strengthening and toughening effects.

10.5 Calcium carbonate and other additives

Calcium carbonate ($CaCO_3$) is one of the most commonly used inorganic fillers in PP.[63] Several authors reported that mechanical properties of PP filled with nano-sized calcium carbonate particles are essentially improved.[64] Chan *et al*. prepared nanofilled PP fibres by adding 9.2 vol% surfactant treated $CaCO_3$. The impact strength of the modified PP was more than twice as high when compared with the neat PP. The intrinsic toughness of the PP matrix influences the toughening effect of the nanoparticles. The highest increase in toughness was found in the case of the moderate matrix toughness.[63] In attempts to prevent the agglomeration of nanoparticles several surface modifications of the nanoparticles have have reported, e.g. nano-$CaCO_3$ treated with titanate coupling agent, silane coupling agent, etc.[63]

The particle size (0.07–1.9 μm) has no influence on the thermal composite's properties, and also the particle content does not affect the melting temperature or the crystallinity of PP. Surface treatment of the particles by the stearic acid coating showed an important positive effect on the impact strength due to the improved dispersion of the $CaCO_3$ particles. In addition PP molecular weight should be considered when designing a $CaCO_3$–PP nanocomposite due to its profound impact on the toughening properties.[65]

10.5.1 Carbon black-filled polypropylene composites

Carbon additives are used in polymer composites as fillers, reinforcing agents and pigments. In addition, carbon black is used to enhance UV stability, electrical conductivity and weather resistance.[12] PP geotextiles containing carbon black are applied for soil reinforcement, filtration and other construction purposes.[11, 12] In addition, carbon black can be used for preparation of magnetostrictive materials which are defined as materials that undergo a change in shape due to the change in the magnetization state of the material.[66] Carbon black, which has a polyaromatic structure containing various oxygen functional groups, is produced by partial combustion of liquid or gaseous hydrocarbons. Its antioxidant activity is due to the catalytic decomposition of peroxides and free radical scavenging, which is more effective at low temperature.[11]

The effect of carbon black on thermal and photo-oxidative degradation of oriented PP geotextile tapes was studied by Horrocks *et al*.[11] The influence of particle size (16–60 nm), structure, aggregate shape, specific surface volatile content and concentration was determined. Significant increases in thermal stabilities were observed when increasing carbon black content in PP composite.

However, the opposite effect of the carbon black with highest volatile content on thermal stability was observed.[12] This phenomenon is attributed to the adsorption of antioxidant by the carbon black surface or to the sensitization of thermal oxidative reactions by the surface oxygenated groups present.[11] It has been proved that different behaviour is related to the volatile content, due to the presence of carboxylic and sulphonic acid groups.[12] Not only are the temperature and rate of decomposition influenced by embedded carbon black particles, but also the decomposition products. The presence of 1-alkene oligomers with $3n$ C atoms is reduced, while 2-alkenes and 1-alkenes with $3n+1$ C atoms are increased. Carbon black promotes chain scission and participates in the radical transfer reactions.[12] Incorporated particles of carbon black, especially those with small particle size, improve UV durability.[11]

10.5.2 Alumina nanoparticle-filled polypropylene

Nanocomposites containing 1.5–5.0 wt% of spherical alumina (Al_2O_3) nanoparticles, which were pre-treated with silane coupling agent, were prepared by Zhao and Li.[67] Tensile tests show that Young's modulus and the yield strength of the nanocomposite increase with the particle content increasing, suggesting that the interfacial interaction between the nanoparticles and the matrix is relatively strong. Structural investigation, i.e. X-ray analysis, differential scanning calorimetry (DSC) and optical microscopy measurements, show that a small amount of the β-crystal form results after adding the Al_2O_3 nanoparticles. The Al_2O_3 nanoparticles reduce the size of PP spherulites and enhance the crystallization temperature of PP, by acting as an effective nucleating agent.[67]

10.5.3 Polypropylene-polyhedral oligomeric silsesquioxane nanocomposites

Polyhedral oligomeric silsesquioxanes (POSS) were first synthesized in 1946. They belong to the group of silsesquioxanes characterized by the general formula $(RSiO_{1,5})_n$, where R is hydrogen or an organic group, such as alkyl, aryl or any of their derivatives. POSS can be easily functionalized by chemically altering the R substituent group, thus having the potential to undergo copolymerization or grafting reactions. The addition of the thermally robust POSS moiety drastically modifies the polymer thermal properties supplying greater thermal stability to the polymer matrix, also allowing the tailoring of the polymer glass transition temperature by varying the POSS concentration.[68] The addition of POSS also improves mechanical properties and reduces polymer composite flammability.

Fu *et al.*[69, 70] first prepared octamethyl-POSS/PP composites by melt blending and studied their crystallisation behaviour.[69] Fina *et al.*[68] investigated

the influence of the POSS substituent groups on the morphological and thermal characteristics of melt-blended POSS/PP composites by varying the aliphatic chain length. Composites with octamethyl-, octaisobutyl- and octaisooctyl-POSS were prepared. Increasing alkyl chain length provoked substantial differences in morphology of the composites, i.e. the compatibility between POSS and PP, nucleating ability, spherulitic morphology formation, etc.[68] Recently the same authors reported about thermal and thermo-oxidative degradation of PP-based composites, using different metal containing POSS. Metal POSS derivatives (Al and Zn) were prepared by deprotonation of incompletely condensed POSS trisilanol (i-$C_4H_9)_7Si_7O_9(OH)_3$ with either triethylaluminium or diethylzinc.[71]

10.6 Conclusion

In recent years, nanostructured materials have attracted much attention because of their potential for large gains in mechanical and physical properties as compared with standard structural materials. Although numerous different nanofilled products were developed, there are still unlimited challenges for researchers and technology.

10.7 References

1. Lewin M., Pearce E.M., *Handbook of Fiber Chemistry,* New York, Marcel Dekker, 1998.
2. Benetti E.M., Causin V., Marega C., Marigo A., Ferrara G., Ferraro A., Consalvi M., Fantinel F., 'Morphological and structural characterization of polypropylene based nanocomposites', *Polymer*, 2005 **46** 8275–8285.
3. Cook J.G., *Handbook of Textile Fibres, II Man-made Fibres*, Durham, Merrow Publishing, 1984.
4. Poole C.P., Owens F.J., *Introduction to Nanotechnology*, Hoboken, New Jersey, Wiley Interscience, 2003.
5. Manias E., Touny A., Wu L., Lu B., Strawhecker K., Gilman J.W., Chung T.C., 'Polypropylene/silicate nanocomposites, synthetic routes and materials properties', *Polymeric Materials: Science & Engineering*, 2000 **82** 282–283.
6. Chatterjee A., Deopura B.L., 'High modulus and high strength PP nanocomposite filament', *Composites Part A – Applied Science and Manufacturing*, 2006 **37/5** 813–817.
7. Kearns J.C., Shambaugh R.L., 'Polypropylene fibers reinforced with carbon nanotubes', *Journal of Applied Polymer Science*, 2002 **86/8** 2079–2084.
8. Hine P., Broome V., Ward I., 'The incorporation of carbon nanofibres to enhance the properties of self reinforced, single polymer composites', *Polymer*, 2005 **46** 10936–10944.
9. Li J., Wang Q., Chan C., Wu J., 'Effect of molding temperature on crystalline and phase morphologies of HDPE composites containing PP nano-fibers', *Polymer*, 2004 **45** 5719–5727.

10. Gubin S.P., 'Metal-containing nano-particles within polymeric matrices: preparation, structure, and properties', *Colloids and Surfaces, A: Physicochemical and Engineering Aspects,* 2002 **202** 155–163.
11. Horrocks A.R., Mwila J., Miraftab M., Liu M., Chohan S.S., 'The influence of carbon black on properties of oriented polypropylene, 2. Thermal and photodegradation', *Polymer Degradation and Stability*, 1999 **65** 25–36.
12. Jakab E., Omastova M., 'Thermal decomposition of polyolefin/carbon black composites', *Journal of Analytical Applied Pyrolysis*, 2005 **74** 204–214.
13. Jain S., Goossens H., van Duin M., Lemstra P., 'Effect of *in situ* prepared silica nano-particles on non-isothermal crystallization of polypropylene', *Polymer,* 2005 **46** 8805–8818.
14. Hribernik, S., Sfiligoj Smole, M., Stana-Kleinschek K., Strnad S., Bele M., Ribitsch V., 'Preparation of nanocomposite cellulose fibres' 4th Symposium of science and technology of nanomaterials in Slovenia, *Slonano* 2005.
15. Mozetič M., Zalar A., Panjan P., Bele M., Pejovnik S., Grmek R., 'A method of studying carbon particle distribution in paint films', *The Solid Films*, 2000 **376** 5–8.
16. Stakne K., Dissertation, University of Maribor, 2004.
17. Perrin–Sarazin F., Ton-That M.T., Bureau M.N., Denault J., 'Micro- and nano-structure in polypropylene/clay nanocomposites', *Polymer*, 2005 **46** 11624–11634.
18. Kawasumi M., Hasegawa N., Kato M., Usuki A., Okada A., 'Preparation and mechanical properties of polypropylene-clay hybrids', *Macromolecules* 1997 **30** 6333–6338.
19. Manias E., Touny A., Wu L., Strawhecker K., Lu B., Chung T.C., 'Polypropylene/ montmorillonite nanocomposites. Review of the synthetic routes and material properties', *Chemistry of Materials*, 2001 **13** 3516–3523.
20. Privalko V.P., Shumsky V.F., Privalko E.G., Karaman V.M., Walter R., Friedrich K., Zhang M.Q., Rong M.Z., 'Viscoelasticity and flow behaviour of irradiation grafted nano-inorganic particle filled polypropylene composites in the melt state', *Journal of Materials Processing Technology*, 2003 **137** 208–213.
21. Carter L., Hendricks J.G., Bolley D.S., US Patent 2,531,396, 1950 (assigned to National Lead Co.), 31.
22. Vaia R.A., Ishii H., Giannelis E.P., 'Synthesis and properties of 2-dimensional nanostructures by direct intercalation of polymer melts in layered silicates', *Chemistry of Materials*, 1993 **5** 1694–1696.
23. Filho F.G.R., Mélo T.J.A., Rabello M.S., Silva S.M.L., 'Thermal stability of nanocomposites based on polypropylene and bentonite', *Polymer Degradation and Stability*, 2005 **89** 383–392.
24. Ray S.S., Okamoto M., 'Polymer/layered silicate nanocomposites: a review from preparation to processing', *Progressin Polymer Science*, 2003 **28** 1539–1641.
25. Alexandre M., Dubois P., Sun T., Garces J.M., Jérôme R., 'Polyethylene-layered silicate nanocomposites prepared by the polymerization-filling technique: synthesis and mechanical properties', *Polymer*, 2002 **43** 2123–2132.
26. Han B., Ji G., Wu S., Shen J., 'Preparation and characterisation of nylon 66/ montmorillonite nanocomposites with co-treated montmorillonites', *European Polymer Journal*, 2003 **39** 1641–1646.
27. Tang Y., Hu Y., Song L., Zong R., Gui Z., Chen Z., Fan W., 'Preparation and thermal stability of polypropylene/montmorillonite nanocomposites', *Polymer Degradation and Stability*, 2003 **82** 127–131.
28. Rong M.Z., Zhang M.Q., Zheng Y.X., Zengh H.M., Friedrich K., 'Improvement of

tensile properties of nano-SiO_2/PP composites in relation to percolation mechanism', *Polymer*, 2001 **42** 3301–3304.
29. Rong M.Z., Zhang M.Q., Zheng Y.X., Zengh H.M., Walter R., Friedrich K., 'Structure–property relationships of irradiation grafted nano-inorganic particle filled polypropylene composites', *Polymer*, 2001 **42** 167–183.
30. Zhang M., Liu Y., Zhang X., Gao J., Huang F., Song Z., Wei G., Qiao J., 'The effect of elastomeric nano-particles on the mechanical properties and crystallization behaviour of polypropylene', *Polymer*, 2002 **43** 5133–5138.
31. Wei Q., Gao W., Wang X., 'Preparation and characterisation of functionally nanostructured fibres' *2nd International Textile Clothing & Design Conference, Magic World of Textiles*, Dubrovnik, 2004, 151–156.
32. Mareri P., Bastide S., Binda N., Crespy A., 'Mechanical behaviour of polypropylene composites containing fine mineral filler: effect of filler surface treatment', *Composites Science and Technology*, 1998 **58** 747–752.
33. Lagaly G., Ziesmer S., 'Colloid chemistry of clay minerals: the coagulation of montmorillonite dispersions', *Advances in Colloid and Interface Science*, 2003 **100–102** 105–128.
34. Nam P.H., Maiti P., Okamoto M., Kotaka T., Hasegawa N., Usuki A., 'A hierarchical structure and properties of intercalated polypropylene/clay nanocomposites', *Polymer* 2001 **42** 9633–9640.
35. García-López D., Picazo O., Merino J.C., Pastor J.M., 'Polypropylene–clay nanocomposites: effect of compatibilizing agents on clay dispersion', *European Polymer Journal*, 2003 **39** 945–950.
36. Ding C., Jia D., He H., Guo B., Hong H., 'How organo-montmorillonite truly affects the structure and properties of polypropylene', *Polymer Testing* 2005 **24** 94–100.
37. Kim J.H., Koo C.M., Choi Y.S., Wang K.H., Chung I.J., 'Preparation and characterization of polypropylene/layered silicate nanocomposites using an antioxidant', *Polymer*, 2004 **45** 7719–7727.
38. Lee J.H., Jung D., Hong C.E., Rhee K.Y., Advani S.G., 'Properties of polyethylene-layered silicate nanocomposites prepared by melt intercalation with a PP-g-MA compatibilizer', *Composites Science and Technology,* 2005 **65** 1996–2002.
39. Mlynarčiková Z., Kaempfer D., Thomann R., Mülhaupt R., Borsig E., Marcinčin A, 'Syndiotactic polypropylene/organoclay nanocomposite fibres: influence of the filler and compatibilizer on the fibre properties', *2nd International Textile Clothing & Design Conference*, *Magic World of Textiles*, Dubrovnik, 2004.
40. Gorrasi G., Tortora M., Vittoria V., Kaempfer D., Mülhaupt R., 'Transport properties of organic vapors in nanocomposites of organophilic layered silicate and syndiotactic polypropylene', *Polymer*, 2003 **44** 3679–3685.
41. Mucha M., Królikowski Z., 'Application of DSC to study crystallization kinetics of polypropylene containing fillers', *Journal of Thermal Analysis and Calorimetry*, 2003 **74** 549–557.
42. Lew C.Y., Murphy W.R., McNally G.M., Abe K., Yanai S., 'Metallocene–catalyzed polypropylene nanocomposite fibers: the effect of melt spinning on the exfoliation of layered-silicates', *Polymer Fibers 2004*, Manchester 2004.
43. Bertini F., Canetti M., Audisio G., Costa G., Falqui L., 'Characterization and thermal degradation of polypropylene–montmorillonite nanocomposites', *Polymer Degradation and Stability,* 2006 **91** 600–605.
44. Modesti M., Lorenzetti A., Bon D., Besco S., 'Effect of processing conditions on

morphology and mechanical properties of compatibilized polypropylene nanocomposites', *Polymer*, 2005 **46** 10237–10245.
45. Utracki L.A., Sepehr M., Li J., 'Melt compounding of polymeric nanocomposites', *International Polymer Processing*, 2006 **21** (1) 3–16.
46. Marcinčin A., Jurenkova M., Kubičkova M., Hricova M., Borsig E., Brejka O., 'Nanocomposite fibres for advanced textiles', *2nd International Textile, Clothing and Design Conference*, *Magic World of Textiles*, Dubrovnik 2004
47. Sfiligoj Smole M., Stakne K., Stana Kleinschek K., Gregor Svetec D., Ribitsch V., 'Properties of nanocomposite PP fibres' *SPIE Opto-Ireland 2005 Nanotechnology and Nanophotonics*, Dublin 2005, 306–313.
48. Sfiligoj Smole M., Stakne K., Gregor Svetec, D., Stana Kleinschek K., Bele M., Ribitsch V., Musil V., 'Nanofilled PP fibres', *Polymer Fibres 2004*, Manchester 2004.
49. Joshi M., Shaw M., Butola B.S., 'Studies of composite filaments from nanoclay reinforced polypropylene', *Fibres and Polymers*, 2004 **5**(1) 59–67.
50. Zhou Y., Rangari V., Mahfuz H., Jeelani S., Mallick P.K., 'Experimental study on thermal and mechanical behaviour of polypropylene, talc/polypropylene and polypropylene/clay nanocomposites', *Materials Science and Engineering*, 2005 **402** 109–117.
51. Zhang S., Horrocks A.R., 'A review of flame retardant polypropylene fibres', *Progressin Polymer Science*, 2003 **28** 1517–1538.
52. Marosi G., Márton A., Szép A., Csontos I., Keszei S., Zimonyi E., Toth A., Almeras X., Le Bras M., 'Fire retardancy effect of migration in polypropylene nanocomposites induced by modified interlayer', *Polymer Degradation and Stability*, 2003 **82** 379–385.
53. Qin H., Zhang S., Zhao C., Feng M., Yang M., Shu Z., Yang S., 'Thermal stability and flammability of polypropylene/montmorillonite composites', *Polymer Degradation and Stability*, 2004 **85** 807–813.
54. Montanari G.C., Fabiani D., Palmieri F., 'Modification of electrical properties and performance of EVA and PP insulation through nanostructure by organophilic silicates', *IEEE Transactions on Dielectrics and Electrical Insulation* 2004 **11** (5) 754–762.
55. Wu C.L., Zhang M.Q., Rong M.Z., Friedrich K., 'Tensile performance improvement of low nanoparticles filled-polypropylene composites', *Composites Science and Technology*, 2002 **62** 1327–1340.
56. Rong M.Z., Zhang M.Q., Zheng Y.X., Zengh H.M., Walter R., Friedrich K., 'Structure–property relationships of irradiation grafted nano-inorganic particle filled polypropylene composites', *Polymer*, 2001 **42** 167–183.
57. Rong N.Z., Zhang M.Q., Zheng Y.X., Zengh H.M., Friedrich K., 'Improvement of tensile properties of nano-SiO_2/PP composites in relation to percolation mechanism', *Polymer*, 2001 **42** 3301–3304.
58. Wu C.L., Zhang M.Q., Rong M.Z., Friedrich K., 'Silica nanoparticles filled polypropylene: effect of particle surface treatment, matrix ductility and particle species on mechanical performance of the composites', *Composites Science and Technology*, 2005 **65** 635–645.
59. Stöber W., Fink A., 'Controlled growth of monodisperse silica spheres in the micron size range', *Journal of Colloids and Interface Science*, 1968 **26** 62–69.
60. Bikiaris D.N., Vassiliou A., Pavlidou E., Karayannidis G.P., 'Compatibilisation effect of PP-g-MA copolymer on iPP/SiO_2 nanocomposites prepared by melt mixing', *European Polymer Journal*, 2005 **41** 1965–1978.

61. Zhang Q., Yang H., Fu Q., 'Kinetics-controlled compatibilization of immiscible polypropylene/polystyrene blends using nano-SiO_2 particles', *Polymer*, 2004 **45** 1913–1922.
62. Reddy C.S., Das C.K., Narkis M., 'Propylene–ethylene copolymer nanocomposites: Epoxy resin grafted nanosilica as a reinforcing filler', *Polymer Composites* 2005 **26/6** 806–812.
63. Yang K., Yang Q., Li G., Sun Y., Feng D., 'Morphology and mechanical properties of polypropylene/calcium carbonate nanocomposites', *Materials Letters*, 2006 **60** (6) 805–809.
64. Weon J.I., Gam K.T., Boo W.J., Sue H.J., Chan C.M., 'Impact-toughening mechanisms of calcium carbonate-reinforced polypropylene nanocomposite', *Journal of Applied Polymer Science*, 2006 **99/6** 3070–3076.
65. Zuiderduin W.C.J., Westzaan C., Huétink J., Gaymans R.J., 'Toughening of polypropylene with calcium carbonate particles', *Polymer* 2003 **44** 261–275.
66. Nai-Xiu D., Mao-Sheng Z., 'Magnetostrictive properties of carbon black filled polypropylene composites', *Polymer Testing*, 2004 **23** 523–526.
67. Zhao H.X., Li R.K.Y., 'Crystallization, mechanical and fracture behaviours of spherical alumina-filled polypropylene nanocomposites', *Journal of Polymer Science B – Polymer Physics*, 2005 **43** (24) 3652–3664.
68. Fina A., Tabuani D., Frache A., Camino G., 'Polypropylene–polyhedral oligomeric silsesquioxanes (POSS) nanocomposites', *Polymer*, 2005 **46** 7855–7866.
69. Fu B.X., Yang L., Somani R.H., Zong S.X., Hsiao B.S., Phillips S., Blanski R., Ruth P., 'Crystallization studies of isotactic polypropylene containing nanostructured polyhedral oligomeric silsesquioxane molecules under quiescent and shear conditions', *Journal of Polymer Science Part B – Polymer Physics*, 2001 **39** (22) 2727–2739.
70. Fu B.X., Gelfer M.Y., Hsiao B.S., Phillips S., Viers B., Blanski R., Ruth P., 'Physical gelation in ethylene-propylene copolymer melts induced by polyhedral oligomeric silsesquioxane (POSS) molecules', *Polymer*, 2003 **44** (5) 1499–1506.
71. Fina A., Abbenhuis H.C.L., Tabuani D., Frache A., Camino G., 'Polypropylene metal functionalised POSS nanocomposites: a study by thermogravimetric analysis', *Polymer Degradation and Stability*, 2006 **91** (5) 1064–1070.